JOURNAL OF THE

Electrochemical Society

ol. 112, No. 4 April 1965

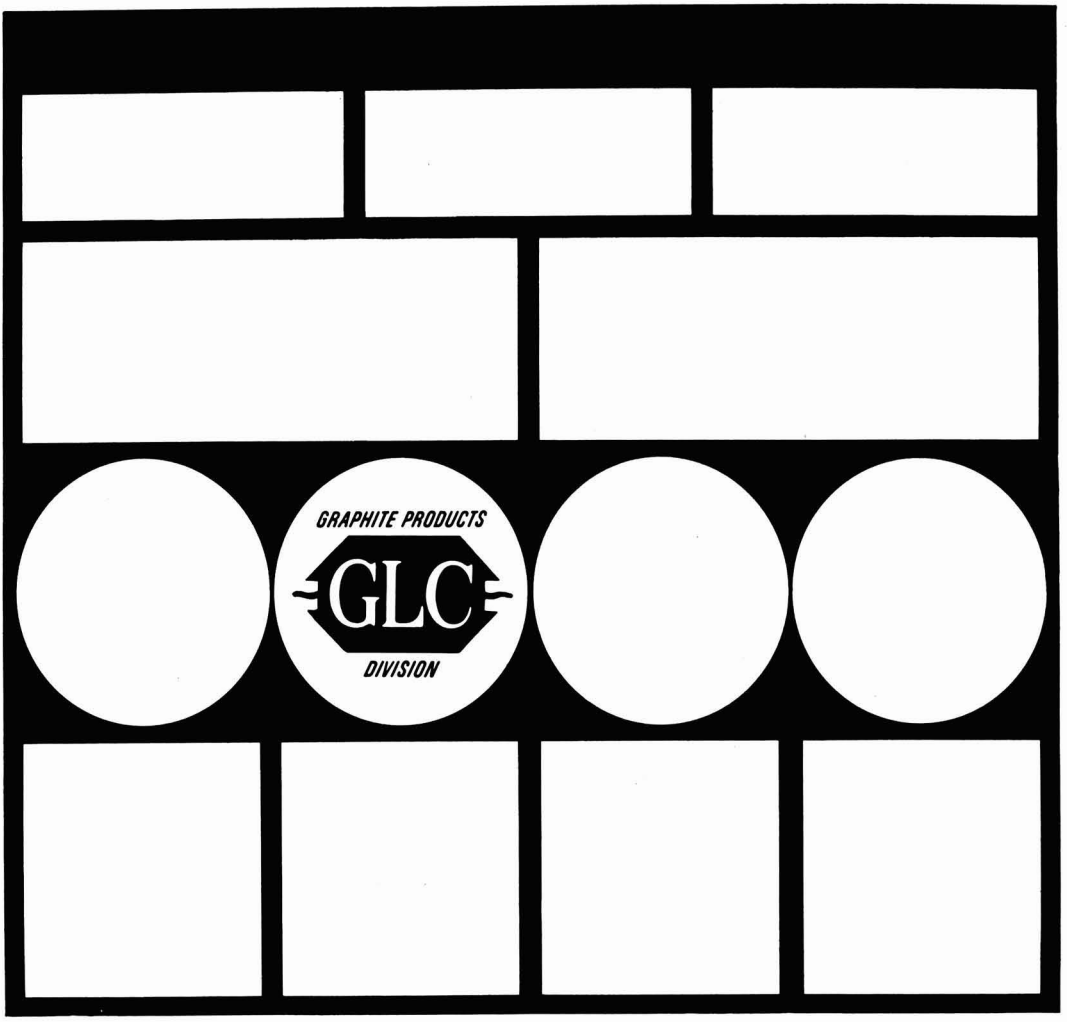

GLC ANODES:

leaders of dependability in electrolytic cell operation for more than a decade.

PRODUCTS GRAPHITE PRODUCTS GLC DIVISION YOU CAN TRUST ®

GREAT LAKES CARBON CORPORATION

18 East 48th Street • New York, N. Y. 10017

OFFICES AND AGENTS IN PRINCIPAL CITIES AROUND THE WORLD

Great Lakes Carbon Corporation is one of the world's largest manufacturers of graphite for electrochemical and electrothermic processes—and for aerospace, nuclear, metallurgical and other industrial uses.

WHAT MAKES A STACKPOLE ANODE BETTER?

Rigid processing control. At Stackpole, close supervision of mixing, baking, graphitizing and impregnating produces a product of the highest quality and uniformity.

For instance, Stackpole's oil treating process impregnates the anode for keeps. Bleeding during operation is cut to a minimum. This means fewer diaphragm changes for you . . . longer cell life, lower maintenance costs.

Stackpole GraphAnodes® can be designed with any feature you need, such as holes, slots or bevels. Careful planing of all anode surfaces insures perfect cell alignment for maximum efficiency and life.

Let us tell you more about the difference in GraphAnodes, write: Stackpole Carbon Company, Carbon Division, St. Marys, Pa. Phone: 814-834-1521 TWX: 814-826-4808.

STACKPOLE
CARBON DIVISION

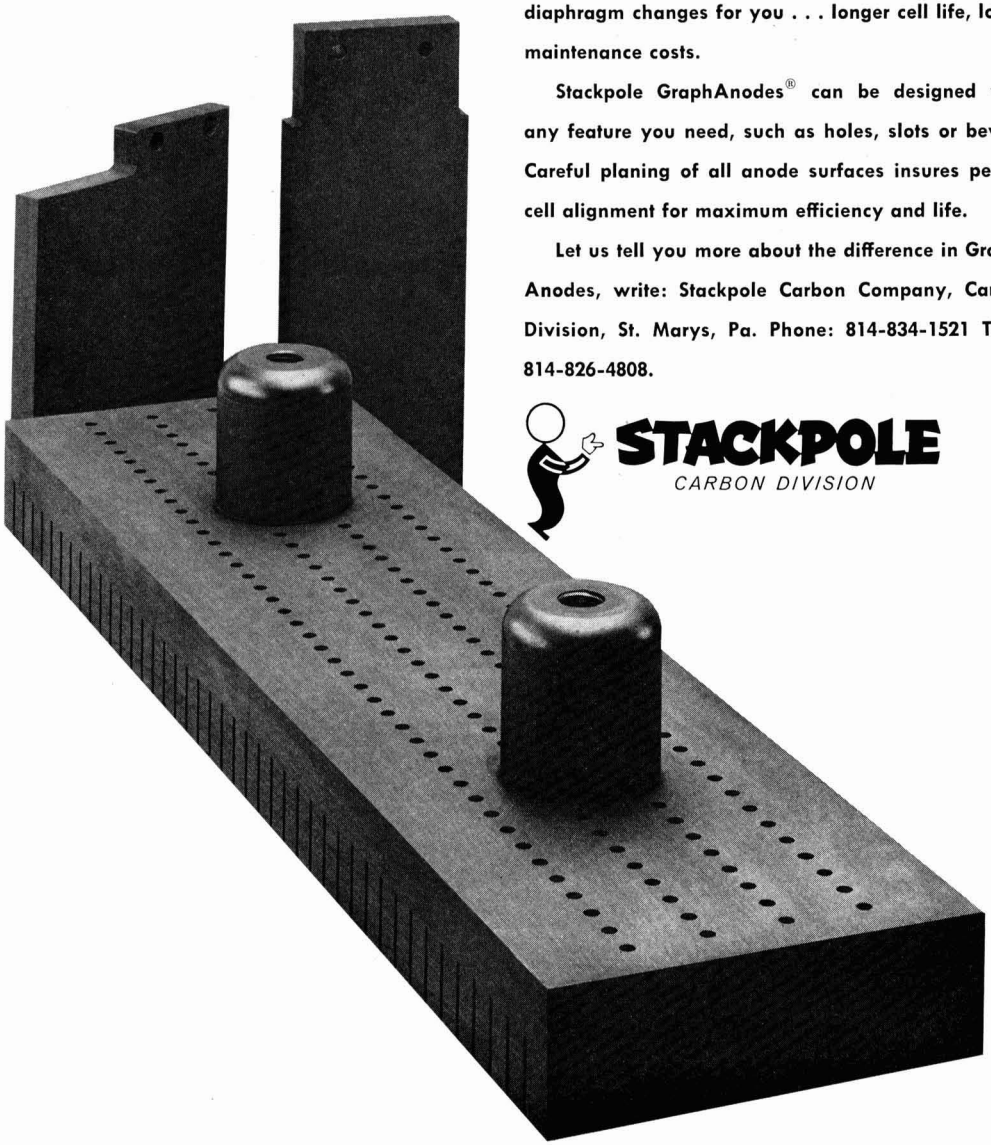

JOURNAL OF THE

C. L. Faust, Chairman, Publication Committee
R. A. Kolbe, Manager of Publications

EDITORIAL STAFF

Cecil V. King, Editor
Norman Hackerman, Technical Editor
Ruth G. Sterns, Managing Editor
H. W. Salzberg, Book Review Editor
Daniel J. Immediato, Assistant Editor

DIVISIONAL EDITORS

W. C. Vosburgh, Battery
Paul C. Milner, Battery
G. A. Marsh, Corrosion
A. C. Makrides, Corrosion
Morris Cohen, Corrosion
Harry C. Gatos, Corrosion—Semiconductors
Newton Schwartz, Electric Insulation
Seymour Senderoff, Electrodeposition
Ephraim Banks, Electronics
Simon Larach, Electronics
Charles S. Peet, Jr., Electronics—Semiconductors
F. A. Trumbore, Electronics—Semiconductors
P. Wang, Electronics—Semiconductors
Sherlock Swann, Jr., Electro-Organic
Stanley Wawzonek, Electro-Organic
John M. Blocher, Jr., Electrothermics & Metallurgy
J. H. Westbrook, Electrothermics & Metallurgy
Scott Lynn, Industrial Electrolytic
C. W. Tobias, Theoretical Electrochemistry
A. J. deBethune, Theoretical Electrochemistry
R. M. Hurd, Theoretical Electrochemistry
M. W. Breiter, Theoretical Electrochemistry

ADVERTISING OFFICE
ECS

30 East 42 St., New York, N. Y., 10017

ECS OFFICERS

Lyle I. Gilbertson, President
207 Dogwood Lane,
Berkeley Heights, N. J.

E. B. Yeager, Vice-President
Western Reserve University,
Cleveland, Ohio

H. J. Read, Vice-President
Dept. of Metallurgy
Pennsylvania State University
University Park, Pa.

H. C. Gatos, Vice-President
Depts. of Met. & Electrical Engrg.,
Massachusetts Institute of Technology,
Cambridge, Mass., 02139

R. A. Schaefer, Treasurer
The Electric Storage Battery Co.,
Yardley, Pa.

Ivor E. Campbell, Secretary
220 Gentry Rd.,
Coraopolis, Pa.

Ernest G. Enck, Executive Secretary
National Headquarters, The ECS,
30 East 42 St., New York, N. Y., 10017

Robert A. Kolbe, Assistant Executive Secretary
The ECS, 30 East 42 St., New York, N. Y., 10017

APRIL 1965

EDITORIAL

TECHNICAL PAPERS

ELECTROCHEMICAL SOCIETY

VOL. 112 • NO. 4

Manuscripts submitted to the Journal should be sent, in triplicate, to the Editorial Office at 30 East 42 St., New York, N. Y., 10017. They should conform to the revised Instructions to Authors published on pp. 366-45C of the Mar. issue. Manuscripts so submitted become the property of The Electrochemical Society and may not be published elsewhere, in whole or in part, unless permission is requested of and granted by the Editor.

The Electrochemical Society does not maintain a supply of reprints of papers appearing in its Journal. A photoprint copy of any particular paper, however, may be obtained by corresponding direct with the Engineering Societies Library, 345 E. 47 St., New York, N. Y., 10017.

Inquiries re positive microfilm copies of volumes should be addressed to University Microfilms, Inc., 313 N. First St., Ann Arbor, Mich.

Walter J. Johnson, Inc., 111 Fifth Ave., New York, N. Y., 10003, have reprint rights to out-of-print volumes of the Journal, and also have available for sale back volumes and single issues, with the exception of the current calendar year. Anyone interested in securing back copies should correspond direct with them.

Published monthly by The Electrochemical Society, Inc., at 215 Canal St., Manchester, N. H.; **Executive Offices, Editorial Office** and **Circulation Dept.**, and **Advertising Office** at 30 East 42 St., New York, N. Y., 10017, combining the JOURNAL and TRANSACTIONS OF THE ELECTROCHEMICAL SOCIETY. Statements and opinions given in articles and papers in the JOURNAL OF THE ELECTROCHEMICAL SOCIETY are those of the contributors, and The Electrochemical Society assumes no responsibility for them.

Claims for missing numbers will not be allowed if received more than 60 days from date of mailing plus time normally required for postal delivery of JOURNAL and claim. No claims allowed because of failure to notify the Circulation Dept., The Electrochemical Society, 30 East 42 St., New York, N. Y., 10017, of a change of address, or because copy is "missing from files." Subscription to members as part of membership service; subscription to nonmembers $24.00 plus $1.50 for postage outside U.S. and Canada. Single copies $1.70 to members, $2.25 to nonmembers.

© 1965 by The Electrochemical Society, Inc.

Entered as second-class matter at the Post Office at Manchester N. H., under the act of August 24, 1912. Postage paid at Manchester, N. H.

ห้องสมุด กรมวิทยาศาสตร์
25 พ.ค. 2509

Editorial

The World Needs Truth and Honesty

THERE is probably no more untruthfulness and dishonesty in the world now than in the past, but we would like to hope that there will be less in the future. Civilization has formed only a thin veneer of respectability on mankind, and all too often we see the sad results when this veneer is punctured. Education and the ability to convert natural resources into materials of ease and comfort are the means of advancing our civilization, provided that too much ease and comfort do not bring apathy, neglect of responsibility and the eventual downfall of the comfortable society.

The resignation (under pressure) of 100 cadets from the U.S. Air Force Academy has touched off a spate of controversy about the honesty and morality of the well-fed, best educated part of our younger generation. A few cadets stole examination questions and induced others to help distribute them (for cash). Many others were accused of knowing what had happened but failing to report to the authorities, a definite requirement of the honor system to which all had subscribed. Parents of some of the young men in the latter group were indignant; they had taught their sons from childhood, they said, to be honest but not to tell tales on their brothers or friends. However, it is one thing for a boy to keep mum if his pal accidentally breaks a window, quite another to condone harmful misbehavior in a dignified college. And we feel only contempt for the witness to an accident or a crime who silently steals away ("I didn't want to get involved with the police"). Where does morality end and immorality begin?

Reporters studying the Academy affair tell us there is evidence that at least 55% of all college students cheat at one time or another. If this is true in any serious way it has to mean that college administrators and teaching staffs are negligent and apathetic, at the least. The honor system can be extended too far: why tempt immature students unnecessarily? Examination questions can be protected from theft and alternative sets can be ready. It is hardly cheating if fraternities collect old examinations for the brothers to study; the departments ought to be able to hand out all old questions for this very purpose. It is hard to get convincing evidence of plagiarism and ghostwriting, but if these are suspected it is easy to let the student know it will do him no good.

We are accustomed to the Big Lie in the dictator countries, where history may even be rewritten to fool the people, maybe the dictators too. It is hard to condone the apparently increasing tendency of our own government bodies and officials to cover up mistakes, inefficiency and waste by silence, evasion and all too often by downright untruths. We are told that the budget is balanced, that the budget will be balanced, that the imbalance is noninflationary, that the small rise in prices is noninflationary (what *is* inflation?). We are told that a Red Cuba is no menace, that Cuba has no dangerous weapons, that all dangerous weapons have been removed from Cuba. We are told that only a few guerrillas remain in Viet Nam, that the Viet Nam war is being won, that the serious setback will soon be reversed, that a few more . . .

It seems that the U.S. Information Service has been making a color movie of the war in Viet Nam. An Associated Press correspondent found the cameras shooting scenes of Vietnamese troops, assisted by spotter planes, "capturing an enemy village". The correspondent found that plenty of other troops were on guard to make sure that the Viet Cong did not interfere. A USIS man explained that they did not want blood and bodies in the film, but wished to sell Viet Nam to the world by minimizing the brutality and emphasizing the personal aspects of the war.

As the Editor of *Air Force Magazine* says, this kind of an effort to tell something other than the truth about the war in Viet Nam is nothing new; only now the Hollywood touch has been added. —CVK

Equilibrium Pressures of Oxygen over MnO_2-Mn_2O_3 at Various Temperatures

Earl M. Otto

National Bureau of Standards, Washington, D. C.

ABSTRACT

Oxygen pressures of the pyrolusite form of MnO_2 have been determined in a temperature range of 441°-642°C. The dissociation reaction $4MnO_2(c) \rightleftarrows 2Mn_2O_3(c) + O_2$ (g) has been found to reach a steady state in the forward direction; reaction in the reverse direction was exceedingly slow and did not reach a steady state. $\Delta H°$ and $\Delta S°$ for the reaction at 813°K are 37.87 kcal[1] and 51.28 cal/deg, respectively. With little error these values can be used in the equation

$$-4.5756 \log pO_2(\text{atm}) = 37{,}870/T - 51.28$$

to calculate the pressure for any temperature in the above mentioned range. Conversion to 298.15°K resulted in $\Delta H°_{298} = 38.8$ kcal and $\Delta S°_{298} = 52.8$ cal/deg for the dissociation. The limits of uncertainties are not given here because equilibria were not attained by recombination.

Although many investigations of original experimentation, theoretical calculations and collation of data reported in the chemical literature give information which relate temperature of MnO_2 and oxygen pressure, there is such a lack or omission of critical detail and there is so much disagreement that it was felt desirable to attempt to clear up the discrepancies. There is a lack of measuring and/or reporting precise temperatures and pressures. Frequently there is evidence that no equilibrium was reached. For example, in many instances the temperature of the MnO_2 was raised a few degrees per minute. Preparation of the sample is not always specified, nor is there assurance the sample was dry or desiccant included in the system. Among the investigators there is disagreement not only in the pressure-temperature relationship, but also regarding composition, crystal structure, and nomenclature of the sample and regarding the existence of reversibility of the MnO_2 dissociation. Table I gives in very concise form, pertinent observations made by the various investigations (1-24). When sufficient data were available, pressure-temperature graphs were made and some of these are shown in Fig. 5.

Values for thermodynamic constants of oxides of manganese have been determined experimentally in recent years by Millar (25), Siemonsen (26), Southard (27), Shomate (28), Moore (29), Kelley and Moore (30), Orr (31), and King (32). These values have been collated, adjusted to correlate with newly accepted reference values, and are tabulated by Kelley (33), Rossini (34), Brewer (35), Coughlin (36), Glassner (37), Mah (38), and Dushman (39). Brewer has stated (40) that "further work at higher temperatures and with long heating times is necessary to clarify the equilibrium limits of the solid-solution ranges."

It became evident, therefore, that precise determinations of oxygen pressure-MnO_2 temperature relationships at equilibrium were needed. Furthermore, the question of reversibility needed to be studied.

[1] One thermochemical calorie = 4.1840 joules. $R \ln pO_2 = 2.302585 \times 8.31433$ joules ÷ 4.1840 joules/cal = 4.57563 cal log pO_2.

Experimental

For the lowest two temperatures (441° and 491°C) the apparatus was identical with that previously described by this author (41). A diagrammatic sketch of the apparatus is shown in Fig. 1. For 555°C the sample was contained in a Vycor cup set in a nickel bomb. A nickel delivery tube led outside the furnace to ⅜-in. stainless steel tubing attached by Swagelok fittings to a heavy wall glass manometer containing mercury. Steel capillary tubing then lead to a 250 psi gauge and a high-pressure valve. From mercury to pressure gauge and almost to the valve the system was filled with

Table I. Observations of various investigators

Literature reference	Brief summary of pertinent observations
Moissan (1)	H_2 over heated MnO_2. Reaction began at 230°.
Wright and Luff (2)	H_2 over heated MnO_2. Reaction began at 390°.
Gorgeu (3)	Several varieties MnO_2 heated in air. O_2 evolved at about 400°.
Meyer and Rötgers (4)	MnO_2 prepared from $Mn(NO_3)_2$. Decomposed at 530° in air and at 565° in O_2; 86 hr required; no reversibility.
Askenasy and Klonowski (5)	MnO_2 heated in closed system; 0.26 atm in <5 hr at 478° and >1.37 atm in <5 hr at 536°; reversibility claimed.
Kendall and Fuchs (6)	MnO_2 heated in closed system; 1 atm as 419°; reversibility claimed.
Drucker and Hüttner (7)	MnO_2 heated. Pressure equilibria not constant; reversible below 480°.
Simon and Feher (8)	MnO_2 heated; 0.9 atm at 525°.
Bahr and Sackur (9)	MnO_2 heated in closed system: 1.07 atm at 572° in 68 hr; irreversible.
Von Krüll (10)	MnO_2 heated. Concluded no definite decomposition temperature obtainable.
Blumenthal (11)	Pyrolusite, crystalline, amorphous. See Fig. 5 for pyrolusite.
LeBlanc (12)	X-ray diffraction studies. No solid solutions exist.
Dubois (13)	Various types MnO_2 heated. Decomposed at 300°-600°. Proposes $MnO_{1.90}$.
Herman and Slonim (14)	Several natural MnO_2 ores. No >0.4 atm at no >583°. X-ray diffractions showed no solid solutions.
Kapustinskii and Bayushkina (15)	Heated MnO_2 prepared from $Mn(NO_3)_2$. See Fig. 5.
Sakai, Hukuyama and Okuno (16)	Several kinds MnO_2 heated in air. Decomposed at 500°-580°.
Matsuno (17)	Pyrolusite heated. Decomposed about 650°; temperature depends on crystal size.
Tatievskaya (18)	Decomposition temperature of 627° at 1.24 atm calculated by thermodynamics.
Kulp and Perfetti (19)	In DTA (12.5° rise/hr) break in curve at 580°-670°.
Brenet and Grund (20)	Thermogravimetric analysis. Weight loss at 500°.
McMurdie and Golvato (21)	DTA of pyrolusite. Endothermic break at 670°.
Pascal (22)	More than 150 oxides of manganese exist.
Grasselly and Klivenyi (23)	Product analysis after heating for 3 hr in air. Weight loss at 460°.
Földvari-Vogl and Koblencz (24)	DTA of pyrolusite. Endothermic break at 640°.

All temperatures are in °C. DTA = Differential Thermal Analysis.

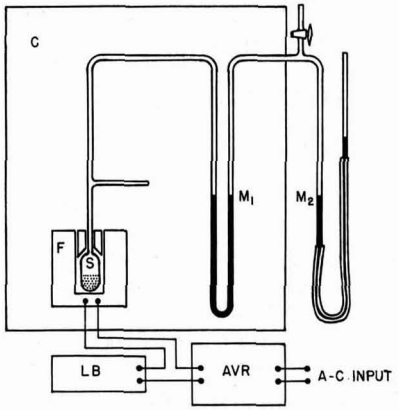

Fig. 1. Diagrammatic sketch of apparatus: C, temperature controlled cabinet; S, Vycor tube containing sample, M_1 and M_2, manometers, M_2 serves as leveling device; AVR, automatic voltage regulator; LB, lamp bank; F, furnace.

trichlorethylene on which the pressure could readily be increased by passing cylinder nitrogen through the high-pressure valve. For 642° the sample was again in a Vycor cup. Now the nickel bomb was very thick walled and was attached to nickel tubing and then stainless steel capillary tubing. A 2500 psi gauge and an oxygen servicing high-pressure valve completed the system. For all temperatures except 642°, pressure readings were taken at constant volume.

In all cases the furnace was located in the thermostatted cabinet (c). Regulated constant current was continuously supplied by means of an automatic voltage regulator connected in series with a lamp bank and the furnace.

The manganese dioxide used was reagent grade pyrolusite assaying 99.5% MnO_2. In a sieve test 9% remained on the 100 mesh sieve, 88% on the 200 mesh, and 3% through the 200 mesh. Further grinding was done sometimes. The sample was dried at 120°C overnight and then weighed into the Vycor capsule. Further drying was done by operating the furnace at 350°C while the system was being evacuated for several hours. The furnace temperature was increased and then held constant for hundreds or several thousand hours while the pressure was approaching an equilibrium or steady value. At each temperature, data on pressure-time relationships were obtained and plotted. Figures 2 and 3 are typical.

By lowering the temperature or by increasing the oxygen pressure attempts were made to reverse the dissociation reaction. The resulting reduction in pressure was so slow in contrast to Mn_2O_3 dissociations (41) that at first it was considered that there was no reduction and the dissociation is irreversible. Figures 2 and 4 show that there is recombination, but that equilibrium was never re-established.

The first sample used in this investigation was mortar ground so fine that it all readily passed through a 100 mesh sieve. After drying the sample at 300°C the system was evacuated to several mm pressure and sealed. The temperature was raised to 513° for a few hours during which time the pressure rose to 1200 mm. The system was cooled to 441°, again evacuated and resealed. It was concluded after 1199 hr that the equilibrium pressure had been reached. That the supply of oxygen was not exhausted was proven by again evacuating and heating to a higher temperature during which time the pressure reached 7.3 atm. The second sample reported was likewise heated to about 500° and the system evacuated before being stabilized at 491° for a total of 524 hr, 336 hr being required to reach a steady pressure. The third sample was preheated to about 580° and the evolved oxygen (18 atm) removed. Then, after 477 hr at 555° by which time the pO_2 was 14 atm and after a partially successful reversal, a second build-up of pressure was allowed to take place, this one reaching 15 atm in 1400 hr and maintaining that pressure for

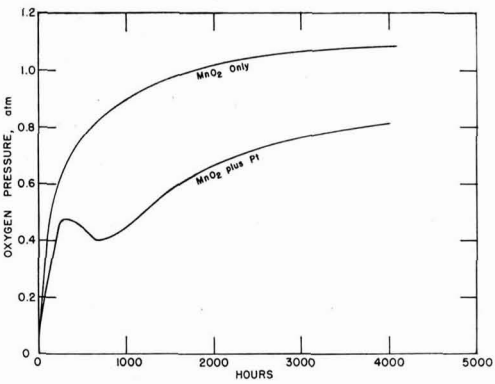

Fig. 3. Dissociation of pyrolusite. Effect of time on attainment of equilibrium at 474°C; also the effect of the presence of platinum black at 474°C.

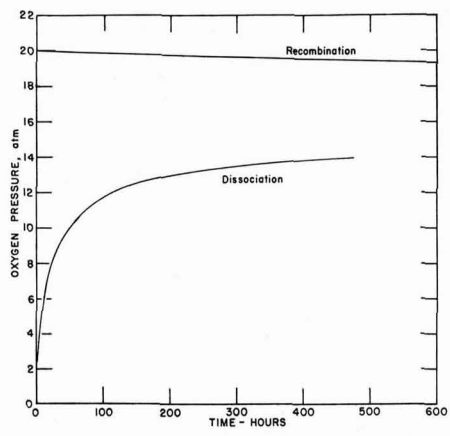

Fig. 2. Dissociation of pyrolusite. Effect of time on attainment of equilibrium at 555°C; also evidence of partial recombination at 555°C.

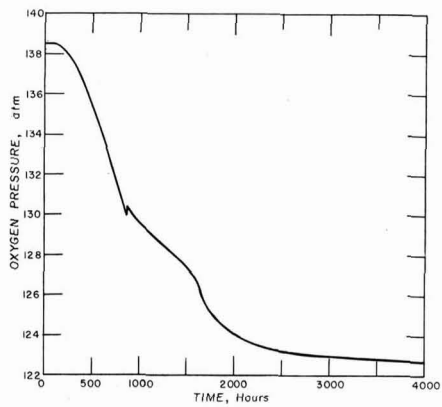

Fig. 4. Reoxidation at 475°C of pyrolusite dissociated at 642°C. Equilibrium pressure is 1.4 atm.

Table II. Equilibrium data for four temperatures

Temperature, °K	pO_2, atm	Compressibility factor	Fugacity, atm	$-R\ln$ fugacity	"Correction" C	$\Delta Y°/T$, cal/deg
714.15	0.410	1.0001	0.4100	+1.7716	−0.0222	+1.7494
764.15	2.45	1.0007	2.4517	−1.7822	−0.0066	−1.7887
828.15	15.0	1.0046	15.069	−5.3907	−0.0028	−5.3934
915.15	142.7	1.045	149.12	−9.9457	−0.0145	−9.9602
[813]						[−4.6884*]

Compressibility factors were obtained by interpolation and extrapolation of data taken from "Tables of Thermal Properties of Gases" Circular 564 National Bureau of Standards. Fugacity equals the compressibility factor times the pressure.

* This is the predicted value of $\Delta Y°/T$ at 813° as given in the section on Treatment of Data.

1600 additional hr. A noteworthy observation is that 800 hr were needed to reach 14 atm in the second build-up compared to 477 hr in the first. The sample studied at 642° was evacuated at 350° and slowly heated to 642° until the pO_2 was 125 atm. Some oxygen was released; the pressure fell to 110 atm. From 1500 to 1800 hr at 642° the pressure was constant at 142.7 atm. Following this experiment the temperature was raised, and it was noted that, after thermal equilibrium was obtained, the pO_2 again rose indicating some MnO_2 was dissociating. An unsuccessful attempt was made to reach the equilibrium pressure by lowering the temperature from 642° to 475°. Figure 4 shows that the Mn_2O_3 did not undergo recombination in the first 200 hr. Recombinations then became relatively rapid until a total of 870 hr had passed, at which time there was a temporary rise in oxygen pressure and then a decrease, but at a lower rate than the initial. If the recombination taking place between 3000 and 4000 hr were to continue at the same rate, the remaining pressure drop of 115 atm to the equilibrium pressure of 1 atm at 475° would have required a number of years. After the partially successful reversal attempt sufficient MnO_2 remained to obtain essentially the equilibrium pressure at 530° in 3700 hr. The equilibrium data obtained for the four temperatures are given in Table II and Fig. 5. For comparison purposes experimental data from the literature are included in Fig. 5. It is to be noted that the oxygen pressures observed in the present investigation are much greater than any heretofore observed for corresponding temperatures.

Platinum black was blended with pyrolusite in an attempt to catalyze the dissociation of MnO_2 or the reverse action. Figure 3 shows that the platinum actually consumed much of the oxygen and was of no benefit to the study.

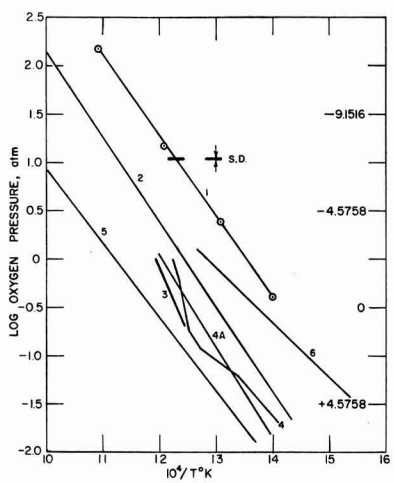

Fig. 5. Oxygen pressure-manganese dioxide temperature. Curve 1, present work on pyrolusite; line thickness aside curve 1 shows the uncertainty of the fit of the equation at 813°K; curve 2, Mah; curve 3, Meyer and Rötgers; curve 4, Blumenthal (experimental) curve 4A, Blumenthal (calc.); curve 5, Ulich and Siemonsen.

Treatment of Data

In spite of the inability to attain complete reversibility, it is assumed that equilibrium was reached in the forward direction. Since the range in oxygen pressure exceeded 100 atm, it is necessary to use fugacity (fO_2) in calculating values for thermodynamic constants (heat and entropy) of the reaction to give precise correlation of pressure and temperature. In other respects the treatment of the data is similar to that used in the previous paper (41). The method of Prosen (42) was again used to convert the data to yield a theoretical straight line plot of $\Delta Y°/T$ against $1/T$, where this line is the tangent to the $\Delta F°/T$ curve at a selected temperature of 813°K, an approximate midpoint temperature in this study. The pertinent equations involved are

$$\Delta Y°/T = \Delta H°_{813}/T - \Delta S°_{813}$$

and

$$\Delta Y°/T = -4.5756 \log fO_2 + C$$

where C is the correction given by

$$C = -\Delta(H°_t - H°_{813})/T + \Delta(S°_t - S°_{813})$$
$$= -1/T\,\Delta C°_p\,dT + (\Delta C°_p/T)\,dT$$

The $\Delta C°_p$ value for the reaction, obtained from data given by Kelley (33), is

$$\Delta C°_p = -9.78 + 8.00 \times 10^{-3}\,T + 8.66 \times 10^5/T^2$$

For the 813°K region the correction is

$$C = 3.9311 + 0.004T - 6{,}374.45/T$$
$$+ 4.33 \times 10^5/T^2 - 22.5233 \log T/813$$

Table II gives in successive columns for each equilibrium the temperature, the observed pressures, the compressibility, the fugacity, R ln of fugacity, the Prosen correction, and $\Delta Y°/T$. Also Fig. 5 indicates there is no noticeable difference on this scale between the plot of pO_2 against $1/T$ and the theoretical tangent at 813°K. The constants of this tangent

$$\Delta Y°/T = \Delta H°_{813}/T - \Delta S°_{813}$$

were determined to be

$$\Delta H°_{813} = 37.87 \pm 0.56 \text{ kcal}$$

$$\Delta S°_{813} = 51.28 \pm 0.70 \text{ cal/deg}$$

and the predicted value at 813 was

$$\Delta Y°/813 = -4.688 \pm 0.065 \text{ cal/deg}$$

The indicated uncertainties are the standard deviations of the associated quantities as determined from the least squares fit to the four points of Table II. The uncertainty in the log pO_2 value at 813°K is indicated by the standard deviation shown by the thickness of the line aside curve 1 of Fig. 5. This is evidence that the difference from the other curves cannot be accounted for by errors in measurement. Systematic error due to not actually reaching equilibria could only mean

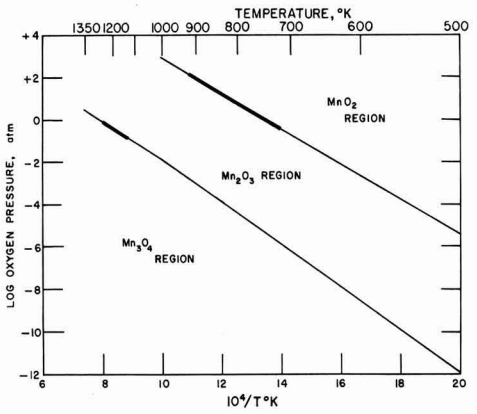

Fig. 6. Regions of stable existence of oxides of manganese

that pressures would have been even higher than those shown here.

If one subtracts from the above constants −0.88 kcal, $(H_{813} - H_{298})$, and −1.50 cal/deg, $(S_{813} - S_{298})$, calculated from the tabulated heat content and entropy data given by Kelley for the substances involved, the resultant constants for the reaction at 298.15°K become

$$\Delta H^\circ_{298.15} = 38.76 \pm 0.6 \text{ kcal}$$

$$\Delta S^\circ_{298.15} = 52.78 \pm 0.7 \text{ cal/deg}$$

Then

$$\Delta F^\circ_{298.15} = 23.0 \text{ kcal}$$

These values may be compared with those given in the literature. Rossini *et al.* (34) selected −124.5 kcal for the ΔHf°_{298} of MnO_2 and −232.1 kcal for that of Mn_2O_3. These yield +33.8 kcal for ΔH°_{298} for the reaction. Mah (38) selected −124.4 kcal for ΔHf°_{298} of MnO_2 and −228.4 kcal for that of Mn_2O_3 giving +40.8 kcal for the reaction. Brewer (35) chose −124.2 kcal and −229.2 kcal for these respective constants which result in 38.4 kcal for the reaction. Using the newly determined value of −228.7 kcal derived by Otto (41) for the ΔHf°_{298} of Mn_2O_3 one obtains for the ΔHf°_{298} of MnO_2 a value of −124.0 kcal. This is in good agreement with those cited above.

The value of ΔS°_{298} may also be compared with that obtained from entropy values given in the literature. Glassner (37) selected entropies at 298°K for MnO_2, Mn_2O_3, and O_2 as 12.7, 26.4, and 49.0 cal/deg, respectively. These yield 51.0 cal/deg for the dissociation of MnO_2 while the value obtained as a result of this investigation is 52.8 cal/deg.

It may be of interest to compare, in tabular form, the present results with those given by Mah.

Tcmp, °K	298	700	800	900	1000
Present work, atm	4.3×10^{-17}	0.242	7.23	101.5	849
Mah's table, atm	1.71×10^{-19}	0.0238	0.855	14.1	132

Now that equilibrium studies of MnO_2-Mn_2O_3 and Mn_2O_3-Mn_3O_4 have been completed, it is possible to delineate the mutual boundaries of these oxides. By use of tables (38) of entropy and heat-content changes the boundaries (Fig. 6) have been extended above and below the range of temperatures and pressures of the experimentation. At an oxygen pressure of 1.000 atm the equilibrium temperature is 468°C (741°K), while in air at 1.000 atm it is 424°C (697°K).

Acknowledgment

The author wishes to express his gratitude to Dr. W. J. Hamer under whose direction the work was conducted and who maintained keen interest in the study despite the thousands of hours required to obtain equilibria.

Manuscript received Aug. 6, 1964. This paper was presented at the Boston Meeting, Sept. 16-20, 1962.

Any discussion of this paper will appear in a Discussion Section to be published in the December 1965 JOURNAL.

REFERENCES

1. H. Moissan, *Ann. Chim. Phys.*, [5] **21,** 231 (1880).
2. C. R. A. Wright and A. P. Luff, *J. Chem. Soc.*, **33,** 522 (1878).
3. A. Gorgeu, *Compt. rend.*, **110,** 1134 (1890).
4. R. J. Meyer and K. Rötgers, *Z. anorg. Chem.*, **57,** 104 (1908).
5. P. Askenasy and S. Klonowski, *Z. Elektrochem.*, **16,** 104 (1910).
6. J. Kendall and F. Fuchs, *J. Am. Chem. Soc.*, **43,** 2017 (1921).
7. C. Drucker and R. Hüttner, *Z. Phys. Chem.*, **131,** 237 (1928).
8. A. Simon and F. Feher, *Z. Elektrochem.*, **38,** 137 (1932).
9. F. Bahr and O. Sackur, *Z. anorg. chem.*, **73,** 101 (1912).
10. V. F. Von Krüll, *Z. anorg. u. allgem. chem.*, **208,** 134 (1932).
11. M. Blumenthal, *Bull. soc. chim. (France)*, **53,** 1418 (1933).
12. M. LeBlanc and G. Wehner, *Z. phys. chem.*, **168,** 59 (1934).
13. M. P. Dubois, *Ann. chim.*, [11] **5,** 432 (1936).
14. Z. Herman and Ch. Slonim, *Monatshefte,* **70,** 84 (1937).
15. A. F. Kapustinskii and K. C. Bayuskhina, *Zhur. fiz. khim. (USSR)*, **11,** 77 (1938).
16. W. Sakai, H. Hukuyama, and T. Okuno, *J. Soc. Chem. Ind. Japan,* **45,** 25 (1942).
17. S. Matsuno, *ibid.*, **46,** 605 (1943).
18. E. P. Tatievskaya, G. I. Chufarov, and V. K. Antonov, *Izvest. Akad. Nauk. SSSR,* 371 (1948).
19. L. Kulp and J. Perfetti, *Mineralog. Mag.*, **29,** 239 (1952).
20. J. Brenet and A. Grund, *Compt. rend.*, **240,** 1210 (1955).
21. H. F. McMurdie and Golvato, *U. S. Natl. Bur. Standards J. Research,* **41,** 589 (1948).
22. P. Pascal, "Nouveau Traité de Chimie Minerale," Vol. XVI, p. 748, Masson et Cie, Paris (1960).
23. G. Grasselly and E. Klivenyi, *Acta Univ, Szegediensis Acta Mineral. Petrog.*, **9,** 15 (1956).
24. M. Foldvari-Vogl and V. Koblencz., *ibid.*, **9,** 7 (1956).
25. R. W. Millar, *J. Am. Chem. Soc.*, **50,** 1875 (1928).
26. H. Siemonsen, *Z. Elektrochem.*, **45,** 637 (1939).
27. J. C. Southard, *J. Am. Chem. Soc.*, **63,** 3142 (1941).
28. C. H. Shomate, *ibid.*, **66,** 928 (1944).
29. G. E. Moore, *ibid.*, **65,** 1398 (1943).
30. K. K. Kelley and G. E. Moore, *ibid.*, **65,** 782 (1943).
31. R. L. Orr, *ibid.*, **76,** 857 (1954).
32. E. G. King, *ibid.*, **76,** 3289 (1954).
33. K. K. Kelley, *U. S. Bur. Mines Bull. 584* (1960).
34. F. D. Rossini, *U. S. Natl. Bur. Standards Circ. 500* (1952).
35. L. Brewer, *Chem. Rev.*, **52,** 1 (1953).
36. J. P. Coughlin, *U. S. Bur. Mines Bull. 542* (1954).
37. A. Glassner, *U. S. Argonne Nat. Lab. ANL 5750* (1957).
38. A. D. Mah, *U. S. Bur. Mines Repts. Invest. 5600* (1960).
39. S. Dushman, "Scientific Foundations of Vacuum Techniques," p. 742, 2nd Ed., John Wiley & Sons, New York (1962).
40. L. Brewer, Private communication.
41. E. M. Otto, *This Journal,* **111,** 88 (1964).
42. E. J. Prosen, To be published.

Effects of Foreign Ions on Nickel Hydroxide and Cadmium Electrodes

E. J. Casey, A. R. Dubois, P. E. Lake,* and W. J. Moroz

Defence Chemical Biological and Radiation Laboratories, Ottawa, Ontario, Canada

ABSTRACT

The behavior of individual positive and negative electrodes of the sintered-plate nickel-cadmium battery system in the presence of foreign ions in KOH solutions has been examined. Carbonate choke: The variation of electrochemical capacity as a function of carbonate contamination of the electrolyte, temperature, and current density was measured for both positive and negative electrodes. The effect of carbonate on the negative cadmium electrode is much greater than on the positive. The general mechanism and the role of intermediate complexes are discussed. Nitrate shuttle: Self-discharge occurs in cells containing nitrate, as a result of reduction of NO_3^- to NO_2^- at the cadmium electrode with subsequent reoxidation to NO_3^- at the nickel hydroxide electrode. Cations on the positive: Addition of Li^+, Ag^+ Sb^{+3}, Al^{+3}, and As^{+3} to the electrolyte had effects on capacity and on charge-retention of well-formed nickel hydroxide positive electrodes. Lithium promoted the highest average oxidation, particularly at high temperatures (55°C). Arsenic was the best inhibitor of loss of charge. Possible mechanisms are discussed.

Carbonate.—Previous investigations have had as their objective the understanding of the effects on nickel-cadmium batteries of the carbonate which is formed by the reaction of the alkali electrolyte with carbon dioxide absorbed from the air (1). The interest of this Laboratory in these phenomena was awakened several years ago when it was observed that sintered-plate cells with more than 5% carbonate by weight sometimes behaved very peculiarly (2) and always delivered less capacity (3, 4) at low temperatures. However, the unpredictability of when and where it would occur made the verification of a true carbonate effect difficult.

On cadmium metal surfaces the mechanism of the carbonate effect has been studied (4-7) at a more fundamental level, in the absence of the porous sintered nickel matrix. It was concluded (6) that $CO_3^=$ competes with OH^- for adsorption sites on the underlayer which forms as the primary product of the oxidation reaction; and, further, that this competition varies with variation in current, electrolyte composition, and temperature. The important role of an inner double layer, in the underlayer, was stressed.

Another way of looking at this effect might be through the model of Croft and Tuomi (8-9). In their model the polarizations of the electrode are related to the number and kind of structural defects principally at the electrolyte-oxide interface and in the covering layer itself. The number and kinds of defects are determined by their rate of formation by the anodic current, their rate of combination with each other and with existing defects, and their rate of reaction with the components of the electrolyte.

The fibrous nature and the probable role of the hydroxycarbonate anodic reaction products on cadmium were discussed by Huber (10). Although their chemical composition was reported as early as 1936 (11), and that of the related bicarbonates since 1957 (12), there is still no reliable means of identifying small quantities formed on an anode. To complicate matters, these compounds are unstable. The problem of identification will be discussed in a subsequent report.

The nickel hydroxycarbonates are better known. Gagnon *et al.* (11, 13) showed chemically that nickel hydroxycarbonates can be formed if precipitating conditions are carefully controlled. However, like the cadmium compounds, sufficiently rapid identification of small quantities formed at electrodes is still not possible. There have been some very good recent studies made of the chemical precipitation and properties of nickel hydroxycarbonates (14) which may be used as a starting point in the attempt to understand at least qualitatively the electrochemical behavior. Thus compounds of the general formula $y\mathrm{NiCO_3 \cdot Ni(OH)_2 \cdot H_2O}$, where $y = 1$, 3, or 4 have been identified chemically, and they give unique x-ray diffraction patterns (14). They are unstable in strong caustic. Longuet-Escard and Méring (15) have tackled the critical problem of the distortion of the nickel hydroxide lattice by incorporated carbonate ions; and Vasserman and Fomina (16) have followed changes in composition and in x-ray diffraction pattern during ageing, the compound becoming more basic at high *p*H (~12) and less basic at low *p*H (~7). Feitknecht (17) has given a broad and informative perspective of this problem.

Nitrate.—The loss of charge of a nickel-cadmium cell via the "nitrate shuttle" (18) was not recognized until cells with little or no free electrolyte were manufactured. Observations of odd effects of nitrate on voltage have been noticed [*e.g.*, (19)]. It seems to be a unique redox system: both the oxidized (NO_3^-) and reduced (NO_2^-) species are soluble in the electrolyte, are uncomplexed with either the electrolyte or the electrodes, and diffuse at a rate which increases with concentration gradient and temperature. Because nitrate is readily reduced by cadmium metal, and nitrite readily oxidized by charged nickel hydroxide, a mechanism for loss of charge exists by means of electron exchange within the cell.

Positive ions.—Following up a rather ingenious prediction from the solid-state structure of cadmium and its hydroxide, Fleischer (20) was able to demonstrate that the addition of indium metal to the cadmium negative electrode made a sharp decrease in the loss of capacity which usually occurs during cycling. With the above exception, most of the published work within the past few years on cationic additions, including that undertaken by this Laboratory, has dealt with their effect on the behavior of the nickel hydroxide electrode. The addition of lithia to the electrolyte has been standard practice in the pocket-plate battery industry for years. Its effect has been described in the trade as keeping the nickel hydroxide active material "loosened up," with the result that the electrochemical storage capacity does not decrease with prolonged use of the battery. Normally lithia does not need to be added to the sintered-plate battery; this is presumed to be so because the positive active material is spread so thinly over the surface of the sintered matrix that it is substantially all available for electrochemical action at normal temperature. However, to facilitate the formation of plates made by the thermal impregnation

* Present address: 448 Briar Avenue, Ottawa, Ontario, Canada.

process (21) used now by at least two manufacturers, it is sometimes necessary to add lithia to the electrolyte during the forming process. That lithium ions are also beneficial in the sintered plate positive at high temperatures will be demonstrated later.

Although cobalt hydroxide has often been incorporated in pocket-plate batteries since the time of Edison, the introduction of cobalt into the positives of sintered-plate batteries was first made by a European manufacturer during the early 1950's, and most other manufacturers have since followed suit. An additional stimulus for the commercial introduction of cobalt was Winkler's paper (22) in 1955 in which he reported "brilliant improvement" in performance. In general terms, cobalt raises the voltage of the electrode during discharge (*i.e.*, either it raises the reversible emf or it lowers the overvoltage). Further, cobalt has been reported (19) to improve greatly the charge-retention of the positive, and data published recently (23) support this view. After Winkler's paper, the first published systematic study on the effects of cobalt was that of Doran in 1958 (24). With lightly impregnated plates he demonstrated that, in contrast with plates containing pure nickel hydroxides, whose electrochemical storage capacity slowly decreases toward a final steady value (about 60% of the original) during repetitive cycling, the "electrodes containing moderate proportions of cobalt maintain indefinitely a capacity at least as high as that of the pure nickel hydroxide electrode at its transient best." He also found that whereas other ions (Zn^{++}, Mn^{++}, and Cd^{++}) made only minor modifications to the charge (oxidation) and discharge (reduction) curves, Mg^{++} had the very important practical effect of raising the discharge voltage (*i.e.*, lowering the cathodic overvoltage of the positive) by about 50 mv. However, Mg^{++} ions were found to increase the rate of loss of charge from the oxidized nickel hydroxide mass during an idle period.

Further, Doran found (25) that replacement of 5% of the nickel ions by cobalt and 5% by magnesium ions combined the best characteristics of both additions; thus, a stabilized high capacity, as well as discharge at a higher voltage resulted. In his paper, Doran cautioned that one could not extrapolate from his results, obtained with lightly impregnated plates, to battery performance. Subsequent evaluations of complete cells have been inconclusive (26).

In later work (27) it was demonstrated that scandium alone has the combined beneficial effects of the $Mg^{++} - Co^{++}$ addition, and that the discharge voltage is even higher with scandium than with magnesium. Further, "compared with the pure nickel electrode, in addition to the much higher discharge potential, the separation of anodic and cathodic potential is less, and the oxygen overpotential (top-of-charge potential) is higher." Of course, all of these effects are desirable in battery applications.

A basic difficulty arises in a study such as the present one, because the crystal structure of the active nickel hydroxide mass may be different from one experiment to the next on the same material, or from one preparation to another [see ref. (28), *e.g.*]; and, further, the crystal structure may change with "age" and even during "rest" when it is not being oxidized and reduced (8, 29, 30). One preparation (loose, open structure) may be expected to show marginal effects of positive ion additions, while another preparation (more perfectly formed crystallites) may show marked effects. These and other published claims [ref. (31-58)] about electrochemical effects of positive ions have been collected and are recorded in Table I, for comparison later with results of the present work.

Consider what might be the effects of foreign cations on the electrical conductivity of the active nickel hydroxide mass. Two concepts provide the background: (*a*) the mass consists of lamellar hexagonal arrays of positive ions, negative ions and water molecules whose positions are known from x-ray diffraction studies [colorfully described and illustrated by Doran (24), *e.g.*]; and (*b*) the idea (59), that the oxygen atoms of the water and hydroxide ions of the mass remain relatively fixed in the lattice while protons from the electrolyte and electrons from the metallic grid move into the mass during discharge (reduction) and out of the mass during charge (oxidation). Divalent foreign cations should distort the lattice, being of different size, and introduce anion (OH^-) vacancies as the mass becomes oxidized. Into these vacancies water molecules may fit, and facilitate protonic conduction. Doran's results on Mg^{++} and Sc^{++} especially tend to support

Table I. Reported effects of added cations on properties of nickel hydroxide electrodes

	Ionic radius, Å	Coulombic capacity, C	Capacity-stabilization with cycling	Voltages: disch	Voltages: chge	Voltages: o'chge	Charge retention (open circuit)	Potential decay (open circuit): b_A	Potential decay (open circuit): b_B	Potential decay (open circuit): b_C	Electrical conductivity of oxides	Rate of recrystallization of hydroxides	References
Li^+	0.68	++	+	0	0	++	+	0	+	+	++	(−)	(35), (29), (55), (45), (39), *, (83), (86)
Na^+	0.97	0	0	0	0	0	0	0	0	0		0	**, (33), (83)
K^+	1.33	+				(−)	(+)	0	0	0		(−)	(48), (50), (52), (83)
Rb^+	1.48	(+, −)			(−)	(+)							(41), (58), (86)
Cs^+	1.69	(+, −)			(−)	(+)							(41), (58), (86)
Ag^+	1.26	+			+	0	0	0	d	d		(−)	*
Mg^{+2}	0.65	+	+		+	(0)	0		−				(25)
Cu^{+2}	0.69				(−)	(+)							(25)
Ni^{+2}	0.69											+	(40), (42)
Zn^{+2}	0.74	0, =	=		0, −	0	0	0					(25), (55), (56), (87)
Cd^{+2}	0.97	0			0	0	0	0					(24), (57)
Hg^{+2}	1.10	++	+										(43)
Ba^{+2}	1.34	+, −	+, −				−						(85), (29), (2), (55), (44), (76)
B^{+3}	0.35	(−)											(36)
Al^{+3}	0.51	0			−	+	+	0	d	0			*
Fe^{+3}	0.53	+, −	+										(35), (49)
Ce^{+3}	0.63	+, 0	+		+	+	−	+	+	+	+	(−)	(20), (25), (54), (31), (47), (51), (55), (22), (38), (23)
Sc^{+3}	0.81	+			+	+	0	+					(25), (27)
Mn^{+4}	<0.80 (+2)	0, −			0	0							(25), (46)
Sn^{+4}	0.75	+											(64)
Sb^{+5}	0.62	+			0	+	0	+	0	d	0		*
As^{+5}	0.56	+			0	+	+	++	0	d	0		*
Bi^{+5}	<1.16 (+3)											+	(35)
Mo^{+6}	<0.68 (+4)						−						(47)
Cr^{+6}	<0.55 (+3)						−						(47)
W^{+6}	0.64						−	0					(87)

0, no change; +, increased; − decreased; $b = \partial E/\partial \log t$, where t is time and E is potential; A, B, and C, 1st, 2nd, and 3rd sections of open-circuit voltage decay; d, disappeared; *, this work; **, taken as standard or reference behavior.

this idea. Monovalent cations should do the same, even to the discharged mass [as $Ni(OH)_2$]. Trivalent cations may introduce cation vacancies and so facilitate electronic conduction; or trivalents may be more heavily hydrated, because of smaller size, and facilitate protonic conduction. If electronic conduction through the mass can be made lower relative to protonic conduction, the mass can be anodically oxidized to a higher free energy state at the mass-electrolyte interface before oxygen evolution sets in. An attempt has been made to study these possibilities experimentally.

The rate of self-discharge during an idle period following charging may also be affected by foreign cations. The present work has been designed around the simple premise that the charge, or the oxidation capability of the charged mass, is composed of two parts: (*a*) the "normal capacity," associated with the transformation $Ni(OH)_2 \rightarrow NiOOH$;[1] and (*b*) the "over-capacity"—extra oxygen forced into the NiOOH during charging and trapped there. Thus the charged mass may be represented as

$$\beta\text{-NiOOH[O]}$$

where the extra O is in, as well as on, the crystallites. [See ref. (65) for discussion of $(\beta\text{-NiOOH})_2(O)_{ads.}$] Both the overcapacity and the normal capacity are lost during an idle period, the former faster than the latter. In the present work an attempt has been made to separate the two and then to assess the effects of monovalent and trivalent foreign ions on each decay.

Experimental Methods

The experimental cells consisted of the test electrode suspended between two counter electrodes in a lucite or nylon container. A reference electrode (Hg/HgO), with Luggin capillary tip which was proximal to the test electrode, was added. The stock electrolyte was 30% KOH in distilled water, and protected from rapid CO_2 absorption by a ½-in. layer of mineral oil. The electrolyte was replaced when necessary.

Experiments were of two kinds: (*a*) Charge-discharge cycles were done on a program (Table II) which has been shown [see ref. (3), for example] to reflect quantitatively and reliably the operational electrochemical properties of the electrode. The capacity (charge delivered), 5-sec and mid-point discharge voltages, the shape of the charging curve, and the top-of-charge voltage were recorded at several current densities. (*b*) Charge-retention studies were also carried out: potential decay and capacity loss as a function of time were carefully measured. The decay of open-circuit potential (test electrode to Hg/HgO reference electrode) was traced by one of three methods: (i) continuous recording on a potentiometer which was fed only a fraction of the potential of the cell via a high resistance (200,000 ohms) voltage divider; (ii) intermittent measurements of cell potential at appropriate intervals with a L&N slide-wire potentiometer; and (iii) continuous recording of potential by a Type 1230-A General Radio electrometer-amplifier (input impedance minimum 10^9 ohms) coupled with an Esterline Angus recording ammeter. The precision of the measurements was: for the recording potentiometer ±2 mv; L&N ±0.1 mv; 1230-A electrometer ±2 mv.

The cycling and charge-retention programs [(*a*) and (*b*) above] were carried out on duplicate cells to which Li^+, Ag^+, $Sb^{+3} \cdot As^{+3}$ or Al^{+3} had been added. No study of charge retention was done on carbonate-contaminated electrodes. Duplicate controls, containing no additive, were run simultaneously. All cells containing positive ion additives were thermostated at 55° ± 1°C during most of experiments, with cycling at 27°C done both before and after the high-temperature studies. The electrodes used in the positive ion studies were prepared from commercial (Clevite) sintered nickel plaques made from carbonyl nickel. Impregnation was carried out by the thermal method (21). The plates were then formed, and given 14 electrical cycles on the routine outlined in Table II. This procedure established the "normal" behavior of the electrode. After the characteristics had stabilized, the impurities were introduced into the electrolyte: the Ag^+ first as nitrate, later as oxide, the Li^+ as hydroxide, the As^{+3} as oxide, the Sb^{+3} as oxide and the Al^{+3} as oxide.

Table II. Cycling routine and program used to study output vs. current density

Cycling routine* Discharge at the following rates:		Test program for each added cation	
1.	3 hr	I	At 27°C, with no additive; then
2.	20 hr		
3.	3 hr	II	At 27°C, with additive; then
4.	1 hr	III	At 55°C, with additive, then charge-retention studies at 55°C; then
5.	6 min		
6.	3 hr		
7.	3 hr	IV	At 55°C, with additive; then
8.	3 min	V	At 27°C, with additive
9.	3 hr		
10.	2 min		
11.	3 hr		
12.	3 hr		
13.	20 hr		
14.	3 hr		

* All charging done at the 1-hr rate for 2 hr.

For the carbonate studies, electrodes from two commercial sources [prepared by the electrolytic method (66, 67)] as battery plates (by North American and European manufacturers) were used. After electrochemical cycling in 30% KOH (7.2*N* KOH) to constant "normal" capacity, the electrodes were cycled in electrolyte made up of mixtures of various proportions of 7.2*N* KOH and 7.2*N* K_2CO_3 so that the concentration of K^+ remained constant at 7.2*N*. These mixtures correspond roughly to the practical situation after 30% electrolyte has absorbed CO_2 from the air. Experimental data were collected at temperatures of 27°, −18°, −40°, and −54°C. Electrodes were charged at the 1-hr rate for 2 hr, put on open circuit stand for approximately a half-hour, and subsequently discharged at current densities of 3.9, 15.6, or 39 ma/cm² of electrode. Electrolyte compositions[2] of 0, 5, 10, 25, 50, 75 and 100 equivalent % carbonate were used (0% being only nominal, the actual $CO_3^=$ concentration being closer to a value of 1-1.5%). As a check on reproducibility, at least two electrodes of the same type were used for each experiment. The cycle was repeated from two to five times with each electrode and the results for each particular condition were averaged. In addition, some cadmium electrodes were examined to determine whether the capacity loss during aging is temporary or permanent. The early experiments (3, 4) have been carefully repeated by further experiments on plates from different sources. Selected results which establish the main features of the processes are reported in this paper.

After introduction of the impurity, cycling was continued (Table II) until new stable characteristics had been obtained. In the carbonate studies it was found advantageous to re-cycle in 30% KOH at room temperature before changing the electrolyte composition; but in the positive ion studies this was done only at the very end of the experiment. During the cycling of cells containing added positive ions the experiments were interrupted at convenient times so that measure-

[1] Note that although the composition NiOOH is manifested in three fairly well-defined physical structures (see X-ray diffraction patterns and cell constants, Fig. 1 and Table I of ref. (60), for example), there is still no unequivocal evidence that the nickel in the compound is trivalent. On the contrary, the x-ray K-edge absorption results of Hanson and Milligan (61) offer no evidence at all for valences other than two in the "higher oxides." Tsutsumi (62) later found similar results with higher oxides, but introduced an uncertainty which has not yet been clarified (63). Perhaps $Ni(OH)_2$ is simply a good container for O and OH, with certain compositions [4 $Ni(OH)_2 \cdot NiOOH$, $Ni_3O_2 \cdot Ni_3O_2(OH)_4$, NiOOH] more stable than others. However, it is believed that trivalent and tetravalent nickel can be stabilized in complexes with certain foreign elements such as phosphorus and arsenic (64).

[2] $100\left[\frac{\text{equiv. of } CO_3^=}{\text{equiv. of } CO_3^= + \text{equiv. of } OH^-}\right]$, called "equiv. % $CO_3^=$"

ments of both the decay of voltage and the loss of charge during open circuit stand could be taken. For charge-retention studies the charge was measured as the coulombic output during reduction at the 2-hr rate. The minimum stand time was 30 min, and the longest was six weeks.

Some x-ray diffraction spectra were taken in support of this work by the Physics Section of this Laboratory. In addition, standard qualitative chemical analytical techniques were employed for the identification of impurity ions found at the end of the experiment in both the electrolyte and the electrodes. Corroborative analytical work was done by the Analytical Section. Mines Branch, Ottawa. Basicity and carbonate were determined by double titration, with phenolphthalein and methyl purple indicators. The nickel in the electrodes which was soluble in hot NH_4Cl-NH_4OH was determined quantitatively by the dimethylglyoxime method (68).

Changes in nitrite concentration in the electrolyte were followed by the sensitive sulfanilic acid-alpha naphthylamine hydrochloride color development for NO_2^-, as described by Snell and Snell (69).

Results and Discussion

The Carbonate Choke

The aim of this series of experiments, which was to establish the effects of contamination by carbonate ion on nickel hydroxide and cadmium electrodes and to be able to predict carbonate effects on nickel-cadmium batteries, has not been fully achieved. The results on single electrodes were reproducible to within only about ±10%, even when a fixed parallel geometrical arrangement was used and when the most obvious variables, temperature, concentration and charge and discharge rate, were carefully controlled. The work has pointed up the importance of further variables, some of which cannot be controlled in experiments in which the active material is held within the pores of a sintered plaque. For instance, until more is known of the physical properties of anodically formed hydroxides and hydroxycarbonates of cadmium and nickel, the full explanation of the effects of carbonate contamination, and under what conditions these effects will occur, cannot be predicted. However, the results obtained in the present work permit certain general conclusions to be made and point out suitable directions for further study. The results are discussed in the following two sections.

On cadmium electrodes.—The general trends and measurements on a particular plate for a particular set of conditions were reproducible, but the detailed behavior varied from plate to plate, and also was found to be dependent on the age and electrical history of the plate. In this report the results are summarized in terms of a qualitative model which, in our opinion, includes the principal dependent variables. The general behavior is illustrated with examples selected from experimental results on plates. Essentially the model [summarized in ref. (28)] is as follows: Cd metal oxidizes anodically to a "CdO" underlayer, the primary product,[3] and in all but the very initial stages either metal ions or oxygen-containing species must penetrate the film of CdO if reaction is to continue. Therefore the thickness of CdO is important. It is removed at the CdO-electrolyte interface by a "conversion reaction," in which CdO is complexed into the adjacent electrolyte as $Cd(OH)_4^{-2}$ or $Cd(CO_3)_3^{-4}$ (7), at a rate depending on the composition of the electrolyte at the interface, and settles out on the surface of the CdO layer as $Cd(OH)_2$, $CdCO_3$, or as a hydroxycarbonate. The reaction can continue as long as ions can penetrate the CdO more easily than water can be oxidized to oxygen and the electrons so liberated penetrate the CdO in the opposite direction. Therefore the rate of the conversion reaction is of prime importance: if it is slow, the available capacity will be low. This rate increases with temperature and exposed area. The reaction can go by two routes, via the hydroxy-complex (at rate v_{OH^-}) and via the carbonate-complex ($v_{CO_3^=}$). These complexes are not very soluble and probably also precipitate on the CdO surface. Hence the complicated problem of physical interference by reaction product logically arises, and it cannot be avoided. This introduces the second variable.

The second variable thought to be important is the specific volume of final precipitate. In addition to the complexes $Cd(OH)_4^{-2}$ and $Cd(CO_3)_3^{-4}$, solid, basic cadmium carbonates, $xCdCO_3 \cdot Cd(OH)_2$, can also be formed. Huber stated (10) that these are formed as fibrous (gelatinous) precipitates at the reaction interface where Cd^{++} from the metal meets OH^-, $CO_3^=$, and H_2O from the electrolyte. Several years ago Gagnon *et al.* (11), using a controlled precipitation of weak $Cd(NO_3)_2$ and K_2CO_3 solutions, formed two such compounds, which were chemically distinguishable, corresponding to $x = 10$ and $x = 5$. We have repeated, confirmed, and extended this work and, chemically, have been able to distinguish a third compound corresponding to $x = 4$ (Fig. 1). By the time they were dried and mounted, all gave x-ray spectra basically of $CdCO_3$, but sometimes with additional weak lines due to $Cd(OH)_2$, splitting in two of the three strongest lines and with intensity differences at short spacings. All three are quite unstable, and change composition, to $Cd(OH)_2$ or $CdCO_3$, if washed for a long time or digested in the mother liquor depending on the *p*H. Details of this work will be published elsewhere.

The precipitates found after $Cd(NO_3)_2$ solutions are mixed with 7.2*N* ($KOH + K_2CO_3$) solutions in which the concentration is varied from 0 to 100 equivalent % K_2CO_3 show some striking physical difference (see Fig. 2). In the central, 20-70 equivalent % region, the precipitates are voluminous and gelatinous and when analyzed are found to be composed of $Cd(OH)_2$, K_2CO_3, and $CdCO_3$ with slight variations in x-ray spectra. Those in the end regions of concentration (<20%, >70%) are nearly pure hydroxide or carbonate and

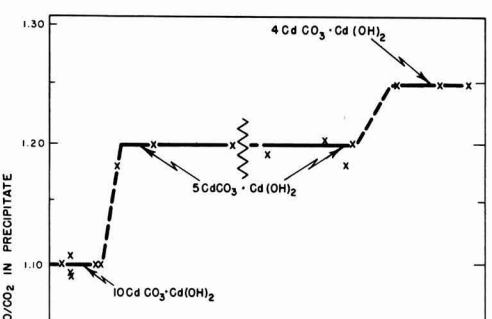

Fig. 1. Analytical results on precipitates and their mother liquors made by controlled mixing of $Cd(NO_3)_2$ with K_2CO_3 of different concentrations.

[3] There has been discussion on this point in the recent literature. We called it "CdO" for reasons discussed in ref. (6) on the basis of interference colors, existence of the conversion reaction, carbonate effects, exponential decay of overpotential, and consideration of likely primary processes. CdO was earlier (70) reported found by electron diffraction techniques, and was found again more recently (71), but others have tried to find it without success (8, 65). This divergence of experience can be rationalized as follows: The rate of the conversion reaction is high, and the underlayer very thin. Thus, during oxidation of cadmium planar electrodes at 0.33 ma cm^{-2} at 27°C in 7.2*N* KOH, the rate of conversion was found (5) to have a value equivalent to 0.26 ma cm^{-2} when the conversion layer was thin, and smaller values as the conversion layer built up. As conversion slows down the thickness of the underlayer increases. Its maximum thickness, at passivation, was estimated (28) to be a few hundred angstroms during current flow. It is rapidly converted to $Cd(OH)_2$ or $CdCO_3$ once the circuit is broken.

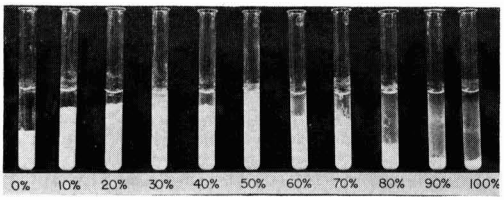

Fig. 2. Precipitates formed by mixing one part of 0.5N $Cd(NO_3)_2$ with one part of 7N K^+ in which the K^+ is present from 0 to 100 equiv. % carbonate in hydroxide.

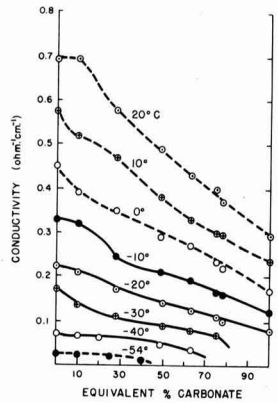

Fig. 3. Conductivity of mixed KOH-K_2CO_3 electrolytes at different temperatures. Total alkalinity: 7.2N K^+.

are flaky and/or granular. The specific volume of the final reaction product could be quite important in a porous electrode. For example, a small weight of precipitate could conceivably have a volume large enough to block the "neck" of a pore or displace the electrolyte and cut off all ionic contact between active material and the bulk of the electrolyte. This would make the active material within the pore unavailable for further electrochemical oxidation or reduction.

The third variable is the group of transport properties of the bulk electrolyte: conductance, diffusion, and fluidity. Electrical conductance, for example, falls off nearly linearly with increasing equivalent % carbonate, as is shown in Fig. 3, drawn from our earlier work (4). Presumably, as is usually the case, the corresponding specific rates of diffusion and fluid flow fall off similarly. At high rates and at low temperatures, soon after reduction starts, the ohmic voltage drop almost immediately reduces the cell voltage below the acceptable, useable, cut-off or end value. Decreased diffusion of KOH and K_2CO_3 in the solutions with higher equivalent % carbonate would also be expected to have the same effect, because the concentration gradients set up in the pores of the plate can disperse only slowly. Convective effects within pores and "extrusion" or forced flow of electrolyte into or out of pore due to changes in volume or physical structure of active material are not well understood but, such a transfer of fluid could dramatically affect the electrical output of heavily impregnated plates.

Figure 4a is a schematic illustration of speed of the processes on which the electrical output is thought to depend. A trend downward in the function plotted means there will be a trend downward in the coulombic output obtained. Since the processes are consecutive, the slowest one limits the output. Each of these curves represents a family of similar curves, there being a member for each set of experimental conditions. For example, the curves of Fig. 4b are the results of linear combinations of members of the four families introduced in Fig. 4a. Thus capacity *vs.* composition

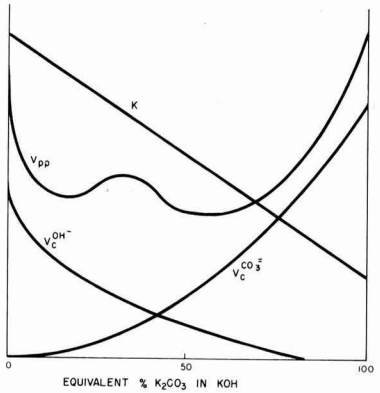

Fig. 4a. Schematic curves depicting how the rates of four critical processes probably vary with increasing carbonate in 7.2N K^+ electrolyte during anodic oxidation of cadmium.

$V_c^{OH^-}$ — rate of conversion reaction via $Cd(OH)_4^{-2}$

$V_c^{CO_3^=}$ — rate of conversion reaction via $Cd(CO_3)_3^{-4}$

K — specific conductance

V_{pp} — rate of penetration of reactants and products through precipitate (i.e. $V_{pp} \propto 1/$ volume)

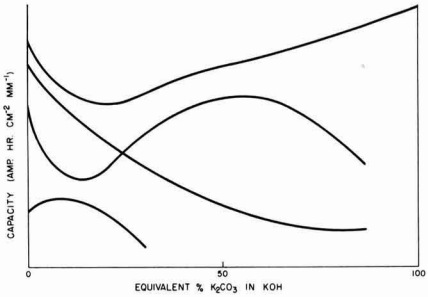

Fig. 4b. Effects of electrolyte composition on charge delivered by negative electrodes under various conditions (schematic).

(C/c) curves may take many shapes. Figures 5 to 7 are examples of results chosen from both the earlier report (4) and our more recent confirmatory work.

In addition to the transient effects on the three variables just considered, the results show that plates used in carbonated electrolyte can "age" or develop a permanent decrease in capacity. Although no cadmium has left the plate, some of it becomes passivated in the sense that it cannot be oxidized or reduced. This may be due to a permanent sealing of pores, to a redistribution of the active materials, or to the formation of a nonconducting (salt? oxide?) mass. The three sets of curves in Fig. 5 (25°C) were taken on plates which had a substantial history (at least 100 cycles) in batteries before these tests were done. Not only is the transient carbonate concentration effect very pronounced, but also in two cases, the capacity permanently "lost" was very large. Figure 6 (data at −18°C) illustrates this point even better: the output of a plate (No. 12) early in the tests is contrasted against the output of the same plate near the end of the tests, about 100 cycles later: the capacity *vs.* composition characteristic has changed markedly. Apparently the internal physical character of the plate has changed (*i.e.*, the plate has "aged") so that the capacity *vs.* composition curve has moved to the left and down, as if some solid carbonate had become permanently sealed into the plate, accounting for part of the loss (the permanent loss), while the carbonate in the electrolyte had caused

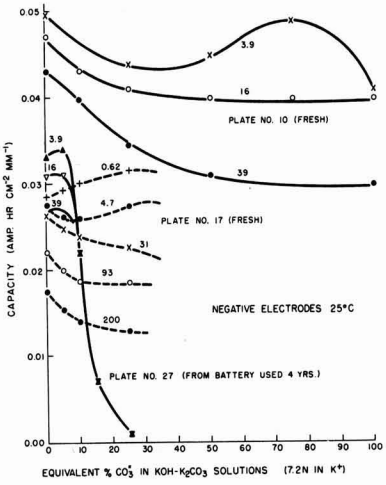

Fig. 5. Electrochemical capacity delivered, at c.d. shown (ma cm^{-2}), by good fair and poor cadmium negative plates at 25°C.

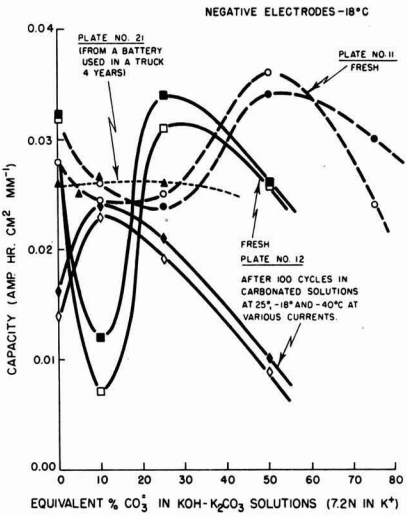

Fig. 6. Electrochemical capacity delivered, at c.d. of 160 ma cm^{-2}, by three different cadmium negative plates at —18°C, in KOH-K_2CO_3 mixtures. Solid symbols, charged at 25°C; open symbols, charged at —18°C.

the rest (the transient loss). The initial characteristics of another plate from the same group (No. 11) and with the same history, are also plotted in Fig. 6. Note the similarity of trend but difference in detailed behavior between supposedly duplicate specimens, plates 11 and 12.

Although somewhat tedious to obtain, these characteristic capacity *vs.* composition (*C/c*) curves clearly display the important, though subtle, differences between supposedly identical porous plates. They are much more sensitive than the Peukert curves (log *C vs.* log cd), which have been used to good advantage in assessing the early stages of development of the sintered plate technique [See ref (3) and (21), for example].

Figure 7 shows that differences in detail can be very pronounced at —40°: remarkably good output can be obtained from some plates, very much less from others. These differences are more pronounced the higher the discharge current density. The figure also illustrates the fact that better capacities can usually be obtained at low temperatures (—40°) if charging is also done at low temperatures. Generally at low temperatures the differences are less reproducible than at room temperature. Charge acceptance may be better at low temperature, but it seems to be more likely that the extra charge is due to hydrogen trapped in the pores and in grain boundaries of the nickel sinter, and as nickel hydride.

In summary, there now exists an accumulation of evidence that two kinds of detrimental effects due to carbonate occur on the negative plate: permanent effects related to the history of the plate and due to carbonate locked in the pores, and transient effects related to pore dimensions and the composition of the electrolyte. These effects have been observed on planar cadmium electrodes (5), and now, amplified greatly, on sintered negative plates. Three dependent variables seem to be important: the rate of the conversion reaction, the volume of reaction product (discharge), and the transport properties of the bulk electrolyte. These variables are dependent on electrolyte composition, temperature, and apparent current density, and probably also on pore size, pore size distribution, and interconnections of pores (*i.e.* electrolyte channels) within the plate.

On nickel hydroxide electrodes.—No appreciable effect of carbonate was found on the coulombic capacity of the nickel hydroxide electrode at 25°C. Transient effects, but no permanent effects, were found at low temperatures, during studies on 12 plates with upwards of 100 cycles per plate. Since the mechanism of discharge of the positive is still poorly understood, the presentation here is limited substantially to the effects of carbonate found experimentally.

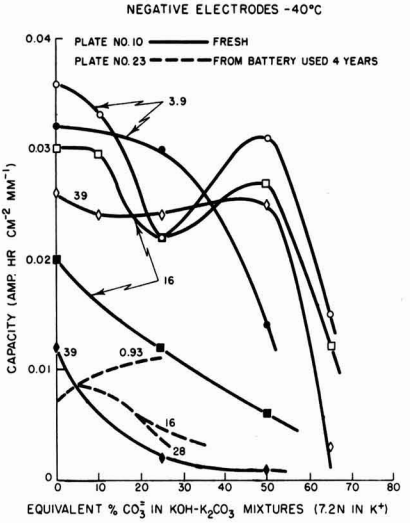

Fig. 7. Electrochemical capacity delivered, at c.d. shown (ma cm^{-2}), by two cadmium negative plates at —40° in KOH-K_2CO_3 mixtures. Solid symbols, charged at 25°C; open symbols, charged at —40°C.

At —18° and —40°C, the loss in capacity due to carbonate was found to be larger for plates which contained a greater amount of active material. In the more heavily loaded plates the capacity was a multivalued function of composition, a behavior similar to that of the negative. Figure 8 shows output at —18°C (following charge at —18°C) for two different plates, one twice as heavily loaded as the other. The general downward trend of the capacity as the electrolyte became more

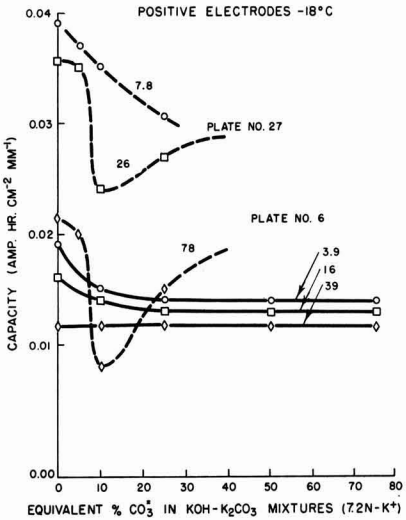

Fig. 8. Electrochemical capacity delivered at —18°C, at c.d. (ma cm^{-2}) shown, by two positive plates, which differ by a factor of two in the amount of nickel hydroxides per unit volume, in KOH-K_2CO_3 mixtures.

heavily carbonated is a behavior similar to that of the negative and is probably related to the decreasing rate of mass transport. The minimum at 10% may be the influence of the formation of bulky nickel hydroxycarbonates as intermediates in the process of electrochemical reduction, for it is evident that the effect was manifested only in the more heavily loaded plates. Unfortunately with nickel, as with cadmium, very little is known about the formation of its hydroxycarbonates as intermediates in the electrode process. Alternatively, possibly the carbonate acts by its ability to penetrate the layer lattice of the nickel hydroxide and distort it (15).

Figure 9 shows capacities delivered at —40°C. It is rather striking that the effect is actually fairly small until the carbonate content becomes so high that the electrolyte becomes glassy (at about 60 equiv. % carbonate), when the rate of transport of water, needed for the discharge reaction

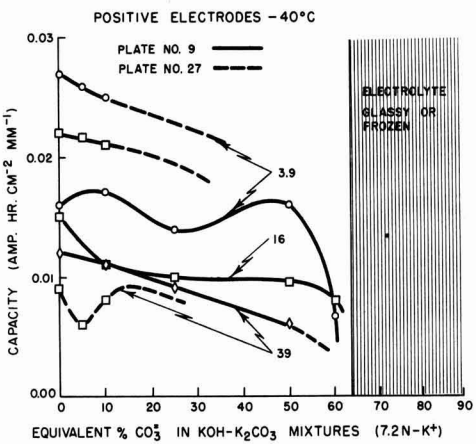

Fig. 9. Electrochemical capacity delivered at —40°C, at c.d. shown (ma cm^{-2}), by two nickel hydroxide plates in KOH-K_2CO_3 mixtures. All charging done at —40°C. (Charging at 25°C gave about the same outputs).

$$H_2O + e^- + NiOOH = Ni(OH)_2 + OH^-$$

falls practically to zero. Perhaps the readily available carbonate ions are literally frozen out of the layer lattice at —40°.

The Nitrate Shuttle

During preliminary work in this study, some positive ions were added to the electrolyte as nitrates. The most notable effect of the additions was the rather impressive loss of capacity during charged stand. Although the loss of charge was first attributed to the cation, a systematic elimination of possibilities by adding oxides instead of nitrates, and finally by adding KNO_3 itself, revealed that the anion was responsible for the effect. The results of experiments with the active materials added directly to the KOH electrolyte showed that Cd metal reduces nitrate rapidly to nitrite and that the oxidized positive plate material (nominally NiOOH) oxidizes nitrite to nitrate. Tests on a three-plate cell confirmed the suspicion that the $NO_3^- - NO_2^-$ couple can conduct a shuttle for electrons from the negative to the positive plate, and thus discharge the cell. Results are shown in Fig. 10. Since negative capacity was well in excess of positive in the test cells, the additive always ended up as nitrite, after the positive had become fully discharged. Subsequently it was shown that charged positive active material can stand alone in nitrate-containing KOH without accelerated self-discharge.

From these results the general mechanism of the nitrate shuttle is clear. Nitrate ion diffuses to the negative and is reduced to nitrite; the nitrite diffuses to the positive and is oxidized to nitrate. The result reported, for the cell containing 7 x 10^{-3} moles/1 KNO_3, in Fig. 10 was the approximate electrical equivalent at 55°C of a 100-ohm resistor connected directly across the terminals. The shuttle probably operates at a rate which is transport-controlled, since the reactions with the solids seemed to be relatively very fast at both the positive and negative electrodes. Since the transport rate (and hence the value of the equivalent resistance) is a function of cell geometry, concentration of nitrate, and temperature, as well as of the permeability constant of the separator, no detailed examination of transport for the experimental cells was worthwhile, and such work was not undertaken.

As a check on current industrial practice, sealed cells (4 AH) from the production line of two manufacturers were opened, and the contents refluxed in a Soxhlet extractor with distilled water for 3 hr. The leachant was then made neutral, and tested for nitrate. Tests for nitrate in both were positive. One had enough nitrate to make the electrolyte of the cell 0.005*N* in nitrate! The nitrate effect and its implications were reported briefly in an earlier paper (18). Reduction of NO_3^-

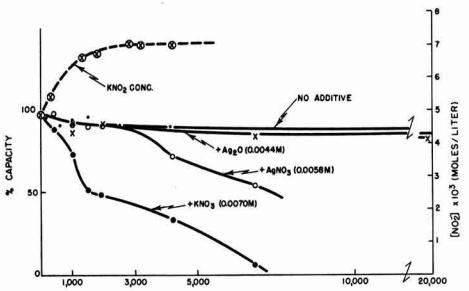

Fig. 10. Effect of nitrate ion on charge retention of positive plates in a 3-plate test cell; 7.2*N* KOH; 55°C; total nitrate added: 7x10^{-3}M. % capacity = 100 $C_t/C_{30\ min}$, where C_t is capacity after charged stand of t min, and $C_{30\ min}$ is capacity after charged stand of 30 min.

ultimately to NH_3 and N_2 in sealed cells at high temperatures during prolonged charged stands has been recently reported (72).

A search was made for other possible shuttles, but none was found. The requirements are actually quite stringent: good solubility of both the oxidized and reduced form; rapid oxidation of the reduced form by the charged positive; rapid reduction of the oxidized form by the charged negative; (redox potential E between $Cd/Cd(OH)_2$ and $NiOOH/Ni(OH)_2$ in 7N KOH). This search consisted of examination of the redox tables, and then experimentation with likely candidates (*e.g.*, I^-/IO_3^-, Tl^{+1}/Tl^{+3}, quinhydrone, etc.). All these couples lack at least one of the pertinent qualifications. The nitrate shuttle seems to be unique in the alkaline Ni-Cd system. [The iron (Fe^{+2}/Fe^{+3}) shuttle is well known in the $Pb/H_2SO_4/PbO_2$ system.]

There was some indication in this work that the nitrate-nitrite system depressed the voltage of the test cells during overcharge, but more work is required to establish this point.

Foreign Cations in the Nickel Hydroxide Electrode

General observations.—The effect of positive ion additions on (*a*) electrochemical capacity and (*b*) charge-retention and voltage-decay during charged stand were measured and analyzed. The experiments were intended to test the lamellar hydroxide-proton transfer model of nickel hydroxide electrodes.

Duplicate test cells were made up with added Li^+, Ag^+, Al^{+3}, and As^{+3}. These positive ions were added to the electrolyte of the test cells as $Al(OH)_3$, Sb_2O_3, As_2O_3, LiOH, and silver ion as Ag_2O. They were put through a cycling program and a charged-stand program at 55°C, at which temperature the aging effects should be accelerated. Although the information was gained under conditions (full impregnation, high temperature) in which the plate is often found in practice, it may be that introduction of the rapid aging effects has precluded the possibility of isolation of any but the gross effects of the ions added, *i.e.*, all the subtle effects may have been masked by the changes in crystalline form which occur during aging (8, 29, 30). Hence our discussion is limited to those effects which were observed under the specific conditions of this study.

The end-of-charge voltage did not vary appreciably from cycle to cycle. All charging (oxidation) was done for 2 hr at the 1-hr rate based on the theoretical capacity. The shapes of the charging curves varied (slightly), both from cycle to cycle and with different additives, but in no systematic fashion, and are not discussed here. [Lightly impregnated plates show some systematic variations (25).] High end-of-charge voltages with correspondingly high "overcapacities" were obtained with the Li^+-containing cells. This fact will be discussed later.

Other than one isolated inhibition caused by aluminum, no inhibition of the electrochemical oxidation or reduction which could be ascribed to the mono- or trivalent foreign ions was observed on the positive. A fast, sensitive amplifier-oscillograph apparatus was used for several high-rate (5-min) discharges at normal temperatures and at low temperatures (down to −30°C), but no large effects on overpotential were observed which could be ascribed unambiguously to foreign cations. This result may be a significant blow to the proton transfer theory of charge transfer within the active mass, because trivalent cations were expected to trap out anion vacancies into which protons could jump. However, there may be other explanations.

The cations are not as easily lost cathodically from the electrolyte as one might imagine. No silver was found plated out on cadmium; nor was any of the alloy AgCd detected by x-ray diffraction. Aluminum and lithium cannot be plated out in KOH_{aq}. Although AsH_3 and SbH_3 are evolved rapidly, along with H_2, from a cathode in acid solution, the processes are somewhat different in basic solution. Thus, the silver nitrate-paper test for arsine revealed that when arsenic is added as As_2O_3 to KOH solution it does escape at the cathode as AsH_3, whereas if added as As_2O_5 it does not escape. The As_2O_3 added to a cell behaves as if it were quickly converted to As_2O_5 at the positive and then stayed there. No stibine could be detected either, but the case of antimony is not certain because analysis is difficult.

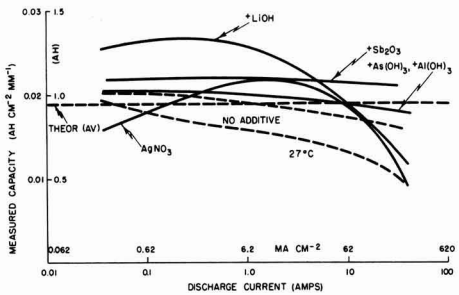

Fig. 11. Charge delivered at 27°C as a function of discharge current density for nickel hydroxide electrodes whose charge retention had been studied for nearly 2 years at 55°C.

Charge delivered during reduction.—A progressive increase in the measured capacity with prolonged use was observed for all positive plates. The greatest increase was obtained with those containing foreign cations. This was reflected at all discharge rates, from the 20-hr to the 2-min rate. Better use is made of the active material within the plate when cycled at 55° than at 27°C. Once the "active mass" has become fully active at 55°C, however, the output at 27° approaches that at 55°C, behavior that perhaps could have been predicted from earlier work (73) on the role of water and alkali in the active mass. Figure 11 shows the charge delivered at 27°C by seven plates following protracted studies of charge retention at 55°C, conducted over a two-year period.

The source of increased capacity with life was determined by chemical analysis of the plates. The question posed was: Is the same amount of nickel hydroxide oxidized to a higher average level of oxidation (*i.e.*, to contain more oxygen), or is some of the sintered metal plaque oxidized slowly to give an extra amount of chargeable hydroxides? At the end of the tests the plates were washed in distilled water until neutral; the hydroxides were leached out in warm $NH_4OH = NH_4Cl$, and the leachant analyzed for soluble nickel using the dimethylglyoxime method (68, 69). A substantial increase in soluble nickel occurred during the tests [Table III: row (4) minus row (1)]. The fact that some of the original sinter was converted into active material was confirmed by the loss in weight of the sintered plaques, *i.e.*, 10-15% of their original weight per unit volume. The oxidation probably occurred during the prolonged (weeks) charge-retention tests at 55°C, not during the relatively insignificant charging time (2 hr). The rate of this corrosion reaction is doubtless a function of purity of the nickel powder from which the sinters were made.

The definite effects which could be ascribed unambiguously to the presence of the foreign cations were: (*a*) In all cells containing foreign cations, the sintered nickel matrix oxidized more during the tests than did the control electrodes with no foreign cations. (*b*) One positive in a cell containing $Al(OH)_3$ at one stage (cycle 55) was fully charged, yet could not be electrolytically reduced (discharged). This "passivation" was finally broken by an anodic pulse of high current density. Perhaps it was the physical breakdown of a skin of gamma alumina (an electronic conductor at high field strengths) formed on the exposed active sites of the active mass. This condition was observed only once.

Table III. Theoretical and measured electrochemical capacity of nickel hydroxide electrodes

Condition	100 × capacities, amp-hr cm^{-2} mm^{-1}				
	Normal	+ LiOH	+ $As(OH)_3$	Sb_2O_3	+ $Al(OH_3)$
1. Theoretical, based on weight gain (before tests)	1.80	1.85	1.80	2.05	1.97
2. Last measured (3-hr rate) 27°C	1.6	1.8	1.5	1.4	1.6
3. Last measured (3-hr rate) 55°C	2.3	2.8	2.4	2.1	2.2
4. Theoretical, based on soluble nickel (after tests)	3.0	3.6	2.6	3.0	2.8

Notes on each condition: 1, All weight gained during impregnation was assumed to be due to $Ni(OH)_2$; 2, cycle 56; 3, cycle 80; 4, Leached in a mixture of 1*N* NH_4OH + 1*N* NH_4Cl at 60°C for at least 24 hr.

Although values given for theoretical capacities are averages of 4 determinations, the errors are such that the numbers are reliable to only ±5%. In addition, numbers in row 1 might be systematically low because of excess drying; numbers in row 4 might be systematically low because of incomplete leaching. Reproducibility of measurements of electrochemical capacity during test program (Table II), as determined from the 3-hr rate discharge was ±4%.

(c) Positives in Li^+-containing cells consistently showed high "overcapacities," to be discussed next.

Charge retention.—Figures 12 and 13 show the charge (normalized: $C_r \equiv C/C_{Theor}$) delivered at the 2-hr rate by 12 plates after they had been stored for various lengths of time in the electrolyte at 55°C. This converging decay is linear in log time (t) for upwards of 2 months at 55°C, and can be expressed as

$$C_r \propto \log (t + \theta)$$

where θ is very small, of the order of minutes. [The same relationship was found by others, for example Conway and Bourgault (74), who measured the oxygen evolved from the charged active material at 25°C]. Beyond about 40 days the relationship breaks down. Thus a linear plot C_r *vs.* t, from 10^3 to 10^5 min, discloses that the decay rate, $-\partial C_r/\partial t$, at long times is more or less constant [similar observations have been reported before (75)]. If C_r^o is defined as C_r at the first marked deviation from the linearity of the C_r *vs.* log $(t + \theta)$ curve, and if it is assumed that to a first approximation all C_r above this value is excess capacity over that due to $NiOOH/Ni(OH)_2$, that is, "overcapacity," one can analyze the decay of this overcapacity, $Q(\equiv C_r - C_r^o)$, by standard kinetic techniques. Figure 14 shows a linear plot of Q *vs.* stand-time. Tangential slopes $(-dQ/dt)$ express the rate of decay, v, at various values of the excess capacity. If the order of the reaction with respect to concentration of overcapacity is n, then

$$v \propto Q^n$$

from which

$$\partial \log v/\partial \log Q = n$$

From plots of log v *vs.* log Q for all the results, n was found to be about 5 (consider the insensitivity of the log-log plot). Integration and introduction of the boundary condition that Q must have some well-defined value, Q_o, at the end of charge (*i.e.*, at a stand-time of zero) gives

$$Q = Q_o(1 + 4k\,Q_o^4\,t)^{-0.25}$$

where k is the specific rate constant for the decay. In Fig. 15 the charge retained after different times of charged stand is plotted up for four electrodes in a manner which displays the inverse quarter-power dependence upon time.

In the system under study here, an order of reaction of about five can be interpreted in at least two ways, neither of which directly results from the chemistry of the system:

1. An unknown concentration-dependent force may be operative when excess higher oxide material begins to accumulate. This could be a physical repulsion of oxygen (as O_2?; as OH?; as O?) trapped under high internal pressure (dU/dV) in distorted (stretched ?) crystallites; or possibly an electrostatic repulsion of trapped OH^- ions, since high orders of reaction are observed when strong repulsive forces can become operative.

2. An erosion reaction, very rapid at first, but slowing down quickly, may be operative, perhaps a recrystallization, or a "digestion," as suggested by

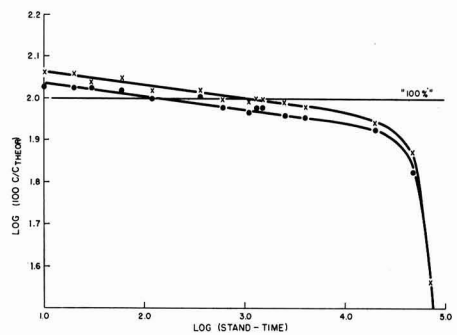

Fig. 12. Charge retention of thermally impregnated nickel hydroxide electrodes at 55°C, with no foreign ions added to the electrolyte, stand-time in minutes.

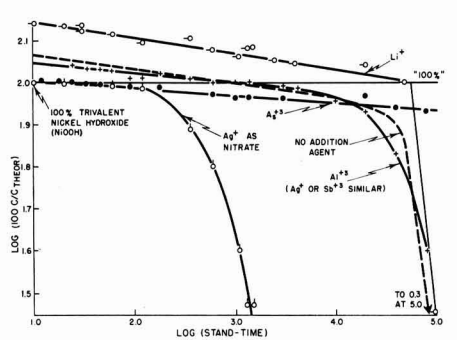

Fig. 13. Charge retention at 55°C, of thermally impregnated nickel hydroxide electrodes with foreign cations added to the electrolyte, stand-time in minutes.

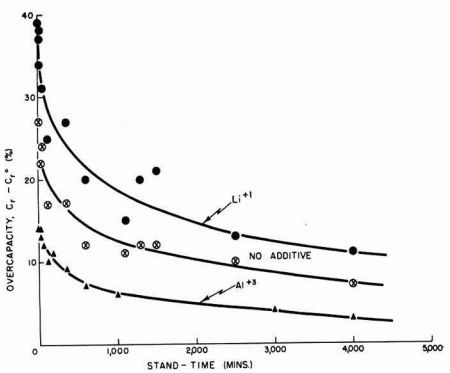

Fig. 14. Decay of overcapacity (C_r—C_r^o) of fully impregnated sintered plate nickel hydroxide electrodes at 55°C.

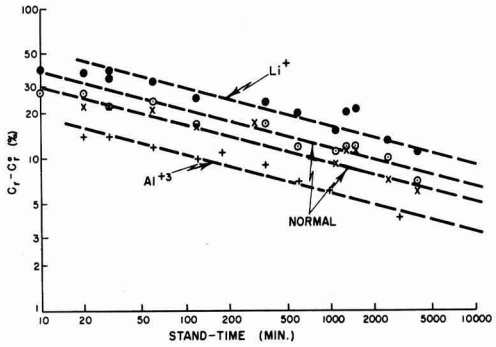

Fig. 15. Decays plotted as log ($C_r - C_r^\circ$) *vs.* log (stand-time), with broken lines drawn in at slopes consistent with 5th order decay.

Seiger *et al.* (76). In this case the rate of decay of the overcapacity would simply follow the rate of the physical erosion of the mass, because it would be the erosion reaction which presents the overcapacity to the electrolyte.

On the assumptions that crystallites of charged active material have some particular (normal ?) size distribution, that little ones lose their extra oxygen faster (higher area/volume), and that Li^+ acts either by making the crystallites uniformly large or by helping to trap the extra oxygen in the crystallites, a study of the kinetics of loss of charge from very thin films, of the order of a few molecular layers in average thickness, has been started. Results on nickel wire, and then on nickel foil (Fig. 16) have shown, first, that the loss of charge is very much more rapid from open surfaces than from porous ones, and, second, that early in the decay from open surfaces the order of reaction with respect to overcapacity is only 2 not 5. We infer that the loss of charge from porous electrodes immediately after anodic oxidation is not controlled by an erosion reaction, but rather by the movement of trapped oxygen-containing species from the inside of the crystallites to the surface. The effect of the foreign cations, then, and of lithium in particular, can be ascribed to their modifying the elastic restoring forces, within the crystallites. This view is consistent with known modifications of lattice dimensions observed by Briggs (30) in 1957 in doped crystallites of nickel hydroxides.

Overpotential decay.—During studies of charge-retention of impregnated, sintered plate nickel hydroxide electrodes, the cell was allowed to stand on open circuit, and the open-circuit potential was traced as a function of time. The values so obtained were plotted in the manner introduced by Armstrong and

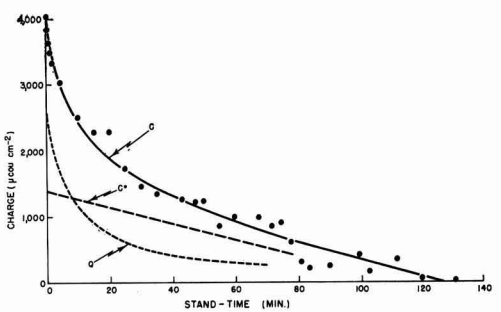

Fig. 16. Charge, *C*, delivered at 12 $\mu a/cm^2$ by oxidized nickel foil electrodes after various lengths of charged stand; $T = 30°C$; *Q*, overcapacity; *C°*, normal capacity.

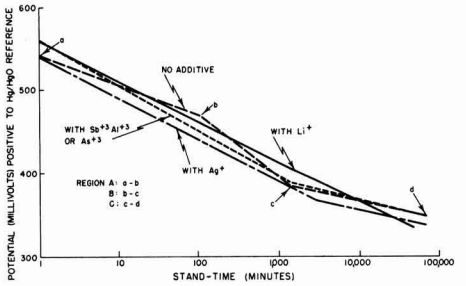

Fig. 17. Open-circuit decay of overpotential of nickel hydroxide electrodes, with and without foreign cations added.

Butler (77), *i.e.*, as *E vs.* log $(t + \theta)$. The slope, related [see ref (78), *e.g.*] to Tafel's "*b*" $(\partial E/\partial \log i)$ could be evaluated. Figure 17 shows a typical plot. Three distinct regions A, B, and C are evident from inspection of the potential decay curves. Two of these regions, A and C, have been discussed rather fully by Conway and Bourgault (74); B is a transition region between A and C which has been examined by Seiger *et al.* (76). Average values of $\partial E/\partial \log t$ for the three regions are given in Table IV.

The three regions were not always observed in an electrode. For instance, plates containing Li^+ did not make the transition from A to B, and the C region was never observed. By contrast, plates with no additive spent most of their stand life in the C region. More or less complete loss of capacity did not further affect the open-circuit potential of the cells which had no additives: they remained in the C region.

As Conway and Bourgault, and earlier, Bockris, pointed out, if certain assumptions are made, the slopes, or *b*-values, may be interpreted in terms of specific rate determining steps in the self-discharge process. For instance, one can compare the value of 26 ± 2 mv for region C with the value of 25 (*i.e.*, 2.3 $2RT/5F$ at 55°C), which by Bockris' analysis is consistent with a rate-determining step in which HO_2 is being formed on the surface as follows

$$O_{ads} + OH^- \rightleftharpoons HO_2 + e^- \qquad [1]$$

However, the reaction

$$O_{ads} + OH_{ads} \rightleftharpoons HO_{2\,ads} \qquad [1a]$$

should give (78) a slope 2.3 $RT/3F$, or 22; which, although it is slightly less than our assignment of precision would allow (Table IV), would agree explicitly with the reaction assigned by Conway and Bourgault (74) to their values.[4]

Table IV. "b"-Values for different regions of self-discharge of nickel hydroxide electrode

Decay	Region	$b = -\partial E/\partial \log t$ (mv/decade of time) No additive	Monovalent additive	Trivalent additive
Overcapacity	A	45 ± 8 (42 ± 0.2)*	50 ± 12	50 ± 12
	B	70 ± 5	None	None
	C	26 ± 2 (22 ± 0.3)*	None	22 ± 3
Normal capacity		Same as C	Same as C	Same as C

* Values given in parentheses are from reference (74) Table I, recalculated for 55°C. In our work individual decay plots did not give *b*-values (slopes) with high precision. However, repeated runs with the same electrode did not reproduce the value so exactly, and the accuracy reflects the variation observed.

[4] An undetected constant error is not impossible here although calibrations were done periodically to reduce the probability. The presence of Cd negatives may have made our decay slopes high. Further, the theoretical deductions of the numerical value of "b" invariably, and apparently quite arbitrarily for oxide electrodes, assume a "symmetry factor" of 0.5, which has not yet been unequivocally proven. With these reservations in mind, such an explicit statement of the reacting species gives the clue that it is O (and OH ?) which accounts for the overcapacity described earlier; and that self-destruction of NiOOH is slow.

Within the reproducibility in measurements, more than one deduced slope (said to be a characteristic of a certain step of the decay) can sometimes be made to fit the facts. The slope $-\partial E/\partial \log t$ of the reaction

$$OH_{ads} + OH^- \rightleftharpoons O_{ads} + H_2O + e^- \quad [2]$$

is said (78, 79) to be 2.3 $2RT/5F$, or 42 mv/decade of time at 55°C. This value falls within the range of values observed in the A region, and could be taken as an indication that this is the rate-controlling step early in the decay. Although such a reaction may exist under conditions of high overvoltage, the result on plates with Li^+ added show that this region of decay can continue to either the B or the C regions, and well below the overvoltage at which transition usually occurs. In this interpretation, Li^+ either promotes reaction [1] or inhibits reaction [2].

The B region has been given no assignment to date. It is short (a few hours) in solutions with no additives; it is absent altogether in weak caustic, and in solutions with additives (Fig. 17, Table III).

Milner's treatment [see ref (80)], and more recently Hale's (81), would involve diffusion processes, not necessarily activation processes alone, to explain the facts. Especially interesting is the fact that antimony and to a greater extent arsenic inhibit the loss of overcapacity. Perhaps arsenate is adsorbed on and poisons sites which would otherwise be involved in oxygen evolution.

Present status of the problem.—Many reported effects of cations on the measurable properties of the nickel hydroxide electrode are poorly founded in fact. Table I contains a summary of the claims and inferences drawn by various workers who have studied the question. Controlled experiments have been done in only a few cases, and the reported effects of others have to be considered more as lore than as scientific fact. This is understandable if the premise is accepted that the effect of a cation on the parameter being investigated is closely related to the physical condition of the nickel hydroxide (*viz.*, crystallite size distribution, defect structure, water content of the layer lattice, etc.) during the measurement. Reproducibility is bound to be poor. Of the reports on effects of 24 ions, reports on 7 draw particular attention: Li^+, Mg^{+2}, Zn^{+2}, Hg^{+2}, Co^{+3}, Sc^{+3}, and As^{+5}. The suppression of charge available from the electrode in the presence of Zn^{+2} and the increased charge available in the presence of both Hg^{+2} and Mg^{+2} ions require confirmation, for if the effects of divalent cations on coulombic capacity are as claimed (Table I), at least two interesting possibilities exist to account for the effects: (i) polarization of water of hydration might exist due to the strong electric field about the small Mg^{+2} ion (Doran's suggestion), and (ii) the layer-lattice crystallites might retain less water of hydration at the important defects occupied by large ions such as Hg^{+2} and Ba^{+2}.

Information on the transition metal cations is sparse and conflicting, with the exception of that on cobalt. Cobalt must exist as Co^{+3} even in the discharged nickel hydroxide material. There seems to be some agreement that Co^{+3} improves charge retention, stabilizes capacity during repetitive cycling, raises the charge and discharge voltages and increases the b-values, all indications that it promotes higher overcapacities. In this respect its effects resemble those of the Li^+ ion. The scandium ion seems to belong to this group also. However, its trivalent cousins (Fe^{+3}, Al^{+3}, B^{+3}), which have a strong tendency to form insulating oxides, clearly do not.

Arsenic and antimony, which must be present as pentavalent ions at the potential of the nickel hydroxide electrode, suppress the B region of potential decay and promote better charge retention; perhaps they adsorb, as AsO_4^{-3} or SbO_4^{-3}, on the oxygen evolution sites and inhibit the process. The fact that the arsenic ion can stabilize higher valence states of nickel (82), and increases the overpotential during charge and overcharge is supporting evidence.

Nickel hydroxide remains an enigma. As a semiconductor NiO will change conductivity by many orders of magnitude if it is doped with Li^+. The proton-transfer theory of ionic conduction seems well entrenched in the literature. Indeed the recent experiments on proton-penetrable Ni foil electrodes even permit the evaluation of the proton-transfer current during anodic oxygen evolution (83). (This current is highest in KOH, less in NaOH, and lowest in LiOH.) The present work emphasizes a possible movement of oxygen-containing species in the active mass, akin to mass transfer processes suggested for MnO_2, V_2O_5, and PbO_2 (84). Crystal deformation of the layer lattice can be effected by several cations (30), by carbonate (15) and probably by other anions such as nitrate. At the present time we may usefully consider nickel hydroxide to be a remarkable matrix through which electrons (or positive holes) and protons and oxygen-containing species can be forced, at relative rates which depend intimately on a time-dependent molecular structure, as well as on the nature of the applied force, or potential gradient. In this sense, nickel hydroxide may indeed be the most versatile, and *ipso facto* the most exasperating, member of the electrochemically active (hydr)oxide family.

General Summary

1. Electrodes were studied in which the electrochemically active material was supported within the pores of sintered nickel plaques. Detrimental effects of carbonate ion have been demonstrated on both the nickel hydroxide positive and cadmium negative electrodes.

2. On negative electrodes both permanent and transient effects occur, both of which lower the coulombic or ampere-hour output. The transient effects are a complicated function of the amount of carbonate in the electrolytes, and are dependent also on current density and temperature. Processes which seem to be involved are rate of conversion of primary reaction product into hydroxide or carbonate, specific volume of precipitate, and transport properties of electrolyte through the porous mass. Aging effects were demonstrated via the capacity *vs.* composition data.

3. On positive plates only transient carbonate effects were observed, quite complicated if the plate is heavily loaded.

4. Interpretations of these effects have been offered. Quantitative prediction of when they will occur is not yet possible. The possible roles of the hydroxycarbonates of cadmium and nickel as reaction intermediates are discussed.

5. The mechanism of the "nitrate shuttle" has been demonstrated. The nitrate-nitrite redox system within the cell seems to be unique in that it can be oxidized and reduced by the positive and negative, respectively. Since both species are soluble, it acts as an electronic short-circuit. A search for other systems which would do this was unsuccessful.

6. Prolonged (1-2 years) operation of pure nickel hydroxide electrodes at high temperature (55°C) resulted in a marked increase in the electrochemical capacity of the electrode. Analyses for soluble nickel showed that most of the increase could be attributed to oxidation of the sintered nickel matrix. However, there is evidence that the electrode gradually becomes able to be charged to a higher average oxidation state, especially in the presence of Li^+.

7. Practical conclusions from parts 1 to 6 include: (*A*) Nitrate from the processing of plates must be removed from cells, otherwise self-discharge may be rapid. (*B*) Special precautions must be taken to keep CO_2 from the air and carbonate from other sources (oxidation of separator ?) from processed plates and from assembled cells, otherwise the capacity may not be reproducible and the plates may show aging effects

and unpredictable outputs, especially at low temperatures. (C) Only extra high purity nickel powder should be used for the sintered matrix for nickel hydroxide electrodes, if corrosion of the matrix at high temperatures is to be avoided.

8. Loss of charge by charged nickel hydroxide seems to occur by two main processes: a rapid but convergent decay of the overcapacity, and a slower, linear decay of the normal capacity. The former may take days in a sintered plate, minutes on a nickel foil. The latter takes weeks in the sintered plate, hours on a foil.

9. Decay of the overcapacity consists of two, and perhaps three, consecutive steps, separable by analysis of the concurrent potential decay, and rather markedly affected by foreign cations. Possible controlling reactions are discussed. Kinetic analysis of the decay of charge, and analysis of the concurrent overpotential decay, suggest that the controlling reactions involve adsorbed oxygen atoms which are continuously supplied from within the crystallites.

10. Reported effects of foreign cations on the behavior of the nickel hydroxide electrode were collected and reviewed. The roles of certain uni- and trivalent positive ions on the nickel hydroxide electrode were investigated at length. None had any reproducible measurable effect on the ability of well-formed, charged nickel hydroxide to deliver its charge, even up to very high (20-min) rates, from 25° to −30°C. All promoted the oxidation of the sintered nickel matrix to active material at 55°C.

11. At 55°C Li^+ increased the overcapacity, and it also lowered the rate of loss of overcapacity. It blocked the onset of the second and third (B and C) stages in the potential decay which runs concurrent with the decay of overcapacity.

In an isolated, but interesting, instance, Al^{+3} blocked the reduction of a fully oxidized electrode, an effect that was finally broken by a strong anodic pulse of current. Arsenic, probably as As^{+5}, adsorbed on cathodic sites, affected the potential decays during loss of overcapacity, and then seemed to inhibit the protracted decay of the normal capacity which followed.

12. Inferences are drawn about the mechanisms of the various processes studied, and the present status of each is given.

Acknowledgments

Mr. D. G. Scraba, a summer student from the University of Alberta, did the nitrite analyses, and along with Mr. J. L. Lackner contributed technical assistance. Dr. J. R. Coleman, and Drs. I. H. S. Henderson and T. E. King who read the manuscript, offered many very helpful suggestions.

A special word of thanks is offered to the many friends in other laboratories who have encouraged the preparation of this paper.

Manuscript received Dec. 11, 1961; revised manuscript received Dec. 15, 1964. The manuscript is issued as DCBRL Report No. ———.

Any discussion of this paper will appear in a Discussion Section to be published in the December 1965 JOURNAL.

SYMBOLS

equivalent % of carbonate:

$$\frac{\text{Equiv. of } CO_3^=}{\text{Equiv. of } OH^- + \text{Equiv. of } CO_3^=} \times 100$$

x = No. of moles of $CdCO_3$ contained in solid basic cadmium carbonate of general formula $x\ CdCO_3\ Cd(OH)_2$.

C = measured electrochemical capacity, or charge, in ampere-hours per unit volume (cm^2 area x mm thickness of electrode)

C_{Theor} = theoretical capacity based on weight gain during impregnation of sintered plaque, it being assumed that all weight gain is due to $Cd(OH)_2$ (negative) or $Ni(OH)_2$ (positive)

C_r = reduced, or normalized, capacity = $100\ C/C_{Theor}$ (%)

c.d. = current density

C_r° = value of C_r at which the linear C_r *vs.* log $(t + \theta)$ relationship breaks down, denoting last of the overcapacity

$Q = C_r - C_r^\circ$ = overcapacity (normalized)

Q_o = overcapacity immediately at the end of charging

v = $-d(C_r - C_r^\circ)dt$, rate of decay of overcapacity

n = order of reaction (decay of overcapacity) with respect to overcapacity

k = specific rate constant for decay of charge

U = internal energy; V, specific volume; $\partial U/\partial V$, internal pressure

E = potential (mv) positive to Hg/HgO reference

b = $-\partial E/\partial \log t$ during open-circuit stand

REFERENCES

1. A. P. Hauel, *Trans. Electrochem. Soc.*, **76**, 435 (1939); U. B. Thomas, Private communication, 1953; E. J. Casey, *Proc. 4th DRB Symposium*, p. 51-61, 1952.
2. E. J. Casey and B. Ogden, "Some Factors Affecting the Low Temperature Operation of Sintered Plate Nickel Cadmium Batteries," DRCL Report No. 117, October, 1952.
3. P. E. George and E. J. Casey, "The Electrical Output of Sintered Plates of Nickel Cadmium Batteries. I," DRCL Report No. 156, March, 1954.
4. P. E. Lake and E. J. Casey, "Sintered Plates of Nickel Cadmium Batteries. II. Extent of Effects of Carbonate Contamination on Electrical Output," DRCL Report No. 186, April, 1955.
5. P. E. Lake and E. J. Casey, *This Journal*, **105**, 52 (1958); **106**, 913 (1959).
6. P. E. Lake and E. J. Casey, *ibid.*, **106**, 532 (1960).
7. P. E. Lake and J. M. Goodings, *Can. J. Chem.*, **36**, 1089 (1958).
8. D. Tuomi, Private communication, 1963.
9. G. T. Croft and D. Tuomi, *This Journal*, **108**, 915 (1961).
10. K. Huber, *Z. Elektrochem.*, **62**, 675 (1958).
11. L. Cloutier, P. E. Pelletier, and P. E. Gagnon, *Trans. Roy. Soc. Can.*, **33**, III, 149 (1936).
12. K. C. Grover and L. M. R. Noyar, *Agra Univ. J. Res.*, **6**, Part 2, 67 (1957).
13. P. E. Gagnon, L. Cloutier, and R. Martineau, *Can. J. Res. B.*, **19**, 179 (1941).
14. J. T. Carriel and W. J. Singley, *J. Am. Chem. Soc.*, **76**, 3839 (1954); O. Bagno, *Compt. rend.*, **236**, 1275 (1953); J. Francois-Rossetti and B. Imélik, *J. Chim. Phys.*, **51**, 451 (1954); and *Bull. soc. chim. France*, p. 1115 (1957).
15. J. Longuet-Escard and J. Méring, *Compt. rend.*, **246**, 1231 (1958).
16. I. M. Vasserman and E. A. Fomina, *Zhur. Priklad. Khim.*, **34**, 90 (1961).
17. W. Feitknecht, *Kolloid Z.*, **136**, 52 (1954). See also *Kolloid Z.*, **93**, 66 (1940).
18. T. E. King, E. J. Casey, and I. H. S. Henderson, *Proc. 16th Annual Power Sources Conf.*, USASERDL, May, 1962.
19. R. Hérold, Private communications, 1960-1962.
20. A. Fleischer, "Vented Ni-Cd Batteries," *Proc. 11th Ann. Battery Research and Development Conference*, p. 83, U.S. Army Signal Engineering Lab., 1957.
21. P. L. Bourgault, P. E. Lake, E. J. Casey, and A. R. Dubois, *Can. J. Tech.*, **34**, 495 (1957); U.S. Pat. No. 2,831,044, Dec. 13, 1956; E. J. Casey, *Proc. 10th Annual Battery Conference*, USASCEL, Fort Monmouth, N. J., May, 1956.
22. H.Winkler, *Elektrotechnik*, **8**, 300 (1955).
23. J. P. Harivel and J. F. Laurent, *Electrochim. Acta*, **9**, 703 (1964).
24. R. J. Doran, "Impurity Effects in Metal Hydroxide Electrodes", Paper Y, *Proc. 1st Internat. Symposium on Batteries*, Signal Research and Development Laboratories, Christchurch, England, October, 1958.
25. R. J. Doran, "Further Studies of Aging and Impurity Effects in the Nickel Hydroxide Electrode", Paper 26, *Proc. 2nd Internat. Symp. on Batteries*, Signal Research and Development Establishment, Christchurch, England, October 1960; Brit. Pat. No. 848,922 (1960).
26. R. J. Doran, Private communication, 1962.
27. R. J. Doran, "The Nickel-Scandium Hydroxide Electrode", *Proc. 3rd Internat. Symp. on Bat-*

teries, Admiralty Engineering Labs., West Drayton, England, 1962; Brit. Pat. Appl. No. 34429/60.
28. E. J. Casey, *Chem. in Canada,* **12,** 49 (1960).
29. T. A. Edison, U.S. Pat. No. 678,722, July 16, 1901, and many others since.
30. G. W. D. Briggs *et al., Trans. Faraday Soc.,* **51,** 1433 (1955); *ibid.,* **52,** 1272 (1956); *J. Chem. Soc.,* **1957,** 1846; *Electrochim. Acta,* **7,** 241 (1962); *ibid.,* **7,** 249 (1962).
31. T. A. Edison, U.S. Pat. No. 1,083,356, Jan. 6, 1914.
32. Edison's notebooks, which contain his work over many years, are available to the public at the Edison Library and Museum, Orange, N. J. They have never been edited with respect to his work on addition of foreign ions to alkaline cells.
33. V. I. Kosul'nikov and V. A. Tikhov, Russian Pat. No. 51, 380, July 31, 1937.
34. F. M. Bowers, Prog. Rept. by Thos. A. Edison Co. to U.S. Army Signal Corps on Contr. W36-039-sc-32137, Sept. 2, 1947.
35. R. L. Tichenor, *Ind. Eng. Chem.,* **44,** 973 (1952); see also E. J. W. Verwey, in "Semiconducting Materials," p. 151, Pergamon Press, Amsterdam (1951).
36. S. Z. Roginskii and N. I. Element, *Isvest. Akad. Nauk SSSR, Otdel. Khim. Nauk,* **1951,** 350.
37. J. M. Moulton, U.S. Pat. No. 2,634,303, April 7, 1953.
38. K. Sakata, T. Sakata, and K. Kigoshi, *Rept. Inst. Sci. and Technol.,* Univ. Tokyo, **8,** 39 (1954).
39. F. J. Morin, *Phys. Rev.,* **93,** 1195 (1954).
40. M. C. Rastogi, *Z. anorg. u. allgem. Chem.,* **276,** 316 (1954).
41. R. S. Coolidge, U.S. Pat. No. 2,683,102, July 6, 1954.
42. O. Bagno and J. Longuet-Escard, *J. Chim. Phys.,* **51,** 434 and 438 (1954); *Mem. serv. chim. etat* (Paris), **40,** 215 (1955).
43. I. P. Samokhvalov, D. B. Zlotnikova, and A. A. Maklyarskaya, USSR Pat. No. 108,324, Oct., 1957.
44. N. A. Marasonov, and B. V. Ershler, USSR Pat. No. 108,327, Oct. 25, 1957.
45. I. Sanghi and W. F. K. Wynne-Jones, *J. Sci. Ind. Research* (India), **16B,** 376 (1957).
46. I. I. Koval and V. N. Vorob'eva, *Vestnik Elektroprom.,* **29,** 46 (1958).
47. G. P. Loschinina and A. M. Murtazaev, *Dokl. Akad. Nauk. (SSSR),* **11,** 37 (1958).
48. B. C. Bradshaw, "Adsorption Measurements on Nickel Oxide Electrodes," *Proc. 12th Ann. Battery R. and D. Conf.,* USASRDL, Fort Monmouth, N. J., 1958.
49. V. Herold, U.S. Pat. No. 2,646,454.
50. H. Winkler, *Proc. CITCE Mtg.,* **1958,** 383.
51. H. Winkler, German (East) Pat. No. 14,368, Feb. 17, 1958.
52. Ya. I. Tur'yan and I. A. Gershkovich, *Zhur. Fiz. Khim.,* **35,** 1879 (1961), by analogy with effects of Li^+, Na^+, and K^+ on cobalt.
53. J. M. Moulton, U.S. Pat. No. 2,870,234, Jan. 20, 1959.
54. S. Januskiewicz, "Addition of Cobalt to Ni-Cd Batteries." *Proc. 13th Ann. Power Sources Conf.,* USASDRL, 1959.
55. V. N. Flerov, *Zhur. Priklad. Khim.,* **32,** 1306 (1959).
56. V. N. Flerov, *Trudy Gor'kovsk Politekh, Inst.,* **15,** 41 (1959).
57. Y. A. Gindelis, USSR Pat. 125,589, Jan. 15, 1960.
58. Inference only, by analogy with behavior of silver oxide electrodes: C. M. Shepherd and H. C. Langelan, U.S. Naval Research Lab. Report No. 5635, July, 1961.
59. W. Feitknecht, *Bull. Soc. Chim. France,* **1949,** 15. The germ of this idea goes back at least to 1933 (*Helv. Chim. Acta,* **16,** 427), when in a paper on the layer structure of basic salts Feitknecht states "Attack takes place along the layers, not perpendicular to them."
60. J. Labat, *J. Chim. Phys.,* **60,** 1253 (1963); H. Bode, *Angewandte Chem.,* **73,** 553 (1961).
61. H. P. Hanson and W. O. Milligan, *J. Phys. Chem.,* **60,** 1144 (1956).
62. K. Tsusmi, *J. Phys. Soc. Japan.* **13,** 586 (1958).
63. R. A. Van Nordstrand, *Adv. in Catalysis,* **12,** 149 (1960).
64. J. D. Moulton, Unpublished result, 1948.
65. S. U. Falk, *This Journal,* **107,** 661 (1960).
66. A. Fleischer, *J. (and Trans.) Electrochem. Soc.,* **94,** 289 (1948).
67. H. W. Koren and G. Baumstark, U.S. Pats. No. 2,708,211 and 2,708,212, May, 1955.
68. I. Kolthoff and E. B. Sandell, "Textbook of Quantitative Inorganic Analysis," 3d ed., Macmillan New York (1952).
69. F. D. Snell and C. T. Snell, "Colorimetric Methods of Analysis," Vol. II, p. 334 for nickel, p. 803 for nitrite. D. Van Nostrand Co., Inc., New York (1949).
70. K. Huber, *This Journal,* **100,** 376 (1953).
71. S. Yoshisawa and Z. Takehara, *Electrochim. Acta,* **5,** 240 (1961).
72. S. F. Pensabene and A. J. Catotti, *Extended Abstracts,* Battery Div., Electrochemical Soc., Oct., 1964.
73. See, *e.g.,* F. Kornfeil, Proc. 12th Ann. Battery Research and Development Conference, USASRDL, Fort Monmouth, N. J., 1958, p. 18.
74. B. E. Conway and P. L. Bourgault, *Can. J. Chem.,* **37,** 292 (1959).
75. U. B. Thomas and R. J. Baker, Private communication, 1955.
76. H. N. Seiger, R. C. Shair, *et al.,* Gulton Industries, Inc., Final Report (Report No. 8) on U. S. Army Contract No. DA 36-039-SC-85390. June, 1962.
77. G. T. Armstrong and J. A. V. Butler, *Trans. Faraday Soc.,* **29,** 1261 (1933).
78. J. O. Bockris, *J. Chem. Phys.,* **24,** 817 (1956), Eq. 4.144.
79. B. E. Conway and P. L. Bourgault, *Trans. Faraday Soc.,* **58,** 593 (1962); B. E. Conway and E. Gilsadi, *ibid.,* **58,** 2493 (1962).
80. P. C. Milner and U. B. Thomas, "The Nickel Cadmium Cell," in "Advances in Electrochem. Eng.," in press.
81. J. M. Hale, "Kinetics in the Nickel Hydroxide Electrode," *Proc. 4th Internat. Symp. on Batteries,* Brighton, England, Sept., 1964.
82. R. S. Nyholm, *Chem. Rev.,* **53,** 263 (1964).
83. G. Ya. Slaidin and P. D. Lukovtsev, *Dokl. Akad. Nauk SSSR,* **142,** 1130 (1962).
84. See, *e.g.,* J. J. Coleman, *Trans. Electrochem. Soc.,* **90,** 545 (1946); F. Kornfeil, *This Journal,* **109,** 349 (1962); N. V. Watson and A. B. Scott, *Extended Abstracts,* Battery Division, Electrochem. Soc., Oct., 1964; B. N. Kabanov, E. S. Weisberg, I. L. Romanova, and E. V. Krivolapova, *Elektrochim. Acta,* **9,** 1197 (1964).
85. M. Seiger and R. Shair, "Studies on Sealed Ni-Cd Batteries," *Proc. 15th Ann. Power Sources Conf.,* U. S. Army Signal R&D Lab., Ft. Monmouth, N. J., 1961.
86. F. Alliegro, W. E. Ryan, G. Baumstark, and A. B. Mundel, "Design and Manufacture of Sealed Ni-Cd Cells of Cylindrical Design," Final Report by Sonotone Corp. to U. S. Army Electronics R&D Lab., March 31, 1963.
87. P. D. Lukovtsev and G. Ya. Slaidin, *J. Phys. Chem. USSR,* **36,** 1227 (1962).

Studies of the Oxidation of Nickel in the Temperature Range of 900° to 1400°C

Kazuo Fueki[1] and J. Bruce Wagner, Jr.

Materials Research Center and Department of Materials Science, Northwestern University, Evanston, Illinois

ABSTRACT

The parabolic oxidation of nickel has been studied between 900° and 1400°C at pressures from the dissociation pressure of nickel oxide to 1 atm of oxygen. The activation energies in various atmospheres were found to range from 36.3 to 43.6 kcal/mole. The usual equation for parabolic oxidation, $k_p = c[p_{O_2}{}^{1/n} - p_{O_2}{}^{1/n}$ (eq.)] did not hold over the entire pressure range because the value of $1/n$ varied with temperature. A marker study showed that the markers were located close to the metal-oxide interface. A method for obtaining the self-diffusion coefficient of the more mobile ionic species in the oxide is proposed.

The dependence of the parabolic constant of metal oxidation on the oxygen partial pressure can provide valuable information about ionic transport in the oxide and the mechanism of oxidation. In the early work of Wagner and Grünewald (1) on the oxidation of nickel, the parabolic constants were found to be proportional to $p_{O_2}{}^{1/5}$. The electrical conductivity of nickel oxide was found by von Baumbach and Wagner (2) to be dependent on $p_{O_2}{}^{1/4}$. On the basis of these results it was concluded that nickel oxide is a metal deficit p-type semiconductor and that the nickel oxide layer on nickel grows by the simultaneous diffusion of nickel ions via cation vacancies and of electron holes. Baur and his collaborators (3) carried out a study of the pressure dependence of nickel oxidation between 1000° and 1200°C at oxygen pressures from 6.5×10^{-3} to 20.4 atm. They found that the measured rates above 1 atm are insensitive to oxygen pressure and that the rates below 1 atm closely followed $p_{O_2}{}^{1/4}$. The pressure dependence was explained on the basis of Langmuir's adsorption isotherm and of vacancy creation by adsorbed oxygen. Since both oxidation studies and the measurements of diffusion (4, 5) and electrical conductivity (2, 6, 7) of nickel oxide have been confined to pressures above about 10^{-4} atm of oxygen, it has not been confirmed that the aforementioned mechanism still holds in lower oxygen pressures.

Marker studies are useful for identification of the predominant ionic species diffusion through oxides during metal oxidation. Sartell and Li (8) observed in their marker study that the nickel oxide formed on nickel consists of a black outer layer and a green inner one and that the markers were always located at the boundary between the two layers. They proposed a mechanism whereby the outer layer grows by the outward diffusion of nickel ions and that the inner layer grows by the inward diffusion of oxygen ions.

The results of von Baumbach and Wagner and of Baur and his collaborators are not consistent with that of Sartell and Li. To clarify further the ionic transport in nickel oxide, the present authors have studied the oxidation rate of nickel over a wide pressure range between the dissociation pressure of nickel oxide and 1 atm of oxygen. Marker studies have also been carried out. It is the purpose of this paper to report the results of these measurements and also to propose a method by which the self-diffusion coefficient is obtained as a function of oxygen partial pressure from oxidation data.

Table I. Analysis of nickel sheet*

	%
Silver	0.001
Aluminum	0.01
Cobalt	0.004
Chromium	0.001
Copper	0.002
Iron	0.02
Manganese	0.002
Molybdenum	0.001
Lead	0.04
Silicon	0.01
Tin	0.001
Titanium	0.001

* The above analysis was furnished by the Charles C. Kawin Company of Chicago, Illinois.

Experimental and Results

Oxidation rate measurement.—Nickel sheet, 6 mil thick, containing impurities listed in Table I was used in these studies. Specimens, 1 cm wide by 2 cm long, were cut from the sheet, polished using 1/0, 2/0, 4/0 metallographic papers and using Linde "A" fine abrasive on a polishing wheel, washed with soap and water and with acetone, and then dried. The polished specimens were annealed in hydrogen at 550°C overnight to remove strain and to reduce any surface oxide.

The gravimetric measurements below 1190°C were carried out using an Ainsworth automatic-recording balance and its accessories described by Pettit and Wagner (9). Measurements above 1300°C were made using the weighing apparatus described by Pettit, Yinger, and Wagner (10) with modifications to the furnace and reaction tube. An ATT-type Globar tubular heating element, 1⅛-in. ID and 22-in. long, was used for the furnace. Through the hollow of the heating element an alumina reaction tube, 9/16-in. in ID and 36-in. long, was placed. There was a 3-in. section in the center over which the temperature was constant within ±3°C at 1400°C. The temperature was controlled at a given point within ±2°C by means of a platinum-10% rhodium thermocouple and a L&N Speedomax G.

The oxidizing atmospheres were oxygen of 1, 10^{-1}, 10^{-2}, 5×10^{-4}, and 1.35×10^{-4} atm, CO_2, and CO-CO_2 mixtures containing 0.25 and 0.50% CO at a total pressure of 1 atm. When a pressure of oxygen less than 1 atm was required, purified argon was used as the diluent gas. Flow rates of 0.9 and 2.7 cm/sec were employed below 1190° and above 1300°C, respectively.

Figures 1 and 2 show the parabolic plots of oxidation in various atmospheres at 1190°C. The slope changes with time during the initial oxidation period and eventually reaches a constant value. As seen from the comparison of two runs for 10^{-2} atm of oxygen, the rate for the later period is more reproducible than that for the initial period. Therefore, in this paper the parabolic constants were determined from the slope for the later period.

The Arrhenius plots of parabolic constants in various atmospheres are given in Fig. 3. The plots for oxidation in high oxygen pressures and in CO_2 are straight over the entire temperature range, but those

[1] Present address: Department of Industrial Chemistry, University of Tokyo, Tokyo, Japan.

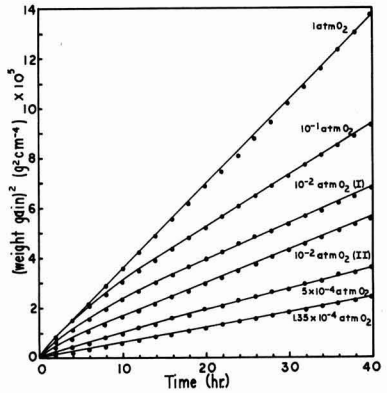

Fig. 1. Parabolic plot of oxidation at 1190°C

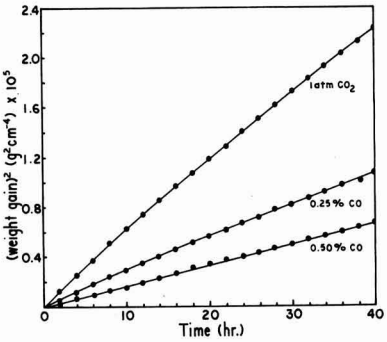

Fig. 2. Parabolic plot of oxidation at 1190°C

for low oxygen pressures and for CO-CO_2 mixtures are curved. The activation energies determined from the slopes of the straight-line portions are listed in Table II. For comparison, results obtained by previous investigators are summarized in Table III.

When an oxide with metal deficit and predominant electronic conduction is formed, the pressure dependence of parabolic constant is usually analyzed by the equation (16, 17)

$$k_p = c[p_{O_2}{}^{1/n} - p_{O_2}{}^{1/n}(\text{eq.})] \qquad [1]$$

where p_{O_2} and p_{O_2} (eq.) represent the oxygen partial pressures at the gas-oxide interface and at the oxide-metal interface respectively, c is a constant, and $1/n$ is a constant characterized by the mechanism of creation of a vacancy and electron hole(s), in this case, trivalent nickel. Figure 4 shows the plots of log k_p *vs.* log $[p_{O_2}{}^{1/n} - p_{O_2}{}^{1/n}(\text{eq.})]$ at constant temperatures. The oxygen pressures for CO-CO_2 mixtures were calculated assuming that the equilibrium of the reaction $2CO + O_2 \rightleftarrows 2CO_2$ was attained at the surface of nickel oxide. The value of n was chosen so that as many data points as possible could be located on a straight line with a slope of unity. As seen in Fig. 4 the data for low oxygen partial pressures deviate from the straight line except for the reactions at 1300° and 1400°C. A similar deviation has been reported by Pettit and Wagner for the oxidation of cobalt (9).

The data for oxidation in CO_2 were also plotted in Fig. 4. The oxygen partial pressures were calculated assuming that the equilibrium of self-dissociation $2CO_2 \rightleftarrows 2CO + O_2$ was attained on the surface of nickel oxide. These data, denoted by the symbol, *X*, are located close to the straight lines.

Marker study.—Platinum paste was put on a polished nickel specimen and heated at 900°C for 30 min

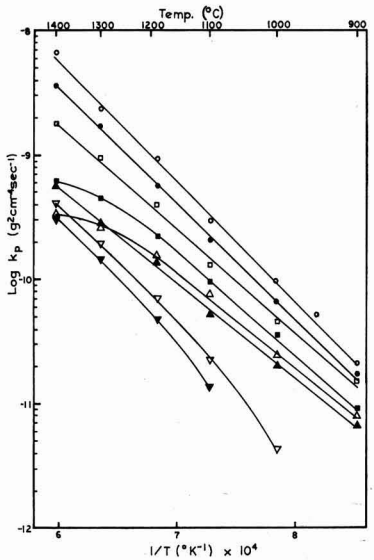

Fig. 3. Temperature dependence of parabolic constants in various atmospheres: ○, 1 atm O_2; ●, 10^{-1} atm O_2; □, 10^{-2} atm O_2; ■, 5 x 10^{-4} atm O_2; △, 1.35 x 10^{-4} atm O_2; ▲, 1 atm CO_2; ▽, 0.25% CO—CO_2; ▼, 0.50% CO—CO_2.

in a 1:1 mixture of CO-CO_2 to convert it into a thin and porous metallic film of about 1-2μ thickness. The specimen coated with the thin platinum layer was oxidized in oxygen of 1 atm or in carbon dioxide of 1 atm and cross-sectioned to examine the location of the platinum marker. Figure 5 shows the cross section of a specimen oxidized for 42 hr in 1 atm of oxygen at 1190°C. The oxide consists of a single layer and platinum markers are located close to the metal-oxide interface. When fine alumina powder was employed, markers were found to be located at the metal-oxide interface. The results of the present work clearly differ from those of Sartell and Li and show that nickel ions migrate much faster than oxygen ions.

Discussion

According to Wagner's theory of metal oxidation the rate constant for the formation of an oxide with predominant electronic conduction is given by the equation (16, 17)

Table II. Activation energies for the oxidation of nickel in various atmospheres in the present study

Atmosphere	Temperature range, °C	Activation energy, kcal/mole
1 atm O_2	900-1400	43.6
1 × 10^{-1} atm O_2	900-1400	42.5
1 × 10^{-2} atm O_2	900-1400	39.0
5 × 10^{-4} atm O_2	900-1190	37.7
1.35 × 10^{-4} atm O_2	900-1190	36.7
1 atm CO_2	900-1400	36.3

Table III. Comparison of activation energies

Investigators	Temperature range, °C	Activation energy, kcal/mole
Sartell and Li (8)	950-1200	67.0
Gulbransen and Andrew (11)	900-1050	68.3
Berry and Paidassi (12)	1000-1400	49.0
Frederick and Cornet (13)	800-1400	51.0
Baur, Bartlett, Ong, Jr., and Fassel (3)	1000-1200	50.0
Zima (14)	980-1260	45.1
Phillips (15)	700-1300	38.0

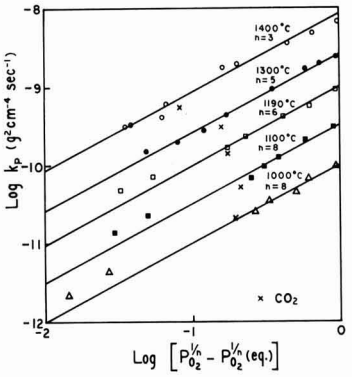

Fig. 4. Plots of log k_p vs. log $[p_{O_2}{}^{1/n} - p_{O_2}{}^{1/n}$ (eq.)]

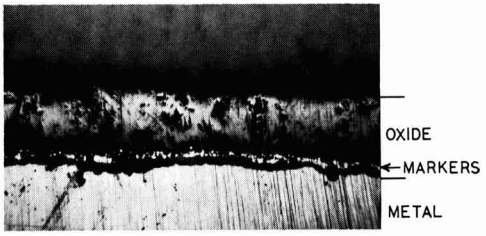

Fig. 5. Cross section of an oxide film with platinum markers. (1190°C, 1 atm O_2, 40 hr). Magnification 135X.

$$k_r = c_{eq} \int_{a_{x'}}^{a_{x''}} \left(\frac{Z_1}{|Z_2|} D_1{}^* + D_2{}^* \right) d \ln a_x \qquad [2]$$

where k_r is "rational rate constant" in equivalents per centimeter per second, $D_1{}^*$ and $D_2{}^*$ are the self-diffusion coefficients of cations and anions, respectively, Z_1 and Z_2 are units of charge on the cations and anions, respectively, a_x is the activity of nonmetallic element,[2] and c_{eq} is the concentration of ions in equivalents per cubic centimeter. Equation [1] is derived from Eq. [2] under the following assumptions: (*a*) oxidation is governed by the diffusion of cations via cation vacancies; (*b*) cation vacancies are created by a mechanism whereby n is independent of oxygen partial pressure, and (*c*) $D_1{}^*$ is proportional to the vacancy concentration. As shown above, Eq. [1] does not hold for the parabolic oxidation of nickel. Moreover, it is difficult to interpret a value of $n = 8$ for oxidation at 1000° and 1100°C. Therefore, a new method for the analysis of the pressure dependence of parabolic oxidation is proposed. As seen in Eq. [2], k_r consists of two kinds of terms, one of which is a function of a_x'' and the other a function of a_x'. a_x' is not a variable but a constant at a constant temperature. Therefore, k_r is differentiated by $\ln a_x''$ as follows,

$$\frac{Z_1}{|Z_2|} D_1{}^* + D_2{}^* = \frac{1}{c_{eq}} \cdot \frac{d\, k_r}{d \ln a_x''} \qquad [3]$$

In the case of the oxidation of nickel $Z_1/|Z_2|$ is unity and $D_2{}^*$ is eliminated because the marker study showed that cations migrate much faster than anions. Moreover, $d \ln a_x''$ is replaced by $\frac{1}{2}\, d \ln p_{O_2}$. Accordingly

$$D_1{}^* = D_{Ni}{}^* = \frac{2}{c_{eq}} \frac{d\, k_r}{d \ln p_{O_2}} \qquad [4]$$

c_{eq} is represented by the molecular weight M_{NiO} and the density ρ_{NiO} of nickel oxide (7.44 g/cc) as follows

$$c_{eq} = \frac{2 \rho_{NiO}}{M_{NiO}} \qquad [5]$$

[2] In the present case the single prime refers to the activity at the oxide-metal interface and the double prime that at the oxide-gas interface.

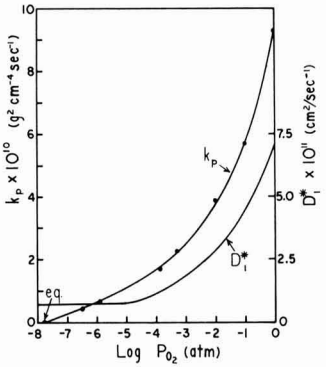

Fig. 6. Plots of k_p and $D^*{}_1$ as functions of p_{O_2} (1190°C)

For the present studies, the rational rate constant, k_r in units of eq/cm-sec, is related to the rate constant, k_p in units of $g^2 \cdot cm^{-4} \cdot sec^{-1}$, by an equation

$$k_r = \frac{M_{NiO}}{M_o{}^2 \rho_{NiO}} \cdot k_p \qquad [6]$$

where M_o is atomic weight of oxygen. Insertion of Eq. [5] and [6] into Eq. [4] yields

$$D_1{}^* = D_{Ni}{}^* = \left(\frac{M_{NiO}}{M_o \rho_{NiO}} \right)^2 \frac{d\, k_p}{d \ln p_{O_2}} = 0.1704 \cdot \frac{d\, k_p}{d \log p_{O_2}} \qquad [7]$$

Equation [7] shows that the self-diffusion coefficient of nickel ions is obtained as a function of log p_{O_2} by differentiating k_p with respect to log p_{O_2}. Figure 6 shows the plots of k_p *vs.* log p_{O_2} and of $D_1{}^*$ *vs.* log p_{O_2}. $D_1{}^*$ was obtained by differentiating the curve of k_p graphically and multiplying a factor of 0.1704. The plots of log $D_1{}^*$ *vs.* log p_{O_2} at different temperatures are given in Fig. 7. The value of log $D_1{}^*$ is independent of log p_{O_2} in the low-pressure range below about 10^{-6} atm and increases linearly with log p_{O_2} in the intermediate pressure range. The slopes determined in this range are given in Fig. 7. In the high-pressure range the slope appears to decrease gradually. In the intermediate

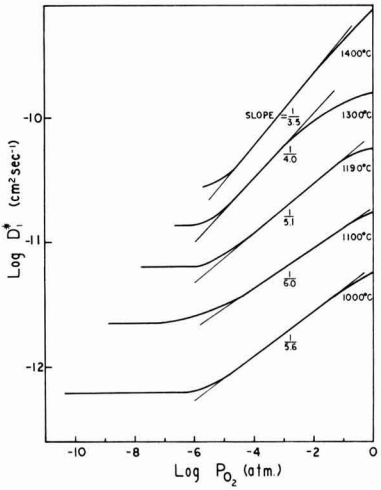

Fig. 7. Pressure dependence of self-diffusion coefficient $D^*{}_1$ calculated by the proposed method.

pressure range, the cation vacancies would be created by the following mechanisms

$$\frac{1}{2}O_2 \rightleftarrows [Ni_{\square''} \cdot \oplus] + \oplus + NiO \qquad (I)$$

or

$$\frac{1}{2}O_2 \rightleftarrows Ni_{\square''} + 2\oplus + NiO \qquad (II)$$

where $Ni_{\square''}$ is a cation vacancy and $\oplus$ is an electron hole. At 1300° and 1400°C the slope of the plot of log D_1^* *vs.* log p_{O_2} is about ¼. Mechanism (I) is inferred to predominate at these temperatures. Mechanism (II) would be predominant at 1000° and 1100°C. It is difficult to reconcile values of n in the pressure dependence of the parabolic rate constant (Fig. 4) and of the self-diffusion coefficient (Fig. 7) which decrease with increasing temperature. Such behavior would not be predicted on the basis of the ideal mass action law whereby the activities of each of the species are equated to their respective concentrations and whereby any trapping or association of electron holes onto vacancies would be expected to be more prevalent at the lower temperatures than at the higher temperatures.We do not have an explanation for this behavior. Additional data on the thermodynamics (activity coefficients of the respective species) are needed. The layers of NiO found in the present study were always adherent and free from pores under microscopic examination. While some oxygen transport in the NiO layers may aid in explaining the foregoing, the agreement of the present diffusion data with tracer diffusion studies (see below) suggests that the present analysis is correct.

There are no data available for the oxygen pressure dependence of the self-diffusion coefficient of nickel. One possible explanation for the apparent independence of D_{Ni}^* on oxygen pressure in the low-pressure range is as follows: In the low pressure range, the concentration of cation defects created by the excess oxygen would be small. Near the stoichiometric composition the defects would be created by a Frenkel mechanism,

$$\text{null} \rightleftarrows Ni_{\square''} + Ni_{O}'' \qquad (III)$$

or by a Schottky mechanism

$$\text{null} \rightleftarrows Ni_{\square''} + O_{\square}'' \qquad (IV)$$

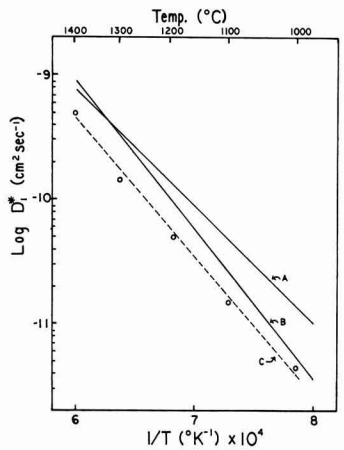

Fig. 8. Comparison of diffusion data: A, Shim and Moore, $D = 3.9 \times 10^{-4} \exp(-44.2/RT)$ cm² sec^{-1}; B, Lindner and Åkerström, $D = 1.7 \times 10^{-2} \exp(-56.0/RT)$ cm² sec^{-1}; C, This work, $D = 1.1 \times 10^{-3} \exp(-50.3/RT)$ cm² sec^{-1}.

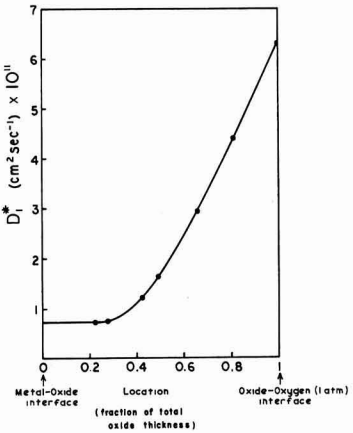

Fig. 9. Self-diffusion coefficient as a function of location in the oxide layer growing in 1 atm of oxygen at 1190°C.

where $Ni_{\square''}$ is a cation vacancy, Ni_{O}'' is an interstitial ion, and $O_{\square}''$ is an anion vacancy. If the concentration of defects created by mechanism (III) or (IV) greatly exceeds that created by the excess oxygen at low oxygen pressures, the mass action law yields

$$[Ni_{\square''}] \cdot [Ni_{O}''] = K_{III}(T) \qquad [8]$$

and

$$[Ni_{\square''}] \cdot [O_{\square}''] = K_{IV}(T) \qquad [9]$$

Since $[Ni_{\square''}]$ is equal to $[Ni_{O}'']$ or to $[O_{\square}'']$ as the case may be, the constant concentrations of cation vacancies and interstitial cations result in the self-diffusion coefficient being independent of oxygen pressure.

Baur and his collaborators found that the parabolic constant is insensitive to oxygen above 1 atm. In the present studies, the gradual decrease in the slope of k_p in the high-pressure range might be due to the transition to the pressure insensitive region. The Arrhenius plot of calculated D_1^* values at 0.2 atm is given in Fig. 8. The diffusion data of Shim and Moore (4), and of Lindner and Åkerström (5) are also plotted for comparison. The values of the self-diffusion coefficient of the nickel oxidation data agree well with those obtained independently using tracer techniques. This shows the self-consistency of the foregoing analysis.

The equilibrium oxygen pressure in a growing oxide decreases gradually from p_{O_2}, the oxygen partial pressure of ambient gas, to p_{O_2} (eq,), the dissociation pressure of the oxide. The location in the growing oxide where the equilibrium oxygen pressure is p_{O_2}' (p_{O_2} (eq.) $\leqq p_{O_2}' \leqq p_{O_2}$) is given by $(k_p'/k_p)^{1/2}$, where k_p' and k_p are the parabolic rate constants when the oxygen partial pressures are p_{O_2}' and p_{O_2}, respectively. Since the self-diffusion coefficient of nickel as a function of oxygen pressure is given in Fig. 7, one can obtain a relationship between the value of the self-diffusion coefficient and the location in terms of fraction of the total oxide thickness in the growing nickel oxide. Figure 9 shows the self-diffusion coefficient as a function of location in nickel oxide growing in 1 atm of oxygen at 1190°C. The linear gradient of D_1^* is seen in the outer portion of oxide and the independence of D_1^* on location is seen in the inner portion.

Summary

From the results of parabolic oxidation and of marker studies, the self-diffusion coefficient of nickel ions in nickel oxide is obtained as a function of oxygen partial pressure. The calculated self-diffusion coefficient is independent of oxygen pressure in the low

oxygen pressure range and is proportional to $p_{O_2}^{1/6}$ to $p_{O_2}^{1/3.5}$ in the intermediate pressure range. The dependence on $p_{O_2}^{1/4}$ is explained by the ionization of one electron hole from the cation vacancy while a $p_{O_2}^{1/6}$ dependence results if 2 electron holes are ionized. The calculated self-diffusion data at 0.2 atm of oxygen agree well with published tracer-diffusion values.

Manuscript received July 20, 1964. This work was supported by a grant from the Advanced Research Projects Agency through Northwestern University's Materials Research Center.

Any discussion of this paper will appear in a Discussion Section to be published in the December 1965 JOURNAL.

REFERENCES

1. C. Wagner and K. Grünewald, *Z. physik. Chem.*, **B24**, 455 (1938).
2. H. H. von Baumbach and C. Wagner, *ibid.*, **B24**, 59 (1934).
3. J. P. Baur, R. W. Bartlett, J. N. Ong, Jr.. and W. M. Fassell, Jr., *This Journal*, **110**, 185 (1963).
4. M. T. Shim and W. J. Moore, *J. Chem. Phys.*, **26**, 802 (1957).
5. R. Lindner, and Å. Åkerström, *Discussion Faraday Soc.*, **23**, 133 (1957).
6. S. P. Mitoff, *J. Chem. Phys.*, **35**, 882 (1961).
7. N. G. Eror and J. B. Wagner, Jr., *Amer. Ceram. Soc.* 65th Annual Meeting, April 27-May 2, 1963; Abstract No. 33-B-63. *Am. Ceram. Soc. Bull.*, **42**, No. 4, 199 (1963); to be published.
8. J. A. Sartell and C. H. Li, *J. Inst. Metals*, **90**, 92 (1961-62).
9. F. S. Pettit and J. B. Wagner, Jr., *Acta Met.*, **12**, 41 (1964).
10. F. S. Pettit, R. Yinger, and J. B. Wagner, Jr., *ibid.*, **8**, 617 (1950).
11. E. A. Gulbransen and K. F. Andrew, *This Journal*, **104**, 451 (1957).
12. L. Berry and J. Paidassi, *Compt. rend.*, **255**, 2253 (1962).
13. S. F. Frederick and I. Cornet, *This Journal*, **102**, 285 (1955).
14. G. E. Zima, *Trans. A.S.M.*, **49**, 924 (1957).
15. W. L. Phillips, Jr.. *This Journal*, **110**, 1014 (1963).
16. C. Wagner, *Z. physik. Chem.*, **B32**, 447 (1936).
17. C. Wagner, "Diffusion and High Temperature Oxidation of Metals," "Atom Movements", Am. Soc. for Metals, Cleveland, p. 153 (1951).

Determination of the Refractive Index and Thickness of Oxide Films on Anodized Zirconium from Transmission Interference Measurements

J. C. Banter

Oak Ridge National Laboratory, Oak Ridge, Tennessee

ABSTRACT

A method is described for the determination of the refractive index of thin oxide films stripped from anodized zirconium by dissolution of the metal. This new technique involves measurement of the interference patterns produced in the light transmitted through the films at various angles of incidence. The film thickness is also calculated from the data, and results show the refractive index does not vary with film thickness for films approximately 3000 to 5500Å thick. These films exhibit normal dispersion behavior over the ultraviolet, visible, and near infrared regions of the spectrum, with the refractive index varying from 2.07 to 2.50 at wavelengths of 1μ and 250 mμ, respectively.

In recent years, many experiments in the field of metallic corrosion have concerned the measurement of the optical properties and thickness of the thin oxide films formed in the early stages of corrosion. Frequently, reflection interference methods were used to make these measurements (1-4), but transmission measurements would serve just as well. This paper describes a transmission interference method applied to the determination of the refractive index and thickness of thin oxide films formed on zirconium. The technique was developed using anodically formed films with the hope of extending the measurements to films formed in other corrosive environments such as high-temperature water, air, and steam.

Theory

As the wavelength of light incident on a thin film is varied, the intensity of the transmitted beam exhibits alternate maxima and minima due to interference effects in the film. The wavelengths at which these extremes occur depend on the optical properties and thickness of the film as well as on the angle of incidence of the light. Vasícek (5) gives the equation describing the intensity, I_t, of light transmitted by a thin homogeneous film as

$$I_t = \frac{(1 - r'^2)(1 - r''^2)}{1 + r'^2 r''^2 + 2 r' r'' \cos X} \qquad [1]$$

where r' and r'' are the Fresnel amplitude reflection coefficients for light incident from the same direction on the first and second surfaces of the film, respectively, and

$$X = 4\pi\eta_1 d_1 \cos\phi_1/\lambda \qquad [2]$$

η_1 and d_1 are the refractive index and thickness of the film, respectively, ϕ_1 is the angle of refraction of the light into the oxide, and λ is the wavelength of the incident light. Since $r'' = -r'$, the maxima occur at those wavelengths where $X = 2m\pi$; and the minima at those wavelengths where $X = (2m + 1)\pi$ with m, the order of interference, being an integer.

As the angle of incidence increases, the positions of the extremes for any given order of interference shift to shorter wavelengths in the spectrum. If the angle of incidence is increased sufficiently, the position of a given maximum or minimum can be shifted to the same wavelength as the minimum or maximum which was immediately adjacent to it at a lower wavelength at normal incidence. With known order numbers (which are easily determined) values for X as given by Eq. [2] can be calculated for both the extremes at normal incidence and those at the higher angle of incidence. Since $\cos\phi_1 = 1$ at normal incidence, the ratio of these two values of X yields $\cos\phi_1$ for the higher angle of incidence. The refractive index at this wavelength can then be calculated from Snell's law of refraction

$$\eta_0 \sin \phi_0 = \eta_1 \sin \phi_1 \quad [3]$$

where η_0 is the refractive index of the medium from which the light is incident on the film, and ϕ_0 is the angle of incidence of the light. The film thickness is determined by then substituting this value of η_1 into Eq. [2].

Experimental Procedure

Specimens ¾ in. x 1¾ in. were cut from 0.020-in.-thick zirconium foil and the surfaces chemically polished in a solution consisting of 50 ml lactic acid, 50 ml nitric acid, 20 ml water, and 10 ml hydrofluoric acid. Specimens were washed with copious amounts of water, dried, then anodized at constant voltages in a solution consisting of 40 ml glycerin, 20 ml lactic acid, 70 ml water, 120 ml ethyl alcohol, 10 ml phosphoric acid, and 4g citric acid. Specimens were anodized in such a manner that oxide film was formed on all surfaces. The film was then abraded from the center of one side of the specimen over an area approximately ⅜ x ⅝ in., and the metal in this area was dissolved by immersing the specimen in a 20% solution of bromine in ethyl acetate. This left a clear window of the oxide film supported by a surrounding frame of the undisturbed metal. The film and frame were then carefully washed in ethyl alcohol to remove all traces of bromine and dried in a stream of warm air.

The variation with wavelength of the intensity of light transmitted through these windows was measured in a Perkin-Elmer Model 4000 A spectrophotometer. For this purpose, two special specimen mounts were designed which allowed the rotation of the specimen about a vertical axis passing through the center of the spectrophotometer light beam. Figure 1 shows these two specimen mounts, one of which was used to make the measurements in air and has a specimen mounted in place. The second mount allows the measurements to be made with the specimen immersed in a liquid with refractive index higher than that of air. This mount was used with water as the immersion liquid in those instances where coincidence of the extremes could not be achieved at reasonable angles of incidence in air. The water immersion reduces the angle of incidence required to obtain coincidence of the extremes by increasing η_0.

Transmitted intensity measurements were first made on each specimen at normal incidence in the visible and/or ultraviolet regions of the spectrum, and then the angle of incidence at the appropriate wavelengths was gradually increased to obtain the angles required to produce coincidence of the extremes. Equation [2] was then applied to obtain η_1 and d_1 at each wavelength.

Results

Figure 2 shows typical interference patterns developed in the visible regions of the spectrum for one of the anodic oxide films and illustrates the shift to shorter wavelength of a given extreme as the angle of incidence is increased. At $\phi_0 = 60°$, maximum A has not shifted quite enough to come into coincidence with the position of minimum B at normal incidence,

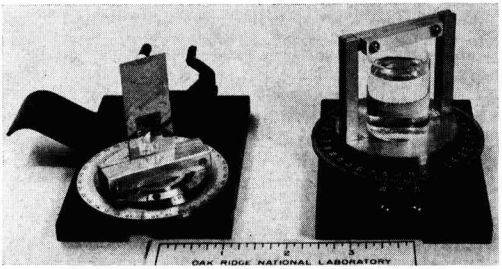

Fig. 1. Special mounts used to hold oxide film specimens in the spectrophotometer.

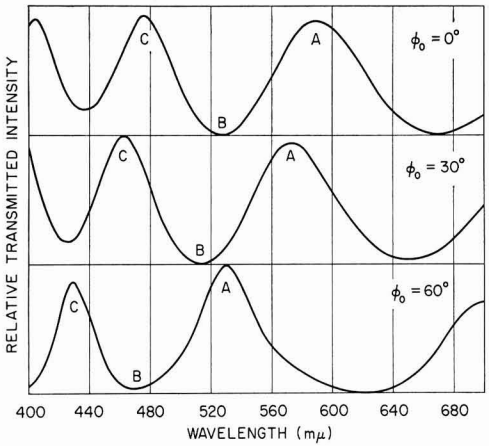

Fig. 2. Interference patterns developed in the visible regions of the spectrum at various angles of incidence by a film formed at 400v. A, 4th order maximum; B, 4th order minimum; C, 5th order maximum.

while minimum B has shifted beyond coincidence to a wavelength lower than that corresponding to the position of maximum C at normal incidence. Data for the calculation of η_1 and d_1 for this specimen in the visible region of the spectrum and the results of the calculation are listed in Table I. The average value for d_1 taken from this calculation was used in Eq. [2] to calculate values for η_1 at other wavelengths where extremes occurred outside the visible region. The calculated variation of the refractive index with wavelength of films formed at 200, 300, and 400v is shown in Fig. 3. The thicknesses of these films were calculated as 3159, 4318, and 5493Å, respectively.

Unfortunately, strong adsorption of light in the visible and ultraviolet regions of the spectrum obliterated the interference patterns of oxide films which were formed in high-temperature water and air to such an extent that this method could not be applied to them.

Discussion

Calculated values for both the refractive index and film thickness of the anodic zirconium oxide films are believed to be accurate to 1% or better, and within this limit the refractive index does not appear to change with film thickness. The refractive index of these films exhibits normal dispersion behavior with no appreciable absorption throughout the ultraviolet, visible, and near infrared regions of the spectrum, and varies from 2.07 at a wavelength of 1μ to 2.50 at a wavelength of 250 mμ. It should be noted, however, that the refractive index measured by this technique is not necessarily the same as that of the oxide film

Table I. Data for the calculation of the refractive index and thickness of an oxide film formed on zirconium anodized at 400v. Measurements were made with the specimen immersed in water.

Wavelength, λ, Å	Angles of incidence for coincidence of extremes	Order of interference of extremes $\phi_0 = 0°$	Order of interference of extremes $\phi_0 > 0°$	Index of refraction	Film thickness
6575	54° 12′	3	3	2.096	5490
5797	49° 48′	4	3	2.104	5510
5132	46° 24′	4	4	2.112	5460
4682	43° 48′	5	4	2.125	5508
4293	41° 48′	5	5	2.145	5504
3973	40° 12′	6	5	2.170	5493
3700	38° 48′	6	6	2.193	5483
Average					5493 ±33

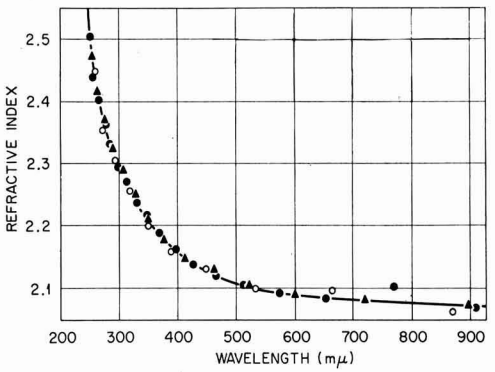

Fig. 3. Dispersion curve for three anodic zirconium oxide films. Anodized at: ●, 400v; ▲, 300v; ○, 200v.

in situ on the metal since the removal of the metal from the films tends to relieve certain strains existing in the film. These strains would be expected to affect the optical properties of the oxide. However, the calculated film thicknesses should not be appreciably different from those of the films in place.

The transmission interference method described here cannot, of course, be used with films such as the thermally formed films mentioned above which are strongly absorbing in both the visible and ultraviolet regions of the spectrum. The method is further limited by a lower limit on the thickness of the film for which coincidence of the interference extremes can be obtained at angles of incidence which are practically and accurately measurable. Proper choice of the liquid for use in the immersion mount can lower this limit considerably.

This method has one distinct advantage over the reflection interference methods often used for refractive index and thickness measurements. It completely eliminates the phase change occurring on reflection at the oxide-metal interface from the interference equations. This factor is often improperly treated. For example, Charlesby and Polling (6) developed interference equations for measurements similar to those reported using reflection techniques. Although these equations contained the phase change, its variation with angle of incidence was neglected completely in their use.

Furthermore, this method can undoubtedly be applied to other oxide films, both anodic and thermal, which can be separated from the substrate metal and which do not absorb strongly enough to obliterate the interference patterns normally developed.

Acknowledgment

The author wishes to express gratitude to Dr. M. L. Picklesimer for his many discussions of this project and his criticism of the manuscript.

Manuscript received Oct. 14, 1964. This paper was presented at the Washington Meeting, Oct. 11-15, 1964. The research was sponsored by the United States Atomic Energy Commission under contract with the Union Carbide Corporation.

Any discussion of this paper will appear in a Discussion Section to be published in the December 1965 JOURNAL.

REFERENCES

1. F. Abeles. *J. Phys. Radium*, **11**, 310 (1950).
2. N. J. M. Wilkins, *Corr. Sci.*, **4**, 17 (1964).
3. W. P. Ellis, *J. Opt. Soc. Am.*, **53**, 613 (1963).
4. O. S. Heavens, "Optical Properties of Thin Solid Films," Butterworths, London (1955).
5. Antonin Vasícek, "Optics of Thin Films," North-Holland, Amsterdam (1960).
6. A. Charlesby and J. J. Polling, *Proc. Roy. Soc. (London)*, **227A**, 434 (1954).

The Role of Copper During the Oxidation of Transformer Oils

John J. Melchiore and Ivor W. Mills

Research Laboratories, Sun Oil Company, Marcus Hook, Pennsylvania

ABSTRACT

Air oxidation of two transformer oils, differing mainly in the fact that one contained metal deactivator, was studied at 95°C in the presence and absence of metallic copper. Power factor, hydroperoxide and carbonyl oxidation intermediates, and copper contents were measured as a function of time. In the absence of metallic copper, oxidation of the two oils is quite similar. Curves of power factor and oxidation intermediates show no striking differences. There appears to be a relation between power factor and carbonyl content in these cases. In the presence of metallic copper, the oil containing metal deactivator is capable of resisting the catalytic effects of copper. The oil without deactivator is grossly degraded by <0.2 ppm soluble copper which the oil rapidly dissolves. The relation between copper content, hydroperoxide content, and power factor is discussed in terms of a proposed mechanism.

It is well known that oxidative degradation of electrical oils results in the loss of electrical insulating properties of the oil. This has led to a search for electrical oils with superior oxidation resistance, especially in the presence of copper. A number of comparative accelerated laboratory tests have been devised, hopefully to predict what will actually happen to a transformer oil in service over a period of years. A particularly convenient and useful comparative test involves periodic measurement of the power factor of an oil at 95°C exposed to air and copper over a period of several days. Although the correlation of this test with actual oil performance in use has yet to be demonstrated, the mechanism of oil degradation should be the same, since in both cases the oil at elevated temperature is exposed to air and metallic copper. This test, described in detail in the Experimental Section, was used throughout the present study.

The mechanism of oil degradation in the presence of copper is not clear. Proposals for both heterogeneous and homogeneous copper catalysis have been made (1), but more convincing evidence has been reported supporting the homogeneous theory (2). Although transformer oils in service are reported to dissolve about 0.2-0.6 ppm copper, the ability of an oil to retain soluble copper apparently depends on many diverse factors (3). However, detailed quantitative data on copper solubility during the early hours of oxidation are lacking as well as the mechanisms responsible for copper solubilization. Similarly, the role of metal deactivators is another related aspect of the over-all problem. The work presently reported, there-

Table I. Properties of transformer oils A and B

Physical	ASTM method	Transformer oil A	Transformer oil B
Specific gravity, 60°F	D1250	0.904	0.904
Flash, OC, °F	D92	295	295
Fire, °F	D92	325	325
Viscosity, SUS/100°F	D446	60	58.6
Pour point, °F	D97	−50	−50
IFT, dynes/cm	D971	40	41
Dielectric strength, kv	D877	32	35
Differential infrared and UV spectra		No Detectable Differences	
Refractive index/20°C		1.4951	1.4963
Chemical			
Neutralization No., mg KOH/g	D974	0.00	0.00
Inorganic chlorides & sulfates	D878	0	0
Free sulfur	D989	0	0
Total sulfur, weight per cent (w/o)		0.12	0.12
Average molecular weight, osmometric		271 ± 5	260 ± 5
Total aromatics, w/o		35	34.5
Monocyclic, w/o		27.4	25.7
Dicyclic		6.3	7.9
Tricyclic		1.3	0.9

fore, was undertaken to help answer these questions, with particular emphasis on the processes occurring during the early hours of oxidation.

In this investigation, air oxidations of two transformer oils, A and B, were studied at 95°C in the presence and absence of metallic copper. Power factors of the oxidizing oils were recorded automatically each hour. From small aliquots withdrawn periodically, hydroperoxide and carbonyl contents were measured polarographically. The soluble copper content was determined by neutron activation analysis. Thus, data are available for plotting continuous curves of power factor, copper content, and oxidation intermediates.

Physical and chemical properties of oils A and B are summarized in Table I, with infrared and ultraviolet spectra given in Fig. 1 and 2. The most important difference between these oils is the fact that oil B contains a metal deactivator, that is, a material capable of significantly decreasing the catalytic activity of copper. This metal deactivator was derived

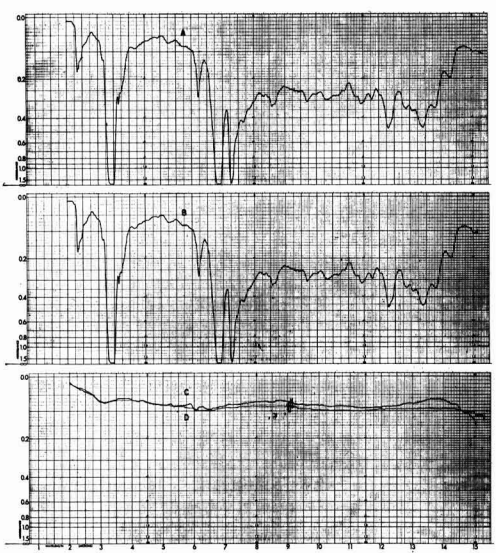

Fig. 1. Infrared spectra. Curve A is conventional transformer oil (A), liquid phase, 0.1 mm thickness. Curve B is oil containing metal deactivator (B), 0.1 mm thickness. Curve C is the differential spectrum of oil A *vs.* oil B, 1.008 mm thickness. Curve D is the differential spectrum of oil A *vs.* oil A, 1.008 mm thickness. Absorbance *vs.* wavelength.

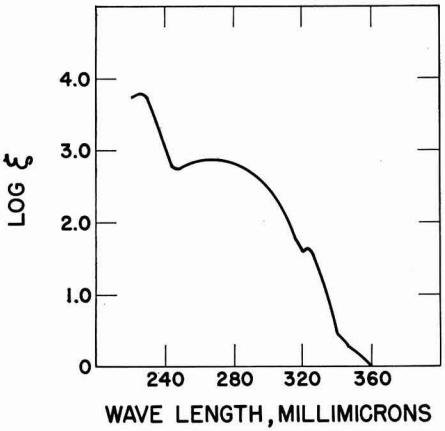

Fig. 2. Ultraviolet spectrum of conventional transformer oil (A) in isooctane, with cell thickness of 1 cm. Spectrum of oil containing metal deactivator (B) is identical. Log molar extinction coefficient (ε) *vs.* wavelength.

from naturally occurring sulfur compounds contained in oil A by the method detailed in the Experimental Section. The concentration of deactivator present in oil B is estimated to be about 100 ppm. Due to difficulties imposed by its low concentration, the exact chemical structure of this deactivator has not yet been determined. The effectiveness of deactivator is indicated in Fig. 3, which shows that deliberately introducing soluble copper does not markedly catalyze the oxidation of oil B, whereas the same quantity of copper grossly degrades oil A. Further evidence for the effectiveness of this deactivator is presented in Fig. 4, showing that a minor amount of oil B will protect oil A from the catalytic effect of soluble copper. These charts are presented simply to show the effectiveness of the deactivator when soluble copper is deliberately added to the oil to accelerate oxidation. In actual use, transformer oil is exposed to metallic copper and, in many cases, to air as well. Therefore, the studies described here were aimed at a better understanding of interactions between oil and metallic copper in the presence of oxygen.

Experimental

Generation of deactivator in situ.—Transformer oil A is obtained from a naphthenic distillate stock by treating the stock conventionally with sulfuric acid and

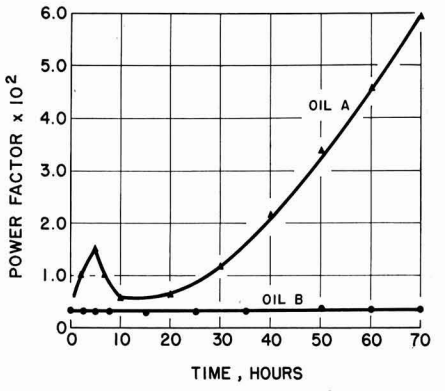

Fig. 3. Effect of 0.5 ppm Cu^{+2} and air on the power factor of conventional transformer oil (A) and oil containing metal deactivator (B) at 95°C.

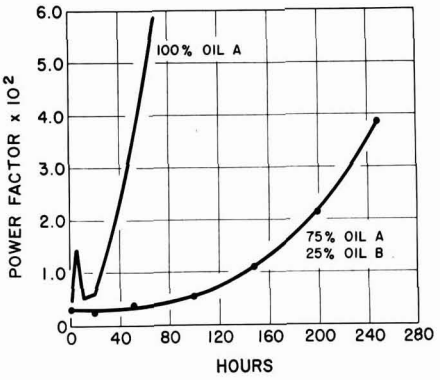

Fig. 4. Effect of 0.5 ppm Cu^{+2} and air on the power factor of blended transformer oils at 95°C.

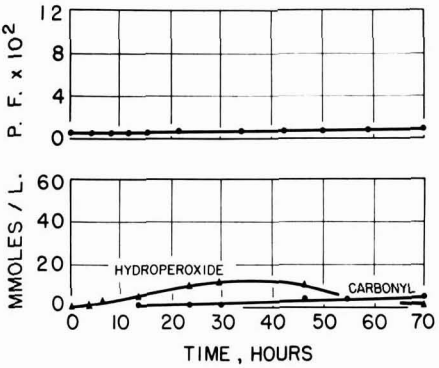

Fig. 5. Air oxidation of conventional transformer oil (A) at 95°C in the absence of copper. Power factor values and oxidation intermediates concentrations vs. time.

adsorptive clay according to procedures widely used in the petroleum industry. When oil A is reacted with sodium isopropoxide, species capable of deactivating copper are generated in very low concentrations (~100 ppm). Specifically, the deactivated oil, oil B, is typically obtained by the following laboratory procedure.

A 1-liter Morton flask, equipped with thermometer, high-speed stirrer, reflux condenser, and gas inlet tube, containing 500 mls oil A and 2.3g sodium, is heated to 110°C under nitrogen with vigorous agitation in order to disperse the sodium. The contents are cooled to room temperature and 7g anhydrous isopropanol are added. The oil and sodium isopropoxide are reacted at 110°-140°C for 30 min, continuing good agitation. When cooled below 90°C, the contents are added carefully, with agitation, to 1 liter of cold distilled water. The oil phase is separated and thoroughly washed five times with equal volumes of water. After drying at 105°C under vacuum, 14g adsorptive clay are added and slurried with the oil for 20 min at 105°C. The oil is then filtered through paper and finally vacuum filtered through a 0.45μ millipore filter.

Oxidation procedure.—Before oxidation, each oil is refiltered through a 0.45μ millipore filter, and 250 ml of filtered oil is then preheated in an oven to 95°C. The oil is placed in a thoroughly cleaned test tube 11 x 2½ in. A stainless steel cell, containing two concentric electrodes, is immersed in the oil. This cell has an air capacitance of 47 x 10^{-12} farads or a measured capacitance of 105 x 10^{-12} farads using material of dielectric constant of 2.2. A coil containing 100 in. of 0.06 in. diameter copper wire is placed within the cell. An air delivery tube extends to the bottom of the oil, through the copper coil. The test tube containing the oil, electrodes, copper coil, and air delivery tube is immersed in a constant temperature oil bath maintained at 95° ± 1°C. Air is supplied to the oil according to the specifications of ASTM D1904. Once each hour, the d-c conductivity of the oxidizing oil is measured, amplified using a L&N #98360A amplifier and recorded using a Varian G-10 recorder. Current is allowed to flow only 5-6 sec each hour. Using an applied voltage of 2.7v from standard mercury cells and the measured current, the resistance of the oil is calculated from Ohm's law. The power factor is related to the resistivity through the equation

$$\text{Power factor} = \frac{1}{\sqrt{(2\pi fCR)^2 + 1}}$$

where f equals 60 cycles and C is capacitance (assumed constant).

Periodically during the oxidation, 3 ml aliquots are withdrawn. Using the Sargent XXI polarograph according to the method of Loveland (4), the hydroperoxide content is determined on a 1 ml aliquot from the half-wave potential in the —0.9v region and the carbonyl content measured from the half wave at —1.6v (*vs.* saturated calomel electrode). The copper content of the sample is determined from the remaining 2 ml aliquot, using neutron activation analysis (5).

Results and Discussion

Oxidation in the absence of copper.—Data on the oxidation of oils A and B with air at 95°C in the absence of copper are summarized in Fig. 5 and 6. The figures show that the power factors of the oils during the first 70 hr of oxidation remain low and essentially unchanged, indicative of little oxidative degradation during this period.

Also plotted on the same time scale are the relative concentrations of hydroperoxides and carbonyl compounds, namely, aldehydes and ketones. The rate of appearance of these oxidation intermediates is essentially the same for both oils. Within a few hours hydroperoxide is detected, rising to a maximum concentration of about 10 mmoles per liter and gradually falling to a steady state of about 4 mmoles per liter. Carbonyl compounds show a slow steady rise during this oxidation period.

Results are consistent with a generally accepted free radical autoxidation mechanism, with hydroperoxide as the first isolatable oxidation intermediate. Decomposition of hydroperoxide and subsequent rearrangement and oxidation of its fragments would result in the appearance of aldehydes and ketones, fol-

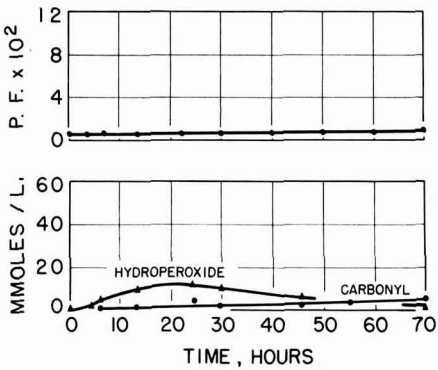

Fig. 6. Air oxidation of oil containing metal deactivator (B) at 95°C in the absence of copper. Power factor values and oxidation intermediates concentrations vs. time.

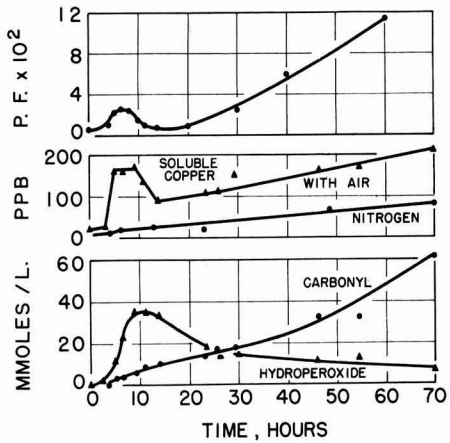

Fig. 7. Air oxidation of conventional transformer oil (A) at 95°C in the presence of metallic copper. Power factor values, parts per billion soluble copper, and oxidation intermediates concentrations vs. time.

lowed finally by the appearance of carboxylic acids. We can also reasonably conclude from the data that both oils, in the absence of copper, oxidize in a similar manner.

Figures 5 and 6 stop at 70 hr; however, if oxidation is continued longer, the power factor curves rise slowly. Although carboxylic acids and alcohols are known to make only small contributions to power factor (6), the parallel rise of power factor and carbonyl content suggests that they are related. Such a relation has not been previously reported, and we have not yet examined it in detail, but it is scheduled for further experimental studies.

Oxidation in the presence of metallic copper.—Power factor, oxidation intermediates, and copper solubility data for the air oxidation of oils A and B in the presence of metallic copper at 95°C are summarized in Fig. 7 and 8. It is immediately obvious that the oxidation of oil A is dramatically catalyzed by copper, whereas oil B is able to resist this copper catalysis.

Oxidation of oil A.—From a detailed examination of Fig. 7 the following observations are made:

1. Oxidative degradation of oil A is rapidly catalyzed by copper although the soluble copper content is less than 200 parts per billion (ppb) for most of the test period.

2. The power factor curve of the oxidizing oil exhibits a peak at 7 hr after which it falls nearly to its initial value before beginning a steady rise.

3. The copper content also rises to a peak between 5 and 10 hr, then drops before starting a gradual rise. The similarity between the power factor and soluble copper curves suggests that conductive copper in solution may affect power factor, particularly in the peak area. This copper solubility data is in sharp contrast to the copper solubility observed when the oil is maintained under nitrogen (Fig. 7). In this case, copper dissolves very slowly over a long period of time, never reaching the level of solubility obtained under oxidizing conditions. The power factor under nitrogen (not shown in Fig. 7) is low and flat over the entire test period.

4. The maximum hydroperoxide content of oil A during copper-catalyzed oxidation is about 3½ times greater than during the noncatalyzed oxidation (Fig. 5). It is interesting to note that maximum hydroperoxide content is achieved after the maximum amount of copper has entered solution, strongly supporting the hypothesis that soluble copper acts catalytically to accelerate hydroperoxide formation. From a comparison of the power factor and hydroperoxide curves, it is evident that hydroperoxides themselves make only a small contribution to the observed power factor.

5. The carbonyl content of the catalyzed oxidation becomes appreciable early in the oxidation and rises rapidly, greatly exceeding the carbonyl content of the uncatalyzed oxidation (Fig. 5) throughout the entire oxidation period, again indicating gross degradation of the oil.

The data are again consistent with a typical free radical chain autoxidation mechanism, catalyzed by soluble copper. The hydroperoxide and carbonyl curves are those that would be expected from such a mechanism. The copper solubility results summarized in Fig. 7 were somewhat unexpected and their interpretation warrants further discussion.

It is interesting to speculate on the nature of the processes occurring during the copper catalyzed oxidation of oil A at 95°C. This oil carried in it, before oxidation, 10-20 ppb soluble copper. Although processes initiating oxidation have received little attention and are not well understood, the initially contained soluble copper may be capable of initiating free radical chains according to previously proposed schemes (7). Once started, the first isolatable product of the oxidation will be hydroperoxides. It has been proposed that reaction of peroxides with metallic copper results in the solubilization of copper (8). It is generally accepted that copper forms an oxide film when exposed to oxygen (9, 10). It has recently been shown that at temperatures in the vicinity of 100°C, copper will form an oxide film having the unusual stoichiometry of $CuO_{0.67}$ (11). This film presumably is a gross defect structure of cuprous oxide. We propose, therefore, that solubilization of copper results from the reaction of hydroperoxide with this oxide film, which for simplicity we will simply consider as cuprous oxide as depicted in Eq. [1]. Possible disproportionation to the cupric salt is depicted in Eq. [2]

$$2ROOH + Cu_2O \rightarrow 2Cu^{+}(O_2R)^{-} + H_2O \qquad [1]$$

$$2Cu^{+}(O_2R)^{-} \rightleftharpoons Cu + Cu^{+2}(O_2R)_2 \qquad [2]$$

Metal salts of hydroperoxides, as proposed in reaction [1], are prepared by reaction of an appropriate metal oxide with hydroperoxide (12). The limited solubility of these salts in hydrocarbon media would depend on the nature of R, the ionic character of the salt, and any further organic material associated or complexed with it. From the coincidence of the power factor and copper solubility peaks of Fig. 7, it seems reasonable to conclude that the power factor peak observed at 7 hr is due largely to the conductivity of soluble copper.

For simplicity we have designated the first isolatable oxidation intermediate simply as hydroperoxide, ROOH. We do not imply that this is simply a hydroperoxide derived from a strictly hydrocarbon precursor. On the contrary, independent evidence indicates that sulfur and/or nitrogen containing organic compounds in the oil are the first to hydroperoxidize and it is these materials which we suspect tend to solubilize copper through reaction [1].

With the soluble copper present in solution, the typical catalytic reactions of metal ions with hydroperoxide would be expected according to Eq. [3] and [4], resulting in the formation of new chains and the appearance of carbonyl compounds from well-known reaction sequences (13).

$$ROOH + Cu^{+2} \rightarrow Cu^{+1} + H^{+} + RO_2\cdot \qquad [3]$$

$$ROOH + Cu^{+1} \rightarrow Cu^{+2} + OH^{-} + RO\cdot \qquad [4]$$

In addition, the postulated copper salts would be expected to be unstable (14) and may decompose by Eq. [5] or [6].

$$Cu^{+}(O_2R)^{-} \rightarrow CuO + RO\cdot \qquad [5]$$

$$Cu^{+2}(O_2R)^{-}{}_2 \rightarrow CuO + RO\cdot + RO_2\cdot \qquad [6]$$

Consequences resulting from Eq. [5] and [6] would be initiation of new chains with subsequent appearance of hydroperoxides, alcohols, and carbonyl compounds, and a mechanism for removal of soluble copper from solution.

Alternate explanations for the observed net decrease in copper content (Fig. 7) are found in known reactions of hydroperoxides and their salts (15). Thus, hydroperoxide is known to react with its salt to produce an alcohol. Using the cuprous salt as an example, the reaction is summarized in Eq. [7].

$$Cu(O_2R) + ROOH \rightarrow ROH + O_2 + CuOR \quad [7]$$

Alternatively, primary and secondary alcohols are known to react with hydroperoxide salts according to Eq. [8].

$$Cu(O_2R) + RCH_2OH \rightarrow CuOH + ROH + R\text{-}CHO \quad [8]$$

The copper hydroxide produced would not be soluble in hydrocarbon media. The polar alcohol and carbonyl compounds produced via Eq. [7] and [8] or from the free radical chain autoxidation would be adsorbable on the copper oxide surface film, thus decreasing the rate of copper solubilization by reaction [1]. Eventually copper removal by Eq. [5], [6], or [8] predominates, resulting in a net decrease of soluble copper.

Although the experimental data clearly indicate a decrease in soluble copper content, visually we do not see any dispersed insoluble material, no doubt due to the extremely low concentration of soluble copper. The oxidizing oil and the aliquots withdrawn from it are perfectly clear. We do, however, observe the formation of varnish colored deposits on the copper coil and on the electrodes, after prolonged oxidation. The nature of these deposits was not investigated due to the minute quantities involved.

After passing through a minimum at about 14 hr, the copper content starts to rise again, probably due to the known solubilizing tendencies of carbonyl compounds and carboxylic acids (16).

Oxidation of oil B.—Oxidation data for oil B in the presence of copper, summarized in Fig. 8, is markedly different from oil A, since oil B contains material capable of reducing, but not completely eliminating, catalysis by copper. The oxidation is characterized by the following:

1. The power factor curve exhibits no peak early in the oxidation and rises only slightly over the entire oxidation period.

2. Oil B dissolves less copper than oil A. At equilibrium, oil B dissolves approximately 50 ppb soluble copper. Significantly, the copper concentration curve does not peak early in the oxidation, in good agreement with the lack of peak noted for the power factor curve.

3. The hydroperoxide curve approximates that found for oil B in the absence of copper. The carbonyl content is several times greater than that observed without copper, but still substantially less than that observed in oil A.

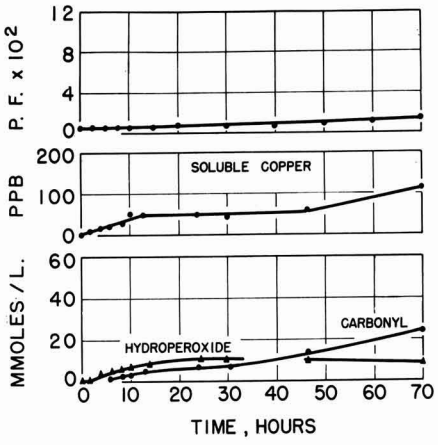

Fig. 8. Air oxidation of oil containing metal deactivator (B) at 95°C in the presence of metallic copper. Power factor values, parts per billion soluble copper, and oxidation intermediates concentrations vs. time.

The results clearly demonstrate that the catalytic effects of copper have been sharply reduced, but not completely eliminated. A striking difference is noted in the abilities of oils A and B to solubilize copper under oxidizing conditions. Oil B dissolves substantially less copper than oil A, although oil B oxidizes to produce appreciable hydroperoxide early in the oxidation. In fact, oil B after 4 hr of oxidation contains enough hydroperoxide to dissolve at least 70 ppm copper. Why then, if our postulated solubilization mechanism between hydroperoxide and copper oxide film is correct, does not more copper dissolve? A reasonable explanation is simply that the polar metal deactivator is adsorbed on the copper oxide surface, thus decreasing the solubilization of copper by Eq. [1]. Copper contained in solution, although at low concentrations, is capable of exerting some catalytic activity as evidenced by the increased carbonyl content over oxidation conducted in the absence of copper.

Therefore, based on this study, the function of metal deactivator appears to be twofold: (*a*) to coat the copper oxide surface and thus decrease the quantity of copper solubilized, and (*b*) to decrease the catalytic activity of solubilized copper, presumably by chelation.

Summary and Conclusions

This study of the processes occurring during the early hours of transformer oil oxidations has indicated that the oxidation rate of similar oils is slow and almost identical in the absence of copper, even though one contains metal deactivator. Dielectric loss, as measured by power factor, seems to be related to the carbonyl content of the oil in these cases.

The situation in the presence of copper is quite different. The oil without deactivator is rapidly degraded in the presence of metallic copper. The solubiltiy of copper rises quickly during the early hours of oxidation to a peak concentration of 170 ppb. The coincidence of this soluble copper peak and the observed power factor peak strongly suggests that copper enters solution in a conductive form contributing to power factor losses in the early stages of the oxidation. A mechanism of copper solubilization has been proposed, involving reaction of hydroperoxide derived from nitrogen and/or sulfur containing impurities in the oil, and a copper oxide surface film. The catalytic effect of the soluble copper is clearly demonstrated from the rate of appearance and concentration levels of hydroperoxide and carbonyl compounds.

In the presence of copper, a metal deactivator is very effective in preserving the oil. The quantity of copper dissolved is less, the rate of appearance and concentration of oxidation intermediates is also less. A twofold effect for the metal deactivator is apparent; namely, a coating effect on the metal which decreases copper solubilization and a decrease of catalytic activity of the soluble copper due to chelation.

Continuous power factor measurements have interesting but largely unexploited potential for following the oxidation of organic substances. Further fundamental work on factors contributing to observed power factor is needed to extend its usefulness. Particularly, quantitative correlations of power factor with oxidation intermediates and with valence and nature of soluble metal species are needed.

Finally, the present study emphasizes the effect of truly trace quantities of copper. The quantitative aspects of this effect could not have been appreciated were it not for the advent of neutron activation anal-

ysis, a superb tool for this and other trace element studies. It is hoped that this and later studies will contribute not only to a better understanding of oil oxidation as catalyzed by copper but to eventual significant improvement in the useful life of electrical oils.

Acknowledgments

The authors wish to acknowledge Mr. G. R. Dimeler and Mr. I. H. Johnson for their helpful assistance in polarographic analyses and power factor determinations, respectively.

Manuscript received Aug. 20, 1964. This paper was presented at the Toronto Meeting, May 3-7, 1964.

Any discussion of this paper will appear in a Discussion Section to be published in the December 1965 JOURNAL.

REFERENCES

1. F. Morton and R. T. T. Bell, *J. Inst. Petrol.*, **44**, 268 (1958).
2. C. N. Thompson, *ibid.*, **44**, 295 (1958).
3. J. C. Wood-Mallock, H. Steiner, and L. G. Wood, *ibid.*, **44**, 320 (1958).
4. J. W. Loveland, G. R. Dimeler, L. G. Bostwick, and L. J. Cali, *Proc. A.P.I., Div. of Refining*, **40**, 410 (1960).
5. R. W. King, C. C. Cerrato, and J. J. Melchiore, *29th Meeting of A.P.I., Div. of Refining*, May 12, 1964, Preprint No. 25-64.
6. A. R. Von Hippell, "Dielectric Materials and Applications," Chapter on Liquid Dielectrics, p. 16, John Wiley & Sons, New York (1954).
7. W. O. Lundberg, "Autoxidation and Antioxidants," Vol. 1, chapter by N. Uri, "Physico-Chemical Aspects of Autoxidation," pp. 95-99, John Wiley & Sons, New York (1961).
8. E. D. Eich, G. Fieck, and W. F. Olds, Paper presented at the Philadelphia Meeting of this Society, May 3-7 (1959).
9. U. R. Evans, "Corrosion and Oxidation of Metals," p. 32, Edward Arnold Publishers, London (1960).
10. L. Young, "Anodic Oxide Films," p. 308, Academic Press, London (1961).
11. H. Wieder and A. W. Czanderna, *J. Phys. Chem.*, **66**, 816 (1962).
12. A. G. Davies, "Organic Peroxides," Butterworth & Co., London (1961).
13. C. Walling, "Free Radicals in Solution," p. 445, John Wiley & Sons, New York (1957).
14. E. G. E. Hawkins, "Organic Peroxides," p. 11, F. F. Spon Ltd., London (1961).
15. A. G. Davies, *loc. cit.*, p. 187.
16. J. C. Bailar, "Chemistry of the Coordination Compounds," pp. 41-45, Reinhold Publishing Co., New York (1956).

Growth Mechanism of Thin Anodic Oxide Films on Tantalum

I. Self-Anodization Using an External Load Resistor

R. Dreiner, K. Lehovec, and J. Schimmel

Research Laboratories, Sprague Electric Company, North Adams, Massachusetts

ABSTRACT

The growth of an anodic oxide film on tantalum metal immersed in diluted sulfuric acid has been investigated using potential and capacitance measurements. The tantalum metal was connected through an external resistance to a platinum electrode in the electrolyte. An analysis of voltage *vs.* time confirms the exponential field dependence of the ionic current for the later phases of oxide growth. Analysis of current (I) *vs.* time (t) measurements provides BF_0 and λF_0 where B is the field coefficient,[1] F_0 is the initial field in the oxide, and λ is the growth rate per unit current, provided that the emf of the reaction, E, is known. E can be determined by matching the B-values derived from I *vs.* t to those derived from capacitance measurements. For sufficiently thin oxide films the growth rate exceeds the value expected from Faraday's law based on the external current which indicates the presence of internal electron currents for which the empirical expression

$$I_E = I_{E^0}\, e^{-d/l}$$

with $I_{E^0} \sim 3 \times 10^{-4}$ amp/cm^2 and $l \sim 3.0$Å, was obtained. There are indications that either the inverse Tafel slope, B, or the emf, E, varies with film thickness in the range where the internal electron current is appreciable.

It has been found (1) that the ionic current promoting the growth of anodic oxide layers depends exponentially on the field across the oxide. Determination of the constants involved in this relation usually requires the measurement of the oxide thickness by such techniques as capacitance-, optical-, or weight-measurement.

We have explored the applicability of the exponential field law for very thin anodic oxide films on tantalum. Since the determination of the oxide thickness becomes increasingly difficult the thinner the oxide film, a method was used which does not involve thickness measurements, namely, the analysis of the time dependence of the external current through a resistor connecting Ta and Pt electrodes in an electrolyte. This current arises from the electromotive force of the reaction of Ta with water and decreases with time as the oxide grows on the tantalum.

This general procedure of analysis could be applied also to cases where an external power source is placed in series with the external resistor. However, in order to investigate the growth of thin oxide films we must limit the external current to fairly small values to obtain a slow growth rate. Initially the oxide resistance is very low so that the current is limited by the external resistor. In this range the current *vs.* time relation is not sensitive to the oxide resistance. In order to investigate the properties of thin oxide films we must reduce the external resistor as much as possible which is incompatible with the former condition of a fairly small current if a large external voltage were employed. For this reason we have not applied an external voltage and have studied in detail the growth of thin anodic films by means of the emf associated with the formation of Ta_2O_5 (so-called self-anodization).

We have compared the experimental time dependence of the external current with a theoretical equation based on well-known relations valid for thick oxide films, but not necessarily applicable to the thin oxide films here investigated. By this comparison the numerical values of certain parameters for thin oxide films were determined and the following anomalies were discovered:

[1] Sometimes referred to as "inverse Tafel slope."

1. The presence of electron currents through the oxide which govern the growth of sufficiently thin oxide films, and
2. Some time or thickness dependence of the "emf" or of the "inverse Tafel slope" for the ionic current.

These anomalies have then been investigated in more detail using capacitance measurements.

Experimental Procedure

Tantalum foil of 99.9% purity supplied by Fansteel was degreased, chemically polished, leached in boiling deionized water for 10 min, "vacuum" annealed at pressures less than 10^{-4} Torr at 2100°C for 30 min, etched in hydrofluoric acid, briefly rinsed in deionized water, and immediately inserted in 0.1% (by weight) aqueous sulfuric acid at room temperature. The sample had a narrow neck extending out of the H_2SO_4 solution to provide an electric contact. The macroscopic contact area with the electrolyte was 18.8 cm^2. The tantalum was connected through a load resistor, R_L, to a platinum electrode immersed into the electrolyte, and the current through the load resistor was measured as a function of time. Resistors of 10^3 ohms were used to investigate the current decay over many orders of magnitudes within a reasonable time, *i.e.*, about one day. Resistors of 10^5 ohms were used when emphasis was placed on the capacitance measurements during the initial phase of oxide growth. The external resistors were large with respect to the electrolyte resistance so that the potential drop across the electrolyte could be neglected.

The voltage between the platinum electrode and the electrolyte (during a run) was monitored by using a saturated calomel electrode in the electrolyte. Except during the initial few seconds, no significant variation in polarization was observed. The voltage was about 0.6v with the platinum (Pt) positive with respect to calomel.

The initial voltage across the resistor was about 1v (tantalum negative) for freshly etched foils.

The equivalent series capacitance of the cell was measured at 1000 cps with a General Radio impedance comparator and a recorder. This permitted the continuous recording of the capacitance with time. The equivalent series resistance observed was approximately 50 ohms which agreed reasonably well with the specific resistivity of the electrolyte and the geometry of the electrolyte cell. From this capacitance an "oxide thickness," d^*, was derived by

$$d^* = S\epsilon\epsilon_0/C \qquad [1]$$

where S is the area, and ϵ is the dielectric constant of tantalum oxide. This procedure ignores capacitances of space charge layers in the electrolyte adjacent to the platinum and adjacent to the tantalum oxide. By investigating the equivalent series capacitances of gold *vs.* gold and gold *vs.* platinum in the electrolyte, we have found that the capacitance for the platinum electrode could indeed be ignored. The solution double layer capacitance adjacent to the tantalum oxide should remain fairly constant during the oxide growth, so that the true oxide thickness would be smaller than the oxide thickness, d^*, by a constant amount, Λ. The equivalent series capacitance of the arrangement Au-electrolyte-Au was found to be $C_S = 2.4\ \mu F/cm^2$.[2] If the solution double layer capacitance adjacent to the tantalum oxide were the same as that adjacent to gold, we would have $\Lambda = S\cdot\epsilon\cdot\epsilon_0/2C_S = 5.1$Å.

Since the capacitance depends somewhat on frequency, the significance of an "oxide thickness" as derived by Eq. [1] for capacitance measurements at the frequency of 1000 cps may be questioned. It has been observed on niobium oxide (3) that the frequency dependence between 60 cps and 8 kcps is the same for various oxide films of thicknesses ranging from a few tens of angstroms to several 1000 angstroms. If this is the case in our films, the correction factor for converting the apparent thickness (*i.e.*, that of Eq. [1], as calculated from C at 1000 cps) to the true thickness should be the same for all values of d, and the frequency dependence of the capacitance may be taken into account by a corresponding frequency dependence of the dielectric constant. When using the capacitance value at 1000 cps in Eq. [1], we must then use the dielectric constant at 1000 cps which was determined by Young (4) to be $\epsilon = 27.6$ based on the density $\rho = 7.93$.

[2] The equivalent series resistance per double layer Au/electrolyte was 20 ohms/1 cm^2 area.

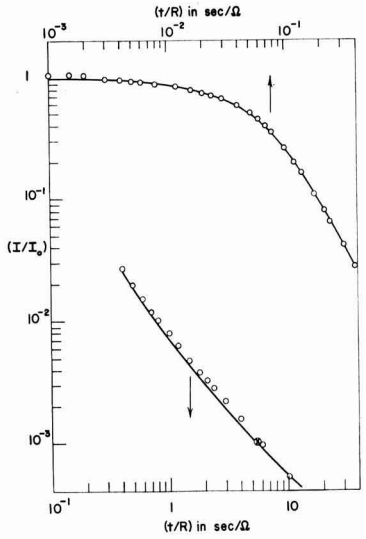

Fig. 1. Current decay during self-anodization of tantalum of area $S = 18.8\ cm^2$ in 0.1% aqueous H_2SO_4. Tantalum connected to a platinum electrode through a resistor R = 1000 ohms. Experimental points; Theoretical curve by Eq. [2] matched to the experimental points by using the following parameters: $I_o = 1.1$ ma, $E = 1.83$v, $BF_o = 35.6$, $\lambda F_o = 13.75$ v/coul.

Analysis of Current Density during Oxide Growth

Figure 1 shows the dependence of the current, I, in the external circuit on time. The ordinate is the ratio of the observed current to an extrapolated initial current, I_o, which was obtained by a procedure to be described later. The theoretical curve drawn represents the equation

$$\lambda F_o t/R = \left(1-\frac{1}{BF_o}\right)\ln\frac{I_o}{I} + \frac{E}{RI_o}\,\frac{BF_o}{[BF_o-\ln(I_o/I)]^2}\left(\frac{I_o}{I}-1\right) \qquad [2]$$

which follows from the accepted field dependence of the ionic current density

$$I_I = A\,e^{BF} \qquad [3]$$

with

$$F = (E-RI)/d \qquad [4]$$

and from Faraday's law

$$\frac{\partial d}{\partial t} = \lambda\cdot I_I \qquad [5]$$

with the ionic current I_I equal to the current, I, in the external resistor

$$I_I = I \qquad [6]$$

Equation [2] was derived as follows: Substitute d of Eq. [4] into [5], and replace $\frac{\partial F}{\partial t}$ by $\frac{1}{BI}\frac{\partial I}{\partial t}$ using [3] and [6] to obtain

$$\lambda I = \left[-\frac{R}{F}\left(1-\frac{1}{BF}\right) - \frac{E}{BF^2 I} \right] \frac{\partial I}{\partial t} \qquad [7]$$

Since F changes quite slowly (logarithmically) with I according to [3], we may treat F in Eq. [7] as a constant when integrating to obtain

$$\lambda t/R = \frac{1}{\bar{F}}\left(1-\frac{1}{B\bar{F}}\right)\ln\frac{I_o}{I} + \frac{E}{RI_o}\frac{1}{B\bar{F}^2}\left(\frac{I_o}{I}-1\right) \qquad [8]$$

where $\bar{F}$ is a suitable average value of F over the integration interval $0 \leq \tau \leq t$. Equation [2] was obtained by using the terminal value

$$F_{\tau=t} = F_o\left(1+\frac{1}{BF_o}\right)\ln\frac{I_{\tau=t}}{I_o} \qquad [9]$$

for $\bar{F}$ in the second term on the right of Eq. [8], since the largest contribution in the integration of Eq. [7] comes from the values near the boundary $\tau \approx t$. In the first term on the right of Eq. [8] $\bar{F}$ can be replaced simply by F_o since this term is important only in the range where $I_\tau \sim I_o$. The error committed by using [9] for $\bar{F}$ is estimated in Appendix I.

For $(I_o/I) - 1 << 1$ one may approximate $\ln (I_o/I) \approx (I_o/I) - 1$, showing that initially the ratio of the second term on the right of Eq. [2] to the first term is $\dfrac{E}{RI_o(BF_o - 1)}$. Since E/RI_o is of the order of unity, but BF_o is about 30, the first term dominates initially. It is interesting to note that the first term arises essentially without the aid of Eq. [3]. If we consider the field F in Eq. [4] as a constant, then it follows from Eq. [5] and [4] that $\lambda Ft/R = \ln I_o/I$ which is very approximately the first term of Eq. [2] since $BF_o >> 1$. Thus good agreement between Eq. [2] and the experimental data in the range $(I_o/I) - 1 << 1$ does not necessarily indicate that Eq. [3] is satisfied.

The second term on the right side of Eq. [2] results from the approximate variation of the field with thickness $F \approx E/d$, which is approached once $RI << E$, in conjunction with the exponential field dependence of the ionic current, Eq. [3], and Faraday's law, Eq. [5]. The second term on the right side of Eq. [2] is also pertinent to the decay of current with time when a constant voltage, V_A, is applied. The emf, E, is then to be replaced by $E + V_A$, and one obtains

$$I = \frac{B(E+V_A)}{[BF_o - \ln(I_o/I)]^2 \lambda t} \qquad [10]$$

Similar forms of the $1/t$-law of current decay during constant voltage formation have been previously derived (5, 6). However, Eq. [10] should be valid only if electron leakage currents through the sample are absent, if Faraday's law (5) and the field dependence (3) of the ionic current are fulfilled, and if there is no field distortion by space charges in the oxide.

Figure 2 shows a plot of $I(t)$ on a semilogarithmic scale. The straight line fits the experimental data well in the range $0.6 \lesssim RI \lesssim 1.05$v, *i.e.*, 400 sec $< t \lesssim$ 4500 sec. Such a straight line relationship is expected from Eq. [2]. Deviations of the experimental points from the straight line for $t \gtrsim 4500$ sec are expected due to the second term on the right side of Eq. [2]. The deviations of the experimental data from the straight line for $t \lesssim 30$ sec indicate that one or several of the Eq. [4]-[6] are not satisfied in this range. This will be discussed in more detail in conjunction with the capacitance measurements. Extrapolation of the straight line to $t = 0$ yields I_o, while its slope, according to Eq. [2] is

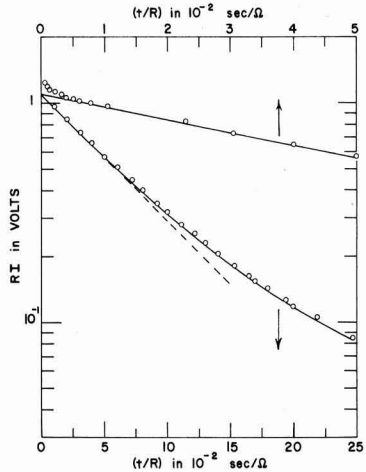

Fig. 2. Current decay during self-anodization of tantalum of area 18.8 cm² in aqueous 0.1% H_2SO_4 with $R = 10^5$ ohm connecting the tantalum to a Pt electrode. The straight line approximation provides $I_o = 1.1 \times 10^{-5}$ amps and $(\lambda F_o)^\circ = 13.2$ v/coul. Experimental points; —— theoretical curve Eq. [2] with $I_o = 1.1 \times 10^{-5}$ amp, $E = 1.83$v, $BF_o = 30.75$, $\lambda F_o = 13.48$ v/coul.

$$\left(\frac{\partial \ln (I_o/I)}{\partial\, t/R}\right)_{t\to 0} = \frac{\lambda F_o}{1 + \dfrac{(E/RI_o) - 1}{BF_o}} \equiv (\lambda F_o)^\circ \qquad [11]$$

As seen from Fig. 1, Eq. [2] fits well the entire range of experimental data $I(t)$ except for the initial range, as already mentioned. The constants BF_o and λF_o required to calculate the theoretical curve in Fig. 1 have been determined by matching the theoretical curve to the experimental data using the procedure described in Appendix 2.

Numerical values for BF_o and λF_o for four samples are listed in Table I, based on the value $E = 1.83$v. The value $E = 1.83$v was selected by comparing data of BF_o and λF_o derived from $I(t)$ with those derived from the capacitance measurements to be discussed in the next section. The values of λF_o differ very little among the four samples. The variation in BF_o is somewhat larger, which suggests that either B differs among various samples or that E might vary. The latter is not impossible considering that E in Eq. [4] is not only the emf but may include some contact potential.

Table I. Evaluation of the current *vs.* time relationship for self-anodization of tantalum oxide, assuming $E = 1.83$v

Sample	R, ohms	RI_o, v	BF_o	λF_o, v/coul	B/λ, farads	B^*, 10^{-6} cm/v	A^{**}, amp
1/21/63	10^6	1.1	35.6	13.75	2.59	8.03	3.8×10^{-19}
II	10^5	1.1	30.75	13.48†	2.28	7.07	4.9×10^{-19}
I	10^5	0.87	23.9	14.23	1.68	5.21	3.6×10^{-16}
1/16/63‡	10^4	0.45	27.1	14.02	1.93	5.98	7.6×10^{-17}

* Using $\lambda = 3.1 \times 10^{-6}$ cm/coul.
** $A = I_o e^{-BF_o}$.
‡ Sample remained unetched following the vacuum anneal.
† $\lambda F_o = 13.2$ using Eq. [11] and taking the denominator to equal 1.

Table II. Dependence of BF_o and λF_o on the choice of E for sample II

E, v	BF_o	λF_o, v/coul
1.7	20.08	13.45
1.83	30.75	13.48
1.9	31.61	13.50

To indicate the influence of the choice of E on the values of BF_o and λF_o of Table I, we have listed in Table II values of BF_o and λF_o for sample II, which would result from three different values of E.

Inserting the values of I_o and of BF_o into Eq. [3], the pre-exponential factor A has been calculated. These values scatter considerably. However, an error in BF_o by 10% would account for the large deviations of A from the mean value of about 10^{-17} amp.

Time Dependence of Capacitance

The time dependence of capacitance during oxide film growth was measured for the samples I and II listed in Table I. Self-anodization of these samples was carried out with the comparatively large resistance $R = 10^5$ ohm in order to slow down the initial oxidation rate so that fairly accurate capacitance measurements could be made.

As discussed in the previous section, the time dependence of the current is not strongly affected by relation [3] during the initial stages of oxide growth. However, the dependence of current on oxide thickness, obtained from Eq. [3], [4], and [6] is strongly dependent on the field dependence of the ionic current. Using the "apparent film thickness," d^*, derived from capacitance measurements by means of Eq. [1], and the external current, we have derived the field intensity as a function of current by means of Eq. [4] with $d = d^*$. These values are quite sensitive to the choice of the emf, E. In Fig. 3 these curves are plotted pertaining to the values $E = 1.9$, 1.83, and 1.7v, on a greatly expanded ordinate scale. The sample is the same as used for Fig. 2.

In spite of the scatter of the experimental points, three ranges of $F(I)$ are clearly apparent. The boundaries between these ranges correspond to the "apparent thicknesses" of 30 and 42Å, respectively. The middle range (b) becomes less pronounced for increasing E.

Range (a): For $d > 42$Å, the field decreases linearly with the logarithm of current as expected from Eq. [3] with [6]. The straight lines fitting the experimental data of Fig. 3 in this range have slopes from which the values of B[3] (the first line of Table III) have been obtained. Extrapolation to $I = I_o$ of Table I provides F_o, and extrapolation to $F = 0$ provides the pre-exponential factor, A, of Eq. [3]. These values are listed in the second and last lines of Table III.

Comparison of BF_o values of Table III with the values derived from the analysis of $I(t)$ (Table II) shows that fairly good agreement exists for $E = 1.83$v. This value will be adopted, therefore, in the subsequent discussion of sample II. The value $E = 1.83$ has been used also for evaluating the $I(t)$ data of the other samples listed in Table I.

[3] B is defined as $\partial \ln I / \partial F$.

Table III. Evaluation of the straight lines in the region (a) marked in Fig. 3

	$E = 1.7$v	$E = 1.83$v	$E = 1.9$v
B (10^{-6} cm/v)	9.2	7.7	6.8
F_o (10^6 v/ cm)*	3.61	3.94	4.13
BF_o	33.2	30.34	27.85
λF_o (v/coul)**	11.2	12.2	12.8
A (amp)	4.2×10^{-20}	5.1×10^{-19}	1.1×10^{-18}

* F_o is F extrapolated to $I_o = 1.1 \times 10^{-5}$Å.
** Using $\lambda = 3.1 \times 10^{-6}$ cm/coul.

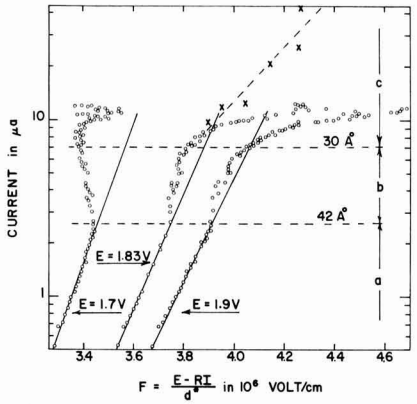

Fig. 3. Field intensity as a function of current, derived by Eq. [4] from current and capacitance measurements during self-anodization assuming three values of E. Values of Table III were derived from the straight line approximations in range (a).

Range (b): In the range corresponding to thickness between 30 and 42Å, the field derived by Eq. [4] changes much more slowly with current (*i.e.*, with time and thickness) than in the range (a).

Range (c): In the range $d \lesssim 30$Å, the field rises quite steeply with the external current.

It is obvious that for $d \lesssim 42$Å, at least one of the Eq. [3] to [6] ceases to be valid or, respectively, the parameters A, B, E, or λ in these equations are not constants but depend on t or d. For instance, the "emf" in this range might be a function of thickness or current density. Or else, the parameters A and B in Eq. [4] might not be constant; *e.g.*, B in the region (b) might be about twice the value in region (a). The region (c) could be explained by an ionic current which is much larger than the external electronic current due to internal flow of electrons so that Eq. [6] becomes invalid. Evidence for this interpretation of the region (c) will be discussed shortly. Lack of validity of Eq. [3] for $d \lesssim 42$Å should not significantly affect Eq. [2] since in the corresponding current range ($I \gtrsim 2 \cdot 10^{-6}$ amp), the condition $I > I_o/BF_o \approx 4 \times 10^{-7}$ amp prevails.

Using the external current, I, and the thickness, d^*, derived from capacitance by means of Eq. [1], we have calculated the "apparent growth efficiency"; *i.e.*, the growth efficiency based on the external current

$$\lambda^* = \frac{1}{I} \cdot \frac{\partial d^*}{\partial t} \qquad [12]$$

These values are plotted in Fig. 4 *vs.* oxide thickness. For thicknesses between 32.5 and 50Å, the average apparent growth efficiency was $\lambda^* = 3.2 \times 10^{-6}$ cm/coul. For smaller thicknesses, the apparent growth efficiency increases with decreasing current. Qualitatively, this accounts for the discrepancies between Eq. [2] and the experimental data in the range $t/R \lesssim 5 \times 10^{-3}$ sec/ohm of Fig. 2. For a given I and t, I_o of Eq. [2] would increase with an increase in λ.

The value $\lambda^*_\infty = 3.2 \times 10^{-6}$ cm/coul, approached by the apparent growth efficiency, λ^*, for $d^* \gtrsim 32.5$Å, is in reasonable agreement with the theoretical value $\lambda = \dfrac{M}{F \cdot \rho \cdot S \cdot 2z} = 3.1 \times 10^{-6}$ cm/coul, where the molecular weight of Ta_2O_5 $M = 442$, the Faraday constant $F = 96{,}500$ coul/g·equivalent, the density $\rho = 7.93$ g/cm^3, and the area $S = 18.8$ cm^2 have been used.

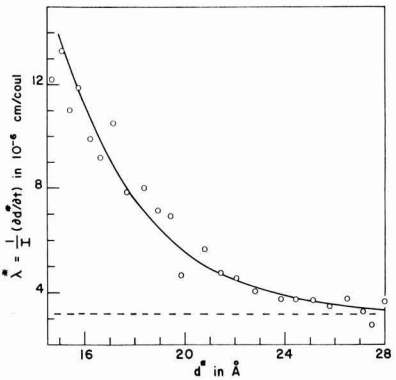

Fig. 4. Apparent current efficiency, λ^*; *i.e.*, current efficiency based on the external current, for oxide growth during self-anodization. Experimental points and theoretical curve from Eq. [13] with [14], assuming $I_E{}^o = 6.0 \times 10^{-3}$ amp, $l = 3.0$Å and $\lambda_\infty = 3.2 \times 10^{-6}$ cm/coul.

The fact that the apparent growth efficiency for $d^* \lesssim 32$Å exceeds significantly the value $\lambda = 3.1 \times 10^{-6}$ cm/coul can be explained by assuming that electrons flow through the oxide film together with the five-valent tantalum ions. This transfer may take place as an ionic current of tantalum ions of valency less than five (*i.e.*, one or several electrons attached to a five-valent ion), or else by electrons flowing through the oxide film unattached to tantalum ions.

Flow of a significant internal electron current, rather than transport by lower-valency tantalum ion, is indicated by the fact that the oxide also grows under open circuit conditions.[4] Considering the range of film thickness with which we are dealing, electron transfer is likely to occur by tunneling. Thus we shall refer to the electron current through the oxide tentatively as the tunnel current, I_E. The tunnel current has been obtained from

$$I_E = I \cdot \left(\frac{\lambda^*}{\lambda^*_\infty} - 1 \right) \qquad [13]$$

The full line drawn in Fig. 4 was calculated from [13] assuming an exponential dependence of tunnel current on thickness

$$I_E = I_E{}^o \, e^{-d/l} \qquad [14]$$

with $I_E{}^o = 6.0 \times 10^{-3}$ amp, $l = 3.0$Å and $\lambda = 3.2 \times 10^{-6}$ cm/coul. The data of Fig. 4 have been used to calculate the total ionic current, $I + I_E$ by means of Eq. [13]. If this total current would have been used as abscissa in Fig. 3 instead of the external current I, the points in the region (c) of the curve would have shifted to the left as indicated by the crosses for the case $E = 1.83$v. Thus correcting for the tunnel current removes much of the steep rise of the curves shown in Fig. 3 in the region (c).

However, the B-value derived by Eq. [3] for the range (c) in Fig. 3, after correction for the tunnel current, still remains significantly lower ($B \approx 3.3 \times 10^{-6}$ cm/v) than that in the region (a) ($B \approx 7.7 \times 10^{-6}$ cm/v).

Instead of the interpretation in terms of a constant E and a variable B, one might postulate a constant B [equal to that in region (a)] and a variable E, in the regions (b) and (c) which would be determined by the intersect of curves $E =$ const. with the extrapolated curve from the region (a). Assuming that $E = 1.83$v in the region (a), the E values would be higher in region (b) but lower in region (c). The changes in E required would be less than 0.1v.

[4] This will be the subject of the next paper in this series.

Discussion

The following discussion concerns mainly the validity of some of the basic equations used and the interpretation of certain parameters occurring in them.

Equation [4] expresses the electric field in the oxide in terms of the emf of the chemical reaction, E, the external voltage drop, RI, and the oxide thickness, d. Equation [4] implies that the electrical field is space independent throughout the oxide, *i.e.*, space charges are neglected. Actually, E is not only the emf of the reaction

$$2Ta + 5H_2O = Ta_2O_5 + 5H_2 \qquad [15]$$

but may include also electrostatic potentials which might exist between the metal and the electrolyte interface in analogy to the contact potential between two solids. This contact potential should be a function of surface states at the oxide-electrolyte interface as might arise from adsorbed ions. Thus E in Eq. [4] is not necessarily the true emf of chemical reaction [15], and its magnitude might change with current density and time during growth, contrary to the assumption of a constant E used in deriving Eq. [2] and the data of Fig. 3. Furthermore E might differ for different samples. The agreement between the value $E \sim 1.83$v derived from the experimental data with the theoretical emf 1.79v [Ta *vs.* Pt equal to Ta *vs.* $H_2 = 0.81$ (2) plus H_2 *vs.* Pt $= 0.98$] is therefore surprising.

Equation [3] contains also the tacit assumption that there is no overpotential during film growth across the space charge layer in the electrolyte adjacent to the oxide. In general, a fraction of the external potential RI might be required to modify the potential across this space charge layer when current flows, and only the remaining portion of RI would modify the field across the oxide.

We have already discussed the difficulties arising from the possible capacitance of the electrolyte space charge layer adjacent to the oxide for the determination of the true oxide thickness. Because of this difficulty the apparent oxide thickness d^* determined by Eq. [1] from capacitance measurements contains an unknown additive constant, Λ, the true oxide thickness being $d = d^* - \Lambda$. This constant, Λ, has been ignored in Fig. 3. The constant Λ has no effect on the effective growth efficiency λ^* of Fig. 4, and on the tunnel current, Eq. [14], derived from λ^*.

The determination of E by matching BF_o as obtained from $I(t)$ to BF_0 derived from capacitance measurements as shown in Fig. 3 is questionable for the following reasons: (a) if the apparent oxide thickness d^* is corrected by Λ to obtain the true oxide thickness, one has

$$\frac{1}{B_\Lambda F_\Lambda} = \frac{1}{BF} \cdot \frac{F_\Lambda}{F} + \frac{RI_\Lambda}{F\,d^{*2}} \cdot \frac{F_\Lambda}{F} \qquad [16]$$

where B_Λ, F_Λ are the values obtained from the corrected thickness, and B, F are those obtained from the uncorrected thickness ($\Lambda = 0$). The corrected product, $B_\Lambda F_\Lambda$, is smaller than the uncorrected one, since $F\Lambda/F > 1$. Thus the corrected values $B_\Lambda F_\Lambda$ would be less than those of Table III and by matching these corrected values to those of Table II a smaller value of the emf, E, would have been derived. Correcting d^* of Eq. [1] by Λ increases the field F by an amount which is larger for smaller d^*, so that the region (b) of Fig. 3 might be removed, and the region (a) would be enhanced.

For $E = 1.83$ and $\Lambda = 6$Å, region (b) in Fig. 3 would just about vanish. However, in order to match F_o and B from Fig. 3 (modified by $\Lambda = 6$Å) to the values obtained from $I(t)$, the value for the emf would have to be decreased to about 1.60v. Since region (b) becomes more pronounced by decreasing the value of E, the increase in Λ and the decrease in E would partially compensate and the region (b) would reappear. The sensitivity of various parameters to the choice of Λ is illustrated in Table IV. The values of BF_o and λF_o

Table IV. Effect of the correction Λ for the oxide-electrolyte capacitance

Λ, Å	E, v	from $I(t)$				from $C(I)$			
		BF_o	λF_o, v/coul	B, 10^{-6} cm/v	F_o, 10^6 v/cm	BF_o	λF_o, v/coul	B, 10^{-6} cm/v	F_o, 10^6 v/cm
0	1.83	30.75	13.48	7.07	4.35	30.34	12.2	7.7	3.94
4	1.83	30.75	13.48	7.07	4.35	23.2	13.7	5.25	4.42
0	1.69	28.8	13.1	6.8	4.23	33.2	11.2	9.2	3.61
4	1.69	28.8	13.1	6.8	4.23	27.2	12.5	6.75	4.03

as determined from the analysis of $I(t)$ and $C(I)$ agree reasonably well for $\Lambda = 0$, $E = 1.83$ and also for $\Lambda = 4$, $E = 1.69$. However there is a large disagreement in BF_o obtained by the two methods for $\Lambda = 4$, $E = 1.83$ and for $\Lambda = 0$, $E = 1.69$.

The value λF_o of Table II is pertinent to the initial range of the $I(t)$ curve, while the value F_o of Table III is derived by extrapolation of F from the later ranges of current flow to the initial range using relation [3]. If this relation is not valid, as suggested by Fig. 3, the values of λF_o from Tables II and III cannot be expected to coincide.

The value of F_o derived from Table II with $\lambda = 3.1 \times 10^{-6}$ cm/coul should coincide with the F-value of Fig. 3 pertinent to the "initial current range," *i.e.*, the current range where the straight line approximation to the semilogarithmic plot of Fig. 2 is valid.

In view of all these difficulties, the B-values derived from Fig. 3 can be accepted only with great caution.

The B-values for region (a) as given in Table I are in reasonable agreement with those of the literature ($B \sim 5 \times 10^{-6}$ cm v^{-1}) (Young, p. 93).

Conclusions

1. The time dependence of the external current during self-anodization of tantalum in an electrolyte can be used to evaluate the combinations BF_o and λF_o of the "Tafel" slope, $1/B$, the growth efficiency, λ, and the initial field strength, F_o, provided that the emf, E, is known.

2. Combining the current *vs.* time measurements with those of capacitance *vs.* time, the emf, E, and the initial field can be derived. However, this evaluation involves some questionable assumptions.

3. For films of thickness $d \gtrsim 40$Å the values of B and λ agree with those observed for the transport of five-valent tantalum ions.

4. At smaller film thicknesses, the following anomalies occur: (a) An electron current flows through the oxide film of magnitude $I_E{}^o \exp^{-d/l}$ with $I_E{}^o \sim 3 \times 10^{-4}$ amp/cm^2 and $l \approx 3.0$Å. (b) This simulates an effective growth efficiency, *i.e.*, a growth efficiency based on the external current which exceeds the value of Faraday's law for five-valent ions. (c) There is some indication that either the inverse Tafel slope of the ionic current varies in this range or else the emf, E, varies with film thickness.

Manuscript received July 16, 1964. This paper was presented at the Toronto Meeting, May 3-7, 1964.

Any discussion of this paper will appear in a Discussion Section to be published in the December 1965 JOURNAL.

REFERENCES

1. For a summary, see L. Young, "Anodic Oxide Films," Academic Press, London and New York (1961).
2. D. A. Vermilyea, *This Journal*, **101**, 389 (1954).
3. L. Young, *Faraday Soc.*, **51**, 1250 (1955).
4. L. Young, *Proc. Roy. Soc.*, **A244**, 41 (1958).
5. W. Ch. van Geel and H. Emmens, *Z. Phys.*, **87**, 220 (1933).
6. A. Charlesby, *Proc. Phys. Soc.*, **66**, 317 (1953).

APPENDIX 1

Estimate of Error in Eq. [2]

The error committed by using [9] for $\bar{F}$ can be estimated as follows. Since

$$F_{\tau=t} < \bar{F} < F_o \qquad [1.1]$$

we expect the relative error of the true t pertaining to the current I to be smaller than $(t_\tau - t_o)/t_o$ where t_τ is calculated from Eq. [8] using $\bar{F} = F_{\tau=t}$ and t_o is calculated from [8] using $F = F_o$. The error increases with decreasing I, and we shall be concerned, therefore, mainly with the range where the $\ln(I_o/I)$ term in Eq. [2] can be neglected *vs.* the I_o/I-term. Then

$$(t_\tau - t_o)/t_o \approx \frac{2}{BT_{\tau=t}} \cdot [\ln(I_o/I)] \cdot \left[1 + \frac{\ln(I_o/I)}{2BF_{\tau=t}}\right] \qquad [1.2]$$

Since the main contributions at the integration of Eq. [7] come from the I-values near the boundary $I_{\tau=t}$, we expect $F_{\tau=t}$ to be a better approximation to $\bar{F}$ than F_o. Thus the error by inserting [9] for $\bar{F}$ should be somewhat less than

$$(t - t_o)/2t_o \approx \ln(I_o/I)/BF_{\tau=t}) \qquad [1.3]$$

For $I_o/I \approx 10^3$ and $BF_{\tau=t} \approx 25$, the error in t by Eq. [2] should thus be somewhat less than 28%. The error can be bracketed closer by the relation

$$F_{\tau=t} < \bar{F} < F_{\tau=t} + \frac{I - I_{\tau=t}}{BI_{\tau=t}} \qquad [1.4]$$

instead of [1.1] where the right side comes from the development of F as a function of I in the vicinity of $I_{\tau=t}$, $F_{\tau=t}$. For $E/RI_o = 1$, $BF_o = 30$ and $I_o/I = 10^3$, the following values are obtained: $\lambda t_o/BR = 1.33$ from Eq. [8] with $\bar{F} = F_o$; $\lambda t/BR = 2.09$ from Eq. [2]; and $\lambda t/BR = 1.69$ by integrating Eq. [7] with $\bar{F}$ replaced by the value on the right side of the inequality [1.4] prior to the integration. The exact value lies between 1.69 and 2.09.

APPENDIX 2

Determination of BF_o and λF_o by Matching Eq. [2] to Experimental Data $I(t)$

From a semilogarithmic plot as shown in Fig. 2, I_o and $(\lambda F_o)^o$ are obtained. Rearranging Eq. [2]

$$BF_o = 2\ln(I_o/I) - \frac{[\ln(I_o/I)]^2}{BF_o} + \frac{\dfrac{E}{RI_o}\left(\dfrac{I_o}{I} - 1\right)}{\dfrac{(\lambda F_o)^o}{R} t\left[1 + \left(\dfrac{E}{RI_o} - 1\right)/BF_o\right] - \left(1 - \dfrac{1}{BF_o}\right)\ln(I_o/I)} \qquad [2.1]$$

with $(\lambda F_o)^o$ defined by Eq. [11]. This form is convenient for calculating BF_o from a single experimental point of $I(t)$ in the range where the second term on the right side of Eq. [2] is dominant and assuming a suitable value of E. Equation [2.1] then becomes a good approximation

$$(BF_o)^{(o)} = 2\ln(I_o/I) + \frac{\dfrac{E}{RI_o}\left(\dfrac{I_o}{I} - 1\right)}{\dfrac{(\lambda F_o)^o}{R} t - \ln(I_o/I)} \qquad [2.2]$$

since the terms containing BF_o on the right side of Eq. [2.1] are only small corrections. By inserting $(BF_o)^{(o)}$ calculated from Eq. [2.2] on the right side of Eq. [2.1] and using an experimental point of $I(t)$,

one obtains the first order approximation $(BF_o)^{(1)}$; inserting $(BF_o)^{(1)}$ into the right side of Eq. [2.1], one obtains the second order approximation $(BF_o)^{(2)}$, etc.[5]

The series $(BF_o)^{(o)}$, $(BF_o)^{(1)}$, etc. converges so rapidly that we have found it rarely necessary to proceed beyond $(BF_o)^{(2)}$.

Using BF_o and $(\lambda F_o)^{(o)}$, one may calculate λF_o by Eq. [11].

SYMBOLS

I_I	ionic current
$I,(I_o)$	current (initial current) in the external resistor
A	preexponential factor in the ionic current-field relation
$F,(F_o),(\bar{F})$	field, (initial field), (time average of the field) across the oxide layer
B	field coefficient or "inverse Tafel slope"
λ	growth rate per unit current
λ^*	apparent growth rate as calculated from the external current
λ^*_∞	apparent growth rate for film thicknesses larger than 32Å
E	emf of reaction
I_E	internal electron current
$I_E{}^o$	preexponential factor in the electronic current-thickness relation
l	attenuation length of the internal electron current
d	true film thickness
d^*	film thickness as calculated from capacitances
Λ	(d^*-d)
C	capacitance
ϵ_0	permittivity of free space
S	area
R	external resistor
t	time
B_Λ,F_Λ	values of B and F after correcting for Λ

[5] Since BF_o is about 30, the first step in this procedure can be saved by inserting 30 for $(BF)^{(o)}$, instead of the value given by Eq. [2.2].

The Structure and Mechanical Properties of Electroless Nickel

Arthur H. Graham,[1] Robert W. Lindsay, and Harold J. Read

Department of Metallurgy, College of Mineral Industries,
The Pennsylvania State University, University Park, Pennsylvania

ABSTRACT

Effects of variations in phosphorus content of electroless nickel from 4.6 to 9.4 w/o on structure, strength, ductility, and hardness were studied. Electron diffraction proved the crystallinity of many as-plated alloys, and x-ray data established a conventional precipitation hardening mechanism during heat treatment. Changes in properties after heat treatment at 200°-750°C have been correlated with structural changes shown by x-ray diffraction and with those revealed in optical and electron back scatter micrographs. Abrupt changes in the structure, strength, and ductility of as-plated alloys and of alloys heat treated at 750°C occurred at phosphorus contents of about 7%.

Although electroless nickel plating has achieved considerable popularity in the somewhat more than a decade and a half since attention was drawn to its possibilities by the work of Brenner (1) and his colleagues, most of the literature on the subject concerns the process rather than the product. Some notice has been given to structure, but aside from hardness measurements, little has been done in the evaluation of mechanical properties.

Goldenstein, Rostoker, Schossberger, and Gutzeit (2) in their study of deposits containing 7-10 w/o (weight per cent) phosphorus concluded on the basis of x-ray diffraction and some other considerations that as-plated electroless nickel is amorphous. Other investigators reached similar conclusions. It is not impossible, however, to account for the typical diffraction patterns through a consideration of the combined effects of extremely small grain size, internal stress, and nonhomogeneous solid solution. Some hint of possible crystallinity in as-plated deposits appears in a paper by Zusmanovich (3), but he made no actual claim in this direction. The relationship between structure and phosphorus content of the deposits has not been studied, although the work of Brenner, Couch, and Williams (4) on electrodeposited nickel-phosphorus alloys contains evidence that phosphorus concentration is an important variable in determining structure.

More attention has been given to optical microstructure than to fine structure, but only a portion of the work has taken into account the phosphorus variable. The changes that take place on heat treatment have been extensively studied and most investigators have claimed that the final microstructure is a dispersion of Ni_3P in a nickel matrix (1, 2, 5, 6). Ziehlke, Dritt, and Mahoney (7) maintain, however, that heat treated, high-phosphorus alloys are dispersions of nickel in a matrix of Ni_3P. Because the mechanical properties would be markedly affected by the nature of the matrix, the effect of phosphorus on this variable needs further study.

The increase in hardness of electroless nickel as a result of heat treatment is a notable effect and has received much attention (2, 3, 5, 7). In general, agreement is good among investigators as to the effects of time and temperature on hardness, and the data resemble those for known precipitation-hardenable alloys. It has been generally assumed, therefore, that precipitation hardening is the mechanism that prevails in spite of the fact that the accepted theory of precipitation hardening, which requires a crystalline lattice, is not compatible with the amorphous structure that is also generally accepted. Only Goldenstein (2) and Ziehlke (7) and their colleagues recognized this point and postulated vague expedients to resolve it.

Almost nothing has been done on the determination of the strength of electroless nickel and most of the work on ductility has involved rather qualitative bend tests on composite samples of deposit and basis metal. Phosphorus content has not been regarded as an important variable, but Lee (5) as well as Ziehlke, Dritt, and Mahoney (7) published some observations that intimate that phosphorus content should not be ignored in work on mechanical properties.

The investigation described here had as its objectives (a) the study of the effects of phosphorus content on structure and mechanical properties, (b) correlation of changes in mechanical properties after heat treatment with structural changes, and (c) elucidation of the mechanism of hardening. Strength and ductility, as measured by the hydraulic bulge test, and microhardness were used to evaluate mechanical pro-

[1] Present address: Engineering Materials Laboratory, Experimental Station, E. I. du Pont de Nemours & Co., Inc., Wilmington, Delaware.

Table I. Details of electroless nickel processes

Designation	Bath composition, g/l	First modification	Second modification	Plating conditions	
Alkaline-chloride process	$NiCl_2 \cdot 6H_2O$	45	45	pH	8.2-8.4
	Sodium citrate dihydrate	82	82	Temperature	90°C
Modification of process developed by MacLean and Karten (10)	NH_4Cl	50	50	Rate of deposition	0.4-0.6 mil/hr
	$NaH_2PO_2 \cdot H_2O$ (rate of replenishment)	16 (2.1 g/l/hr)	24 (2.7 g/l/hr)	Ratio of area plated to bath volume	5 sq in./l
	NH_4OH	added to maintain pH		Agitation	stirrer
Acid-sulfate process	$NiSO_4 \cdot 6H_2O$	75		pH	4.2-5.7
	Sodium acetate	7.5		Temperature	93°C
After Girard (11)	H_3BO_3	8		Rate of deposition	0.6-1.0 mil/hr
	NH_4Cl	6		Ratio of area plated to bath volume	12 sq in./l
	$NaH_2PO_2 \cdot H_2O$	24		Agitation	stirrer

perties. Some preliminary findings on the crystallinity of electroless nickel have been reported previously (8).

Experimental Procedure

Specimen Preparation

Because of the large number of different electroless nickel plating processes that have been developed, it was not possible to select what might be considered a typical one. The selection of plating processes for this study was based principally on their ability to produce deposits that were free from internal stress and that did not contain macrovariations in phosphorus content across a thickness of 1 mil.[2] The microvariations in composition reported by Gutzeit (9) which occure over increments of approximately 0.02 mil in thickness could be tolerated. But, macrovariations in the average phosphorus content across the deposit would severely curtail, if not render impossible, the investigation of the effect of phosphorus on structure and mechanical properties. Internal stresses would also be detrimental to the objectives of this study because they would affect properties and influence the position and breadth of lines in diffraction patterns. The two processes selected for the preparation of specimens are specified in Table I.

Most of the specimens were prepared by alkaline-chloride processes that differ only slightly from the process developed by MacLean and Karten (10). Careful control of the periodic additions to the plating baths resulted in the formation of electroless nickel deposits that were free from internal stress, that is, they were not warped or distorted. Control of the periodic additions of sodium hypophosphite was based on the assumption that the amount required to maintain a constant rate of deposition would be sufficient to replace the amount consumed. The periodic additions of nickel chloride were determined by a calculation of the amount of nickel being deposited based on prior knowledge of the rate of deposition and the surface area of the basis metal.

As a result of the unavoidable changes in bath composition during 500 hr of plating from a particular alkaline-chloride bath, the average phosphorus content of the specimens deposited gradually increased from 4.6 to 9.4 w/o. Fortunately, the bath composition changed so slowly that the average phosphorus content, as indicated by electron-probe microanalysis, was constant across the thickness of deposits from a particular plating run.

The deposits from the acid-sulfate bath developed by Girard (11) were slightly stressed and had a phosphorus gradient that ranged from 5 w/o at the surface adjacent to the basis metal to 10 w/o at the outer surface. The increase in the phosphorus content during plating appeared to be related to the rapid decrease in the pH of the bath. A similar relationship between phosphorus content and the pH of acid electroless nickel baths has been observed by Gutzeit (9).

[2] All specimens were plated to approximately the same average thickness to avoid possible effects of variations in thickness on mechanical properties.

The electronprobe microanalysis traverses in Fig. 1 contrast the uniform distribution of phosphorus across a deposit from an alkaline-chloride bath with the steep phosphorus gradient across a deposit from the acid-sulfate bath. A limited number of specimens was prepared from the acid-sulfate bath to determine whether a significant difference in plating bath composition would affect the structure and the properties of the deposits.

The basis metal for bulge-test specimens was annealed copper sheet attached to a glass plate to give sufficient rigidity for handling. The surface of the copper sheet adjacent to the glass plate was coated with a stop-off lacquer. At the completion of a plating run, the stop-off lacquer was removed with acetone, and the copper substrate was stripped from the deposits in a solution of chromic acid (500 g/l) and sulfuric acid (50 g/l). Extensive experience with this stripping solution has shown that there is neither chemical attack nor mechanical disturbance of nickel or nickel-phosphorus deposits.

Strips of low-carbon steel served as the basis metal for hardness specimens.

Heat treatments were conducted at 200°, 400° 600°, and 750°C in a purified argon atmosphere. At the completion of a heat treatment, the specimens were cooled to below 100°C under the argon atmosphere before they were exposed to air.

X-ray Diffraction Studies

X-ray pinhole transmission patterns were taken of as-plated and heat-treated deposits to reveal the presence of any preferred orientation. Plated coatings with a preferred orientation usually have a fiber texture in which a certain crystallographic direction [hkl] of most of the grains is parallel, or nearly parallel, to an axis normal to the surface of the coating. To reveal the presence of any fiber texture in the electroless nickel deposits, it was necessary to tilt the specimen so that

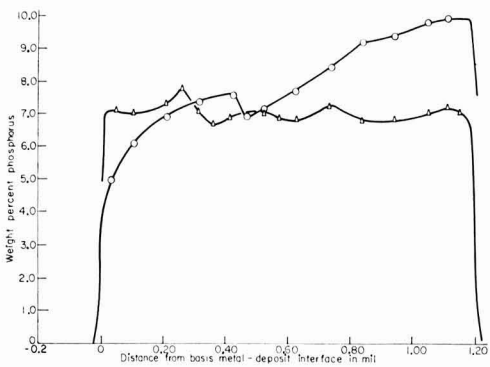

Fig. 1. Typical electron-probe microanalysis traverses of as-plated electroless nickel deposits. △—△, deposit from alkaline-chloride bath; ○—○, deposit from acid-sulfate bath.

the [hkl] fiber axis was not parallel to the x-ray beam. If the fiber axis is parallel to the beam, continuous Debye rings of uniform intensity will appear on the transmission patterns even though a strong preferred orientation exists (12). Preferred orientation will greatly diminish the intensity of many of the Debye rings on the pattern and might eliminate some of them.

An x-ray diffractometer study was conducted on the effect of phosphorus content on the position and breadth of the strong x-ray reflection from as-plated alloys. To compensate for instrumental errors in the diffractometer, the (220) reflection from a powdered-silicon standard was used as a reference for the calibration of the position of the electroless nickel reflection. The breadth of the reflection was measured at half maximum intensity.

The apparent grain size of as-plated electroless nickel alloys was estimated with the Scherrer formula which is based on diffraction broadening, as expressed in the following equation

$$t = \frac{0.9\,\lambda}{B\cos\theta_{hkl}}$$

where t is the apparent thickness of the grain in Å, λ is the wavelength of the radiation in Å, and B is the broadening of the reflection at half its maximum intensity in radians. The estimates of the grain size given by the Scherrer formula were compared with actual grain size measurements made on electron transmission micrographs.

Electron Diffraction Study

The deposits of electroless nickel for the electron diffraction investigation were thinned by electropolishing until they would transmit an electron beam accelerated by a potential of 75 kv. All the diffraction patterns were made with the electron beam perpendicular to the surface of the thin film.

Because excessive heating could cause the crystallization of an initially amorphous film, a finely focused beam and the smallest possible filament saturation current were used to minimize the heating due to electron bombardment. According to Thomas (13), such precautions can decrease the temperature rise of metallic specimens to approximately 20 centigrade degrees. As an additional precaution to insure that the structure of the specimens was not affected by electron bombardment, the beam was focused for diffraction before the specimen was moved into its path in the center of the microscope column. From the instant that the beam touched the specimens up to times as long as 1 hr, no change was observed in the diffraction patterns.

Because of the extremely small wavelength of the electrons (0.04Å), the radius of the Debye ring on a diffraction pattern is directly proportional to the magnitude of the reciprocal lattice vector for the reflection (d^*_{hkl}). A thin layer of polycrystalline nickel oxide or single crystals of nickel sulfate hexahydrate served as internal standards for the determination of the proportionality constant between the radius and d^*_{hkl}. The nickel sulfate hexahydrate crystals became attached to the electroless nickel films during the electropolishing of deposits in a sulfuric acid electrolyte with a high concentration of nickel ions. The thin layer of nickel oxide was intentionally formed on the films by electropolishing at low current densities.

Measurement of Mechanical Properties

The microhardness of the electroless nickel deposits was measured with a Tukon tester equipped with a Knoop indenter. Measurements were made on both the surface and the cross section of an adequate sample of as-plated deposits and heat-treated deposits. A 100-g indenting load was used on most of the specimens. For some specimens that had been heat treated above 400°C, the indenting load was decreased to 50g to avoid the anvil effect and to keep the indents well within the cross section of the deposit. Every hardness number reported is the average of measurements from at least 5 indents that were free from cracks and distortion.

A detailed description of the hydraulic bulge tester used to measure the strength and ductility of the electroless nickel deposits appears in an article by Read and Whalen (14). The theoretical and mathematical interpretation of the test results is presented in an article by Prater and Read (15). Strength is expressed as significant stress at fracture ($\bar{\sigma}$) and ductility is expressed as significant strain at fracture ($\bar{\delta}$). The only experimental data needed for the determination of $\bar{\sigma}$ and $\bar{\delta}$ are the oil pressure measured by appropriate gauges, and the bulge height determined by measurement of the travel of a microscope focused on the center of the bulge.

The significant strain was read directly from a master curve of $\bar{\delta}$ vs. bulge height experimentally determined by Prater.

The significant stress was calculated from the equation

$$\bar{\sigma} = \frac{PR}{2t_i}$$

where P is the pressure, R the radius of curvature of the bulge, and t_i is the instantaneous thickness of the specimen. Values for the instantaneous thickness were calculated by multiplying the original average thickness (t_o) by the ratio of t_i/t_o obtained from a curve determined by Prater.

Results and Discussion

Diffraction Patterns of As-plated Alloys

Although as-plated electroless nickel alloys have been considered to be amorphous by previous investigators, the electron transmission diffraction patterns in Fig. 2 and 3 provide definite evidence that the alloys are crystalline. There can be no doubt as to the crystallinity of the alloys with less than 7 w/o phosphorus because of the appearance of eight to eleven reflections in their diffraction patterns. Difficulties were encountered in the determination of lattice type and in indexing the patterns, but all the reflections could be attributed to nickel regardless of the lattice type assumed. Therefore, the as-plated alloys are supersaturated solid solutions of phosphorus dissolved in crystalline nickel.

Perhaps it should be made clear that as little as 2 v/o (volume per cent) of Ni_3P would produce lines in the diffraction patterns. A deposit with 7 w/o phosphorus would contain 50 v/o of Ni_3P if the phosphorus

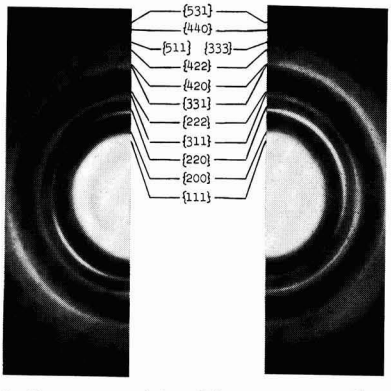

Fig. 2. Electron transmission diffraction pattern of as-plated electroless nickel from the alkaline-chloride bath, phosphorus content 5.0 w/o, indexed according to a fcc structure.

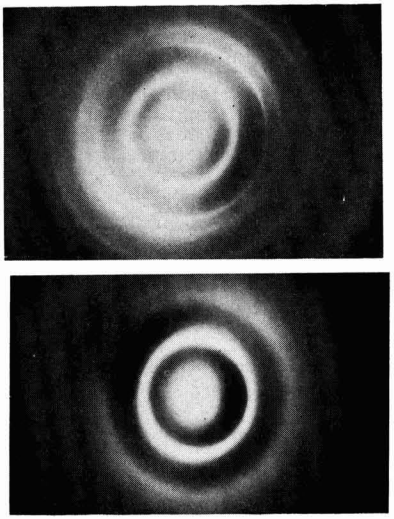

Fig. 3. Electron transmission diffraction patterns of as-plated electroless nickel alloys from the alkaline-chloride bath. (a) phosphorus content 6.6 w/o, (b) phosphorus content 8.6 w/o.

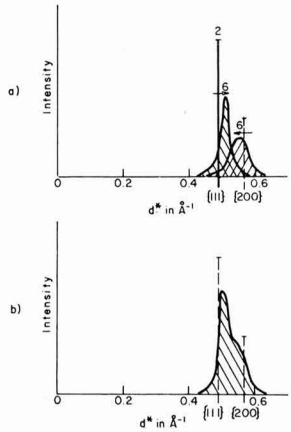

Fig. 4. Schematic sketch of the predicted effect of stacking faults on the {111} and {200} reflections from fcc nickel. (a) Effect on individual components of reflections, heavy vertical line represents unaffected components, shaded areas represent components that are broadened and shifted (after Paterson (16)). (b) Effect on over-all intensity profile.

were all combined with the nickel in the form of the compound. There is no indication that any compound other than Ni_3P is involved. Inasmuch as no compound lines were observed in the patterns, a supersaturated solid solution is indicated.

The patterns from the low-phosphorus alloys with less than 7 w/o phosphorus can be reasonably indexed according to either a hexagonal-close-packed (hcp) or a face-centered-cubic (fcc) structure (hcp nickel has often been reported). The most important factor in attempting to distinguish between the two possible structures is the {200} reflection for the fcc structure. The presence of a strong {200} reflection would be indicative of a fcc structure, whereas its absence would indicate a hcp structure. In all the electron transmission diffraction patterns, the {200} reflection was either absent or extremely weak. The difficulties in indexing can be attributed to stacking faults in the structure of fcc nickel.

The effect of stacking faults on the {111} and {200} reflections from a fcc structure as shown by Paterson (16) is illustrated schematically in Fig. 4a. The presence of stacking faults not only shifts all six components of the {200} reflection to a lower d^* value, but also diminishes their intensity by increasing their breadth. Although the (111) and $(\bar{1}\bar{1}\bar{1})$ components are not affected, the other six components of the {111} reflection are broadened and shifted to a higher d^* value. The predicted over-all intensity profile in the vicinity of the {111} and {200} reflections shown in Fig. 4 closely resembles the observed intensity profile on electron diffraction patterns of as-plated electroless nickel alloys. The d^*_{hkl} for the other reflections indexed in Fig. 2 is compatible with the assumption that the as-plated alloys consist of a single phase having the fcc structure of nickel with a high density of stacking faults. Evidence which might account for the presence of stacking faults in the as-plated alloys is presented in the section on the hardening mechanism.

As the phosphorus content of electroless nickel alloys increases from 7 to 9 w/o, all the reflections in the electron transmission diffraction patterns are severely broadened and many are destroyed. Only three or four reflections are discernible in patterns from alloys with more than 8 w/o phosphorus. However, these alloys still appear to be crystalline if their electron diffraction patterns are compared with patterns from glasses. Electron diffraction patterns of the amorphous structure of glasses have only one diffuse reflection that cannot be accurately located. On the negative of the diffraction pattern in Fig. 3b, which is typical of patterns from electroless nickel alloys with high phosphorus contents, four diffuse rings corresponding to the {111}, {220}, {311}, and {331} reflections are discernible.

Contradiction between Electron and X-ray Diffraction Results

The same specimens of as-plated electroless nickel that yield electron diffraction patterns indicative of a crystalline structure because of the appearance of eight to eleven reflections give x-ray diffractometer and x-ray pinhole transmission patterns that appear to be indicative of an amorphous structure because of the appearance of only one or two reflections. A strong {111} reflection and a weak {222} reflection were observed in diffractometer patterns from the alloys with less than 7 w/o phosphorus. As the phosphorus content increases from 7 to 9 w/o, the {111} reflection becomes less intense and the {222} reflection disappears.

Only the {111} Debye ring appears in x-ray pinhole transmission patterns produced with copper radiation. If an electroless nickel deposit is mounted so that the x-ray beam is perpendicular to its surface, the continuous {111} ring has a uniform intensity as shown in Fig. 5a. When a deposit with less than 7 w/o phosphorus is tilted so that the angle (β) between a normal to its surface and the x-ray beam is approximately 70°, a nonuniform intensity distribution indicative of a weak [111] fiber texture with an axis perpendicular to the surface of the deposit is revealed as shown in Fig. 5b. X-ray pinhole transmission patterns of the copper sheets that served as a basis metal reveal a random orientation; therefore, the preferred orientation in the electroless nickel deposits has no epitaxial relationship to the substrate. The electron transmission diffraction patterns in Fig. 2 and 3a also reveal the presence of the preferred orientation. In both the electron and the x-ray transmission patterns, the preferred orientation becomes weaker and eventually disappears as the phosphorus content increases above 7 w/o.

The detection of a [111] fiber texture in x-ray pinhole transmission patterns tends to support the electron diffraction evidence of crystallinity even though only one or two x-ray reflections are observed. A preferred orientation not only presupposes the existence of order, but also can cause the diminution of the in-

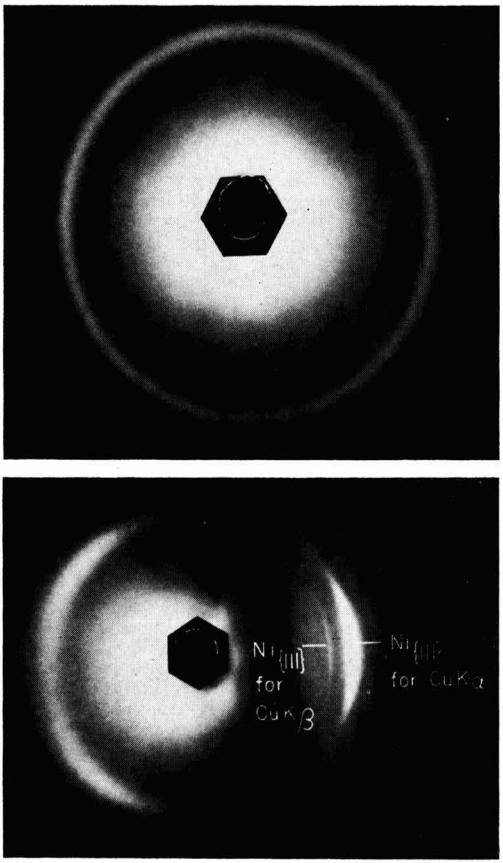

Fig. 5. X-ray pinhole transmission patterns of as-plated electroless nickel from the alkaline-chloride bath, phosphorus content 6 w/o, unfiltered copper radiation. (a) $\beta = 0°$, (b) $\beta = 70°$.

tensities of many x-ray reflections in diffractometer and pinhole transmission patterns. As a result of the basic design of conventional x-ray diffractometers, the crystallographic planes that are responsible for the appearance of a diffraction peak must be parallel to the surface of the specimen. An extremely strong [111] fiber texture perpendicular to the surface of a fcc metallic coating could cause the destruction of all x-ray reflections except those from the {111} planes and similar higher order planes because these would be the only planes parallel to the surface of the specimen. Although the weak [111] fiber texture in the low-phosphorus electroless nickel alloys would diminish the intensities of all the missing reflections in the diffractometer patterns, the preferred orientation is not strong enough to account for the absence of these reflections. The intensities of many reflections in the x-ray and electron transmission diffraction patterns would also be diminished by the weak [111] fiber texture if the beam of radiation were approximately parallel to the fiber axis.

The apparent contradiction between the x-ray diffraction results which led previous investigators to conclude that the structure of as-plated electroless nickel was amorphous, and the electron diffraction results which are indicative of crystallinity can be explained by a consideration of the effects of fine grain size and other factors that diminish the intensities of x-ray reflections. Reflections in x-ray patterns are broadened and become less intense as the grain size decreases to diameters less than 10,000Å. In electroless nickel, the

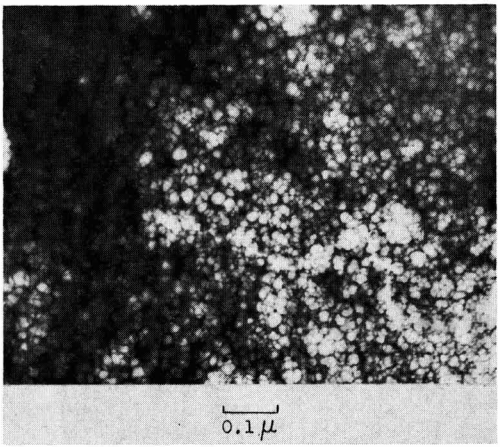

Fig. 6. Electron transmission micrograph of as-plated electroless nickel from the alkaline-chloride bath, phosphorus content 6.1 w/o, X 124,000.

apparent grain size, as indicated by electron transmission micrographs similar to that in Fig. 6, is of the order of 100Å; therefore, only the most intense x-ray reflections should appear. Although the x-ray diffraction pattern of a crystalline material with a particle size of 100Å should probably contain more than one or two reflections, the added effects of internal stress, solid solution, stacking faults, and preferred orientation on the diminution of the intensities of the reflections can reasonably account for the destruction of all but the strong {111} x-ray reflection from as-plated electroless nickel. In the x-ray diffractometer patterns of low-phosphorus alloys, the detection of a weak {222} reflection, which has not been observed by previous investigators, might be due to the absence of internal stress in the deposits prepared for this investigation.

Solution of the Scherrer formula (see section on experimental procedure) for the amount of broadening caused by fine grain size gives the equation

$$B = \frac{0.9\,\lambda}{t \cos \theta_{hkl}}$$

which indicates that the tendency of a fine-grained material to broaden reflections is greatly diminished as the wavelength of the radiation is decreased. The broadening is diminished not only because the numerator of the equation depends directly on the wavelength, but also because the cos θ_{hkl} term in the denominator increases as the wavelength decreases. The fine grain size of the electroless nickel does not preclude the production of electron-diffraction lines because the wavelength of electrons accelerated through a potential of 75 kv is almost two orders of magnitude smaller than the wavelength of x-rays used in diffraction work.

The existence of an abrupt change in the effect of phosphorus content at 7 w/o on the position and breadth of lines in diffraction patterns of as-plated electroless nickel alloys is clearly revealed by the graphs in Fig. 7 for the {111} x-ray reflection. The d_{111} and the peak breadth plotted for alloys deposited from the alkaline-chloride bath are averages of measurements made on the surface of the deposits adjacent to the basis metal and of measurements made on the outer surface. For alloys deposited from the acid-sulfate bath, the measurements from the two surfaces were plotted individually at phosphorus contents determined from electron-probe microanalysis traverses.

Variations in phosphorus content appear to have no significant effect on the position and breadth of the {111} reflection from alloys containing from 4.6 to

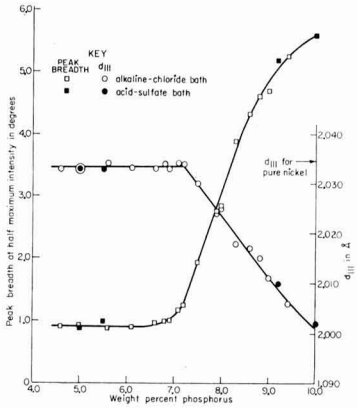

Fig. 7. Peak breadth of the {111} x-ray reflection and d_{111} for as-plated electroless nickel *vs.* weight per cent phosphorus.

7 w/o. As the phosphorus content increases from 7 to 10 w/o, d_{111} decreases and the reflection is broadened considerably. Both the shifting and the broadening of the reflection are associated with the development of an asymmetrical tail on the high-angle side of the {111} diffraction peak.

At present, the exact cause for the effects of an increase in phosphorus content above 7 w/o on diffraction patterns of as-plated electroless nickel alloys can only be the subject of speculation. Even though a decrease in grain size could contribute to the broadening of the {111} reflection, it would not result in asymmetry. Therefore, the observed increase in peak breadth with increasing phosphorus content must be caused by some phenomenon which can result in asymmetrical broadening, such as an increase in the density of stacking faults.

Goldenstein, Rostoker, Schossberger, and Gutzeit (2), in support of their contention that electroless nickel is amorphous, state that the apparent grain size obtained by measuring the breadth of the {111} x-ray peak and applying the Scherrer formula is only a few atomic diameters. The new data reported in Table II show that estimates given by the Scherrer formula are not valid indications of the actual grain size of alloys with more than 7 w/o phosphorus. In Table II, the Scherrer formula estimates, calculated from measured peak breadths that have been corrected for instrumental broadening, are compared with actual grain size measurements made on several electron transmission micrographs similar to that in Fig. 6. For the alloy containing 8.8 w/o phosphorus, the measured grain size is approximately five times greater than the estimate given by the Scherrer formula, which attributes all the broadening to fine grain size. The fact that the estimated grain size for alloys with 5.0 and 6.1 w/o phosphorus is fairly close to the measured value indicates that fine grain size makes a significant contribution to the total breadth of the x-ray reflections from the low-phosphorus alloys.

Table II. Comparison of estimated grain size given by the Scherrer formula with average grain size determined from electron transmission micrographs of as-plated electroless nickel

Weight per cent phosphorus	B radians	Grain size in A: Estimate from Scherrer formula	Grain size in A: Average of measurements on micrographs
5.0	0.0154	98	150
6.1	0.0153	98	150
7.5	0.0335	46	—
8.8	0.0803	19	100
9.4	0.0917	16	—

Effect of Heat Treatment on Preferred Orientation

An observed increase in the strength of the preferred orientation of the nickel phase of all electroless nickel alloys after heat treatments at temperatures ranging from 200° to 750°C is indicative of recrystallization and grain growth. Even the high-phosphorus alloys with more than 7 w/o phosphorus that seemed to have a random orientation in the as-plated condition develop a weak [111] fiber texture at temperatures as low as 200°C. After heat treatments at 200°C, the weak preferred orientation of the as-plated, low-phosphorus alloys is slightly stronger and a very weak {200} reflection appears on the x-ray pinhole transmission patterns. No evidence for the formation of a Ni_3P phase appears in electron or x-ray transmission diffraction patterns of alloys heat treated at 200°C for times as long as 240 min.

The initial particles of Ni_3P that form in alloys heat treated at 400° and 600°C also have a distinct preferred orientation. There seems to be no reason for this behavior unless the deposits are crystalline before heat treatment. This is one more bit of evidence for crystallinity of the as-plated deposits. In the low-phosphorus alloys, the preferred orientation of the Ni_3P phase is still strong after a heat treatment at 400°C for 120 min as shown by the {321} reflection in Fig. 8. An analysis of the preferred orientation in the Ni_3P phase and its implications concerning the hardening mechanism in electroless nickel will be presented in a subsequent section.

The strength of the [111] fiber texture in the nickel phase of all the electroless nickel alloys increases as the temperature of heat treatment increases from 200° to 600°C. At 750°C, the preferred orientation developed in the nickel phase of the high-phosphorus alloys is just as strong, if not stronger, than that developed in the same interval of time at 600°C. In the low-phosphorus alloys heat treated at 750°C for 120 min, the preferred orientation of the nickel phase is considerably weaker than that developed at 600°C, as shown by a comparison of Fig. 9 and 10a. Furthermore, the reflections from the nickel phase of the low-phosphorus alloys heat treated at 750°C are extremely spotty in character compared to the continuous reflections from the high-phosphorus alloys after a similar heat treatment. After heat treatments at 750°C, the differences in the character of the reflections and in the strength of the preferred orientation shown in Fig. 10 are indicative of recrystallization with excessive grain growth in the low-phosphorus alloys and recrystallization with restricted grain growth in the high-phosphorus alloys. Recrystallization is possible only if the as-plated deposits were crystalline.

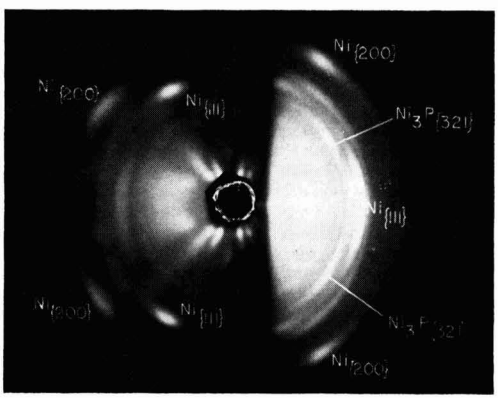

Fig. 8. X-ray pinhole transmission pattern of electroless nickel deposited from the alkaline-chloride bath and heat treated at 400°C for 120 min, phosphorus content 6.1 w/o, unfiltered copper radiation, $\beta = 70°$.

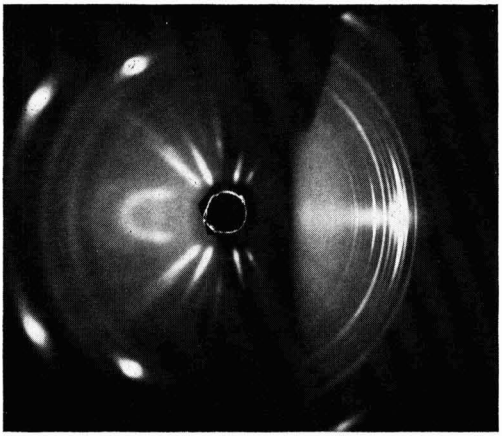

Fig. 9. X-ray pinhole transmission pattern of electroless nickel deposited from the alkaline-chloride bath and heat treated at 600°C for 120 min, phosphorus content 6.1 w/o, unfiltered copper radiation, $\beta = 70°$.

The results of the preferred-orientation study of electroless nickel alloys after heat treatments at temperatures ranging from 400° to 750°C are summarized in Table III. The qualitative estimates of the strength of the preferred orientation that appear in Table III were made on x-ray pinhole transmission patterns similar to those in Fig. 8, 9, and 10. The importance of inclining the specimen at various angles to the x-ray beam cannot be overemphasized, otherwise the variations in [111] fiber texture may not be detected.

Microstructure

The micrographs of as-plated electroless nickel in Fig. 11 and 12 show the lamellar structure observed by previous investigators and also reveal a significant difference in the thickness of the lamellae of deposits from the two plating baths. In the microstructure of the as-plated deposit from the alkaline-chloride bath shown in Fig. 11, the lamellar thickness is approximately 0.2 mil. The lamellae in the microstructure of the acid-sulfate deposit shown in Fig. 12, which closely resembles the appearance of micrographs published in the literature, are only about 0.02 mil thick.

After heat treatments at temperatures as high as 400°C, the microstructures of the electroless nickel alloys have the same lamellar appearance of as-plated alloys even though the supersaturated solid solution has transformed to the equilibrium phases of nickel and Ni_3P.

Heat treatments at 600°C for 120 min result in the disappearance of the lamellar structure, as shown by the micrograph in Fig. 13. The two equilibrium phases

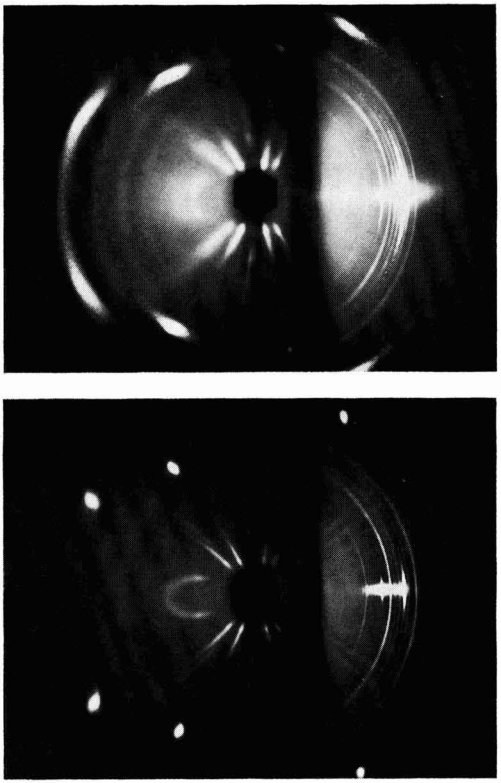

Fig. 10. X-ray pinhole transmission patterns of electroless nickel alloys deposited from the alkaline-chloride bath and heat treated at 750°C for 120 min, $\beta = 70°$, unfiltered copper radiation: (a) phosphorus content 5.0 w/o, (b) phosphorus content 8.8 w/o.

are evident in the micrograph, but the structure is too fine to be clearly resolved.

Optical micrographs of the electroless nickel alloys heat treated at 750°C for 120 min show clearly resolved particles dispersed in a matrix. The electron backscatter micrographs in Fig. 14 definitely establish that there is a change in the phase forming the matrix as the phosphorus content increases from 5.0 to 9.0 w/o. The intensity of electron backscattering diminishes with a decrease in mass density or with a decrease in the atomic number of the elements present. On the electron backscatter micrographs of electroless nickel, the Ni_3P phase should appear as a dark region not only because its mass density is less than nickel, but also because it contains 25 a/o (atomic per cent) of

Table III. Qualitative summary of preferred-orientation study of electroless nickel after heat treatments at temperatures ranging from 400° to 750°C

Phase	Plating bath	Weight per cent phosphorus	Strength of preferred orientation after heat treatment				
			at 400°C		at 600°C		at 750°C
			10-30 min	120 min	14-30 min	120 min	120 min
Ni	Alkaline-chloride	6	W-S	S	S	VS	W-S
		9	W	W-S	S	VS	VS
	Acid-sulfate	5*	W-S	S	S	VS	
		10**	VW	W	S	VS	
Ni_3P	Alkaline-chloride	6	S	S	W-S	VW-R	VW-R
		9	VW	VW-R	VW-R	R	R
	Acid-sulfate	5*	S	S	W-S	VW-R	
		10**	VW-R	R	VW-R	R	

Key: R random orientation, W weak, VS very strong, VW very weak, and S strong.
* Surface adjacent to basis metal.
** Outer surface.

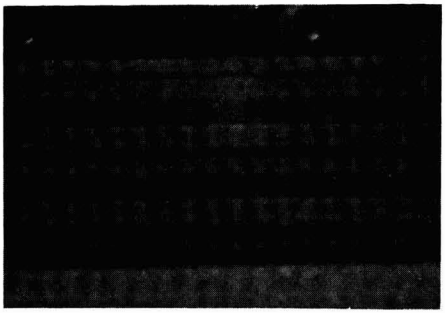

Fig. 11. Microstructure of as-plated electroless nickel from the alkaline-chloride bath, phosphorus content 7.1 w/o, NaCN-$(NH_4)_2S_2O_8$ etch, X 1000.

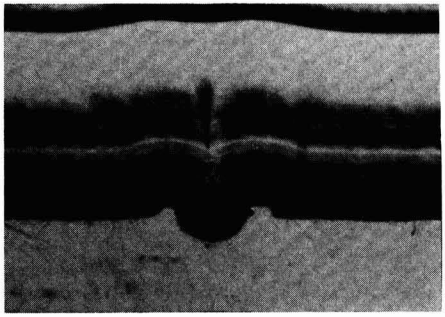

Fig. 12. Microstructure of as-plated electroless nickel from the acid-sulfate bath, phosphorus content varies from 5 w/o at surface adjacent to basis metal to 10 w/o at outer surface, NaCN-$(NH_4)_2S_2O_8$ etch, X 1000.

phosphorus, whose atomic number is considerably below that of nickel. Even though the particles of the dispersed phase are not clearly resolved, the electron backscatter micrographs indicate that the light nickel phase is the matrix in the alloys containing 5.0 w/o phosphorus and the dark Ni_3P phase is the matrix in the alloys containing 9.0 w/o phosphorus.

The evidence from x-ray pinhole transmission patterns for restricted grain growth of the nickel phase of high-phosphorus alloys heat treated at 750°C in contrast to the excessive grain growth in the low-phosphorus alloys can be attributed to the change in the phase forming the matrix as the phosphorus content increases. The continuous Ni_3P phase would act as a natural barrier to the growth of a dispersed nickel phase in the high-phosphorus alloys.

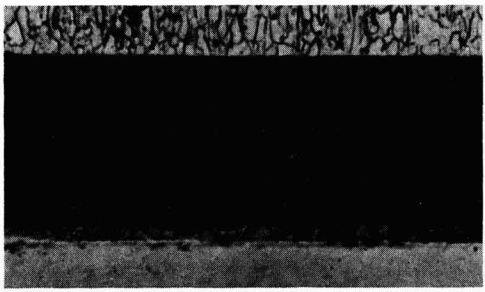

Fig. 13. Microstructure of electroless nickel deposited from the alkaline-chloride bath and heat treated at 600°C for 120 min, phosphorus content 9.0 w/o, NaCN-$(NH_4)_2S_2O_8$ etch, X 1000.

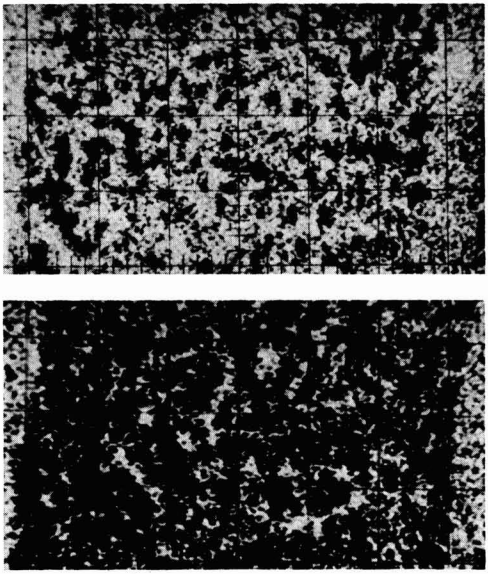

Fig. 14. Electron backscatter micrographs of electroless nickel alloys deposited from the alkaline-chloride bath and heat treated at 750°C for 120 min, unetched, X 2500. (a) phosphorus content 5.0 w/o, (b) phosphorus content 9.0 w/o.

The fact that the change in the phase forming the matrix occurs in the vicinity of 7 w/o phosphorus, which according to the equilibrium phase diagram corresponds to 50 v/o Ni_3P, can be ascertained from the series of micrographs in Fig. 15. The continuous nickel phase appears as light regions on the optical micrograph of the alloy with 5.0 w/o phosphorus in contrast to the gray regions representing the continuous Ni_3P phase in the micrograph of the alloy with 9.0 w/o phosphorus. In the microstructure of the alloy containing 7.1 w/o phosphorus shown in Fig. 15b, neither phase is continuous across the entire thickness of the deposit. The Ni_3P phase appears to be the matrix at the basis metal-deposit interface, whereas nickel seems to be the matrix near the outer surface. All optical micrographs in this section are oriented so that the basis metal is at the bottom.

Mechanical Properties

The bulge-test specimens deposited from the alkaline-chloride bath were grouped according to phosphorus content. As-plated specimens or specimens for a specific heat treatment were randomly selected from a group representative of a particular phosphorus content in order to eliminate any effect that plating conditions during a particular run might have on the properties of the deposits. The strengths and ductilities plotted on the graphs in this section are sample means or averages for measurements on several specimens. The limits of the averages indicated by dashed lines on some of the graphs are 90% confidence intervals for the true mean calculated from Student's "*t*" distribution.

For an adequate sample of as-plated specimens and heat-treated specimens, there was no significant difference between the hardness measurement on the surface of a deposit and the hardness measurement on its cross section. Therefore, it was not necessary to make two measurements on all specimens. If measurements were made on both the surface and the cross section, the Knoop hardness number (KHN) reported was the average of the two measurements. The maximum deviation of two measurements from their mean was less than 5%.

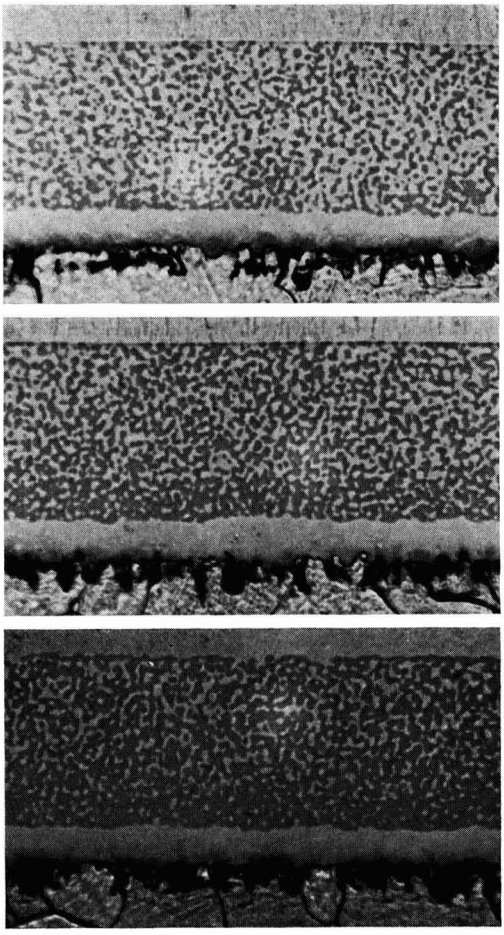

Fig. 15. Microstructure of electroless nickel alloys deposited from the alkaline-chloride bath and heat treated at 750°C for 120 min, NaCN-$(NH_4)_2S_2O_8$ etch, water rinse, 2% nital etch, X 1000. (a) phosphorus content 5.0 w/o, (b) phosphorus content 7.1 w/o, (c) phosphorus content 9.0 w/o.

The graphs in Fig. 16 indicate that both the strength and the ductility of as-plated electroless nickel alloys increase with a rise in phosphorus content. These results contradict qualitative observations of Brenner, Couch, and Williams (4) who reported a decrease in the strength and ductility of similar electrodeposited alloys with increasing phosphorus content. In the vicinity of 7 w/o, both the strength and the ductility of electroless nickel alloys rise abruptly and the strength appears to reach a maximum. The changes in strength and ductility are not reflected in the hardness, which remains practically constant as the phosphorus content increases.

The increase in the strength of the as-plated alloys can reasonably be attributed to either solid solution hardening or to the effects of localized coherency stresses in regions where phosphorus atoms are collecting and attempting to form a nucleus of the phosphide phase. At present, no reasonable hypothesis can be offered to explain the unusual direct relationship between strength and ductility with increasing phosphorus content of as-plated electroless nickel. A similar direct relationship was described by Read in his discussion of the effects of addition agents on the mechanical properties of copper and nickel electrodeposits (17).

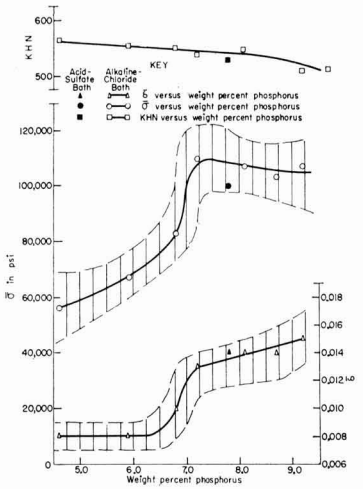

Fig. 16. Effect of phosphorus content on the mechanical properties of as-plated electroless nickel alloys.

The strength and ductilities reported in Fig. 16 for as-plated alloys containing 7 to 10 w/o phosphorus are in good agreement with those obtained by Jovanovic and Smith (18) for similar alloys. These investigators, whose method for analyzing bulge test results differs from that used in this investigation, report strengths at fracture ranging from 109,000 to 120,000 psi and strains at fracture ranging from 0.0069 to 0.0080. If the bulge test results of this study for alloys containing 7 to 10 w/o phosphorus were treated according to the method employed by Jovanovic and Smith, the average strength at fracture would be 106,000 psi and the average strain at fracture would be 0.0095.

Although heat treatments at 750°C for 60 and 120 min significantly improve both the strength and the ductility of the low-phosphorus alloys, they greatly decrease the strength and the ductility of the high-phosphorus alloys as shown by a comparison of the data in Fig. 16 and 17. The fact that alloys with greater

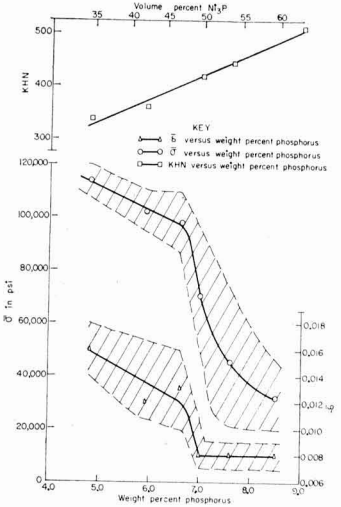

Fig. 17. Effect of phosphorus content on mechanical properties of electroless nickel alloys deposited from the alkaline-chloride bath and heat-treated at 750°C for 120 min.

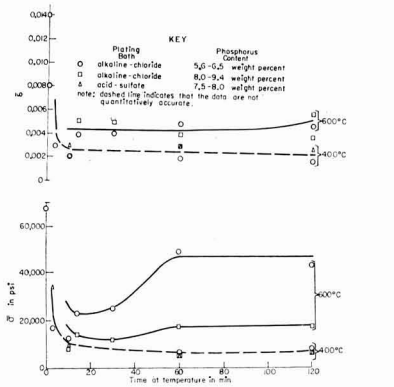

Fig. 18. Effect of heat treatments at 400° and 600°C on the strength and ductility of electroless nickel alloys.

than 7 w/o phosphorus are more brittle after heat treatments at 750°C than as-plated alloys of comparable phosphorus content confirms the qualitative observations of Brenner *et al.* for similar electrodeposited alloys and contradicts claims in the literature that prolonged heat treatments above 600°C improve the ductility of all electroless nickel alloys.

The graphs in Fig. 17 show that the strength and ductility of alloys heat treated at 750°C for 120 min decrease abruptly with increasing phosphorus content in the vicinity of 7 w/o. The abrupt loss in strength and ductility is indicative of the fact that a ductile nickel phase is the matrix in the low-phosphorus alloy and a brittle phosphide phase is the matrix in the high-phosphorus alloy. Once again, hardness measurements give no indication of the potent effect of phosphorus content in the vicinity of 7 w/o on strength and on ductility. The data plotted in Fig. 17 indicate that hardness is not only directly proportional to the weight per cent phosphorus in the alloys, but is also directly proportional to the volume per cent Ni_3P, as suggested by Ziehlke, Dritt, and Mahoney (7).

Heat treatments at 400° and 600°C result in a drastic decrease in the strength and ductility of all electroless nickel alloys as shown by the graphs in Fig. 18. After 10 min at 400°C, the alloys were so brittle that their strength and ductility could not be measured accurately even by the bulge test, which is particularly suitable for the determination of the properties of many brittle metallic coatings. The ductilities reported in Fig. 18 for the specimens tested are not quantitatively accurate because the bulge heights at fracture were far below the lower limit of the calibration graph for the bulge tester. At the lower limit, the curvature of the calibration graph changes rapidly so that precise extrapolation is not possible. Valid measurements of the strength were not obtained because the specimens fractured so early in testing that the oil pressure could not be accurately determined. For alloys heat treated at 400°C, phosphorus content seems to have no effect on the apparent strengths or the apparent ductilities which, at best, are only qualitative indications of these properties.

Even though the quantitative accuracy of the ductilities reported for alloys heat treated at 600°C is also questionable, the strength measurements are considered to be valid because all the specimens fractured at a measurable pressure. Heat treatments of the low-phosphorus alloys for more than 30 min result in the recovery of a significant portion of the original loss in strength. The high-phosphorus alloys are still extremely weak even after 120 min at 600°C.

There are probably many plausible explanations for the severe embrittlement indicated by the drastic decrease in the strength and ductility of electroless nickel after heat treatments at 400° and 600°C. One hypothesis could be based on the assumption that the Ni_3P phase initially precipitates as very thin platelets with edges that act as severe stress raisers. If this assumption were true, the recovery of the strength of the low-phosphorus alloys after prolonged heat treatments at 600°C could be attributed to the elimination of the stress raisers due to the natural tendency of the platelets to form spheroids and thereby decrease their surface energy.

A second hypothesis could be based on the assumption that many of the phosphorus atoms in as-plated electroless nickel alloys are segregated at grain boundaries. If this assumption were valid, the initial phosphorus-rich phase precipitated during heat treatments would form a continuous grain boundary network that could reasonably account for the embrittlement of the alloys. In the low-phosphorus alloys, a phosphide grain-boundary network would also tend to spheroidize during heat treatments at high temperatures. In the high-phosphorus alloys, the grain-boundary network would be stabilized due to the high volume percentage of the phosphide present.

There is some evidence on the x-ray pinhole transmission patterns of alloys heat treated at 400° and 600°C and on the micrographs of alloys heat treated at 750°C which would support both hypotheses suggested to account for the severe embrittlement. The observed preferred orientation of the phosphide phase in the x-ray pinhole transmission patterns suggests that some of the initial Ni_3P particles may precipitate as platelets with a particular crystallographic plane parallel to a habit plane in the parent nickel structure. The preferred orientation of the phosphide phase becomes stronger as the phosphorus content of the alloys decreases. However, even in the low-phosphorus alloys, the preferred orientation is not strong enough to preclude the existence of a randomly oriented precipitate at grain boundaries. The micrographs in Fig. 15a and 15b show irregularly shaped phosphide particles that appear to be the remnants of a grain-boundary network and also reveal small isolated phosphide spheroids which could have originally been platelets.

The data in Fig. 19 indicate that the embrittlement of electroless nickel after heat treatments at 400°C is accompanied by the substantial increase in hardness observed by previous investigators (2, 3, 5, 7). After 3 min at 400°C, the hardness of an alloy containing 6.1 w/o phosphorus is greater than that of an alloy containing 9.0 w/o. However, the hardness of alloys after heat treatments at 400°C for 10 min or longer is not significantly affected by phosphorus content. In Fig. 19, the stability of the maximum hardness developed at 400°C is compared with the rapid decrease in hardness during heat treatments at 600°C. The hardness

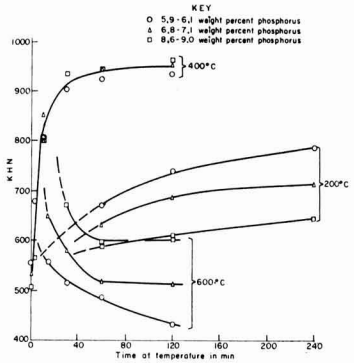

Fig. 19. Effect of heat treatment on the hardness of electroless nickel alloys deposited from the alkaline-chloride bath.

of alloys after identical heat treatments at 600°C appears to be directly proportional to the volume per cent of Ni_3P present.

After heat treatments at 200°C, an increase in the hardness was observed for all the electroless nickel alloys. In the low-phosphorus alloys, the rate of hardening was significantly greater than that in the high-phosphorus alloys as shown in Fig. 19. The observed dependence of the rate of hardening on phosphorus content partially accounts for the contradictory results of previous investigators concerning the tendency of electroless nickel to harden at 200°C. Goldenstein *et al.* (2), who reported no increase in hardness at 200°C, were studying high-phosphorus alloys. Zusmanovich (3) and Lee (5), who observed hardening, probably were studying low-phosphorus alloys.

In the high-phosphorus alloys, the relatively slow rate of hardening at 200°C seems to be indicative of the presence of an activation energy barrier, dependent on the phosphorus content, that retards the initial stages of the transformation and the hardening of the supersaturated solid solution. After a heat treatment at 400°C for 3 min, the low hardness of the alloy containing 9.0 w/o phosphorus compared to that of the alloy with 6.1 w/o phosphorus is further evidence for the existence of an activation energy barrier. If an activation energy barrier were not present, the high-phosphorus alloys should transform and harden faster than the low-phosphorus alloys because the instability of the solid solution and the free energy available for transformation should increase as the phosphorus content increases. Although in a few instances rate of precipitation may decrease with increasing solute concentration, we know of no reason to suspect that such a phenomenon should prevail here.

The strength and the ductility of the alloys heat treated at 200°C increase with a rise in phosphorus content as shown in Fig. 20. The measurements of strength of the alloys heat treated at 200°C for 120 min give a much more positive indication than hardness measurements that the low-phosphorus alloys start to transform before the high-phosphorus alloys. A comparison of the data in Fig. 16 and 20 indicates that a heat treatment at 200°C for 120 min decreases the strength of the low-phosphorus alloys by a factor of two but does not significantly affect the strength of the high-phosphorus alloys. The loss in strength in the low-phosphorus alloys resembles the embrittlement

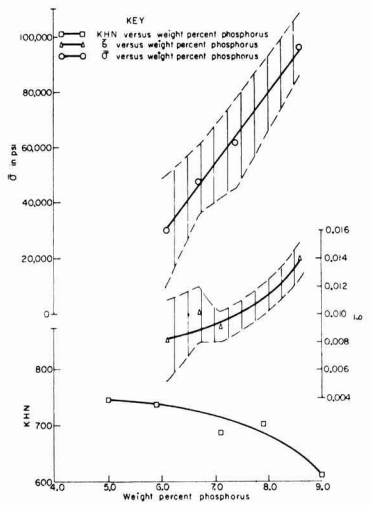

Fig. 20. Effect of phosphorus content on the mechanical properties of electroless nickel alloys deposited from alkaline-chloride bath and heat treated at 200°C for 120 min.

that accompanies the transformation of alloys during heat treatments at 400°C.

The decrease in ductility after heat treatments at 400°C is not observed after heat treatments at 200°C. Although the average values reported for the ductility of as-plated alloys and those reported for alloys heat treated at 200°C are almost identical, it is probably important to note that the scatter in the data for the low-phosphorus alloys heat treated at 200°C is much greater than that for as-plated alloys of comparable phosphorus content. Furthermore, changes in the mechanical properties of brittle materials are almost always indicated by variations in strength rather than in ductility because tests employed to measure strain are not sensitive enough. Even though the hydraulic bulge test is one of the most sensitive tests for detecting slight differences in the strain at fracture for brittle materials, its sensitivity is not very great at the strains at which electroless nickel deposits fracture.

Hardening Mechanism

The structural observations from x-ray pinhole transmission patterns and many of the characteristics of the increase in hardness after the heat treatment of electroless nickel tend to indicate the occurrence of conventional precipitation hardening. In the initial stages of precipitation hardening of a supersaturated solid solution, the atoms of the solute diffuse to a specific crystallographic plane with an atomic arrangement that resembles the array of atoms on a plane in the structure of the precipitate. As the atoms attempting to precipitate collect, they are forced to conform to the structure of the solvent. The forced coherency between atoms of the solvent and atoms attempting to form the structure of the precipitate causes severe, localized, elastic stresses that are responsible for the increase in hardness. When a sufficient number of solute atoms have collected, the structure of the precipitate is formed and the localized elastic stresses are relieved because the forced coherency no longer exists. After the formation of a significant number of precipitate particles at various locations throughout the specimen, the rate of hardening decreases and the hardness approaches a maximum.

The fact that there is no x-ray evidence for the presence of a phosphide precipitate in the low-phosphorus alloys that have been hardened by heat treatments at 200°C or by a heat treatment at 400°C for 3 min is in agreement with the established mechanism for precipitation hardening. After heat treatments at 400°C for more than 10 min, reflections from Ni_3P appear in x-ray diffraction patterns and the hardness approaches a maximum.

The strongest evidence obtained for the occurrence of conventional precipitation hardening in electroless nickel is based on the analysis of the relationship between the [111] fiber texture of the nickel phase and the preferred orientation of the Ni_3P phase, as revealed in the x-ray pinhole transmission pattern in Fig. 8. The presence of a preferred orientation in both the Ni_3P precipitate and the parent nickel phase implies the existence of a plane of coherency between the two crystal structures.

The habit plane on which a precipitate forms in the solvent is usually a plane of low indices. In the pattern in Fig. 8 and similar patterns, an analysis of the locations of the intense arcs on the {321} reflection of Ni_3P indicates that the {111} planes of fcc nickel are parallel to the {110} planes of Ni_3P, which has a body-centered-tetragonal structure with 32 atoms per unit cell. The arrangement of atoms associated with the $(\bar{1}10)$ Ni_3P plane shown in Fig. 21 bears a striking resemblance to the hexagonal array of atoms on the {111} planes of nickel. Furthermore, the average interatomic distance of 2.6Å on the {110} planes of Ni_3P is very close to the interatomic distance of 2.5Å in pure nickel. Therefore, the {111} planes of nickel

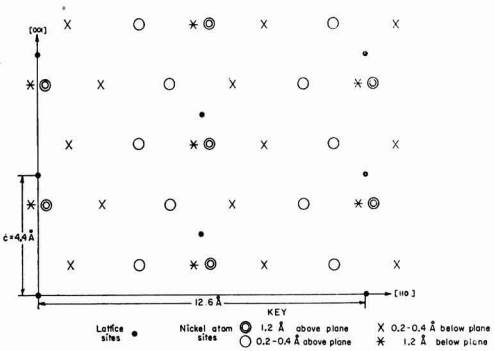

Fig. 21. Schematic sketch of the arrangement of atoms associated with the (110) plane of Ni_3P.

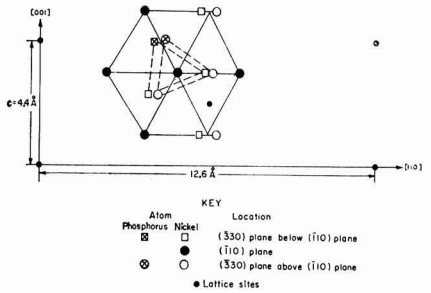

Fig. 22. Schematic sketch showing the pseudo hcp stacking sequence in the vicinity of a nickel atom on the (110) plane of Ni_3P.

satisfy all the requirements of a habit plane for the precipitation of Ni_3P.

The evidence that the {110} planes of the initial Ni_3P particles formed are parallel to the {111} planes of the nickel phase also tends to account for the existence of stacking faults in the as-plated deposits. In the Ni_3P structure, all of the phosphorus atoms may be considered to be located on a set of {330} planes which are immediately adjacent to the {110} planes. If one considers certain nickel atoms on {110} planes of Ni_3P and their nearest neighbors on adjacent {330} planes, a pseudo hcp stacking sequence is apparent, as shown in Fig. 22. This stacking sequence would correspond to a stacking fault in the fcc structure of the supersaturated solid solution in as-plated electroless nickel. If some of the phosphorus atoms in the as-plated alloy were segregated on {111} planes in the structure of the nickel solvent, they would tend to stabilize stacking faults because of the resemblance between the faults and a coherent structure of Ni_3P.

One important characteristic of the hardening of electroless nickel that is markedly different from conventional precipitation hardening is the inverse relationship between hardness and strength. In conventional precipitation hardening, an increase in hardness is accompanied by an increase in strength. The hypotheses that were proposed to account for the loss in strength during heat treatment of electroless nickel at 400°C do not explain why an increase in strength is not observed in the initial stages of hardening. In speculating on a plausible explanation for the unusual inverse relationship between strength and hardness in the initial stages of hardening, it is probably important to note that the established mechanisms and characteristics of conventional precipitation hardening are based on alloys with a grain size two to five orders of magnitude greater than that of as-plated electroless nickel. Very little is known concerning the relationships between strengthening mechanisms and the mechanical properties of extremely fine-grained alloys such as electroless nickel. Some of the characteristics of the hardening in fine-grained alloys might be different from those observed in alloys with a much coarser grain size.

Comparison of Alkaline-Chloride Deposits and Acid-Sulfate Deposits

No significant differences were observed between the x-ray diffraction patterns of alloys deposited from the alkaline-chloride bath and the patterns of deposits from the acid-sulfate bath. In the study of the effect of phosphorus content on the position and breadth of the {111} reflection from as-plated alloys, the data for the acid-sulfate deposits shown in Fig. 7 are extremely close to the curves established for the alkaline-chloride deposits. The data in Table III indicate that heat treatments have similar effects on the preferred orientation of the phases in alloys of comparable phosphorus content from the two baths.

In the microstructure of the as-plated deposits, the difference of one order of magnitude in the thickness of lamellae did not affect the mechanical properties shown on the graph in Fig. 16. However, it is possible that the steep phosphorus gradient across the acid-sulfate deposits obscures the effects on mechanical properties of differences in microstructure and plating bath composition. After heat treatments at 400°C, the mechanical properties of alloys deposited from the two plating baths were also similar, as shown by the data in Fig. 18.

Summary

An analysis of electron and x-ray diffraction patterns indicates that as-plated electroless nickel alloys are supersaturated solid solutions of phosphorus dissolved in crystalline nickel. An increase in phosphorus content above 7 w/o not only broadens and shifts electron and x-ray reflections, but also decreases the strength of a [111] fiber texture in the nickel-rich solid solution. Both the strength and the ductility of the as-plated alloys increase with a rise in phosphorus content whereas the hardness remains constant.

During heat treatments at temperatures ranging from 200° to 750°C, the development of a strong [111] fiber texture in the nickel phase is indicative of recrystallization and grain growth.

Differences in the mechanical properties of alloys after identical heat treatments at 200°C indicate that the phosphorus content affects the kinetics of the initial stages of transformation and hardening prior to the formation of a Ni_3P precipitate. The absence of a Ni_3P phase during the initial stages of hardening at 200° and 400°C is in agreement with the established mechanism for precipitation hardening. Additional definite evidence for the occurrence of precipitation hardening is the existence of a logical habit plane for the coherent precipitation of the Ni_3P phase.

Heat treatments at 400° and 600°C greatly decrease the strength and ductility of all the alloys. Low-phosphorus alloys heat treated for more than 30 min at 600°C recover a significant portion of the original loss in strength, but high-phosphorus alloys are still weak after 120 min at 600°C.

Heat treatments at 750°C that significantly improve the strength and ductility of low-phosphorus alloys greatly decrease the strength and ductility of high-phosphorus alloys. Hardness measurements give no indication of the abrupt changes in strength and ductility with increasing phosphorus content. The loss of strength and ductility in the vicinity of 7 w/o phosphorus indicates that a ductile nickel phase is the matrix in the low-phosphorus alloys, and a brittle Ni_3P phase is the matrix in the high-phosphorus alloys. Evidence in micrographs, x-ray diffraction patterns, and electron-probe microanalysis traverses confirms the change in the phase forming the matrix.

The x-ray diffraction patterns of alloys deposited from the acid-sulfate bath were similar to the patterns of alloys with comparable phosphorus contents deposited from the alkaline-chloride bath. The difference of one order of magnitude in the thickness of lamellae in the microstructure of as-plated alloys from the two plating baths has no apparent effects on mechanical properties.

Acknowledgment

One of the authors (AHG) was supported by a fellowship from the General Electric Educational Foundation during most of this investigation.

Manuscript received April 10, 1964; revised manuscript received Nov. 27, 1964. This paper was presented at the New York Meeting, Sept. 29-Oct. 3, 1964.

Any discussion of this paper will appear in a Discussion Section to be published in the December 1964 JOURNAL.

REFERENCES

1. A. Brenner, "Symposium on Electroless Nickel Plating," Spec. Tech. Publ. No. 265, A.S.T.M., Philadelphia, 1 (1959).
2. A. W. Goldenstein, W. Rostoker, F. Schossberger, and G. Gutzeit, *This Journal*, **104**, 104 (1957).
3. G. G. Zusmanovich, Metal Science and Heat Treatment (Russian), No. 4, 48 (1960).
4. A. Brenner, D. F. Couch, and E. K. Williams, *J. Research Nat'l. Bur. Standards*, **44**, 109 (1950).
5. W. G. Lee, *Plating*, **47**, 288 (1960).
6. W. H. Metzger, Jr., "Symposium on Electroless Nickel Plating," Spec. Tech. Publ. No. 265, A.S.T.M., Philadelphia, 13 (1959).
7. K. T. Ziehlke, W. S. Dritt, and C. H. Mahoney, *Metal Progress*, **77**, 84 (February 1960).
8. A. H. Graham, R. W. Lindsay, and H. J. Read, *This Journal*, **109**, 1200 (1962).
9. G. Gutzeit, *Plating*, **46**, 1158 (1959).
10. J. D. MacLean and S. M. Karten, *ibid.*, **41**, 1284 (1954).
11. A. Kreig, "Symposium on Electroless Nickel Plating," Spec. Tech. Publ. No. 265, A.S.T.M., Philadelphia, 21 (1959).
12. B. D. Cullity, "Elements of X-Ray Diffraction," p. 280, Addison-Wesley, Reading, Mass. (1956).
13. G. Thomas, "Transmission Electron Microscopy of Metals," p. 188, John Wiley & Sons, New York (1962).
14. H. J. Read and T. J. Whalen, *Proc. Am. Electroplaters' Soc.*, **46**, 318 (1959).
15. T. A. Prater and H. J. Read, *Plating*, **36**, 1221 (1949).
16. M. S. Paterson, *J. Appl. Phys.*, **23**, 805 (1952).
17. H. J. Read, *Plating*, **49**, 602 (1962).
18. S. Jovanovic and C. S. Smith, *J. Appl. Phys.*, **32**, 121 (1961).

Relationship between Deposit Thickness and Current Density during the Early Stages of Electrodeposition

Joseph B. Kushner[1]

Engineering School, Evansville College, Evansville, Indiana

ABSTRACT

Some experiments have been performed to determine how long it takes at a given current density to put a continuous copper deposit on a simple planar platinum cathode and what the average thickness of the copper deposit is at that time. The results indicate a hyperbolic power type of relationship between the current density and the time of full coverage and the current density and the deposit thickness at full coverage. A simple theory is proposed to explain the results obtained.

This is a preliminary report in connection with some experiments performed dealing with the origins of stress in electrodeposited metals. In a previous paper (1) the present author proposed that the stress in electrodeposited metals reaches a maximum value at the time the deposit becomes essentially continuous on the cathode. It is of interest therefore to determine for a given current density how thick the deposit is at the time continuity is achieved and how long it takes to arrive at this thickness.

At first glance this appears to be a rather elementary problem, but it is not as simple as it looks. If a deposit grows uniformly over the cathode surface, atom layer by atom layer, then at the time the cathode surface is continuously covered, the thickness of the deposit should be exactly one atom layer. But deposit growth does not occur like this. There is a certain amount of growth normal to the plane of the cathode as well as parallel to it. Furthermore it is well known that electrocrystallization on a cathode begins in many instances only after starting nuclei have formed. Evans and Shome (2) clearly demonstrated that in the case of a simple nickel plating bath growth starts from nuclei formed at the very beginning of the plating process and little or no additional nucleation occurs after that.

Electrocrystallization is very much similar to other kinds of crystallization, and thermodynamic reasoning leads one to the conclusion that the size of these starting nuclei should become smaller as the current density is increased. And since fewer atoms are required to form a nucleus there should be more of them at the start of plating at a higher current density than there would be at a lower current density. Furthermore, as current density is increased the rate of deposition is increased, and each of these starting nuclei grow at a faster rate. In accordance with this, therefore, it can be expected that at high current densities the cathode will be very quickly covered and the deposit thickness at that time will be very small whereas at low current densities, since less nuclei are formed, it will take longer to cover and the deposit will be thicker when full coverage is achieved. The purpose of the experiments described below was to determine what relationship, if any, existed between the current density used and the average thickness of the deposit at the time full coverage of a simple cathode surface occurred.

Experimental Equipment

The electrolyte used for the experiments was a 0.5M copper sulfate, 0.5M sulfuric acid solution. It was chosen because of its simplicity and because over a fairly wide range of current densities it is capable of producing microscopically resolvable deposits. Two liters of solution were made from analytical grade chemicals and distilled water. The solution was filtered through acid washed activated carbon and was preelectrolyzed using a strip of high-purity copper (99.-

[1] Also Director, Joseph B. Kushner Electroplating School, Evansville, Indiana.

999) as anode, as an additional purification. The solution was used in a specifically designed cell made of Lucite which held 16.4 ml of solution. The cell was drained after each test and filled with fresh solution for each succeeding test.

It is well known that exceedingly small amounts of impurities can have important effects in electrodeposition from acid copper sulfate baths, and no doubt the purification given the electrolyte was less than desirable, but it was felt that since each experimental bath would on the average contain the same kind and amount of impurities their effect on the deposit would be the same in all the experiments performed. The platinum strip was handled with considerable care to prevent bending and scratching of the surface beyond that already present in the as-received condition.

The cathode used was a thin strip of C.P. platinum (99.99+). Its dimensions were 0.01 in. thick, 0.25 in. wide and 4.00 in. long. The actual plating because of the cell design, occurred only on one side over a length of 1.00 in. so that the active cathode surface had an area of 0.25 in.^{2} (1.61 cm^2). Platinum was selected because it is known to give a reproducible surface (3, 6).

It has been shown quite convincingly that nucleation takes place at dislocation arrays such as polygonization boundaries, in the presence of impurities which at sometime during the previous history of the cathode have diffused to the dislocations (4, 5). For almost any other metal than platinum, surface cleaning would be sure to affect nucleation centers, leading to irreproducibility. In addition, the platinum surface gave a strong contrast to the pink colored copper deposit, a marked advantage in determining coverage.

The next question was how would continuity of the deposit be established? The criterion was the human eye, both unaided and with a microscopic amplification of 800 diameters. The plated cathode area was deemed fully covered when to the eye the deposit was uniformly spread over the surface and examination of random and selected areas at a magnification of 800 x showed no bare regions greater in area than 1/1000 of the total area of the field of view. Figure 1 shows a result in which the deposit was considered continuous. Figure 2 shows what was considered a discontinuous deposit. The human eye is amazingly sensitive to color, and some preliminary experiments indicated that the eye could detect films of copper only a few hundred angstoms thick.

The temperature of the plating bath was room temperature, 27°C + 1°. The cleaning procedure was as follows: The platinum strip, handled by tweezers at the nonplating end was heated in concentrated nitric acid for 2 to 3 min or long enough to remove the previous copper deposit. It was rinsed thoroughly in running distilled water and then anodically electrolyzed in a 10% solution of C.P. sulfuric acid using another platinum strip as cathode, at a potential of 6v so that there was copious oxygen evolution at the anode. This was followed by a distilled water rinse and then plating was started after permitting the strip to sit in the bath for 2 min without current.

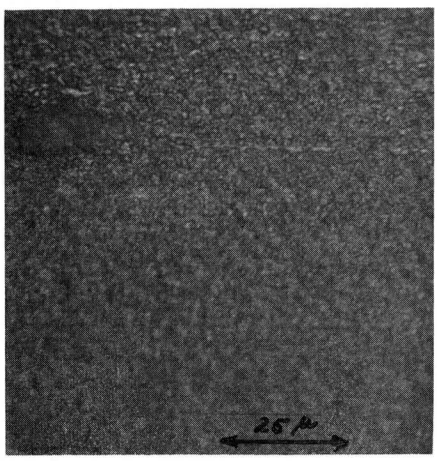

Fig. 1. Continuous copper deposit

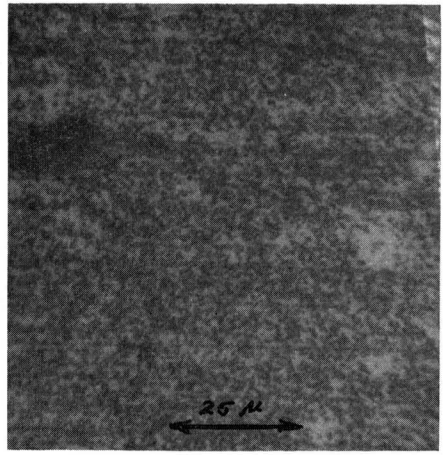

Fig. 2. Discontinuous copper deposit

It has been found by Becker (6) in the case of silver electrodeposition on platinum from a silver nitrate solution that random nucleation is produced whenever the platinum is given a cleaning treatment involving oxidation, such as dipping in nitric or sulfuric-chromate solution or flaming or anodic treatment in acid. He hypothesizes that oxygen is adsorbed on the cathode surface by these treatments, increasing the work of nucleation, and leading more or less to random nucleation. On the other hand he finds that cathodic treatment in nitric acid removes such an adsorbed oxygen layer, if formed, and leads to reproducible nucleation at easy nucleation sites with many many more nucleation sites available.

Use of a cathodic treatment in sulfuric acid was tried at first, but it was found that the hydrogen treatment led to nonuniformity of the copper deposit. Almost invariably for the same number of coulombs of electricity passed at several different current densities, the anodic treatment produced uniform coverage of the surface whereas the cathodic treatment resulted in bare areas. At this time no explanation is offered for this rather strange behavior. Possibly adsorbed hydrogen may be the cause of it. At any rate, on the basis of these tests, the anodic treatment was selected to help insure more random nucleation if this is what was occurring.

In order to determine the time of coverage as closely as possible, a pulse generator[2] producing an essentially square wave was used as the source of current. With this generator it was possible to produce either a single pulse or a series of pulses of known pulse width, spacing, and amplitude. The reasoning behind the use of a pulse generator was that the time element in the plating could be kept under closer control at the higher current densities when the time of plating was short. Thus, at higher current ranges full coverage might be obtained in a second or two with continuous current. With a pulse generator by using pulses of relatively small width compared to the pulse spacing the time factor could be magnified. For example, with a pulse spacing of 100,000 μsec and a pulse width of 10,000 μsec, the time of plating is magnified by a factor of 10.

Before using the pulse generator this way certain points had to be checked out. Basically these were:

[2] Servo Corporation of America, Model 3450D.

(*A*) Would the average thickness of the pulsed deposit be the same as for a continuous d-c deposit at the same number of coulombs? (*B*) Would pulse plating produce the same type of deposit, with reference to grain size, as continuous plating?

Regarding point *A*, it was found at once that some dissolution of the deposit took place during the off time particularly at low current densities. Thus at a current density below 4 ma/cm² the on-off ratio had to be 1 to 1 or better for an efficiency value as good as that for direct current. This was verified a number of times by plating the weighed platinum cathode with d.c. equivalent to the pulsed d.c. in terms of current density and coulombs passed. Efficiencies measured with the d.c. checked out very well with efficiencies at the same current density as measured by Turner (7) on an acid copper solution of similar composition. The efficiency with the pulsed current was likewise determined by weighing the platinum strip after a definite number of pulses producing the same current density and total number of coulombs was passed. These results came to within 2% or less of the d.c. results when the pulse width was at least one-half of the pulse spacing in the lower current density ranges. At higher current densities it was found possible to get results identical to the d.c. results with a wider pulse spacing; that is, a ratio of 1:10 could be used, thus magnifying the time by a factor of 10.

The attack on the copper deposit (and nickel in some other experiments) is no doubt due to the corrosive couple set up between the platinum and the copper. It appears that at relatively high plating current densities the interfacial film is depleted of ions or ion combination (most probably sulfate ions) that are capable of oxidizing the copper. The diffusion back to the interface of these attacking ions takes time and the next pulse puts on another layer of copper and retards the return of these ions. At lower current densities the attacking ions move only a short distance away from the cathode interface or are thinned out less extensively and, if the next pulse does not come quickly enough, some of the copper put on by the previous pulse is dissolved back into the solution, and the overall efficiency of the process becomes less than that of the d-c process. From the few pilot experiments tried, it appears that a considerable amount of information on diffusion and related subjects may be obtained by means of pulsing techniques.

With regard to the nature of the deposits, under the microscope the deposits produced by pulsed d.c. showed the same crystal size and general structure as those put down with the same number of coulombs of d.c. at the same current density. It may be that there are more subtle structure changes but these were not apparent to the eye.

It is also interesting to note that the copper deposits seemed almost invariably to nucleate along rolling lines, scratches, and other defects on the platinum strip. In most of the pictures taken a surface defect which can be seen in Fig. 1 and 2, was used as a landmark for positioning the surface so the same area could be photographed each time when desired. The circuit and apparatus layout is shown schematically in Fig. 3.

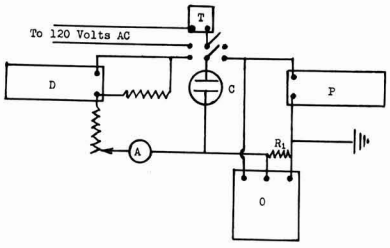

Fig. 3. Schematic of circuit used: T, electric timer; C, plating cell; P, pulse generator; A, ammeter; O, oscilloscope; D, constant current supply d.c.; R_1, precision resistor.

Table I. Time and deposit thickness at full coverage of platinum cathode

Actual plating time, sec, *t*	Coulombs passed, *Q*	Current density, ma/cm², *I*	Average thickness of deposit, Å, *T*
6.00	0.144	14.8*	329
17.5	0.280	9.88	638
30.0	0.360	7.41	822
80.0	0.640	4.94	1460
175.0	1.05	3.70	2400
400.0	1.60	2.47	3640
750.0	2.40	2.06	5470
1330	3.19	1.48	7280

* Measurements above this current density were not made due to difficulty in resolving crystal size.

The instantaneous current in the plating cell during pulses was determined from the measured instantaneous voltage drop across a precision resistor in series with the cell, as determined by means of a calibrated oscilloscope. Continuous direct current when used was produced by a constant current power source[3] and was measured by a precision Weston ammeter. During pulsed plating, the number of coulombs passed was determined by multiplying the number of pulses per second by the pulse width by the instantaneous current through the plating cell. The number of pulses (total) multiplied by the pulse width gave the actual plating time in seconds.

Data were obtained in the following way: At a given total current a known number of pulses were passed. The platinum strip was removed, rinsed in distilled water followed by a pure acetone spray, air dried and examined first with naked eye and then under the microscope at 800X. If the deposit showed bare areas, the strip was cleaned in hot nitric acid as previously described, given an anodic treatment in the 10% sulfuric, and plated again for a longer number of pulses and re-examined until finally the strip appeared to be fully covered (99.9%). The number of coulombs required for full coverage was determined by approaching full coverage from both the low coulomb side and the high coulomb side. The reproducibility of the method was good. It is estimated the maximum error is no greater than 10%. Each coulomb value (or time value) given in Table I is the result of at least two such determinations. The average thickness of each deposit was computed from the known number of

[3] Universal Electronics, Model I020-2A.

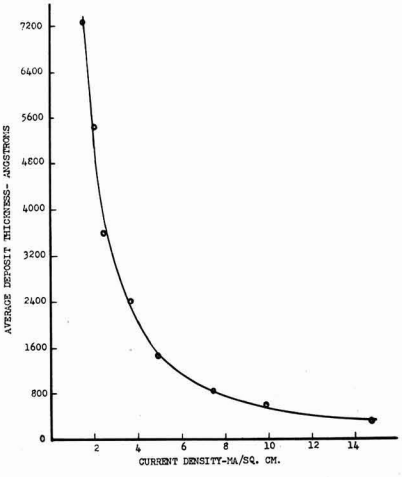

Fig. 4. Relationship between current density and average deposit thickness at time full cathode coverage is reached.

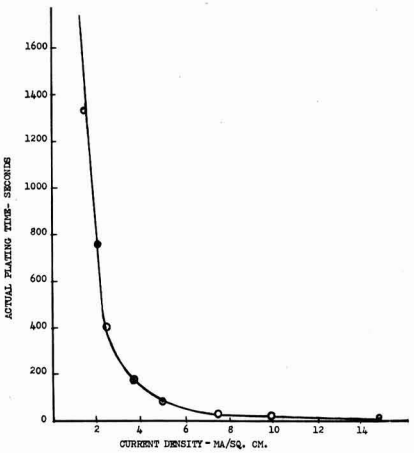

Fig. 5. Relationship between current density and time to reach full cathode coverage.

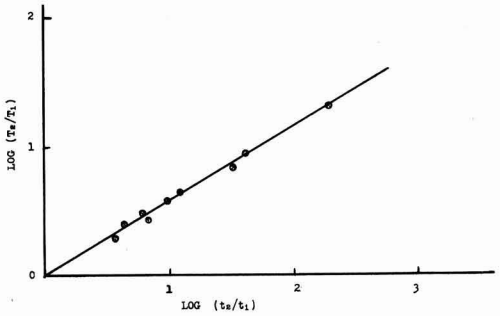

Fig. 6. Relationship between (T_2/T_1) and (t_2/t_1) at time full cathode coverage is reached.

coulombs passed, the nominal plated area, the electrochemical equivalent, and the bulk density of copper. Results for the copper solution described and the platinum strip used are given in Table I.

Three graphs have been plotted from the data. Figure 4 is a plot of the average deposit thickness *vs.* the current density used, at the time full coverage is reached. Figure 5 is a plot of the time to reach full coverage *vs.* the current density used and Fig. 6 is a plot of the log of (T_2/T_1) *vs.* the log of (t_2/t_1) where t_1 is the time in seconds to produce a deposit of average thickness T_1 angstroms, etc. Figures 4 and 5 show a hyperbolic type of relationship betweeen the thickness, time, and a power of the current density. Figure 6 gives what appears to be a straight line, with a slope of 0.57. The reason for this last plot will appear in the theory and discussion which follows.

Theory and Discussion

According to Evans and Shome (2) the area covered by a deposit on a flat cathode of area A_o in time t, is given by

$$A = A_o(1 - e^{-\pi v^2 t^2 N}) \qquad [1]$$

where v is the velocity of lateral spreading of the deposit (assumed constant for a given current density) and N is the number of nuclei originally formed. At the time of full coverage, assuming 99.9% to be full coverage, for different nucleation numbers, velocities, and times (different current densities) it can be said

$$\ln(1000) = \text{constant} = \pi v_1^2 t_1^2 N_1 = \pi v_2^2 t_2^2 N_2 = \pi v_3^2 t_3^2 N_3 \ldots \qquad [2]$$

What this series of equations is saying is that when coverage is complete, the lateral area of each grain deposited, multiplied by the number of grains (number of nuclei) is equal to the total area of the cathode surface A_o, or

$$A_1N_1 = A_2N_2 = A_3N_3 = \ldots\ldots = A_o \qquad [3]$$

and

$$A_1/A_2 = N_2/N_1 \qquad [4]$$

Assuming all directions of lateral growth equally possible, the lateral growth that occurs from a given nucleus in time t must be equal to $a\sqrt{A}$, where a is a geometric constant. As a first approximation, the normal growth or thickness, T, can be assumed to be a simple linear function of the lateral growth. That is, $T = k\sqrt{A}$ where k is some proportionality constant. Solving for A gives $A = (T/k)^2$. Substitution of this value for A in [3] gives

$$(T_1/T_2)^2 = N_2/N_1 \qquad [5]$$

Electrocrystallization is very similar to other forms of crystallization, and by thermodynamic reasoning (8) it can be shown that the minimum radius of a crystal nucleus that will continue to grow is given by $R = Cs/G$ where C is a constant having to do with shape and interfacial relations, s is the surface energy (interfacial energy), and G is the free energy of the newly formed phase, all in consistent units.

In the case of electrocrystallization at a fixed temperature the interfacial energy is constant, and the free energy of the newly arriving metal ions will be measured by the difference between the energy they had as ions in solution and the energy they possess on sitting down on the substrate. This is given by the overpotential for deposition, e, the difference between the equilibrium potential and the actual potential required to produce deposition. Accordingly it can be said that

$$R = K/e \qquad [6]$$

where K is a new constant involving previous factors and the faraday.

If we consider the nucleus to be two dimensional at the start which is probably the case, and r is the radius of each individual atom of metal, then

$$\pi(K/e)^2 = bnr^2\pi$$

where n is the number of atoms in the nucleus and b is a constant having to do with the geometry of the arrangement. As a simple approximation in the case of copper, since the overpotential is relatively small, we can assume that the overpotential is directly proportional to the current density, I. This being so, the number of atoms forming a nucleus at a given current density, is proportional to one over the square of the current density, or

$$n \propto 1/I^2$$

Let m be the number of atoms deposited per unit of time per unit area which according to Faraday's law is proportional to I. Assuming the nuclei are formed in the first instant of time, the average number of nuclei formed at the start will be given by $m/n = N$. Thus N is proportional to $I/(1/I^2)$ or I^3. This line of reasoning, therefore, leads to the result that the number of nuclei formed at the start is proportional to the cube of the current density and as a result,

$$N_2/N_1 = (I_2/I_1)^3 \qquad [7]$$

Substitution of this value for N_2/N_1 in [5], gives

$$T_1/T_2 = (I_2/I_1)^{3/2}$$

or

$$T(I)^{3/2} = T_2(I_2)^{3/2} = T_1(I_1)^{3/2} = \text{a constant} \qquad [8]$$

But the average thickness of an electrodeposit varies directly with the number of coulombs $I\,t$, and accordingly,

$$T_1/T_2 = I_1t_1/I_2t_2$$

If alternate substitutions are made for T and I in [8], using this last relationship, there results

$$t(I)^{5/2} = t_1(I_1)^{5/2} = t_2(I_2)^{5/2} = \text{a constant} \quad [9]$$

and

$$T_1/T_2 = (t_1/t_2)^{3/5} \quad [10]$$

If this theory is correct, we would expect that the relationship between current density and time and current density and thickness to take the forms shown in Eq. [8] and [9]. Likewise if a plot is made of the log of T_1/T_2 against the log of (t_1/t_2) the slope of the straight line, if it is a straight line, should be equal to 0.60 (3/5). The slope of the actual experimental line is 0.57 which is in excellent agreement with the theoretical value. A plot of Eq. [8] and [9] fits the experimental data fairly well but if $T(I)^{1.33}$ = a constant is plotted rather than $T(I)^{1.50}$ = a constant the smooth line through the experimental points shown in Fig. 4 is obtained and if $t(I)^{2.33}$ = a constant is plotted the smooth curve through the points of Fig. 5 results.

By assuming that the growth normal to the cathode is proportional to a power of the lateral growth, *i.e.*, $T = k(A)^{P/2}$ where p is an unknown power, and using the same type of procedure given above, we end up with the following relationships to replace [8], [9], and [10]:

$$T_1(T_1)^{3p/2} = T_2(I_2)^{3p/2} = \text{constant} \quad [8a]$$

$$t_1(I_1)\,\frac{3p+2}{2} = \text{a constant} \quad [9a]$$

$$T_1/T_2 = (t_1/t_2)\,\frac{3p}{3p+2} \quad [10a]$$

If $3p/3p + 2$ is set equal to 0.57, this gives $p = 0.883$ and substitution into [8a] and [9a] of this value gives $TI^{1.33}$ = constant and $tI^{2.33}$ = constant, with a better fit, as can be seen from the figures. It appears therefore on the basis of this evidence that the rate of growth normal to the cathode surface is almost but not quite a linear function of the rate of lateral growth. Because of possible errors in measurement and the appearance of exponential relationships, it may be that the first hypotheses is the correct one. Additional experiments will have to be performed in order to verify this. The hyperbolic power relationship shown here for copper is probably applicable to other deposits from simple solutions, at relatively low activation overpotentials. In the case of nickel which deposits at high activation overpotentials the number of nuclei formed will be very great (very fine crystals), and the technique used here for copper would be difficult to apply. Additional experiments are in progress in connection with the maximum stress in copper deposits in relation to these findings, which will be reported on in future papers.

Acknowledgment

The author would like to thank Mr. Wilfred Hung for assisting with the laboratory work, Mr. Russell Schoene for advice and assistance in connection with the electronic equipment, and Mr. Ed Reine for construction of the cell and other essential equipment.

This work was supported in full by National Science Foundation Research Grant GP-1678.

Manuscript received Sept. 22, 1964; revised manuscript received Dec. 18, 1964.

Any discussion of this paper will appear in a Discussion Section to be published in the December 1965 JOURNAL.

REFERENCES

1. J. B. Kushner, *Proc. Amer. Electroplaters' Soc.*, **45**, 28 (1958).
2. U. R. Evans and S. Shome, *J. Electrodepositers' Tech. Soc.*, **27**, 45 (1950-51).
3. J. K. Prall and L. L. Schreir, *Trans. Inst. Metal Finishing*, **38**, 9 (1961).
4. S. Weissman, *et al.*, Air Force Cambridge Labs., Project, 4608, Report No. 1, July, 1962.
5. T. B. Vaughn and H. J. Pick, *Electrochima Acta*, **2**, 179 (1960).
6. J. J. Becker, *This Journal*, **111**, 480 (1964).
7. D. R. Turner and G. R. Johnson, *ibid.*, **109**, 798 (1962).
8. G. M. Pound, "Liquid Metals and Solidification," p. 90, American Society for Metals, Cleveland (1958).

Growth of Single Crystal Cuprous Oxide from the Melt and Luminescence of Cuprous Oxide

Richard S. Zucker

Astrionics Division, Aerojet-General Corporation, Azusa, California

ABSTRACT

A number of crucible materials were evaluated for melting Cu_2O. Only MgO appears to be sufficiently nonreactive for use in crystal growing. A melt of cuprous oxide contained in a magnesia crucible when cooled at a rate of 2.5°C per hour produced large single crystals. Attempts to accelerate growth by cooling at a rate of 13.5°C per hour produced only small polycrystals. A (100) seed cut from the single crystal along natural cleavage lines was used to pull a crystal from the melt by the Czochralski method. A tendency to grow off-axis resulted in beautiful subsurface facets of transparent ruby-red material. Two new forms of luminescence were observed during rapid cooling of solid cuprous oxide. From 1175° to 1145°C continuous light emission was observed in the yellow-green region. From 1125° to 975°C flashing points of light were observed in the same spectral region.

Polycrystalline cuprous oxide rectifiers have been in use since 1929 as instrument and power rectifiers because of their excellent frequency response, resistance to pulse damage, and exceptionally high reliability and long life. These have been prepared by partial oxidation of copper sheets of the desired shape. Recently large area single crystals have been formed by annealing of polycrystalline cuprous oxide (1). No reports of crystal growth from the melt have been observed in the literature. One observer in 1933 reported failure to obtain crystal growth by the Bridgman or hydrothermal techniques (2). This paper describes the growth of ingots of single crystal cuprous oxide by the Czochralski method and some interesting phenomena observed during these experiments.

Experimental

A graphite resistance heated crystal furnace with sapphire Radiamatic control and linear down-drive (motor-driven downward adjustment of the tempera-

Table I. Evaluation of crucible materials for melting cuprous oxide

Run No.	Crucible material	Results at 1230°C in presence of Cu_2O
1	Alumina[6]	Highly reactive, not satisfactory.
2	Tantalum	Highly reactive, not satisfactory.
3	Graphite	Highly reactive, Cu_2O reduced to Cu.
4	Molybdenum	Reactive, alloys with metallic copper.
5	Magnesia (sintered)[6]	Best of all materials tried, only slightly reactive with melt over long periods of time.
6	Crystolon 63[1] (silicon carbide, oxynitride bonded)	Wetting, partial reduction to Cu, scum on surface.
7	Cerac 4[2] (aluminum nitride 95% silicon carbide 5%)	Violet wetting occurs, N.G.
8	Cerac 6[2] (aluminum nitride 55% silicon carbide 45%)	Violet wetting occurs, N.G.
9	Magnesia (single crystal)[6]	Melting without wetting occurs for 5 minutes. May be OK.
10	Lecotherm ceramic[3]	Soaked right through crucible on melting.
11	Zirconium silicate[4]	Soaked right through crucible on melting.
12	Cerac 2[2] (boron disilicide)	Strongly reductive, glass binder in crucible reactive with melt.
13	Boron nitride[5]	Most violent reaction of all, evolution of gas and ejection of contents from crucible.
14	Thoria[3]	Entire contents reduced to copper, which permeated walls of crucible.
15	Calcium zirconate[3]	Entire contents reduced to copper, which permeated walls of crucible.
16	Quartz[7]	Violently reactive to form copper silicate.
17	Zirconia[6]	Wetting of crucible, but no violent reaction. Scum formation limits time available.

Notes: [1] Carborundum Corp.; [2] Allis-Chalmers Corp.; [3] Leco Corp.; [4] Saxonburg Ceramic; [5] National Carbon Co.; [6] Norton Corp.; [7] Englehard Industries.

ture-set-point of the furnace controller) was used throughout this work. Baker Cu_2O powder was washed with benzene to remove the antioxidant (pine oil), dried, and weighed into the crucible. Argon (99.998%) or helium at 10 CFH was used for the furnace atmosphere. Subsequent experiments proved that the same results were obtained by weighing the unwashed Cu_2O directly into the crucible and removing the antioxidant by a vacuum heat treatment prior to melting. The crucible materials used are shown in Table I. About one-third reduction in volume of the powder is observed prior to melting, and a gradual change in color of the powder from ruby red to violet to black was noted. Norton RM-5480 Magnesia crucibles were used when pulling crystals using (100) seeds 5 x 5 x 25 mm cut from slow cooled runs. The seeds showed an approximate 70°32′ cleavage angle characteristic of (111) $\wedge$ (111) cuprite octahedrons. A natural crystal of cuprite may also be used as a seed. Slow cooling at a linear rate of 2.5°C per hour was easily obtained by automatic reduction of the power input to the furnace. Cooling at a rate of 13.5°C per hour produces polycrystalline material. At the melting point of cuprous oxide (1230°C) a change in apparent emissivity is evident, the melt appearing much brighter than the solid. The optimum pulling rate was found to be 1.75 cm/hr. The crucible was rotated at a speed of 10 rpm throughout all 28 runs in order to minimize uneven heating of the crucible. In addition, during some runs it became necessary to rotate the seed in an opposite direction at the same rate (10 rpm), making a total rotation rate of 20 rpm. The thermal fluctuations observed on the recorder during a typical run at equilibrium at the melting point of Cu_2O amounted to a maximum of 1.7°C, but the actual stepless controls of the furnace provide probably 0.2°C responsivity or better, if properly adjusted. A number of small crystals approximately 1 cm in diameter were easily grown using seeds. However, only one large irregular shaped crystal was grown which is shown in Fig. 4. The maximum diameter of this crystal was about 3 cm. The gross impurity in this crystal consisted of microscopic tree-like growths of metallic copper as determined by viewing a section of the crystal through a strong light. These apparently did not affect the single crystal of Cu_2O. In addition, some areas of this crystal were covered with a thin black surface layer of cupric oxide, CuO, which was easily removed in dilute hydrochloric acid before examination. No spectrographic or other methods were used to determine trace impurities, although from examination of the crucible attack after the run, it is strongly suspected that magnesium was picked up by the melt during a period up to several hours' contact with the molten cuprous oxide. The crystal, when viewed from the top during pulling, will show characteristic fourfold symmetry with light reflected off the (100) facets. These may not be present in all cases, as they seemed to predominate only when the crystal tended to grow off axis. Also, the crystal may tend to be lopsided due to freezing out of crucible reaction products on the crucible walls. Considerably more difficulty in growing cuprous oxide may be expected compared with silicon crystals due to the reactivity of the melt with magnesia. The single crystal character of the pulled crystal was confirmed by x-ray diffraction techniques (forward and back reflection Laue photographs).

After pulling is completed and during rapid cooling (approximately 100°C per min) of the remainder of the solid in the crucible, one or two luminescence phenomena may be observed, depending on the crucible material used. From 1175° to 1145°C the solid will instantaneously emit a burst of yellow-green light, L_1, which will diminish in intensity as the melt cools further, extinguishing at approximately 1145°C. No attempts were made to study the spectral characteristics of this high-temperature luminescence phenomenon, L_1. Over a much wider range of temperature (1125°-975°C) intermittent flashes of yellow-green light of 0.2-2 sec duration, L_2, will be observed. Cinespectrograph film measurements of the radiation of cuprous oxide over the temperature range 1125°-975°C show an absorption band in the yellow region of 0.56-0.60μ, and no emission lines or bands in this region are evident. The cinespectrograph used in this experiment consisted of a conventional slit, collimator, grating, lens, and film system. The film handling mechanism was a 35 mm cine camera permitting a sequence of spectra to be made at a rate of 10/sec. A lens in front of the slit serves as a light-gathering device for use with distant sources. It was not possible to focus this lens on the nearby source used in this experiment. Under these circumstances, therefore, emission lines from a blinking low-intensity point source on top of a 1200°-1300°K black body might easily have remained undetected. The emission wavelength is unknown at the present time. A more elaborate system would be required to determine the wavelength of emission of this radiation. These flashing lights appear at random throughout the solid and are especially intense wherever the Cu_2O has wetted (reacted with) the crucible walls. They remain of constant intensity throughout the above temperature range and then suddenly disappear at approximately 975°C. The high-temperature (continuous) light phenomena will be referred to as L_1, since it is the first to be observed on the cooling curve, and the lower temperature (flashing) light phenomena will be referred to as L_2 throughout the discussion. Both L_1 and L_2 can be repeated at will without any loss of intensity by reheating the contents of the crucible and cooling at the same rapid rate. Neither can be observed by cooling at a slow rate (10°C per min or less) or on the normal heating cycle.

Discussion

The best crucible materials are those which were compacted to the greatest degree during manufacture. To that extent the best results might be obtained from the use of single crystals of the respective materials, if available, by hollowing them out to form crucibles. On the basis of observed order of chemical reactivities with the melt, it might be predicted that crucibles made of beryllia would be less reactive than magnesia

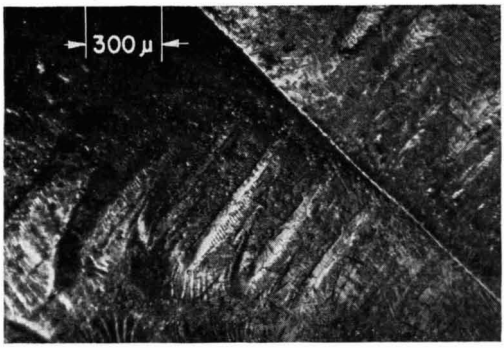

Fig. 1. Single crystal of cuprous oxide showing ridge along (100) sub-surface facet.

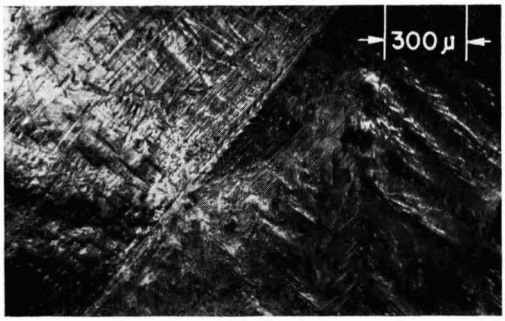

Fig. 2. Single crystal of cuprous oxide showing ridge along (100) sub-surface facet and light reflected off facet (left).

which is less reactive than alumina. Due to toxicity BeO crucibles were not tried, however. Crucibles made by pressing MgO slurries in a laboratory press were unsatisfactory due to porosity. However, use of a Pt crucible coated with MgO has been reported (3).

A microscopic view of the grown surface of a single crystal of cuprous oxide is shown in Fig. 1 and 2. The ridge along the edge of the facet is clearly shown here. The plane angle of the facet measured 90° ± ½°, characteristic of a (100) face (see Fig. 3). However, the vertex of this angle is inclined approximately 45° toward the seed axis indicating a shortening of the third cubic axis to form a rhombohedral pseudo-symmetry (4), although not clearly shown in Fig. 3 or 4. Cuprite (natural cuprous oxide mineral) belongs to the plagiohedral or gyroidal class of the isometric system because the faces of the general form (hkl) are arranged in spiral order. This class is rare among minerals and is represented, almost uniquely, by cuprite. It is interesting to note that because of this character, cuprous oxide may be expected to show circular polarization of light.

All material grown was p-type except one run made in a Ta crucible, which was strongly n-type and highly impure due to reaction of the melt with the tantalum crucible. It is suspected that almost degenerate doping with Ta resulted in this anomaly. Attempts to repeat this with 1% TaC (tantalum carbide) added to Cu_2O in a magnesia crucible resulted only in p-type material. Measurements made on typical crystals using silver paste to provide ohmic contacts are shown in Table II. These results show a hole mobility somewhat higher (about one order of magnitude) than that shown in the literature (5, 6).

A simple etch for revealing grain boundaries was 28% ammonium hydroxide for 5-30 min. For removing CuO deposits 3*N* HCl was found to be suitable.

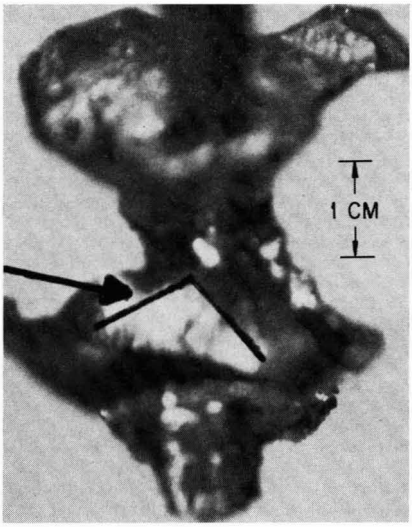

Fig. 3. Side view of pulled crystal of cuprous oxide showing light reflected off sub-surface (100) facet (arrow) and 90° plane angle (lines). Crystal was pulled out of melt rapidly to freeze the growth pattern, hence difference in diameter. The plane angle measured 90 ± ½°. Apparent distortion is due to perspective of the camera.

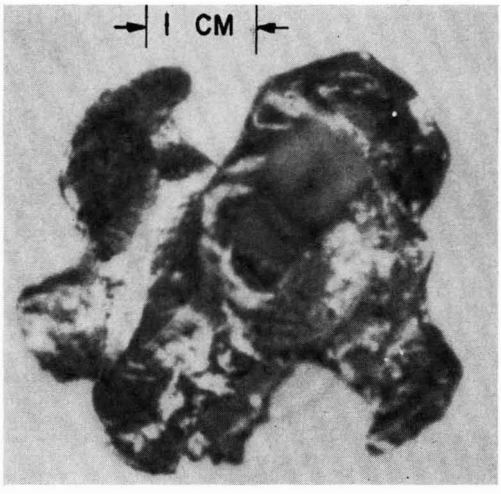

Fig. 4. Top view of Cu_2O crystal showing (100) seed

Luminescence

It is obvious from the limited data presented in this paper that a mechanism for the observed light emission cannot be put forth, particularly in view of the lack of data on the wavelength of emission. The two luminescence phenomena may not even be related in their mechanisms. Furthermore, both phenomena correspond to an "inverse thermoluminescence" since the emission is observed only on the cooling curve and not

Table II. Typical properties of single crystal cuprous oxide

Conductivity type	p
Resistivity, ohm-cm	4×10^3-16×10^3
Hall constant, cc/coulomb	2.1×10^6-2.2×10^7
Mobility, cm²/volt-sec	480-1300
Carrier concentration, carriers/cm³	3×10^{11}-3×10^{12}

on the heating curve. This is exceedingly difficult to explain. One is therefore forced to look for less obvious reasons such as possible phase changes in the system or the excitation of an impurity in the material. A brief review of the literature given below may be of interest at this point.

1. An anomalous vapor pressure curve has been reported for cuprous oxide (7, 8), because of the formation of a eutectic with cupric oxide. The vapor pressure of oxygen in equilibrium with liquid Cu_2O at 1230°C (mp of Cu_2O) is 0.6 Torr. This vapor pressure increases to 402 Torr in cooling to 1080°C (CuO-Cu_2O eutectic). Since the observed emission of L_2 is in the range of 1125°-975°C, this emission may in some cases be related to the CuO-Cu_2O eutectic at 1080°C, since it is known that CuO is present at least on the surface of the melt.

2. A rapid cooling rate of over 100°C per min is certainly a nonequilibrium condition, which may under these circumstances allow electronic transitions to occur which might otherwise be forbidden (9, 10).

3. Differential thermal analysis is indicated to explore the region 400°-1300°C to correlate light emission with perhaps extremely minute changes in the localized rate of cooling. No high-temperature phase changes have been reported for Cu_2O. However, crystallographic changes between 25° and 400°C have been reported (11) for cuprous oxide and similar changes for cuprous chloride (12).

4. The photoconductivity of Cu_2O is very complex (13), a maximum occurring at 0.57μ but complicated by "steps" in the absorption edge due to multiple level transitions, particularly in the yellow and green series of exciton absorption spectra (14) at 77.3°K. It is not known how this might affect the results observed.

In conclusion, it may be said that more precise measurements of the radiation observed will be required to resolve the exact nature of this luminescence. This may be rather difficult, in view of the transient as well as high-temperature nature of the phenomena.

Acknowledgments

The author is pleased to acknowledge the technical discussions of Dr. P. N. Russell and Dr. R. H. McFee. Interpretations of the cinespectrograms by Mr. Carleton W. Clench are greatly appreciated.

Manuscript received Oct. 13, 1964.

Any discussion of this paper will appear in a Discussion Section to be published in the December 1965 JOURNAL.

REFERENCES

1. R. S. Toth, R. Kilkson, and D. Trivitch, *J. Appl. Phys.*, **31**, 1117 (1960).
2. E. Englehard, *Ann. Phys.*, **17**, 501 (1933).
3. F. H. Smyth and H. S. Roberts, *J. Am. Chem. Soc.*, **42**, 2582 (1920).
4. W. E. Ford, "Dana's Textbook of Mineralogy," 4th ed., John Wiley & Sons, New York (1958).
5. J. S. Anderson and N. N. Greenwood, *Proc. Roy. Soc. (London)*, **A215**, 353 (1952).
6. J. Bloem, *Philips Research Repts.*, **13**, 167 (1958).
7. M. Randall, R. F. Nielsen, and G. H. West, *Ind. Eng. Chem.*, **23**, 391 (1931).
8. H. S. Roberts and F. H. Smyth, *J. Am. Chem. Soc.*, **43**, 1061 (1921).
9. J. H. deBoer and J. W. Verway, *Proc. Phys. Soc. (London)*, **49**, 59 (1937).
10. W. Schottky and F. Waibel, *Phys. Z.*, **36**, 912 (1935).
11. T. Ikada, *J. Phys. Soc. Japan*, **4**, 140 (1949).
12. M. R. Lorenz and J. S. Prener, *Acta Cryst.*, **9**, 538 (1956).
13. E. F. Gross, *Uspekhi Fiz. Nauk.*, 575 (1957).
14. F. L. Weichman, Ph.D. Thesis, Northwestern University (1958).

Poisoning and Gettering Effects in Silicon Junctions

E. J. Mets

Rectifier Components Department, General Electric Company, Auburn, New York

ABSTRACT

A study was made to obtain an understanding of the factors involved in the "poisoning" phenomena which are responsible for high reverse currents in silicon junctions. A tentative model has been proposed which describes the conditions by which fast diffusing metal impurities can precipitate within junction regions under certain high-temperature ambients and yet not under others. Oxygen appears to be a significant factor which can control the degree and location of such metal precipitation. The role of oxygen was investigated in its relation to impurities and defects in silicon. Its importance was demonstrated by copper-oxygen reactions, oxygen tie up complexing to form SiO_4^+ donor states, and by the effect of induced dislocations.

Considerable effort has been applied to the study of soft reverse characteristics of p-n junctions as indicated by excess reverse current below their normal avalanche breakdown voltage. The origin of this high leakage current is believed to be localized high electric fields caused by precipitated metal particles within the junction region. Goetzberger and Shockley (1, 2) have shown that metals with temperature dependent solubilities in silicon, such as Cu and Fe, can form precipitates through which current flows by Zener tunneling as a result of the high fields. However, certain diffusion processes do yield devices which have good electrical characteristics whereas other high-temperature processes cause degradation of junctions. Prior to this work no explanation as to why and how these precipitates occur in the bulk and junction regions of Si has been offered. As these undesired impurities are introduced into silicon to some degree by all such processes, there must be some controlling factors which reduce or prevent these impurities from collecting in junction regions in some cases but not in others. It is the purpose of this study to investigate those conditions which lead to the poisoning phenomenon and to establish a tentative model by which such precipitates locate in bulk silicon.

Previous observations.—It has been observed that diffused p-n-p structures as formed by Ga sealed-tube techniques yield "hard" breakdown (*i.e.*, devices which show negligible poisoning effects but exhibit avalanche breakdown characteristics). Subsequent oxidation procedures cause these reverse characteristics to become "soft" or poisoned. Typical characteristics are shown in Fig. 1.[1] Later phosphorus diffusion generally causes a poisoned unit to return to its original characteristics. The following discussion of the effects of each of these

[1] All devices were surface contoured to confine the avalanche regions to the body rather than the surface of the device. Further information concerning this technique can be found in a paper by R. L. Davies and F. E. Gentry entitled, "Control of Electric Fields at the Surface of p-n Junctions," *IEEE Transactions on Electron Devices*, July, 1964.

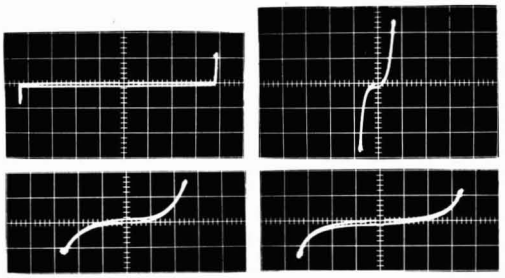

Fig. 1. Typical reverse characteristics of Ga diffused p-n-p junctions showing relative effect of cooling rate exposure to oxygen ambient at 1200°C: Vertical axis 5 ma/div; Horizontal axis 200 v/div. (*a*) (top left) as diffused; (*b*) (top right) furnace cool, 250°C/hr; (*c*) (bottom left) slow cool, 15°C/hr; (*d*) (bottom right) quenched.

three high-temperature operations results in a model which describes mechanisms that affect precipitation of these impurities in junction regions.

The formation of p-n-p structures by the normal sealed tube technique employs a Ga source along with silicon wafers which are sealed in a quartz capsule and back filled with argon through a liquid nitrogen trap. Avalanche-type electrical characteristics are ascribed to three possible effects. (*A*) The system is clean, free of poisoning impurities; (*B*) simple, glassy phase gettering occurs on the silicon surface; (*C*) fast diffusing impurities are removed by surface reactions which occur due to a lower partial pressure of oxygen in the sealed tube. In practice the first two are not probable. Deliberately poisoned Ga p-n-p structures, sealed in argon and heat-treated without a Ga source, are brought back to their original sharp characteristics with a significant increase in minority carrier lifetime. As no liquid phase is present, some other mechanism than glassy phase gettering must take place. This is probably the same means by which good p-n-p structures are originally formed. At the diffusion temperature (1250°C), metallic impurities are considered to be present from the source, quartz, gas ambient and on or in the silicon. The solid solubility of these impurities in silicon will be in equilibrium with phases present (such as oxides or gas) and dependent on temperature. On cooling, precipitation of these metallic impurities can occur because of decreasing solubility. A driving force to the surface is necessary to prevent precipitation in the vicinity of the junction. Such surface reactions can take place under a low partial pressure of oxygen by forming stable compounds of an oxygen complex. It has been shown by Schwuttke (3) that impurities such as copper will locate preferentially at regions of high oxygen concentration. This migration of residual oxygen in the silicon toward the surface would be a sufficient driving force for the removal of these fast diffusing impurities.

Under conditions of open-tube oxidation, silicon is exposed to temperatures 1100°-1250°C under wet or dry oxygen ambient to form an oxide phase on the silicon surface. Simultaneously, oxygen diffuses into the silicon along with undesired impurities. On cooling, precipitation of these impurities will occur at structural defects in the bulk with the size and location of the precipitates governed to some degree by the cooling rate. Sites of high oxygen concentrations can be formed in the bulk, thus preventing the mechanism of transport of fast diffusing impurities to the surface.

In fabricating p-n-p-n devices, phosphorus diffusion of the n-type emitter junctions often will restore p-n-p units which have been previously poisoned by the oxidation-mask step. In this two-step phosphorus diffusion process, first a phosphorus-silicate glass is formed under nitrogen or oxygen. Here an apparent liquid phase gettering effect (1) takes place. Normally, after this first predeposition step, the glass formed is removed prior to a higher temperature diffusion anneal under oxygen. It can be assumed that under these conditions liquid phase gettering is not present but rather some other mechanism is responsible for the prevention of downgrading. This might be explained by high surface doping concentrations which strain the lattice and thereby form dislocations at the surface. Prussin (4) and Quiesser (5) have shown that the stress introduced by solute contraction of phosphorus and boron in silicon is sufficient to generate dislocations. With these dislocations present, a "sink" can be formed, trapping fast diffusing impurities as "atmospheres" of the dislocations or by complexing with oxygen in these regions.

A poisoning model.—The model suggests that a controlling relationship exists between the gas ambient (particularly oxygen) and the type of diffused donor or acceptor impurity in silicon. It appears that the degree and location of such precipitation of fast diffusing metal impurities is influenced by the oxygen movement in the silicon. Clustering or precipitation of these impurities will occur at sites of high oxygen concentration, forming oxygen complexes and thus reducing the metal impurity level in other regions of the silicon. Oxygen will form atmospheres around diffusion induced dislocations thus depleting adjacent areas of oxygen and metallic impurities. Considerable evidence has been obtained to support this concept. These experiments have been based on copper-oxygen reactions, oxygen complexing to form SiO_4^+ donor states and surface induced dislocations.

Experimental

In an effort to determine the source of contamination, various parameters of the open tube systems were evaluated. Ga-diffused p-n-p wafers were chosen for this initial study. These structures offered good initial reverse avalanche-type characteristics which are sensitive to the poisoning phenomena.

Gallium diffused p-n-p structures, which were formed in chemically polished 20-22 ohm-cm n-type Si, generally had a junction depth of 3 mils and a base region of 3 mils so that avalanche voltages of 700-900v were obtained. Wafers were pelletized to a diameter of 0.640 in. and subsequently edge beveled to a 6° angle to eliminate surface effects. In all tests only avalanche type p-n-p wafers were selected for evaluation. Cleaning prior to heat-treatments were kept the same for all tests, except when specifically altered to study the effect of different cleaning cycles. This standard cleaning consisted of hot solvents, hot alkaline cleaning; HF:HNO_3 etch modified with iodine, and HNO_3 boil. Each step was followed by a large number of deionized water rinses.

From these initial experiments it was established that poisoning of the reverse characteristics of Ga p-n-p's could be accomplished at temperatures greater than 700°C under an oxygen ambient. With increasing temperatures, up 1250°C, there appears to be no significant correlation between temperature and the degree of electrical characteristic softening. This effect is observed regardless of prior pellet cleaning treatments and special care observed to prevent contamination by the furnace and the quartz tube, the latter being coated with a sodium-silicate glass to form a gettering sink on the surface. The use of an ultra-pure ambient oxygen did indicate some improvement in reverse currents.

Under a given set of experimental conditions, cooling rate of the p-n-p structures from 1250°C in oxygen did show pronounced effects in the degree of softening observed. Typically, a quenching rate such as 500°C/min in an oxygen ambient causes the least degree of poisoning whereas a furnace cool of 250°C/hr from 1250° to 900°C resulted in the highest degree of poisoning. By approaching equilibrium conditions with a cooling rate of 3-7°C/hr from 1250° to 900°C, harder avalanche breakdowns resulted than the furnace cool.

These typical reverse characteristics are shown in Fig. 1. Interrupted cooling was carried out by furnace cooling from 1250° to 1000°C and holding for 15 hr, then moderately quenched to room temperature by pulling the pellets out of the furnace slowly. The purpose of this experiment was to form SiO_2 precipitates as described by Kaiser (6); these precipitates should serve as complexing sites for metallic impurities. This process did result in considerable improvement over the normal furnace cool with reverse characteristics similar to that obtained by rapid quenching.

The most significant parameter was that effect observed by different gas ambients. No downgrading resulted at any temperature up to 1200°C when exposed to an argon ambient and allowed to furnace cool. On quenching some small degree of softening occurred. From these results it was felt that downgraded units could be "gettered" back under these conditions. Such p-n-p units obtained from various conditions of heat-treatment were sealed in a quartz ampoule under argon, heated at 1200°C for 1 hr, and allowed to furnace cool. In every case avalanche type characteristics were obtained with voltage 10-20% less than the original values. Lifetime values were increased by a factor of two to four above the initial values immediately following diffusion (hereafter defined as "as diffused"). Poisoning was also prevented by exposure of the p-n-p's in a hydrogen ambient at 1000-1100°C. However, electrical characteristics previously softened by oxidation treatments were severely poisoned on exposure to hydrogen. Under nitrogen at temperatures above 800°C, significant softening occurred.

Effect of Oxygen with Impurities and Defects in Silicon

The results from preliminary experiments indicated the oxide phase and/or oxygen ambient have some influence in the transport mechanism of impurities in Si. Motivated by these results, further investigations were made to determine the role of oxygen and its relation to impurities and defects in Si. In these experiments the behavior of oxygen was evaluated by converting the dissolved oxygen into SiO_4^+ donor states. The effects of diffused Cu and surface induced dislocations during oxygen diffusion and the subsequent effect on this oxygen-formed donor level was the basis of evaluation.

Oxygen complex (SiO_4^+).—Oxygen when diffused into Si can form donor states under suitable time and temperature conditions (7). These donor states, SiO_4^+, appear to form by association of groups of four oxygen atoms with one Si atom at a temperature of 450°C and reach a maximum level in about seventy hours. The degree to which the donor level will form is dependent on the dissolved oxygen. Logan and Peters (8) report the maximum solubility of oxygen in Si at 1250°C to be 3×10^{17} at./cm^3, which offers a maximum donor level of 1×10^{15}/cm^3 (8).

Experimentally, oxygen was diffused into polished p-type Si slices of 30-100 ohm-cm resistivity (net impurity concentration less than 3×10^{14} at./cm^3). One half of this lot was sealed in a quartz ampoule under argon, and the other half was used as a control lot. In the sealed tube, a portion of the slices had the oxide removed, and the other half the oxide was left intact. These were heat treated at 1250°C for the same periods of time as they were originally oxygen diffused, *i.e.*, 30 min to 3 hr. After this heat-treatment they were annealed at 450°C for 72 hr along with control slices which were not heat treated previously in argon.

From microscopic examination of stained cross sections, n-type layers were observed on the control slices to depths up to 1.5 mils depending on resistivity of the starting material. Those slices which were argon heat-treated with the oxide removed did not show any conversion. Silicon with the oxide left on converted, but to a lesser degree.

This effect was also observed when cooling rates that approached equilibrium conditions were used following open tube oxidation. In an earlier investigation, we had found that cooling rates of 3-15°C/hr, from 1250° to 900°C, prevented the formation of SiO_4^+ complexes. From these results it was postulated that this cooling rate would permit oxygen to form stable precipitates (SiO_2) or possibly diffuse to the surface of the slice. Under these conditions, therefore, the oxygen is tied up or reduced to level below which the conversion to donors is detectable.

Role of copper and oxygen.—The relationship between oxygen and the poisoning impurity should be determined. It appears that some residual oxygen is required to form favorable sites for nucleation and precipitation of such impurities away from the junction region but near or at the surface. The presence of an oxide phase on Si (always prevalent under an oxidizing ambient) would allow such precipitation to occur internally within the Si at many possible structural defect sites. The size of such precipitates would be governed by the precipitation kinetics of the species involved.

Some idea of these kinetics may be gleaned by examining the effects of Cu and oxygen such as offered by the investigations of Schwuttke (3). Results from that study show Cu to precipitate at regions of high oxygen concentrations with the possible formation of copper-oxygen complexes. It was also shown that dissolved oxygen will form atmospheres around dislocations thereby depleting adjacent areas of oxygen. Therefore, the presence of high concentrations of diffused oxygen should be a favorable location for the precipitation of impurities such as Cu during cooling.

As the normal impurity level of a species such as Cu is too low to be resolved by infrared examination, Cu was diffused into Si to decorate dislocation (9) sites with and without diffused oxygen. By observing the degree of decoration, as to size and shape, and to the level at which it occurs, a correlation with diffused oxygen appeared possible.

Chemically polished 20 ohm-cm n-type Si was oxygen diffused at 1250°C with a maximum surface concentration of 3×10^{17} at./cm^3. The time of diffusion was adjusted so that complementary error function gradient of probable oxygen would result in a level $\sim 1 \times 10^{14}$ at./cm^3 at a distance of three mils from the surface. A shallower diffusion was also made to the same level one mil from the surface. Along with controls containing only residual oxygen, Cu was diffused at 900°C for 10 min and rapidly quenched to room temperature.

By polishing in 0.2 mil increments from the surface and examining the slices with infrared, Cu was found to be precipitated in the high oxygen concentration regions near the surface. Unlike the control slices which showed fine dispersion of decorated dislocation tails, the samples containing oxygen were decorated by copper in the form of star-like clusters. This is similar to that observed by Schwuttke.

Effect of dislocation traps.—Realizing the effect of dislocations as trapping sites for oxygen and impurities such as copper, it was felt that such a site, if it can be introduced at the surface during diffusion, would offer a sink for fast diffusing impurities. The effect of cold working, introducing a stress, and subsequent heat-treatment to elevated temperatures would result in the formation of dislocations. Such line defects must be terminated, either by a surface, a grain boundary, or they may form closed loops. We could expect that in single crystals they would either propagate through the crystal, or form a loop with one surface. If such terminated loops could be produced at the surface, trapping at elevated temperatures of these impurities with an affinity for forming "atmospheres" with dislocations would appear possible.

It is known that a certain amount of damage is introduced into the surface of Si by impact loading, resulting in a stressed surface condition. On heating to some specific temperature, this stress will be re-

lieved with some resultant plastic deformation and subsequent formation of dislocations. Beveled Ga-diffused p-n-p pellets were stressed in this manner by sandblasting the surfaces lightly with a fine grit of 10μ size. Alternate surfaces and both surfaces of beveled pellets were sandblasted to evaluate directional effects of gettering. These units, along with control pellets were exposed to the standard oxidizing conditions of 1200°C for 30 min and furnace cooled. Etching the pellets first in HF to remove the oxide followed by 20 sec in CP-6 modified with iodine was sufficient to obtain the original avalanche characteristics on all the sandblasted units, regardless of the side on which the dislocations were introduced. Control pellets were badly downgraded.

Further experiments were made under longer oxidizing conditions up to 5 hr at 1250°C, always resulting in unpoisoned units. If the sandblasted pellets were quenched very rapidly from any of the oxidizing conditions, downgraded characteristics were obtained. However, reheating at 1200°C in oxygen for 30 min and furnace cooling restored the original electrical characteristics.

To evaluate trapping ability of the introduced dislocation "sponge" at the surface, Ga diffused p-n-p wafers were Cu diffused at temperatures of 900°-1200°C under oxygen and furnace cooled. No poisoning occurred with those pellets having surfaces in a lapped or sandblasted condition. By infrared examination, Cu precipitation effects could not be observed whereas the control slices always showed a large degree of either finely dispersed or gross precipitates in the crystal. Quenching of Cu diffused p-n-p wafers from 900°-1200°C under oxygen always resulted in severely poisoned units. Fine dispersed decorated dislocations were always present in the crystal and subsequent removal of this precipitation was accomplished to a large degree by reheat-treating at 1200°C followed by a furnace cool.

The rapid mobility of copper was first demonstrated by the following experiment: One side of a p-n-p wafer was chemically polished and the other side was finely sandblasted. Then drops of $CuNO_3$ solution were placed on the polished side with care being exercised to keep the sandblasted side free of copper. Next the slice was heat treated in oxygen at 1000°C for 30 min and quenched at a rate of 500°C/min. No downgrading of the reverse characteristics resulted. Moreover, after chemically polishing the sandblasted side, no copper precipitation was observable by infrared examination. However, p-n-p slices that were chemically polished on both sides and subjected to the same process had electrical characteristics which were badly softened and also showed heavy copper precipitation throughout the slices.

Surface induced dislocations on copper and oxygen.— It has been shown in this study that surface induced dislocations have a definite effect in preventing the downgrading phenomena, both in the formation and oxidation of p-n-p units. Copper decoration and infrared examination showed that impurities such as Cu are removed to a very significant degree by dislocation effects. However, it is possible that oxygen also contributes to this mechanism by forming atmospheres around these dislocations sites at the surface.

Oxygen was diffused into p-type Si having chemically polished, sandblasted and lapped surfaces with resistivities of 30, 54, 63, and 100 ohm-cm for 3 hr at 1250°C under wet O_2. One lot was allowed to furnace cool (250°C/hr) and the second lot was quenched to room temperature. After removing the oxide, both lots were annealed at 450°C for 84 hr. These were cross sectioned and stained to reveal any n-type conversion caused by oxygen-silicon interaction to form SiO_4^+. These results are illustrated in Fig. 2. Typically, n-layers were formed in the polished wafers, in some cases with a thin p-layer at the surface. In the lapped and sandblasted wafers, a thin 0.1-0.2 mil but nonuniform n-layer formed at the surface. This thin surface n-region was delineated by a p-type layer and another deeper n-region. Only a p-region more highly doped than the base was observed under the shallow n-surface layer in the sandblasted samples. In the resistivity range tested, no significant difference was observed between the type of structure formed by quenching or furnace cooling. By re-annealing at 575°C for 20 hr, the deep n-type conversion layers formed in the polished and lapped slices were removed. Under these conditions, the SiO_4^+ complex is disassociated. The thin n-surface layer on the lapped and sandblasted slices could not be annealed out at this temperature.

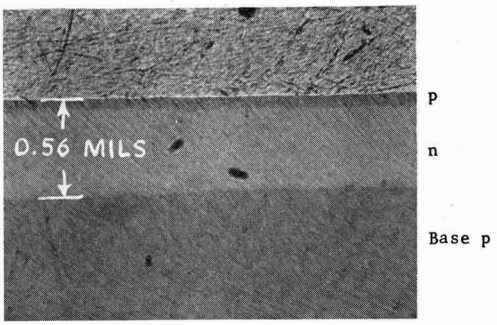

Fig. 2. Typical effect of various surface treatments on the formation of the SiO_4^+ complex from oxygen diffused into 54 ohm-cm p-type Si at 1250°C for 3 hr, 250°C/hr cooling rate; after 72 hr anneal at 450°C; beveled X-section depth magnified 10X. Microscope 60X.(a) Chemically polished surface.

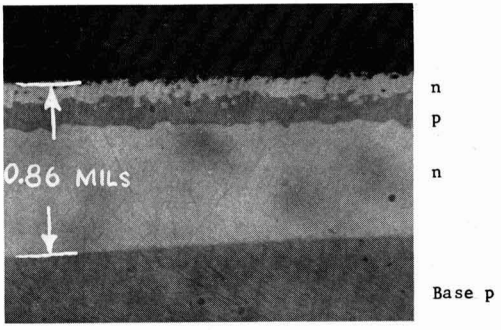

Fig. 2b. Lapped surface

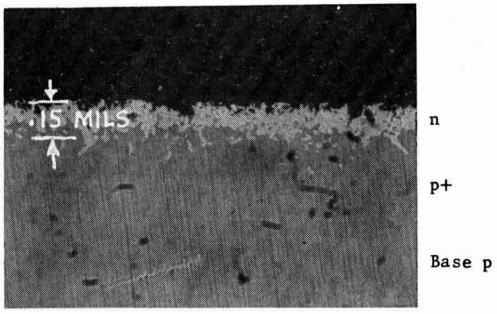

Fig. 2c. Sand blasted surface

The previous experiments were repeated except that Cu was diffused into the oxidized Si prior to annealing at 450°C. The diffusion of Cu was carried out under two temperature conditions; one at 900°C for 15 min and another at 1200°C for 20 min, to obtain different copper solute levels in the Si. A sig-

Fig. 3. Effect of Cu diffusion on the formation of the SiO_4^+ donor level in 54 ohm-cm p-type Si; beveled X-section depth magnified 10X; microscope 60X. (a) Typical n-layer formed by diffused oxygen.

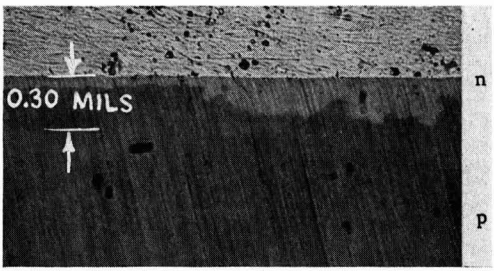

Fig. 3b. After Cu diffusion, 1200°C, furnace cool

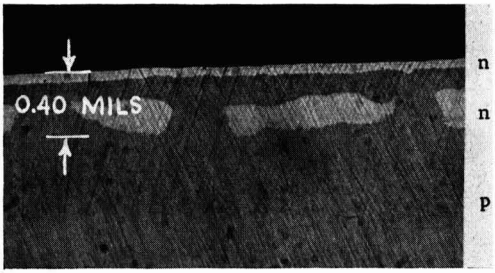

Fig. 3c. After Cu diffusion, 1200°C, quenched

nificant effect of Cu was observed in the donor formation after annealing at 450°C.

Typical results are shown in photomicrographs of Fig. 3. Directly after Cu diffusion from 1200°C, both quenched and furnace cooled polished slices showed an n-layer ~ 0.1 mil deep not observed on slices diffused with Cu at 900°C. After annealing at 450°C, n-layers formed on polished control slices (no Cu) and were partially eliminated on those which were Cu diffused. The effect was more pronounced when the Cu was quenched from diffusion temperatures. No significant effect of Cu on the oxygen formed donor level was found between sandblasted and lapped wafers as compared to polished control slices.

Oxygen-transport concept.—The concept of fast diffusing impurities locating at the silicon surface during nonoxidizing heat-treatments was further tested qualitatively. Wafers of 20 ohm-cm n-type silicon were prepared in three lots having chemically polished, lapped, and sandblasted surface finishes. These were oxidized in wet O_2, forming 12,000Å of oxide on their surfaces. The oxide was removed from one half of each lot and, along with control wafers which were not previously oxidized, they were Ga diffused in the standard sealed tube process. Typically, p-n-p junctions formed through the oxide on the polished slices showed downgraded reverse characteristics. Those formed without an oxide present had hard breakdowns, but the breakdown voltages were slightly less than the standard control slices. Sandblasted and lapped wafers with the oxide left on showed the same hard avalanche voltage breakdown as the control slices; whereas, those units with sandblasted surfaces from which the oxide had been removed, showed slightly higher voltages.

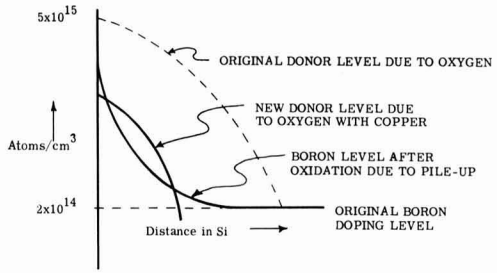

Fig. 4. Concentration profile diagram showing probable effect of Cu on the donor level (formed by oxygen).

Discussion

The purpose of this investigation was to show that a relationship exists between oxygen, the oxide phase, and fast diffusing metal impurities in terms of both the degree and location of metallic precipitation in silicon. The effects of Cu used as an example in these experiments does not necessarily indicate that other fast diffusing metal impurities behave in the same manner. Dash (10) has shown that Au does not offer any observable precipitation. The precipitation kinetics of other metals such as Fe and Ni can be different than that of Cu. However, results have been obtained here which show that such precipitation in the bulk can be effectively prevented without glassy-phase surface gettering. The experiments with Cu and its effects in repressing the SiO_4^+ donor complex indicates ion-pairing as a possible mechanism. The SiO_4^+ donors formed as a result of diffused oxygen can be used as a sensitive measure of the oxygen level and can indicate effectively changes that take place within the silicon.

The effect of Cu on oxygen donor formation on chemically polished slices may be explained as follows. From photomicrographs of Fig. 2a and 3a, we can see the typical donor layer which is formed by oxygen conversion with no added Cu present. In some cases a p-layer has formed on the surface. This can be depicted by the concentration profile diagram of Fig. 4.

From the appearance of the layers formed, the p-type surface layer is assumed to be the result of boron pile-up during oxidation. If this pile-up at the surface exceeds the concentration of donors formed, a p-layer will predominate.

With Cu subsequently diffused into the Si, depending on its solubility level, and whether it was quenched or furnace cooled, the original donor level would be reduced by the tie-up of diffused oxygen and Cu. The p-layer which forms in the lapped wafers can be attributed to boron pile-up. The formation of the shallow n-type surface layer on both the lapped and sandblasted surfaces is probably due to the reaction of oxygen and dislocations. Thus an indication of the depth of damage and of the magnitude of dislocation formation was provided. Sheet resistance measurements indicate this level to be ~ 5 x 10^{15}/cm^3. The absence of oxygen-formed donors in sandblasted specimens might be the result of greater boron pile-up to a level high enough to exceed the donor formation.

To examine more closely the effect of damage to the surface of Si, 2000 ohm-cm, p-type polished wafers were scribed with a diamond pencil leaving a number of scratches on the surface. These were oxidized and annealed at 450°C. As shown in Fig. 5, the depth of

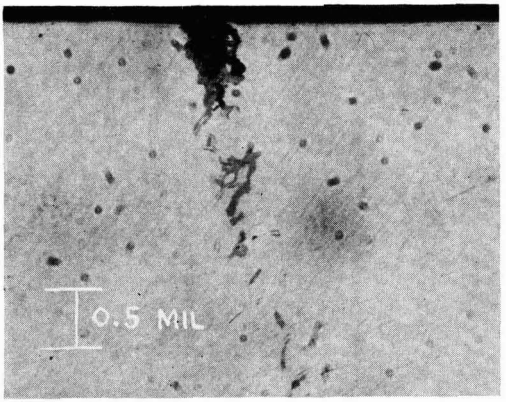

Fig. 5. Photomicrograph showing effect of damage due to scribe mark on polished 2000 ohm-cm p-type Si; after 1 hr oxidation at 1250°C and 450°C anneal for 72 hr; beveled X-section depth magnified 10X. a. Dark p-type regions within oxygen diffused and converted n-region. 75X.

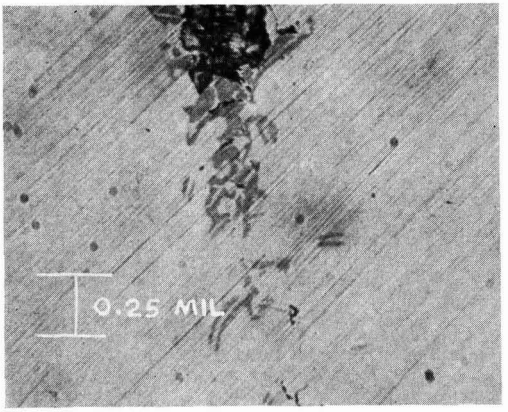

Fig. 5b. Enlarged view showing probable dislocation loops of high oxygen content within depleted dark stained regions. 150X.

the scribe mark was approximately 0.5 mil, but damage and subsequent dislocation formation extended to 2.5 mils. In this region of damage, darkly stained p-regions are present in the background of the n-type region where the latter is obtained because of oxygen conversion. These p-regions are assumed to be areas depleted of oxygen and are adjacent to dislocation loops containing atmospheres of oxygen removed from the depleted regions. From this observation, it is possible that the p-layer, assumed to be due to pile up, is also formed by the depletion of oxygen by reaction with surface induced dislocations.

The evidence indicates that oxygen can react with dislocations thereby forming shallow nonuniform n-type layers on the sandblasted and lapped surfaces. Further, there seems to be a reaction of Cu with oxygen as shown by their effects on the SiO_4^+ complex in polished wafers.

With the effect of a dislocation "sponge" at the surface, reheat-treating under oxygen of previously quenched wafers is of considerable interest. First it indicates that the introduced dislocations are not annealed out even with repetitive temperature cycles up to 1250°C. In addition the recovery of quenched and poisoned p-n-p units shows that fast diffusing impurities are responsible for the downgrading phenomena. A period of time, slower than rapid quenching, is needed to permit the diffusion of these impurities to the dislocation "sponge." As oxygen cannot out-diffuse in the time of cooling evaluated and because the SiO_2 phase is always present on the Si surface, the introduced dislocations must be the major influence in the prevention and recovery of poisoned p-n-p structures.

It was also shown that a metal impurity such as copper can be transported from bulk Si, probably to some surface layer by heat-treatment under argon ambients. Such an ambient also resulted in depletion of the diffused oxygen level from the body of the silicon. The recovery of the reverse characteristics of Cu poisoned p-n-p junctions by this argon treatment would indicate that oxygen-copper complexing or tie-up occurs at or near the surface. Infrared examination of these structures support this view.

An explanation may be offered concerning the effect of cooling rate in an oxygen ambient. In quenching, impurities can precipitate at sites throughout the wafer in a more dispersed form. Under a moderate cooling rate such as a furnace cool, metal impurities can coalesce because of their rapid mobility; however, oxygen levels would not be significantly affected by precipitation or agglomeration. A cooling rate approaching equilibrium conditions affects the oxygen level either by outdiffusion or by precipitation as indicated by the absence of oxygen formed donors. Although the metal impurity level in the bulk Si can be assumed to be the same in all these cases, the resulting reverse leakage currents are not. The lower leakage observed with quenched samples indicates that the over-all effect of more finely dispersed precipitates is less than that of larger coalesced precipitates. If equilibrium cooling resulted in a depletion of oxygen levels by outdiffusion (because of precipitation as SiO_2 at the surface), a significant reduction in reverse currents should be achieved. Therefore, it appears that coalescence of oxygen occurs within the bulk during such a slow cool thus permitting oxygen-metal impurity complexing. Similar reverse currents are obtained to those of slow cooling by holding the slices at 1000°C for long periods of time. Precipitation of oxygen as SiO_2 here causes a reduction in oxygen level within the body of the silicon.

Under nitrogen ambients, downgrading is probably due to a nitride formation. No explanation is offered for the serious poisoning effect of hydrogen on p-n-p slices which have been exposed to oxygen.

Acknowledgments

The author wishes to acknowledge the effort of R. I. Jurgensen, who helped plan and carry out the many experiments in this study and to F. E. Gentry for many helpful discussions and for reviewing this work.

Manuscript received Oct. 22, 1964. This paper was presented at the Washington Meeting, Oct. 11-15, 1964.

Any discussion of this paper will appear in a Discussion Section to be published in the December 1965 JOURNAL.

REFERENCES

1. A. Goetzberger and W. Shockley, *J. Appl. Phys.*, **24**, 1821 (1960).
2. W. Shockley, *Solid State Electronics*, **2**, [1], 35 (1961).
3. G. H. Schwuttke, *This Journal*, **108**, 163 (1961).
4. S. Prussin, *J. Appl. Phys.*, **32**, 1876 (1961).
5. H. J. Quiesser, *ibid.*, **32**, 1776 (1961).
6. W. Kaiser, *Phys. Rev.*, **105**, 1751 (1957).
7. C. S. Fuller and R. A. Logan, *J. Appl. Phys.*, **28**, 1427 (1957).
8. R. A. Logan and A. J. Peters, *ibid.*, **30**, 1627 (1959).
9. W. C. Dash, *ibid.*, **27**, 1193 (1956).
10. W. C. Dash, *ibid.*, **31**, 2275 (1960).

The Preparation of Homogeneous and Reproducible Solid Solutions of GaP-GaAs

M. Rubenstein

Research Laboratories, Westinghouse Electric Corporation, Pittsburgh, Pennsylvania

ABSTRACT

Solid solutions of GaP-GaAs were prepared using the sealed tube iodine transport method. The initial charge was iodine, powdered GaP, and powdered GaAs. These powders were ground and treated with aqueous hydrochloric acid to remove the damaged layers. The resulting GaP-GaAs solid solutions were more homogeneous than other such series of solid solutions which are described in the literature. Polycrystalline sound masses as well as single crystals with reproducible and predictable compositions can be produced using these treated powders.

Solid solutions of two or more compounds or elements can offer a method of changing many characteristics of either of the original constituents. It has been shown that silicon and germanium exhibit continuous solid solution and continuous variation of energy gap over the entire range of compositions (1-4). This type of semiconductor investigation was extended to the III-V compounds (5-10). Investigations on the system GaP-GaAs began in 1955 with Folberth's work (5) and were continued by other workers (11-15).

This paper demonstrates that solid solutions having formula $GaP_{(1-x)}As_x$ (the system GaP-GaAs) can be prepared more homogeneously than previous papers have indicated (13, 14), and the primary reason for this homogeneity is due to the use of powders as the initial charge. The solid solutions prepared in this work involved the sealed tube iodine transport technique (11-17).

Preparation of $GaP_{(1-x)}As_x$

First, the preparation of the solid solutions with formula $GaP_{(1-x)}As_x$ will be sketched quickly since this method has been described in detail (13, 14). Then a detailed description of the preparation of the charge (the powdered GaP and GaAs) will be presented.

The initial charge consists of iodine, GaP, and GaAs. The amount of iodine is such that a maximum pressure of 3 atm would be reached in the ampule if the average temperature were 1000°C, if all the iodine were converted to iodine atoms, if the iodine atoms underwent no reactions, and if no iodine were lost during the evacuation of the ampule. The GaAs and GaP powders (a total of 2g) and I_2 were placed in the ampule (having a volume of about 70 cc) as indicated in Fig. 1. The ampule with the charge was evacuated using a mechanical pump. The ampule was cooled using an ice-water bath to prevent excessive loss of I_2 during evacuation. A liquid nitrogen trap was placed between the pump and ampule to prevent hydrocarbons from getting into the ampule. The pressure in the ampule was about 4×10^{-2} Torr.

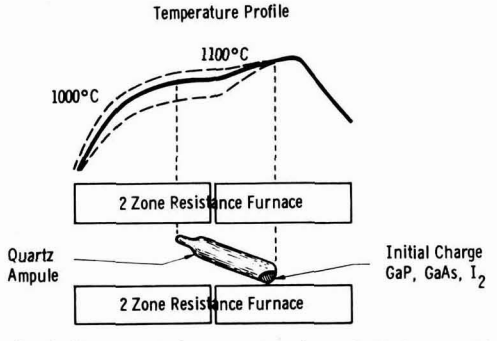

Fig. 1. Diagrammatic representation of ampule in furnace with temperature profiles.

The ampule was sealed off and placed in a temperature gradient such that the maximum temperature was 1100°C and the minimum temperature was between 1090° and 900°C. The time for transport varied between 15 min to four days. No attempt was made to seed the transported material.

Preparation of the Powdered GaP *and* GaAs

The GaP used in the charge for the iodine transport of $GaP_{(1-x)}As_x$ was material grown from a stoichiometric or nearly stoichiometric melt (this GaP was horizontally zone refined at about 1500°C at phosphorus pressures between 10 and 20 atm). The GaP was then crushed in a Plattner's diamond mortar and pestle, ground in a porcelain mortar and pestle, sieved, and then treated with aqueous hydrochloric acid (HCl) to remove contaminants introduced in crushing and sieving and to remove the damaged layer.

Since phosphine is produced when one grinds GaP (this compound is easily identified by its odor), the gallium (or the GaP) must undergo some change. Either Ga_2O_3, Ga_2O, or $GaPO_4$ is formed. Of course, any combination of these three could be produced. Some of the possible reactions which can be written are as follows

$$2GaP + 3H_2O \rightarrow 2PH_3 + Ga_2O_3 \quad [1]$$

$$2GaP + 3H_2O \rightarrow 2PH_3 + Ga_2O + O_2 \quad [2]$$

$$GaP + 4H_2O \rightarrow GaPO_4 + 4H_2 \quad [3]$$

$$GaP + 2\,O_2 \rightarrow GaPO_4 \quad [4]$$

Although GaP is usually considered a rather inert solid, one or more of these reactions could proceed at a damaged layer especially since grinding can produce large local thermal spikes in a material. It is also possible that GaP seems to be rather inert because the oxidized surface film protects the layers under this film.

It is difficult to prove which of these reactions most accurately describes this system since the grinding of GaP does not produce much product. It is fortuitous that a change in body color of the GaP on grinding is quite noticeable to the eyes, and it is also fortuitous that the olfactory nerves are quite sensitive to PH_3. The limit of perceptibility to PH_3 is 1.5-3 ppm, the limit for "serious effects after several hours" is 7 ppm, and the threshold limit is 0.05 ppm (19).

The treatment of the GaP with concentrated hydrochloric acid is an interesting reaction chemically. GaP is attacked very slowly by concentrated hydrochloric acid. GaP which has been ground is attacked at a much faster rate; there is an evolution of bubbles and a change in body color of the GaP. The color change is from brown to red-orange or yellow-orange (de-

Table I. Particle distribution

U.S. sieve No.	Diameter of particles, mm	Designation in this paper
80-100	0.177-0.149	1
100-120	0.149-0.125	2
120-140	0.125-0.105	3
140-170	0.105-0.088	4
170-200	0.088-0.074	5
Smaller than 200	Smaller than 0.074	6
Ground, treated with hydrochloric acid		I
Ground, treated with hydrochloric acid, slurried, decanted, sieved		II
Ground, sieved		III
Ground, slurried, decanted, sieved		IV

pending on the particle size of the GaP).

Table I shows some information about the particle distribution used as well as the treatment used in preparing the GaP powders. In Fig. 2 the diffuse reflectance is presented for all four treatments (as indicated in Table I) for the finest distribution of particles. Figure 3 shows the diffuse reflectance for all four treatments for the coarsest distribution of particles.

The difference between treatments III and IV (Fig. 2) is a slurrying operation. This operation consists of mixing the powder with water and decanting the water. The very fine particles are removed by this operation. The difference between treatments I and II is the same as between III and IV. The difference between treatments I and III is the hydrochloric acid treatment. The same may be said concerning treatments II and IV. This HCl operation increases the diffuse reflectance over the entire range of wavelengths. The change from yellow-orange to brown on grinding GaP can be seen in Fig. 2 and 3 by noting that the diffuse reflectance for the brown material falls off at wavelengths from 0.65 to 0.57μ. At these same wavelengths, GaP which has been treated with hydrochloric acid has a much higher diffuse reflectance.

There is one other observation which was made on GaP which did not have the slurrying and decanting operation. Not only did the coarser particle distributions (after sieving) contain some of the very fine particles, but these larger particles were coated with these very fine particles. Perhaps an electrostatic attraction holds these very fine particles to the coarser particles even during the entire sieving operation. The sieving operation may even be the cause of the electrostatic build-up of charge. The slurrying and decanting operation allows one to obtain samples having particle distributions without the very fine particles.

When one grinds a crystal using a mechanical force, a damaged layer is produced. This damaged layer is composed of a variety of disorders such as a deformed layer, sharp edges, cracks, an increase in the dislocation and vacancy densities, and a reactive surface. Such grinding also produces thermal spikes. These thermal spikes together with a reactive surface could produce a reaction with the surrounding atmosphere. Some of the reactions of GaP with H_2O and/or O_2 mentioned earlier might take place. Grinding GaP produces such a damaged layer which can be observed visually and nasally. There is another technique which can be used to observe a difference between this damaged layer and GaP without this damaged layer, the rate of dissolution. The rate of dissolution of this damaged layer is much larger than the rate of dissolution of GaP without this damaged layer. Any analysis of this rate would include all types of disorders, but since there obviously is a chemical reaction associated with the formation of this damaged layer, it will be assumed that a new compound is, at least, partially covering the surface of the ground GaP.

GaP was ground, slurried, decanted, and sieved. The particle distribution was 0.149-0.125 mm in diameter. Several samples were treated in the following manner. A weighed amount (about 2g) of GaP was placed in aqueous concentrated HCl (about 250 ml) and the mixture was slowly stirred. After 3 hr the GaP was washed with water, dried, and weighed. This weighed sample was returned to the HCl for three more hours, washed, dried, and weighed. This operation was repeated again and again. The curve in Fig. 4 labeled "3 hour runs" is typical of such an experiment. Note that the rate of dissolution of the ground GaP is still falling after a total of eighteen hours of HCl treatment. The curve in Fig. 4 labeled "24 hour runs" was treated in the same way as described above for the "3 hour runs" except the

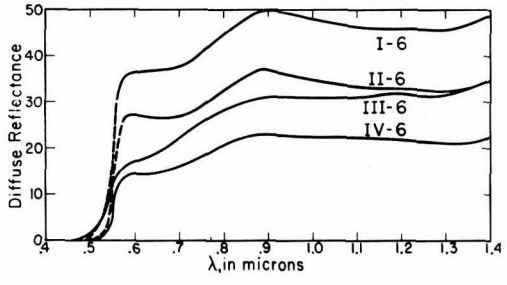

Fig. 2. Per cent diffuse reflectance vs. wavelength for GaP having undergone 4 different treatments (see Table I): the particle distribution is the finest.

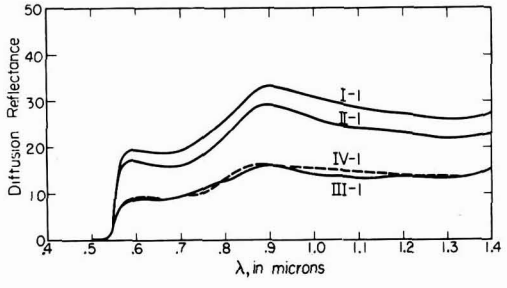

Fig. 3. Per cent diffuse reflectance vs. wavelength for GaP having undergone 4 different treatments (see Table I): the particle distribution is the coarsest.

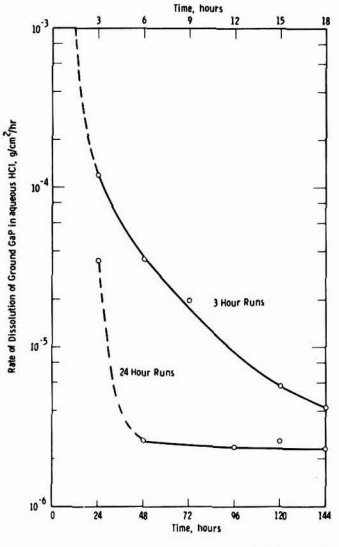

Fig. 4. Rates of dissolution of ground GaP vs. time

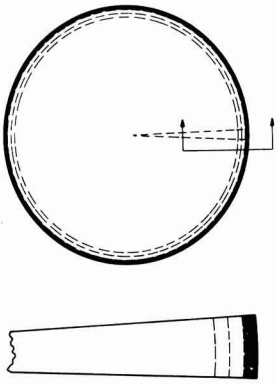

Fig. 5. Diagrammatic cross section of a particle of GaP with a damaged layer (top); (below) portion of sector of cross section of particle with damaged layer.

samples were treated for 24-hr periods instead of 3-hr periods. After 48 hr (two 24-hr HCl treatments) the rate of dissolution of the ground GaP does not fall appreciably. Figure 5 shows diagrammatically what the above experiments show. A particle has a damaged layer but this damaged layer is not a uniform one. It is most damaged on the outer periphery, and as one leaves the surface toward the interior of the particle this damaged layer shows less and less damage. The GaP in Fig. 4 shows a high rate of dissolution initially and a smaller rate of dissolution as more and more of the damaged layer or layers are removed. In the case of the curve labeled "3 hour runs" at the end of 18 hr, all of the damaged layers are not yet removed. In the case of the curve labeled "24 hour runs" at the end of the first 24-hr period the rate is greater than 18 total hr of 3-hr periods because this rate is a combination of higher rates and some lower rates of dissolution. Therefore, the room temperature dissolution rate of GaP with a damaged layer (caused by grinding) is greater than 1×10^{-4} g/cm^2/hr. The room temperature dissolution rate of GaP (without a damaged layer) in aqueous concentrated HCl is 2.3×10^{-6} g/cm^2/hr. The thickness of the damaged layer for several samples were calculated from the weight loss and rate of dissolution experiments to be about 2μ on a radius of about 70μ. After about 20 hr in HCl, GaP is removed at the rate of about 0.01 μ/hr. Initial rates of removal of GaP which has a damaged layer are about two orders of magnitude greater. This discussion may be concluded by saying that the rate of dissolution is not a constant since the degree of damage along a radius of a particle is not constant. It should also be pointed out that the calculation for the area of the particles assumes that these particles are spheres. Since these particles are not spheres, the real surface area is larger than calculated. This would mean that the true dissolution rates are smaller than those presented in this paper.

One other observation may be made correlating damaged layers with visual observation. As one treats ground GaP with HCl, there is a decided color change which one may easily observe from brown to red-orange or to yellow-orange. When the color change is noted, the most damaged material has been removed, and the rate of dissolution has fallen appreciably. The less damaged layers do not have diffuse reflectance much different from GaP without damaged layers and the dissolution rate in HCl of these layers is not much different from GaP without damaged layers. A good discussion on damaged layers and their chemical reactivity may be pursued in ref. (18).

GaAs in many respects is similar to GaP. Although their chemical reactivity is similar, GaAs is somewhat more reactive than GaP with respect to halogens, hydrogen halides, aqueous hydrogen halides, aqua regia, and nitric acid. GaAs powders were prepared in exactly the same way as the GaP powders. The discussion on damaged layers would equally apply to GaAs.

Table II. Lattice constants for 48 samples

State of sample after transport experiment*	Sample designation	Composition $GaP_{1-x}As_x$, x	Per cent transported**	Lattice constant, a_o
Single	20 N-2	0	80	5.4508
Not transported†	20 N-2	0	80	5.4505
	SID	0		5.4506
	S 20 P-2	0.1		5.4706
Single crystal	S 20 P-2	0.1		5.4700
	S 20 P-1	0.1		5.4709
	S 20 P-1	0.1		5.4707
	SIE	0.1		5.4704
	SIF	0.2		5.4894
Single crystal	20 R-2	0.2	40	5.4894
Single crystal	20 R-2	0.2	40	5.4883
Not transported†	20 R-2	0.2	40	5.4883
Transported	20 R-1	0.2	94	5.4893
Not transported†	20 R-1	0.2	94	5.4899
Single crystal	20 R-1	0.2	94	5.4839
Single crystal	20 S	0.3	59	5.5094
Transported	20 S	0.3	59	5.5093
	SIG	0.3		5.5100
Not transported†	S 20 T	0.4	28	5.5317
	SIH	0.4		5.5296
	SIK	0.5		5.5482
	S9E	0.5		5.5486
Single crystal	S9E	0.5		5.5483
Transported	S9D	0.6	65	5.5679
Not transported	S9D	0.6	65	5.5676
Single	S9D	0.6		5.5676
	S 49 W-1	0.6		5.5662
	S 49 W-1	0.6		5.5662
	S 49 W-2	0.6		5.5692
	S 49 W-2	0.6		5.5689
Single crystal	SIL	0.7		5.5895
Not transported	SIL-1	0.7	86	5.5891
Single crystal	SIL-1	0.7	86	5.5889
Single crystal	SIL-1	0.7	86	5.5893
Single crystal	SIL-1	0.7	86	5.5895
Single crystal	S9C	0.7		5.5888
Single crystal	S9C	0.7		5.5890
	SIL-2	0.7		5.5888
Single crystal	SIOH	0.8		5.6103
Single crystal	SIOH	0.8		6.6095
Single crystal	S2E	0.8		5.6104
Single crystal	S2E	0.8		5.6103
	S2M	0.8		5.6107
	S9B	0.9		5.6301
	S 2N-2	0.9		5.6305
Not transported†	S2F	1.0	81	5.6532
	S2F	1.0	81	5.6531
	S2P	1.0		5.6532

* If nothing is indicated concerning the "State of the Sample," the sample was polycrystalline.
** If no per cent transport is indicated, the samples were totally transported.
† Not transported samples were polycrystalline.

Results

$GaP_{(1-x)}As_x$ samples were prepared where $x = 0.1, 0.2, 0.3, \ldots, 1.0$. Table II contains lattice constants for 48 samples prepared in 28 independent preparations in this solid solution system GaP-GaAs. The samples were taken from single crystals and polycrystalline deposits. The samples were taken from preparations in which all of the GaP-GaAs was transported and in which as little as 28% of this material was transported. The time of transport varied from four days to 15 min. The difference in temperature between source and deposit varied from 10° to 200°C. The lattice constants in Table II are plotted in A of Fig. 6.[1] Whether the particle size of the source material had diameters between 0.177-0.149 mm or less than 0.074 mm no differences could be noticed in the material transported or material which did not transport. The length of time of the transport experiments (whether 4 days or 15 min) does not in any way affect the transported or non-transported material, other than the amount which transported. These lattice measurements were made using the Debye-Scherrer technique, a 57.32 mm radius of Straumanis-type camera with nickel filtered copper radiation. A trigonometric extrapolation was used to obtain the precision lattice constants (21).

[1] The lattice constants for GaP and GaAs at 18°C are 5.4505 ± 0.0001A and 5.6534 ± 0.0002A respectively (20).

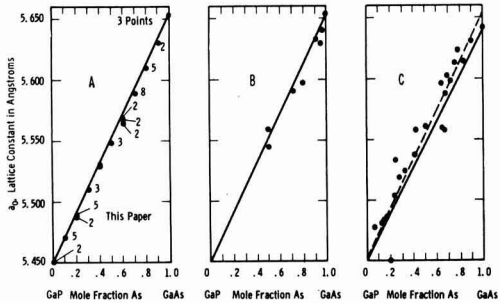

Fig. 6. Lattice constants of $GaP_{(1-x)}As_x$ *vs.* composition. "A" curve is from data obtained in this paper: "B" curve and "C" curve are from ref. (14) and (13), respectively.

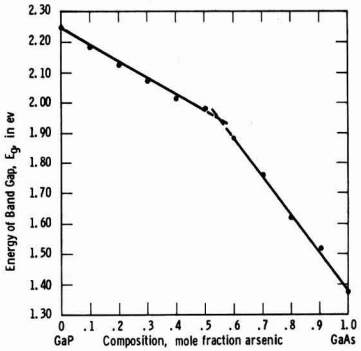

Fig. 7. Energy band gap *vs.* composition for the system $GaP_{(1-x)}As_x$

These points in Fig. 6, Curve A, lie quite close to the line connecting the lattice constants of pure GaP and GaAs; Vegard's law is followed quite well. Also plotted in Fig. 6 are two other curves from the literature (13, 14). The scatter of the points from data in this paper is much less than the scatter observed in data taken from the other two papers. One can observe in Table II that the so-called nontransported material has lattice constants which are either identical with or very close to the lattice constants of the transported material. This was observed not only in these samples listed in Table II, but in a number of other samples. One may conclude that the nontransported powders in these experiments did not remain as GaP and GaAs powders, but rather quickly formed the solid solution under the influence of iodine at a temperature of 1100°C.

Also included in this paper is a plot of band gap energy *vs.* composition, Fig. 7. The data was obtained from room temperature optical transmission measurements on samples which were about 0.4 mm thick. There are enough points plotted in this figure to merit the drawing of 2 straight lines with different slopes rather than a curved line as others have drawn for similar data (5, 13).

Conclusions

GaP and GaAs form a complete range of solid solutions obeying Vegard's law quite well. All of the points in A of Fig. 6 are below the line drawn (assuming Vegard's law is obeyed) indicating slight negative departures from Vegard's law.

One can obtain samples of $GaP_{1-x}As_x$ which are relatively homogeneous and reproducible as indicated in A of Fig. 7 by using crushed GaP and GaAs as the source of an iodine transport experiment.

When one crushes GaP and GaAs a damaged layer is produced. This layer may be removed by treatment with HCl. This treatment not only removes the damaged layer, but also any contaminants introduced on crushing and sieving.

Other workers were not able to obtain, in a reproducible manner, homogeneous solid solutions primarily because they did not know the composition of their solid solutions (their points show a scatter off the Vegard's law line). If they used large pieces of GaP and/or GaAs as their initial charge, the rates of GaP and GaAs leaving the sources and entering the gas phase were determined by the surface area of the source materials. If they crushed the source materials and did not remove the damaged layer, the source materials had already lost phosphorus and/or arsenic, formed oxides and/or phosphates (or arsenates), and were contaminated by impurities on crushing.

The author of this paper has noted (from the lattice constants of nontransported material) that before any solid solution is transported, the solid solution is formed at the source position when powdered GaP and GaAs are used as source material. This is experimental confirmation of a postulate previously set fourth (13). It is easier to understand the homogeneity and reproducibility of the solid solution presented in this paper, if the source material before transport were the solid solution already.

Acknowledgment

The author would like to thank Mr. Donald Sestrich for his help in the experimental efforts in this paper.

Manuscript received Sept. 16, 1964; revised manuscript received Nov. 27, 1964.

Any discussion of this paper will appear in a Discussion Section to be published in the December 1965 JOURNAL.

REFERENCES

1. H. Stohr and W. Klemm, *Z. anorg. Chem.*, **241**, 305 (1939).
2. A. Levitas, C. C. Wang, and B. H. Alexander, *Phys. Rev.*, **95**, 846 (1954).
3. M. Glicksman, *ibid*, **102**, 1496 (1956).
4. F. Herman, M. Glicksman, and R. H. Parmenter, "Progress in Semiconductors" (1957).
5. O. G. Folberth, *Z. Naturforsch.*, **10a**, 502 (1955).
6. F. Seitz and D. Turnbull, "Solid State Physics," Vol. 3, Academic Press, New York (1956).
7. W. Koster and B. Thoma, *Z. Metallkunde*, **46**, 293 (1955).
8. J. C. Wooley, B. A. Smith, and D. G. Lee, *Proc. Phys. Soc.*, **B69**, 1339 (1956).
9. J. C. Wooley and C. M. Gillett, *J. Phys. Chem. Solids*, **17**, 34 (1960).
10. F. A. Trumbore, P. E. Freeland, and A. D. Wells, *This Journal*, **109**, 645 (1962).
11. G. R. Antell and D. Effer, *ibid.*, **106**, 509 (1959).
12. N. Holonyak, Jr., D. C. Jillson, and S. F. Bevacqua, "Metallurgy of Semiconductor Materials," J. B. Schroeder, Interscience Publishers, Aug. 30-Sept. 1, 1961.
13. F. A. Pizzarella, *This Journal*, **109**, 226 (1962).
14. San-Mei Ku, *ibid.*, **110**, 991 (1963).
15. E. M. Hull, Paper presented at the New York Meeting of the Society, Electronics Division Abstracts, **12**, 43 (1963).
16. I. C. Marimace, *I.B.M. J. of R & D*, **4**, 248 (1960).
17. E. S. Wajdo, B. W. Keppenhan, and W. H. White, *ibid.*, **4**, 288 (1960).
18. H. C. Gatos, "The Surface Chemistry of Metals and Semiconductors," John Wiley & Sons, Inc., New York (1960).
19. F. A. Patty, "Industrial Hygiene and Toxicology," Vol. II, Interscience Publishers, New York (1962).
20. Von G. Giesecke and H. Pfister, *Acta Cryst.*, **11**, 369 (1958).
21. A. Taylor and H. Sinclair, *Proc. Phys. Soc.*, **57**, 126 (1945).

Thermal Oxidation of Heavily Doped Silicon

B. E. Deal and M. Sklar

Research & Development Laboratory, Fairchild Semiconductor, Palo Alto, California

ABSTRACT

Oxidation characteristics of heavily doped silicon were investigated in dry and wet (95°C H_2O) oxygen ambients over the temperature range 920°-1200°C for oxide thicknesses of 0.10-1.0μ. Silicon uniformly doped with boron (1×10^{16} to 2.5×10^{20} cm^{-3}) or phosphorus (4×10^{15} to 1.5×10^{20} cm^{-3}) was studied, as well as silicon surfaces predeposited with these two elements. Boron concentrations greater than 1×10^{20} cm^{-3} cause an increase in oxidation rates at all temperatures, the greatest effect occurring in dry oxygen. Above 1000°, no such rate increase occurs for phosphorus doped silicon. At 920°C, however, phosphorus concentrations of 1×10^{19} cm^{-3} or more result in a significant increase of oxidation rates. The latter effect is most pronounced in wet oxygen. The results can be explained satisfactorily by considerations which take into account redistribution of impurities during thermal oxidation of silicon. These considerations also enable a tentative prediction of the effect of heavy doping concentrations of other impurities on the oxidation rate.

Silicon reacts in various oxidizing atmospheres at elevated temperatures to form silicon dioxide (SiO_2). The kinetics of this thermal oxidation of single crystal silicon has been the subject of several recent papers (1-5). The authors of these papers reported no dependence of oxidation rate on bulk impurity concentration over the concentration ranges investigated. These concentrations extended from very low values (intrinsic silicon) to as high as approximately 1×10^{20} cm^{-3} acceptor and donor impurities. It has also been noted, however, that when silicon having surface impurity concentrations greater than 10^{20} cm^{-3} is oxidized, deviations from the standard values of oxidation rate constants are encountered (6, 7). For the most part these deviations have been found with samples subjected to diffusion processes used in device fabrication.

Recently, silicon oxides have assumed an increasingly important role in the development of surface controlled devices and integrated circuits, and the close control of oxide thickness has become of vital interest (8, 9). A study was undertaken therefore to determine the effect of impurity doping, if any, on thermal oxidation rates. This study included both p-type (boron doped) and n-type (phosphorus doped) silicon oxidized in dry and wet oxygen (95°C H_2O) in the temperature range 920°-1200°C. Samples of both uniformly doped crystals and diffused surfaces were examined.

Experimental

Silicon used in this program was obtained from the Kollstan Semiconductor Elements Company, Westbury, New York. It was in the form of circular slices, cut from Czochralski crystals, and lapped to 250μ thickness. In all cases, surface orientation was (111). Material used for subsequent diffusion processing was 1.3-1.5 ohm-cm, either p-type (boron doped) or n-type (phosphorus doped) silicon. Dislocation count was specified to be less than 100 cm^{-2}. For the heavily doped p-type silicon, material with boron concentration of 1×10^{20} and 2.5×10^{20} cm^{-3} was used. Similarly, the heavily doped n-type silicon contained 3.7×10^{19} and 1.5×10^{20} cm^{-3} phosphorus. For both types, the higher values represent the maximum concentration available for boron and phosphorus. In examining these materials some segregation of impurities was noted, especially at the edges of the slices. However it was possible to obtain a sufficient number of slices with large areas of uniform impurity concentration which could be used in this investigation.

Apparatus

The oxidation system was similar to the one described in ref. (3). Both dry oxygen and wet oxygen ambients were used. The latter consisted of oxygen bubbled through deionized water at 95°C. The resulting partial pressure of water vapor in the ambient was assumed to be 634 mm Hg, the vapor pressure of water at 95°C. For the dry oxygen, the gas was dried and purified using a molecular sieve trap. Furnace temperature was controlled to ±1.0°C in the range 920°-1200°C. Silicon slices were placed flat on a thin quartz boat during oxidation. Separate quartz tubes were used for n-type and p-type silicon.

Procedure

The silicon slices were mechanically polished on one side to assure optimum conditions for oxide thickness measurements. Previous experiments had demonstrated no difference in oxidation kinetics between chemically and mechanically polished surfaces for the thickness range studied in this program (3). The slices were cleaned, and resistivity measurements were made on the lapped side. Immediately prior to oxidation, they were carefully cleaned again. The cleaning procedures involved prolonged rinses in organic and inorganic solvents using ultrasonic agitation.

Each particular run, representing a certain oxidation condition, included a standard silicon slice, *i.e.*, $C_B = 1 \times 10^{16}$ cm^{-3}, and two slices of higher impurity concentration. Thickness measurements of the oxides produced were obtained using multiple-beam interferometric techniques. Accuracy and reproducibility of this method is estimated to be ±40Å. Results of the standard sample were compared with corresponding oxides prepared in a separate furnace. The run was repeated if any deviation was noted, although agreement among standard oxides produced in the same furnace with heavily doped crystals and those prepared separately was generally very good.

Dry oxidation characteristics of predeposited[1] silicon were also examined in this program. In these experiments the surfaces were first prepared in regular predeposition furnace systems (9). For boron doped surfaces, methyl borate [$(CH_3)_3BO_3$] and boron tribromide [BBr_3] sources were used. In the case of phosphorus the sources were phosphorus pentoxide [P_2O_5] and phosphorus oxychloride [$POCl_3$]. Surface concentrations of these predeposited surfaces were estimated by measuring junction depths and sheet resistance, and using calculated relationships of the kind presented in ref. (10). A complementary error function-type impurity distribution was assumed. Surface concentration values calculated by this method ranged from $5\text{-}8 \times 10^{20}$ cm^{-3}. The samples were then oxidized at 1200°C. On

[1] "Predeposition," according to common usage, denotes a relatively short diffusion step (the impurity being present in the ambient) usually resulting in a high surface concentration of the impurity (9).

some samples the oxide glass formed during the predeposition step was removed by HF treatment before oxidation; on others it was left on. A standard slice was included in each oxidation, and thicknesses of oxides produced were measured as described above. Again, thicknesses of these standard oxides agreed quite closely with those of corresponding oxides prepared alone in a clean system. Thicknesses of the oxide glasses produced during the predeposition step were also determined.

Results

The oxidation results of silicon uniformly doped with boron or phosphorus are presented graphically in Fig. 1-4. These graphs are log-log plots of oxide thickness *vs.* oxidation time for dry and wet oxygen. Four different oxidation temperatures are included, with data obtained with three different impurity concentrations for each temperature. The lower line for each temperature represents oxidation characteristics of the standard, and these values agree quite closely with previous data (3). The deviation from the standard oxidation rates for more heavily doped boron or phosphorus under certain conditions is readily noted. The significance of these differences is discussed in the following section. In general, experimental values were reproducible to within 100Å, close to the accuracy of the oxide thickness measurement technique.

Oxidation rates obtained using predeposited samples (with the glass removed) were compared with the results in Fig. 1-4. With the exception of the methyl borate samples, the rates fell on the line corresponding to heaviest doping in both the boron and phosphorus cases, *i.e.*, C_B(boron) = 2.5 x 10^{20} cm^{-3}, C_B(phosphorus) = 1.5 x 10^{20} cm^{-3}. The oxides produced on the methyl borate predeposited surfaces were nonuniform in thickness, indicating nonuniform surface concentrations.

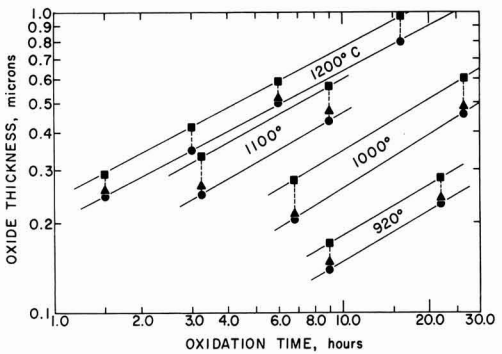

Fig. 1. Oxidation of boron-doped silicon in dry O_2 for three different boron concentrations at four oxidation temperatures: ■, C_B = 2.5 x 10^{20} cm^{-3}; ▲, C_B = 1.0 x 10^{20} cm^{-3}; ●, C_B = 1.0 x 10^{16} cm^{-3}.

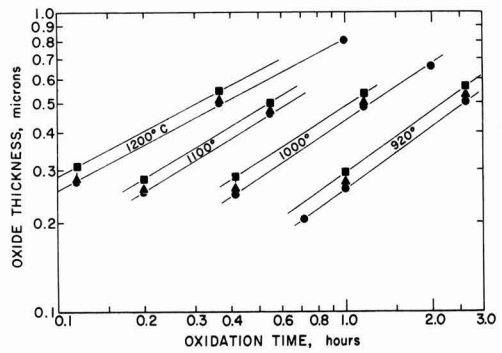

Fig. 2. Oxidation of boron-doped silicon in wet O_2 (95°C H_2O) for three different boron concentrations at four oxidation temperatures: ■, C_B = 2.5 x 10^{20} cm^{-3}; ▲, C_B = 1.0 x 10^{20} cm^{-3}; ●, C_B = 1.0 x 10^{16} cm^{-3}.

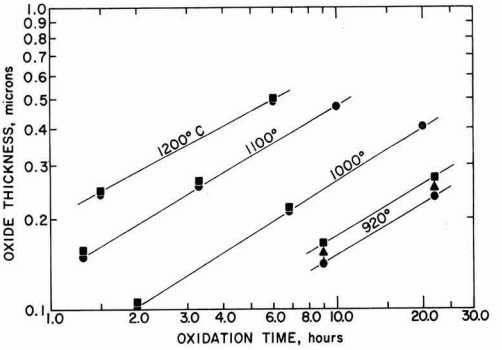

Fig. 3. Oxidation of phosphorus-doped silicon in dry O_2 for three different phosphorus concentrations at four oxidation temperatures: ■, C_B = 1.5 x 10^{20} cm^{-3}; ▲, C_B = 3.7 x 10^{19} cm^{-3}; ●, C_B = 4.0 x 10^{15} cm^{-3}.

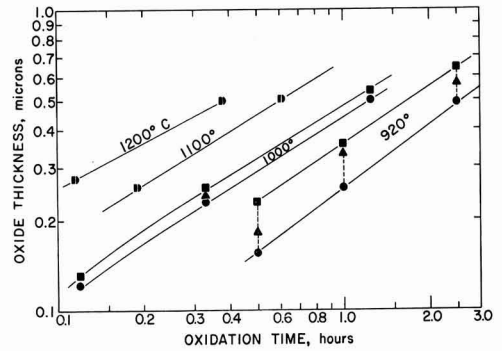

Fig. 4. Oxidation of phosphorus-doped silicon in wet O_2 (95°C H_2O) for three different phosphorus concentrations at four oxidation temperatures: ■, C_B = 1.5 x 10^{20} cm^{-3}; ▲, C_B = 3.7 x 10^{19} cm^{-3}; ●, C_B = 4.0 x 10^{15} cm^{-3}.

Discussion

Boron doped silicon.—In order to interpret the results of Fig. 1 and 2, we must first consider the nature of silicon oxidation. It has been demonstrated (1, 2, 11) that oxidation proceeds by diffusion of some oxidizing species through the oxide already formed to react at the silicon surface. At temperatures above 1000°, the oxidation rate is limited by this diffusion process resulting in the parabolic relationship

$$w = Kt^{1/2}$$

where w is oxide weight or thickness, t, oxidation time, and K is the rate constant, It follows that a change in the oxide structure may affect the oxidation characteristics. By purposely changing the structure, one may observe this effect. The experiments described above concerned with oxidation of predeposited surfaces with boron glass left on the silicon provided an indication of what effect the presence of boron in SiO_2 could provide on further oxidation.

Let us assume a boron glass of thickness 0.2μ is already present on a silicon surface. Then let the sample be exposed to a dry oxygen ambient for 6 hr at 1200°C. Several possibilities arise as to the resulting oxide formation, some of which are shown in Fig. 5. First, if there was no glass present originally, the resulting thickness-time plot would be represented by curve (A) with a final oxide thickness of 0.5μ. Second, if the

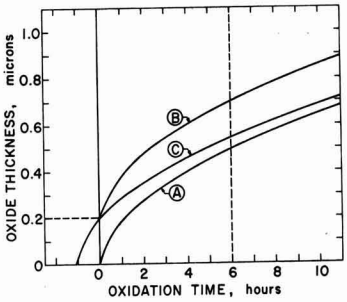

Fig. 5. Possible variations in subsequent oxidation characteristics due to 0.2μ glass formed on silicon surface during predeposition.

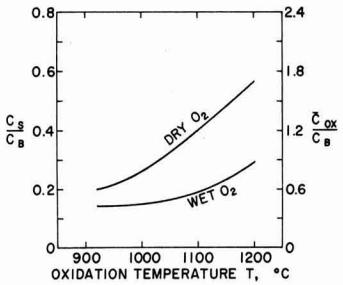

Fig. 6. Predicted boron concentration at the silicon surface (C_s) and in the oxide ($\overline{C}_{ox}$) due to impurity redistribution during thermal oxidation in two ambients at various temperatures.

diffusion of any oxygen species through the glass was much faster than through SiO_2, curve (A) would merely be displaced 0.2μ up along the thickness axis and curve (B) would result. Here the final oxide thickness would be the sum of two thicknesses, *i.e.*, 0.7μ.

The other simple case would exist if both the original glass and the final oxides produced had identical structures, *i.e.*, the diffusion coefficients of oxygen would be the same in both. This case is represented by curve (C), where the additional oxidation starts at the 0.2μ point of the original curve. In other words the original curve is shifted along the time axis so that 0.2μ coincides with 0 min. It can be observed that the final oxide thickness of this case will be 0.55μ. Of course other intermediate possibilities exist where the oxygen diffusivity through the original glass may be greater or less than through the final oxide.

Experiments involving subsequent oxidation of boron predeposited surfaces were performed in several variations. In a typical case the oxidation was conducted in dry oxygen for 90 min at 1200°C. Prior to this oxidation a borate glass was produced by BBr_3 predeposition in an oxygen-nitrogen atmosphere.

The results are: thickness of borate glass, 0.082μ; thickness of oxide on predeposited surface, borate glass removed, 0.294μ; thickness of oxide on predeposited surface, borate glass not removed, 0.372μ; thickness of standard SiO_2, 0.248μ.

It can be noted that the sum of the oxide thickness for the predeposited surface and the borate glass thickness (0.294μ + 0.082μ) is essentially equal to the total oxide thickness where the glass was not removed (0.372μ). Thus the latter result corresponds to case (B) of Fig. 5, and it follows that the borate glass presents very little resistance to the diffusion of oxygen. This effect has been noted previously by Thurston (12) and is in agreement with other comparisons of oxygen diffusion coefficients in glasses (13). The boron probably produces defects in the SiO_2 lattice, resulting in a structure which provides an increase of oxygen diffusion rate.

We are now in a position to discuss the increase of oxidation rates shown in Fig. 1 and 2 for uniformly doped silicon containing high concentrations of boron. These increases can be explained on the basis of the above results if boron is incorporated into the oxide during thermal oxidation. Results of experiments involving redistribution of impurities due to thermal oxidation indicates that this indeed does occur (14, 15). Figure 6 based on considerations of ref. (14, 15) shows the ratio of the boron concentration in the silicon, near the oxide-silicon interface, to the bulk concentration (C_S/C_B) for dry and wet oxygen oxidations as a function of temperature. Since a depletion of boron from the silicon takes place, this ratio is less than one. If a segregation coefficient[2] of 0.33 for the system is also assumed from ref. (14), the average boron concentration in the oxide can also be plotted in Fig. 6 as $\overline{C}_{ox}/C_B$ (see Appendix). At the higher temperatures, there is a considerable amount of boron in the oxide, especially in the dry oxygen case. This boron could cause a weaker bond structure and permit a more rapid oxidation, (assuming that diffusion through the oxide is the rate-determining step at the oxidation temperature). The boron concentration in wet oxides is less according to Fig. 6, and the increase in oxidation rate for heavily doped silicon accordingly should be less pronounced. This is indeed true as shown by comparing Fig. 1 and 2.

Figure 6 also indicates that as oxidation temperature decreases the average boron concentration in the oxide decreases. Thus, the effect of heavy doping should be less pronounced at lower temperatures. This is not observed from Fig. 1 and 2 perhaps because of the change in oxidation mechanism in the vicinity of 1000°C (see ref. 3).

Calculations indicate a dry oxide produced at 1200°C on silicon having a boron concentration of 2.5 x 10^{20} cm^{-3} should contain approximately 1% boron. Gravimetric analysis of such an oxide did show greater boron content than for a standard silicon oxide (C_B(std) = 1 x 10^{16} cm^{-3}), but the method was not sufficiently accurate for quantitative results. Much more significant results were obtained using an infrared examination. Samples were prepared by oxidizing to a thickness of 1.0μ. Using the photoresist and chlorine etch technique (1), a hole was etched through the silicon from the back side. A window of oxide, supported by a frame of silicon, remained on top for infrared transmission examination. Figure 7 shows spectra in the range 6.5-13.5μ wavelength for four different samples. (Total range examined was 2-15μ with no structure indicated beyond the limits included in the figure.) The spectrum for the standard oxide (either wet or dry oxygen) prepared from silicon whose bulk concentration is 1 x 10^{16} cm^{-3} is shown by curve (1). The characteristic absorption peak for fused silica (16) is shown at 9.2-9.3μ. A second peak attributed to an SiO bond, also exists at 12.5μ. Curve (4) represents a wet oxide also on 1 x 10^{16} cm^{-3} material, but covered with a borate layer produced in a methyl borate predeposition system. Additional peaks are now observed at 7.5 and 11.1μ. According to Jellyman and Proctor (17), these peaks are representative of a B_2O_3 glass.[3] Finally, curves (2) and (3) of Fig. 7 are for wet and dry oxygen oxides on 2.5 x 10^{20} cm^{-3} boron doped silicon. The peaks at 7.5μ have shifted slightly to the left (7.2μ) which is more typical of a mixed SiO_2-B_2O_3 system (17). Also present are the boron peaks at 11.1μ. The most significant fact about the two peaks at 7.2μ is the ratio of dry oxygen boron absorption to the wet oxygen value (about 2:1). This same ratio of boron concentration in the oxide is

[2] Segregation coefficient = m = equilibrium concentration of impurity in silicon / equilibrium concentration of impurity in oxide

[3] The data of ref. (17) are based on reflection spectra, but we as well as other investigators have found reasonable agreement between absorption and reflection data.

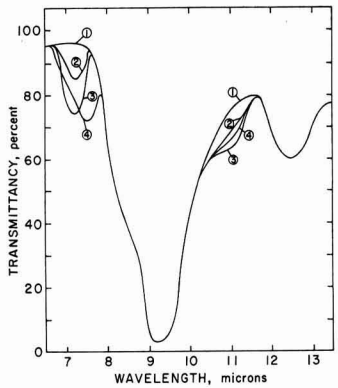

Fig. 7. Infrared absorption spectra of various silicon oxides: 1, standard dry and wet oxide, $C_B = 1 \times 10^{16}$ cm^{-3}; 2, wet oxide, $C_B = 2.5 \times 10^{20}$ cm^{-3}; 3, dry oxide, $C_B = 2.5 \times 10^{20}$ cm^{-3}; 4, wet oxide plus borate glass, $C_B = 1 \times 10^{16}$ cm^{-3}.

predicted from Fig. 6 (at 1200°C, $\bar{C}_{ox}/C_B$ for dry $O_2 = 1.7$, $\bar{C}_{ox}/C_B$ for wet $O_2 = 0.85$). Thus the presence of boron in the oxide is clearly verified by independent means.

Phosphorus doped silicon.—The phosphorus data of Fig. 3 and 4 may be analyzed in a manner similar to the heavily doped boron results. First, experiments involving oxidation of silicon covered with a phosphate glass indicated an increased diffusion rate of oxygen through the glass, although not to the same extent as with the borate glass system. The diffusion coefficient through the glass was estimated to be about 5 times that of pure SiO_2. This finding agrees with the results of Thurston who also noted that phosphorus in fused silica causes an increased rate of oxygen diffusion through the structure, but in a different manner than boron (12). If the phosphate glass data are applied to Fig. 5, the resulting curve would be somewhere in between curves (B) and (C).

Examination of Fig. 3 and 4 reveals that between 1000° and 1200°, a high bulk concentration of phosphorus causes little change in oxidation rates. This is consistent with results of ref. (14, 15): Phosphorus "piles-up" slightly at the silicon surface, and its concentration in the oxide is low. This effect is shown in Fig. 8. Even at 920°, the concentration of phosphorus in a wet oxide (the maximum case) is less than 0.2 that of the bulk. As a result the oxide produced will be essentially SiO_2 and subsequent oxygen diffusion through it will not be significantly affected. However, Fig. 3 and 4 show a marked increase of oxidation rate at 920°C, especially in wet oxygen. This apparent contradiction can be readily explained, however, if the mechanism of silicon oxidation is considered. It has been proposed that below 1000°C, thermal oxidation is no longer completely diffusion controlled, but depends considerably on the reaction at the silicon surface (3). The "pile-up" of phosphorus, especially in wet oxygen, could cause a change in the surface reaction rate and thereby affect the oxidation rate. From Fig. 8 this effect should be more pronounced in wet oxygen, and Fig. 3 and 4 indicate that this is indeed the case.

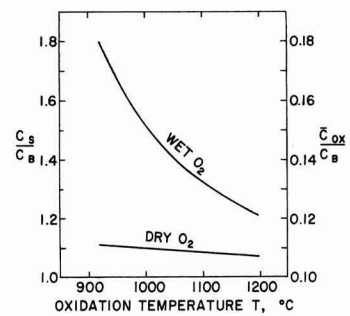

Fig. 8. Predicted phosphorus concentration at the silicon surface (C_S) and in the oxide ($\bar{C}_{ox}$) due to impurity redistribution during thermal oxidation in two ambients at various temperatures.

Table I. Relationship of parabolic oxidation rate constants for heavily doped silicon to standard values

Oxide ambient	Oxidation temp, °C	Rate constant K_{std}, $\mu/\sqrt{hr}$	Boron-doped silicon* K_B/K_{std}	Phosphorus-doped silicon† K_P/K_{std}
Dry O_2	1200	0.206	1.21	1.02
Dry O_2	1100	0.155	1.29	1.03
Dry O_2	1000	0.093	1.31	1.03
Dry O_2	920	(0.050)	1.20	1.18
Wet O_2 (95° H_2O)	1200	0.840	1.11	1.00
Wet O_2	1100	0.675	1.10	1.00
Wet O_2	1000	0.480	1.11	1.09
Wet O_2	920	(0.325)	1.13	1.30

* K_B is the rate constant for $C_B = 2.5 \times 10^{20}$ boron at./cm^3; K_{std} is the rate constant for $C_B = 1 \times 10^{16}$ boron at./cm^3.
† K_P is the rate constant for $C_B = 1.5 \times 10^{20}$ phosphorus at./cm^3; K_{std} is the rate constant for $C_B = 4 \times 10^{15}$ phosphorus at./cm^3.

Thus far, it has not been possible to establish the presence, or perhaps in this case, absence of phosphorus in the oxide by infrared examination. The only P_2O_5 absorption peak (over the wavelength range investigated) falls at 9.2-9.3μ, that of SiO_2. The latter completely masks any effect due to phosphorus.

Correlation of all data.—A general comparison of both boron and phosphorus results may now be made. Table I contains a partial summary of the data plotted in Fig. 1-4. Oxidation rate constants for the silicon with the heavier concentrations of boron and phosphorus ($C_B = 2.5 \times 10^{20}$ and 1.5×10^{20} cm^{-3}) expressed as K_B and K_P, are compared with the standard values, K_{STD}. It should be kept in mind that oxidation at the lower temperatures and for thiner oxides is not truly parabolic. However rate constants are still listed in terms of $\mu/\sqrt{hr}$ for the thicker oxides at each temperature for purposes of comparison. Table I shows a reasonable correlation with Fig. 6 and 8, in that at higher temperatures the concentration of boron in the oxide (Fig. 6) determines the amount of increase in oxidation rate. At 920°C, where the reaction has been proposed to be more surface controlled, wet oxygen oxidation of phosphorus-doped silicon results in the highest surface concentration and also the highest oxidation rate.

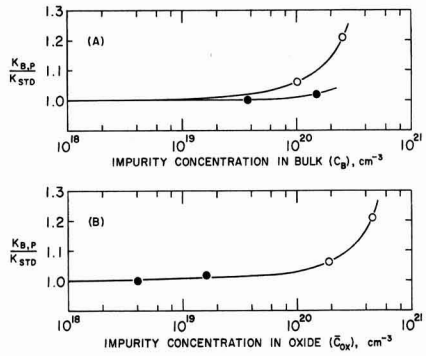

Fig. 9. Dependence of oxidation rate constants for heavily doped silicon on: (A) impurity concentration in the bulk; (B) impurity concentration in the oxide. Data are based on oxidation in dry oxygen at 1200°C; ○, boron; ●, phosphorus.

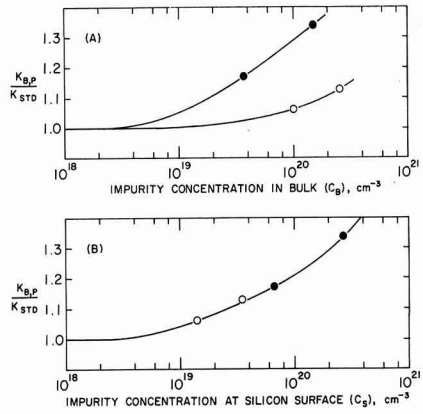

Fig. 10. Dependence of oxidation rate constants for heavily doped silicon on: (A) impurity concentration in the bulk; (B) impurity concentration at the silicon surface. Data are based on oxidation in wet oxygen (95°C H_2O) at 920°C; ○, boron; ●, phosphorus.

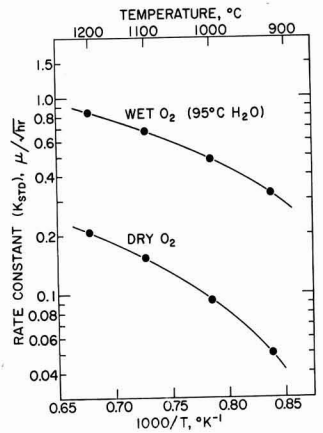

Fig. 11. Log of rate constant, $K_{STD} \equiv w/\sqrt{t}$, plotted against reciprocal of absolute temperature for dry and wet O_2 oxidation of silicon ($C_B = 1 \times 10^{16}$ at./cm^3).

In Fig. 9A, the K_B/K_{STD} and K_P/K_{STD} ratios for dry oxygen oxidation at 1200°C are plotted against bulk impurity concentration C_B. Two separate curves result. However, if the ratios are plotted against average impurity concentration in the oxide, $\bar{C}_{ox}$, one curve is obtained in Fig. 9B. Similarly, 920°C wet oxygen data are plotted in Fig. 10. In this case, whereas ratios of K_B/K_{STD} and K_P/K_{STD} plotted against C_B again result in two curves (see Fig. 10A), a plot of the ratios against surface concentration C_S gives one continuous curve. In this case if the results were plotted against $\bar{C}_{ox}$, the resulting curves would be even more divergent than Fig. 10A.

The above two cases (dry oxygen at 1200° and wet oxygen at 920°C) were selected as examples since they represent the two extremes in the effects of heavy doping on oxidation characteristics. It should be noted that wet oxygen data at 1200°C could be included in Fig. 9 (and dry oxygen data at 920°C in Fig. 10) with reasonable agreement with the existing curves. These results further indicate that the oxidation rate of heavily doped silicon is chiefly dependent on the impurity concentration either in the oxide (above 1000°C) or at the surface (below 1000°C).

A plot of the logarithm of parabolic rate constant versus the reciprocal of absolute temperature is shown in Fig. 11 for dry and wet oxygen silicon oxidation. The points represent the data from Table I for standard rate constants (K_{STD}). The curves help to illustrate the change in oxidation mechanism from one primarily diffusion controlled ($w = K_1 t^{1/2}$) to that where a reaction at the silicon oxide-silicon interface at least partially controls the oxidation rate ($w = K_2 t$). Above 1000°C the curves (based on parabolic rate constants) are more linear while below this temperature a more rapid change in slope is noted. The best fit of a straight line through the points in the 1000° to 1200° region in Fig. 11 will give activation energies of 14.75 and 10.25 kcal/mole for dry and wet O_2, respectively (where $K_{STD} \equiv w/\sqrt{t}$). These values correspond to 29.5 and 20.5 kcal/mole (for $k \equiv w^2/t$) which are in close agreement with previous results (3).

The fact that the curves in Fig. 11 are not strictly linear but have continuously changing slopes indicates that there is no sudden change in oxidation mechanism at any particular temperature. If we consider some concepts of oxidation mechanisms proposed by Evans (18), the nature of these results can be better understood. In the case of silicon, oxidation will depend on two main processes: the diffusion of the oxidizing species through the oxide and the reaction of this species with the silicon at the oxide-silicon interface. The slower of the two processes will be the actual rate-determining step. Temperature will be an important factor in determining the comparative rates and thus the relative importance of these two processes. This is indicated by the changing slopes in Fig. 11. The results described in this investigation involving oxidation rates of heavily doped silicon are also in agreement with this concept.

Mention should be made of the relationship of these results to the few data that have already been presented concerning oxidation of heavily doped silicon. Yeh (6) indicated that the oxidation rate of silicon with an estimated diffused phosphorus surface concentration of 2×10^{21} cm^{-3} increased if the oxidation occurred at 970°C in steam. The only data presented in support of this was a plot of oxide thickness *vs.* square root of time. The slopes and thus the oxidation rate constants, of the two plots ($C_S = 2 \times 10^{21}$ and 2×10^{16} cm^{-3}) were identical, while the intercepts were different. This indicated an initial porous oxide might have been present on the diffused surface, causing a shift of the type shown in Fig. 5 from curve A to curve B. According to the results of the present investigation, Yeh should have obtained a significant increase of oxidation rate in steam at 970° for the surface concentration indicated. Yeh did present data for a boron diffused surface (estimated $C_s = 5 \times 10^{18}$ cm^{-3}) which if plotted in a manner similar to the phosphorus data indicates a rate constant increase of about 10%. This increase would be of a magnitude similar to the boron results given in this paper, but such increases were found only when the boron surface concentration was at least 5×10^{19} cm^{-3}. The difficulty of accurately determining diffused surface concentrations might account for Yeh's results.

The other finding that heavily doped surfaces provide an increased oxidation rate was reported by Ligenza (7). Silicon with a phosphorus surface concentration of 10^{21} cm^{-3} was oxidized at 650°C for 1 hr in 120 atm steam. An oxidation rate five times that of high resistivity silicon was obtained. For this type of oxidation, the oxide thickness-time relationship is entirely linear which means the oxidation is controlled completely by a reaction at the silicon-silicon oxide interface. Such an increase in oxidation rate would therefore be expected from the results and considerations of the present investigation.

Conclusions

It has been shown that the thermal oxidation rate of heavily doped silicon (C_B of boron and phosphorus $\geq 10^{20}$ cm^{-3}) at temperatures above 1000°C depends on

the amount of impurity in the oxide. This finding is consistent with the diffusion-controlled mechanism of thermal oxidation in this temperature range. The amount of impurity in the oxide in turn is a function of the redistribution characteristics of the impurity and the oxidation ambient. Little effect is noted unless the impurity concentration in the oxide is greater than 10^{20} cm^{-3}.

At 920°C, where thermal oxidation is partially controlled by a surface reaction the rate of oxidation is a function of the impurity concentration at the silicon surface. This concentration, determined by redistribution phenomena, must be at least 10^{19} cm^{-3} before an appreciable change in rate occurs.

The effect of other impurities (for $C_B \geqq 10^{20}$ cm^{-3}) on oxidation rates may also be predicted, provided their redistribution characteristics are known. These predictions can be based on the four cases of the redistribution process as presented in ref. (14). Where the oxide rejects impurities and diffusion of these impurities in the oxide is slow (case 2A, ref. 14) such as phosphorus, antimony, and arsenic, no increase in oxidation rate should occur above 1000°C. However the rates should increase below 1000°C. If the oxide takes up an impurity, and again the impurity diffuses slowly in the oxide (case 1A), an increase of oxidation rate should occur at least at temperatures above 1000°C, and possibly below, as with boron. Gallium, aluminum, and indium, which deplete at the silicon surface and also probably diffuse rapidly through the oxide (either case 1B or 2B) should not cause an increase in oxidation rates at any temperature even at high bulk concentrations.

Acknowledgments

The authors are indebted to A. S. Grove, E. H. Snow, and C. T. Sah for helpful discussions regarding various aspects of this program. The calculations in the Appendix were performed by A. S. Grove. R. Tanner assisted in the preparation and evaluation of the oxides.

Manuscript received Sept. 22, 1964; revised manuscript received Nov. 23, 1964.

Any discussion of this paper will appear in a Discussion Section to be published in the December 1965 JOURNAL.

REFERENCES

1. M. M. Atalla, "Properties of Elemental and Compound Semiconductors," Vol. 5, H. Gatos, Editor, pp. 163-181, Interscience Publishing Co., New York (1960).
2. J. R. Ligenza and W. G. Spitzer, *J. Phys. Chem. Solids*, **14**, 131 (1960).
3. B. E. Deal, *This Journal*, **110**, 527 (1963); *ibid.*, **110**, 1292 (1963).
4. H. C. Evitts, H. W. Cooper, and S. S. Flaschen, *ibid.*, **111**, 688 (1964).
5. C. R. Fuller and F. J. Strieter, Paper presented at the Toronto Meeting of the Society, May 3-7, 1964, Abstract No. 74.
6. T. H. Yeh, *J. Appl. Phys.*, **33**, 2849 (1962).
7. J. R. Ligenza, *This Journal*, **109**, 73 (1962).
8. C. T. Sah, *IEEE Trans. Electron Devices*, **ED-11**, 324 (1964).
9. G. E. Moore, Chap. 5 in "Microelectronics," E. Keonjian, Editor, McGraw-Hill Book Co., New York (1963).
10. J. C. Irvin, *Bell System Tech. J.*, **41**, 387 (1962).
11. P. J. Jorgensen, *J. Chem. Phys.*, **37**, 874 (1962).
12. M. O. Thurston and K. D. Kang, "The Mechanisms of Oxidation and Diffusion Into the Oxide," Seventh Quarterly Technical Report No. RF 1233-7Q, U. S. Army Signal Supply Agency Contract No. DA-36-039-SC-87426, October (1962).
13. R. H. Doremus, Chap. 1 in "Modern Aspects of the Vitreous State," Vol. 2, J. D. MacKenzie, Editor, Butterworth and Co., Washington, D. C. (1962).
14. A. S. Grove, O. Leistiko, Jr., and C. T. Sah, *J. Appl. Phys.*, **35**, 2695 (1964).
15. B. E. Deal, A. S. Grove, E. H. Snow, and C. T. Sah, *This Journal*, **112**, 308 (1965).
16. I. Simon, Chap. 6 in "Modern Aspects of the Vitreous State," Vol. I, J. D. MacKenzie, Editor, Butterworth and Co., Washington, D. C., (1962).
17. P. E. Jellyman and J. P. Proctor, *Trans. Soc. Glass Tech.*, **39**, 173T (1955).
18. U. R. Evans, "The Corrosion and Oxidation of Metals," pp. 819-859, Edward Arnold Ltd., London (1960).
19. H. S. Carslaw and J. C. Jaeger, "Conduction of Heat in Solids," Appendix II, Oxford University Press, London (1959).

APPENDIX

The Average Impurity Concentration in the Oxide Layer

Because of the redistribution process taking place during thermal oxidation, some of the impurities which were originally in the silicon substrate will end up within the silicon dioxide film. The resulting average concentration of impurities within the oxide can be readily calculated on the basis of the redistribution theory (14), as follows.

The total amount of impurity (per cm^2) contained within the oxide layer is given by

$$Q_{ox} = \int_0^{z_o} C_1(z,t)\,dz \qquad [A\text{-}1]$$

where z_o denotes the oxide thickness, and $C_1(z,t)$ denotes the concentration of the impurity within the oxide film. [The notation follows that of ref. (14).] Incorporating Eq. [15] of ref. (14) into equation [A-1], and performing the integration yields the average concentration of the impurity in the oxide film

$$\overline{C}_{ox} \equiv \frac{Q_o}{z_o} = C_o + \left(\frac{C_s}{m} - C_o\right)\left[1 + \frac{\text{ierfc}(K/2\sqrt{D_1}) - 1/\sqrt{\pi}}{K/2\sqrt{D_1}}\right] \qquad [A\text{-}2]$$

where ierfc indicates the integral of the complementary error function and is tabulated in ref. (19). C_o denotes the concentration of the impurity at the outside surface of the oxide layer (this concentration is very small if the impurity has a tendency to leave the solid); C_s denotes the concentration of the impurity in the silicon near the oxide-silicon interface; and m is the segregation coefficient. The bracketed term has been evaluated and is shown in Fig. 12 as a function of $K/2\sqrt{D_1}$, the ratio of the parabolic oxidation rate constant to the square root of diffusivity of the impurity in the oxide layer. It can be noted that the limits of very small and very large diffusivities, Eq. [A-2] reduces to

$$\overline{C}_{ox} = C_s/m, \quad K/2\sqrt{D_1} \to \infty \qquad [A\text{-}3]$$

$$\overline{C}_{ox} = C_o, \quad K/2\sqrt{D_1} \to 0 \qquad [A\text{-}4]$$

The first of these equations corresponds to the case of boron and phosphorus; the second to gallium. These are the approximations used in the text of the present work.

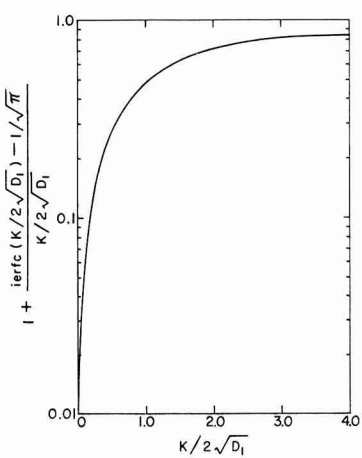

Fig. 12. Value of term used in calculating average impurity concentration in oxide as a function of the ratio $K/2\sqrt{D_1}$.

The Effects of Substrate Orientation on Epitaxial Growth

S. K. Tung

Bell Telephone Laboratories, Incorporated, Allentown, Pennsylvania

ABSTRACT

The effect of substrate orientation on the quality of silicon epitaxial layers was studied in terms of deposition rate and surface topography. The layer was deposited by the hydrogen reduction of silicon tetrachloride. Deposition rate was determined from the time of deposition and from the layer thickness obtained by angle lapping and staining. Deposition rate was lowest on accurately oriented <111> substrates and increased as the degree of misorientation from the <111> direction increased. The frequently observed surface pyramid defect was found to be a function of (*a*) deposition rate and (*b*) substrate orientation. These pyramidal defects were not observed for low deposition rates, and when the substrate was misoriented from the <111> direction. These observations are consistent with the proposal that the deposition rate used in practice is determined by two fundamental rate processes, namely, (*a*) reaction rate and (*b*) growth rate.

During the development of epitaxial deposited silicon layers, there has been interest in the effect of the orientation of the silicon substrate and in the change of orientation after surface processing and layer deposition. This paper reports a study of these effects on the quality of the silicon epitaxial layer in terms of deposition rate and surface topography.

Experimental Procedure and Results

Orientation change during silicon substrate processing.—A silicon substrate surface was lapped and chemically polished before epitaxial deposition. The surface orientation was measured by x-ray goniometry after each processing step, *i.e.*, lapping, chemical polishing, and epitaxial layer deposition. The precision of the employed technique was estimated to be within ± 10 min of arc. The data of this study are summarized in Table I. It is concluded that there was no substantial orientation change of the silicon surface through the orientation range investigated, either after chemical polishing or after layer deposition. The small orientation difference seen in Table I is believed to be experimental error.

Substrate orientation related to deposition rate.—To study the effects of substrate orientation on deposition rate a silicon layer was deposited on a polycrystalline silicon substrate whose surface was mechanically polished. This substrate contained two or three large grains. The orientations of these large grains were determined by the Laue back-reflection technique. An epitaxial silicon layer was deposited by the hydrogen reduction of silicon tetrachloride using a vertical type machine similar to that reported previously (1, 2). This deposition was normally done at a slice temperature of 1200°C and a 0.2 vol % concentration of silicon tetrachloride. After the layer deposition, the grain boundaries were delineated by the differences in thickness of silicon deposited on each grain. Figure 1 shows such a silicon wafer surface after epitaxial layer deposition. The grain boundaries can be seen clearly in this picture, but they could not be located before deposition because the wafer surface had been mechanically polished. The difference in layer thickness is further illustrated in Fig. 2 by an angle-lapped section. In this case the two large grains had <111> and<115> orientations. The layer thickness on the <111> grain was 11.2μ, and on the <115> grain it was 13.0μ. Because the two adjacent grains were deposited in the same run, other deposition parameters such as temperature, silicon tetrachloride vapor concentration, and flow rates were the same. The difference in layer thickness on different grains was thus due to the variation in orientation.

Figure 3 is a plot of deposition rate at 1200°C as a function of substrate orientation. Deposition rate was determined from the time of deposition and from layer thickness obtained by angle lapping and staining. The data of this plot were obtained from depositions on individual single crystal silicon substrates with different orientations. It is of interest to note that the deposition rate increased as misorientation from the <111> direction increased. Also, the curve shows that the <111> orientation had the lowest deposition rate of all low index orientations, while the <110> orientation had the highest deposition rate. These results were similar to those reported by Mendelson (3).

Table I. Surface orientation change after processing

Slice No.	Substrate resistivity, ohm-cm	Orientation, angle from <111> After lapping	After chemical polishing	After deposition
3619-78	0.014	3° 5′	3° 16′	2° 57′
3619-79	0.017	3° 11′	3° 24′	3° 11′
3642-2	0.006	2° 43′	—	2° 55′
3642-3	0.006	2° 46′	—	2° 38′
3642-4	0.006	2° 33′	—	2° 34′
3642-7	0.006	2° 24′	—	2° 29′
3642-8	0.006	2° 27′	—	2° 26′
3642-27	0.006	2° 38′	2° 36′	—
3642-30	0.006	2° 32′	2° 33′	—
3642-31	0.006	2° 26′	2° 29′	—
3642-32	0.006	2° 51′	2° 34′	—
3642-34	0.006	2° 26′	2° 39′	—

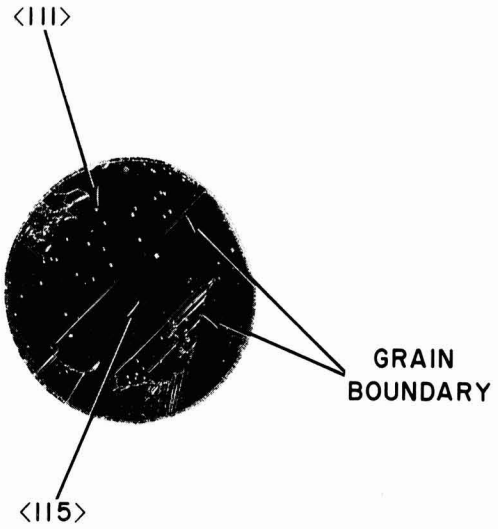

Fig. 1. Surface of silicon layer on polycrystal silicon substrate

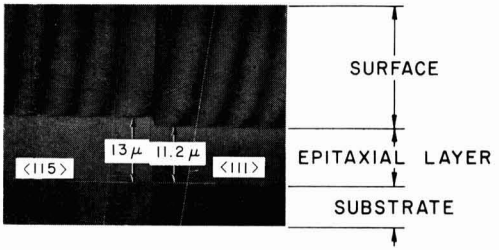

Fig. 2. An angle-lapped picture showing different layer thickness

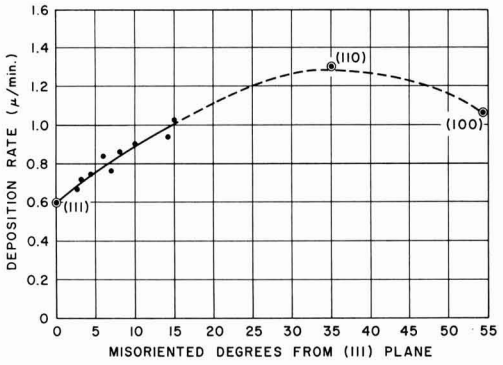

Fig. 3. Deposition rate vs. substrate misorientation

He observed a minimum growth rate and a high stacking fault density on <111> substrates.

Because the deposition rate depends strongly on other processing parameters (2), the orientation effect discussed here can be differentiated only when other process parameters are held substantially constant.

Substrate orientation and surface layer topography.— A surface defect of "pyramidal" shape was found in depositions upon <111> oriented substrates when the deposition rate exceeded a critical value (4). This type of surface defect is shown in Fig. 4. In general, this defect is a prominence on the surface and has a ridgelike tail associated with it. The size of the pyramids varied as the growing conditions changed. Normally, they are easily seen with the unaided eye.

A tetrahedral growth defect has been observed by Miller *et al.* (5) who attributed such a defect to the presence of silicon carbide. It should be emphasized that the type of surface defect observed here developed only when the deposition rate exceeded a critical value for that particular substrate orientation. That is the

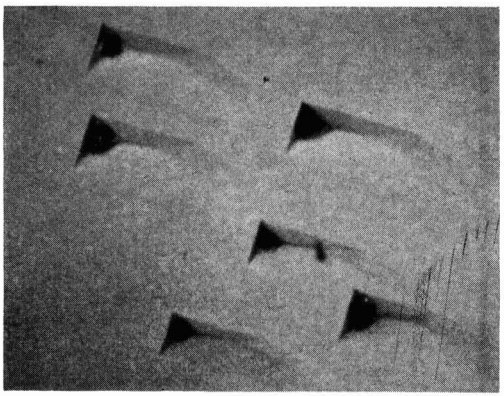

Fig. 4. Surface pyramids. Magnification 50X.

Table II. Summary of data

Substrate orientation	Critical deposition rate
<111>	1.0μ/min ±25%
½° from <111>	1.5μ/min ±25%
2° from <111>	3.5μ/min ±25%

surface defect is a combination effect of both the substrate orientation and the deposition rate. Impurities play a less determining factor. For example, pyramids grew on a substrate with <111> orientation but no pyramids grew on a substrate with <115> orientation when both the substrates were deposited simultaneously at 1200°C with a deposition rate of 1.4 μ/min. In another experiment pyramids did not grow on either <111> or <115> oriented substrates because a lower deposition rate of 0.4 μ/min was used at the same deposition temperature. The deposition rate was adjusted by varying silicon tetrachloride concentrations. In general one can conclude that the pyramids were grown at a certain deposition rate for a particular substrate orientation. In this paper this deposition rate is called the "critical deposition rate" for that orientation.

Because the deposition rate is a function of the substrate orientation, it was expected that the critical deposition rate for pyramids grown depended on the substrate orientation. Experimental results showed that on a silicon substrate which had been misoriented from the <111> direction, a high deposition rate could be utilized without pyramids growing on the surface. Also, when a silicon substrate surface was closely oriented to the <111> direction, pyramids might develop on the surface unless a deposition rate less than the critical deposition rate was used.

The critical deposition rates for various misorientations from the <111> direction were found experimentally. Table II shows the critical deposition rate at 1200°C to be about 1 μ/min for a substrate oriented on the <111> direction, about 1.5 μ/min for a substrate with a ½ degree misorientation from the <111> direction, and about 3.5 μ/min for a substrate with a 2 degrees misorientation from the <111> direction. It should be pointed out that the critical deposition rate is also dependent on the depositing system and the data discussed was derived from the system described in a previous publication (2).

Discussion

One may ask "What is the critical deposition rate?" In answering this question it will be convenient to discuss the results in terms of heterogeneous rate reaction theory (6). In general the over-all deposition process can be separated into two main steps: (*a*) the reaction or series of reactions which take place on or near the substrate surface; this rate will be called the reaction rate; (*b*) the addition of atoms to proper sites of the substrate surface; this will be called the growth rate. These two rate processes complement each other during deposition. The slower process will control the over-all deposition process. Thus the observed deposition rate is either controlled by the reaction rate or by the growth rate. The controlling rate depends on how the deposition process is carried out and how the process parameters are arranged.

Figure 5 shows a schematic drawing of the observed deposition rate *vs.* silicon tetrachloride concentration. One may visualize that the growth rate or the rate at which atoms are added to the substrate surface is dependent on the substrate surface plane. Consequently the growth rate is a strong function of substrate orientation. On the other hand, the reaction rate should not depend too much on substrate orientation. Thus the critical deposition rate on a perfect substrate surface plane can be assumed to be the growth rate. Also, the deposition rate, whether controlled by the reaction rate or by the growth rate, depends on other process parameters in the deposition.

The theoretical treatment of surface structures in crystal growth from the vapor was given by Cabrera

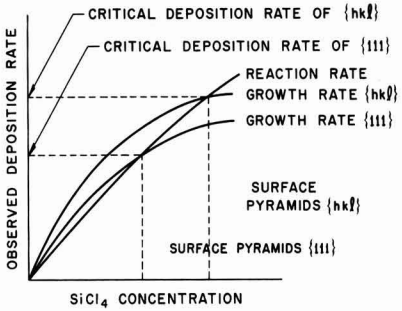

Fig. 5. Schematic drawing of the observed deposition rate vs. silicon tetrachloride concentration.

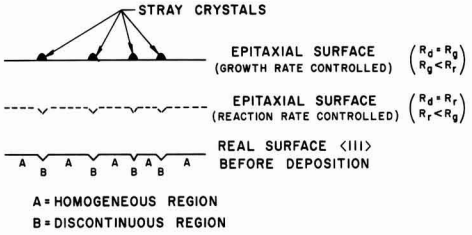

Fig. 6. Schematic drawing of a <111> surface after deposition

Fig. 7. Schematic drawing of a misoriented <111> surface

and Coleman (7). Assume a real surface to be almost homogeneous everywhere but with some inhomogeneities or discontinuities at several locations. These inhomogeneities will also have local orientation changes. It is predicted (7) that the growth rate at such discontinuities will be greater than the growth rate on the homogeneous region because nucleation will occur more readily at the discontinuities than at the homogeneous region. Figure 6 shows a schematic drawing of the epitaxial layer growth on a real surface having <111> orientation. If the deposition process is reaction rate controlled, then the over-all process is not orientation dependent. Consequently there are no differences in the growth features on the homogeneous regions and the inhomogeneous regions. The resultant epitaxial layer surface is merely an image of the substrate surface on which the layer was deposited. This result normally can be accomplished by depositing at a low silicon tetrachloride concentration. However, if the deposition process is growth rate controlled, then the over-all process is strongly orientation dependent and the reaction rate is greater than the growth rate. The difference between the reaction rate and the growth rate is shown by forming a stray crystal at an inhomogeneity at which the growth rate is greater than at other homogeneous regions on the surface. As shown in Fig. 3 the <111> oriented surface had the lowest growth rate when compared to other orientations. Consequently a "pyramid" on the surface is formed. In general, this result can be observed by depositing at a high silicon tetrachloride concentration.

The same general arguments can be applied for the case of a substrate surface which has an orientation other than the <111> orientation. Thus it is proposed that the atomic configuration of a misoriented {111} plane can be resolved into many steps which are parallel to the original {111} plane surface. This is shown schematically in Fig. 7. Such a misoriented {111} plane surface can have a greater growth rate than the {111} plane surface since it is expected that nucleation will occur more readily at the step corners formed by the {111} plane surfaces. Consequently the difference between the reaction rate and the growth rate on a misoriented {111} plane surface is less than the difference between the reaction rate and the growth rate on a {111} plane surface if the reaction rate is considered unchanged. Thus a substrate surface misoriented from the <111> direction can tolerate a higher deposition rate without developing pyramids on the surface.

Conclusions

The deposition rate was found to vary with substrate orientation. The deposition rate increased to a limit as the substrate was misoriented from <111> orientation. The <111> oriented substrate had the lowest deposition rate when compared to other major orientations, *i.e.*, <110> and <100>.

A pyramidal surface defect was found to be a function of both the deposition rate and the substrate orientation. The pyramidal defects were not observed when the deposition rate was slow, and/or when the substrate was misoriented from the <111> direction. These observations were explained by a proposed mechanism in which the deposition rate used in practice is considered to be composed of two fundamental rate processes reaction rate and growth rate which complement each other during the actual deposition.

Acknowledgment

The author wishes to thank Mrs. M. H. Read, Bell Telephone Laboratories, Murray Hill, for her x-ray work in determining the crystal orientations. Also, he is indebted to Dr. R. E. Caffrey for his valuable discussions.

Manuscript received Sept. 23, 1964.

Any discussion of this paper will appear in a Discussion Section to be published in the December 1965 JOURNAL.

REFERENCES

1. H. C. Theuerer, *This Journal*, **108**, 649 (1961).
2. S. K. Tung, *Metallurgy of Semiconductor Materials*, **15**, 87 (1962).
3. S. Mendelson, *J. Appl. Phys.*, **35**, 1570 (1964).
4. Private communication: G. H. Edmunds and W. C. Gibson at Bell Telephone Laboratories, Laureldale, Pennsylvania also reached the same results through their investigations.
5. D. P. Miller, S. B. Watelski, and C. R. Moore, *J. Appl. Phys.*, **34**, 2813 (1963).
6. A. Van Hook. "Crystallization: Theory and Practice," 22 (1961).
7. N. Cabrera and R. V. Coleman, "The Art and Science of Growing Crystals," 3 (1963).

Mechanism of Hydrocarbon Formation in the Electrolytic Reduction of Acetone in Aqueous Sulfuric Acid

Taro Sekine, Akira Yamura, and Kiichiro Sugino

Department of Applied Electrochemistry, Tokyo Institute of Technology, Tokyo, Japan

ABSTRACT

A tentative mechanism or hydrocarbon formation is proposed which, by combining the usual mechanism of pinacol and isopropanol formation, will contribute to one clarification of the over-all electrode process of acetone reduction.

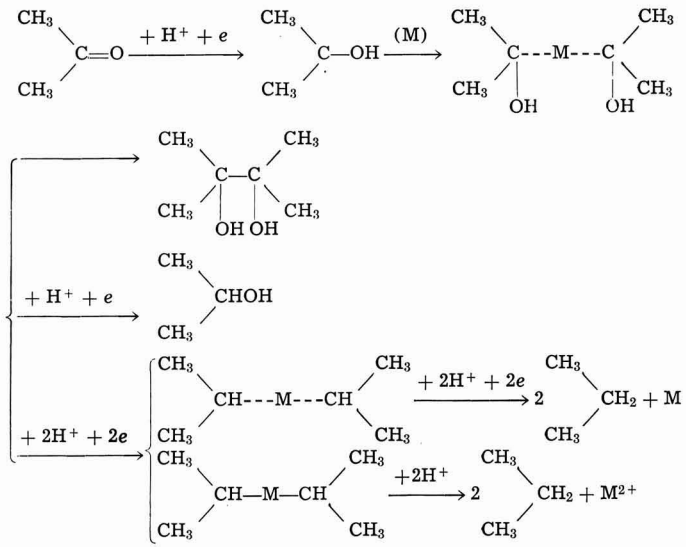

The main point lies in the fact that the radical $(CH_3)_2\dot{C}OH$ is further reduced with dehydration of propane through the isopropyl radical which is combined with the cathode metal. In certain cases (mercury and lead, etc.) the reaction products with metal (organometallic compound) can be isolated in a relatively stable form. Generally speaking, cathode material having a negative standard electrode potential tends to follow this hydrocarbon formation process.

In the electrolytic reduction of aliphatic ketones in acidic medium it is known that pinacol, secondary alcohol, and hydrocarbon are obtained as the main products. In the case of acetone, the reduction products were pinacol, isopropanol, and propane (1). Depending on the kind of cathode used, the amounts of the products obtained will differ considerably; at cadmium (1) and amalgamated zinc (2), the hydrocarbon was mainly obtained.

It is still not clear, however, why the use of different kinds of cathodes produces different types of products. It is impossible at this time to establish a complete mechanism of the electrolytic reduction of aliphatic ketones, although attempts have been made.[1]

The authors have undertaken this study in order to clarify the over-all electrode process of acetone reduction by trying to solve the problem of why the different kinds of cathodes cause the formation of different types of products, and in particular why the hydrocarbon is obtained.

Experimental

Assembly of the apparatus.—Arrangement of the electrolysis equipment and cell design are shown in Fig. 1. Two different types of cell, cylindrical and H type cell, were utilized for the convenience of preparative study and accurate gas analysis.

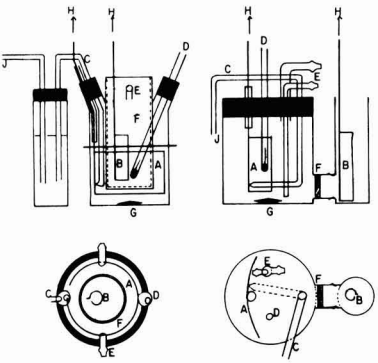

Fig. 1. Cell design: A, cathode; B, anode; C, salt bridge; D, thermometer; E, gas outlet to buret; F, diaphragm; G, stirrer (magnetic drive); H, to controlled potential electrolyzer; J, to saturated calomel electrode.

[1] Recently, S. Swann, Jr. reviewed the electrolytic reduction of keto groups to methylene groups in aliphatic compounds and he showed a tentative mechanism in which the metal of the cathode takes part in the reaction (3). This was originally put forth by Schall *et al.* (9).

Table I. Conditions of gas chromatographic analysis

Product stationary phase, 2m	Pinacol P.E.G.*	Isopropanol P.E.G.	H_2 M.S.†	C_2H_6 S.G.‡	C_3H_8 S.G.	C_4H_{10} S.G.
Carrier gas	H_2	H_2	Ar	H_2	H_2	H_2
Flow rate, cc/min	40	40	40	40	40	40
Temperature, °C	200	100	20	100	100	100
Retention time, min	9.3	7.2	1.8	2.6	7.0	12.0

* P.E.G., polyethyleneglycol 1500.
† M.S., molecular sieve 5A.
‡ S.G., silica gel.

Preparation of electrolyte.—Acetone was purified by distillation after standing for several days with potassium permanganate. HCl-KCl buffer solution (pH 1.55) and 0.2*N* sulfuric acid solution were used for the background solution of polarographic measurement.

Pretreatment of electrodes.—With the exception of mercury, which was carefully distilled before use, lead, cadmium, zinc, aluminum, nickel, tin, and copper cathodes were washed successively with dilute hydrochloric acid and water. The fresh electrodes were used immediately in the following experiments.

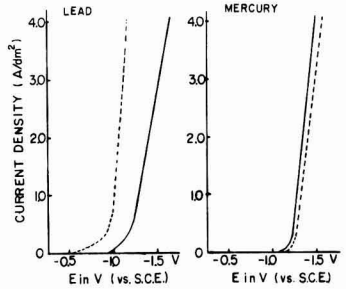

Fig. 2a. I-E curves in acetone sulfuric acid mixture at lead and mercury cathode: ——115g acetone and 28 cc 20% sulfuric acid; - - - - - 130 cc 10% sulfuric acid (reference).

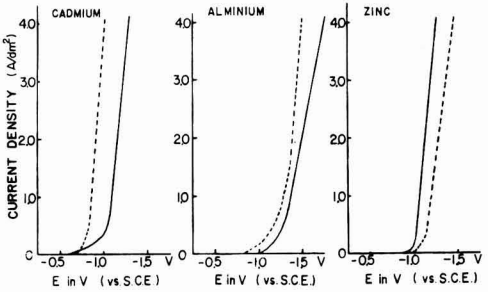

Fig. 2b. I-E curves in acetone sulfuric acid mixture at cadmium, aluminum, and zinc cathode: ——115g acetone and 28 cc 20% sulfuric acid; - - - - 130 cc 10% sulfuric acid (reference).

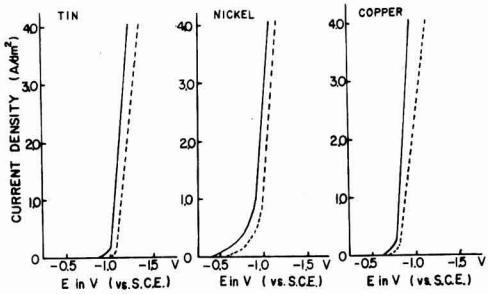

Fig. 2c. I-E curves in acetone sulfuric acid mixture at tin, nickel, and copper cathode: ——115g acetone and 28 cc 20% sulfuric acid; - - - - 130 cc 10% sulfuric acid (reference).

Analysis of the products.—A gas chromatographic technique (4) was utilized to determine the products which were formed during the electrolysis and those formed by the decomposition of organo-metallic intermediate.

The conditions of gas chromatographic analysis used are condensed in Table I.

At the same time, pinacol was separated from the electrolyte and determined by the following procedure.

The catholyte was neutralized with anhydrous potassium carbonate, filtered, and the resulting solution was distilled at reduced pressure to remove acetone and 2-propanol. The residue was extracted with ether and after drying, the ether solution was evaporated. Colorless needles were obtained having a melting point of 38°C.

With the exception of mercury, the ions of metals such as lead, cadmium, zinc, aluminum, nickel, tin, and copper in the electrolyte or in the decomposition product or organo-lead intermediate were determined polarographically at 20° ± 1°C after 5-30 min of deoxygenation by nitrogen. Mercury was determined by E.D.T.A. titration (5).

To confirm the structure of organo-metallic intermediate, the I.R. spectroscopic method was tried by using "Shimadzu I.R. spectrophotometer Type IR-27" at 35°C.

Results and Discussion

Current density-cathode potential curve.—A plot of current density *vs.* cathode potential was made in the catholyte described below by using controlled potential electrolyzer (Yanagimoto EV-3). Figure 2 shows the current density *vs.* cathode potential curves which were measured in a cylindrical cell at mercury, lead, cadmium, zinc, aluminum, nickel, tin, and copper cathodes, respectively. All measurements were carried out at 20° ± 1°C.

Polarographic measurement[2] was also carried out for the catholyte containing 1-10 x 10^{-3} mole/liter acetone in 0.2*N* H_2SO_4 or a HCl-KCl buffer. Polarograms of acetone are shown in Fig. 3. Current increases at mercury in Fig. 2 and 3 were seen at about —1.20v and are considered to be the reduction potential of acetone in sulfuric acid.

Although no noticeable reduction wave (showing half-wave potential) was observed on the polarogram of acetone reduction,[3] the interesting results were observed when the "controlled potential electrolyzer" was used on current-potential curve measurement. That is, at lead, cadmium and aluminum, a negative shift of current-potential curves was induced when

[2] Yanagimoto's High Sensitive Polarograph PA-201 was used.

[3] Nearly the same result was reported by Shikata and Tachi (6) and Zuman (7) for the same conditions.

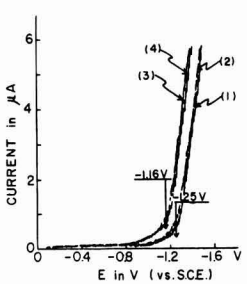

Fig. 3. Polarograms of acetone. 1, 5-500 x 10^{-3} mole acetone in HCl-KCl buffer; 2, HCl-KCl buffer (pH = 1.55); 3, 1-50 x 10^{-3} mole acetone in 0.2*N* H_2SO_4; 4, 0.2*N* H_2SO_4. Sensitivity 0.04 μa/mm.

Table II. Controlled potential electrolysis at various cathodes

Cathode	Hg	Pb	Cd	Zn	Al	Ni	Sn	Cu
Catholyte acetone, g	47	58	110	110	110	145	145	110
20% H_2SO_4 cc	10	13	21	21	21	36	36	21
Cathode potential, v (*vs.* S.C.E.)	−1.375	−1.375	−1.375	−1.375	−1.375	−1.300	−1.200	−1.000
Average current density, amp/dm²	3.0	1.5	3.2	4.3	1.6	5.6	4.0	1.0
Current consumed, amp-hr	12.5	12.3	14.1	12.8	4.6	12.4	5.5	3.6
Current efficiency, %	73	86	90	86	45	1	0	3
Products obtained								
Pinacol, g	0.18	0.74	0	0	0	0	0	0
%*	2.9	7.1	0	0	0	0	—	0
Isopropanol, g	7.9	6.5	0	0.2	0	0	0	0
%*	94.9	67.7	0	3.0	0	0	—	0
Propane, cc	74	930	2596	2157	434	138	0	120
%*	2.2	25.2	100	97.0	100	100	—	100
Hydrogen, cc	1400	730	496	117	1031	5127	2400	1500

* Per cent of total product.

acetone was added to the electrolyte, and at mercury, zinc, nickel, tin, and copper, a positive shift resulted.

Controlled potential electrolysis at various cathodes.—A controlled potential reduction of acetone in sulfuric acid was carried out at a reference potential of −1.375v, at various cathodes (mercury, lead, cadmium, zinc, aluminum, nickel, tin, copper) and was followed by the accurate determination of the products. The condition of electrolysis and its results are shown in Table II.

It was found that even when the reduction potential was the same, the types of products as well as the amounts differed substantially with the cathode used. For example, at mercury, 95% isopropanol, 3% pinacol, and 2% propane were obtained with a current efficiency of 73%. At lead, reduction occurred with a current efficiency of 86%, but the amount of isopropanol decreased to 68% while pinacol and propane increased to 7 and 25%, respectively. In these cases, aside from these reduction products, a small amount of organo-metallic compound which is considered to be reaction product of an intermediate and the cathode, was obtained. On the other hand, at cadmium, zinc, and aluminum cathodes, propane was the only product of electrolysis. At cadmium, reduction, for example, occurred with a current efficiency of 90% and formed 100% yield of propane. The current efficiency for propane formation *vs.* cathode potential is shown more clearly in Fig. 4.

Propane is formed at a potential more negative than −1.10v at a rapid rate and is accompanied by a slow evolution of hydrogen.

At nickel, tin, and copper, current efficiency was very much lower because of the low hydrogen overvoltage and film formation.

To obtain more insight into the mechanism of hydrocarbon formation, the electrolytic reduction of pinacol and 2-propanol was carried out at various cathodes under similar conditions and found to yield no propane.

Isolation of organo-metallic compounds and their decomposition.—The above results give no clue to the mechanism of the hydrocarbon formation and only indicate that a more negative electrode is necessary for the formation of hydrocarbon.

The observation that hydrocarbon formation was accompanied by pitting of the cathode suggested that the electrode had been attacked by a free radical.

This type of reaction was substantiated further by an interesting discovery during our experiments using mercury and lead cathodes. When the catholyte was allowed to stand after the electrolysis, there was a gradual formation of gas which turned out to be propane. Meanwhile, as previously reported (8), the above electrolyses produced also a small amount of oily substances which were considered to be organo-metallic compounds. Therefore, it seems to us that this propane might be formed as a result of the decomposition of the above-mentioned organo-metallic compounds.

To confirm this further, the catholyte containing the oily substance was taken out from the cell after the electrolysis and added to a saturated sodium chloride solution. The rate of decomposition and the composition of gas produced were then determined by gas buret and gas chromatography. The results are plotted in Fig. 5 and are listed in Table III.

As evident from the table, the oily substances seem to be the intermediate for propane formation.[4] Therefore, an attempt was made to isolate organo-metallic compounds and to clarify their properties. Although difficult, we succeeded in obtaining almost pure organo-mercury and organo-lead compound by careful procedure.

[4] An organo-metallic compound was postulated as an intermediate for the first time, by Schall and Kirst (9), in the electrolytic reduction of menthone to menthane.

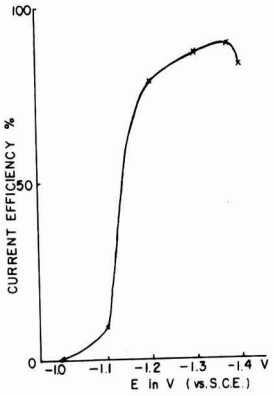

Fig. 4. Influence of cathode potential on current efficiency of propane formation at cadmium cathode.

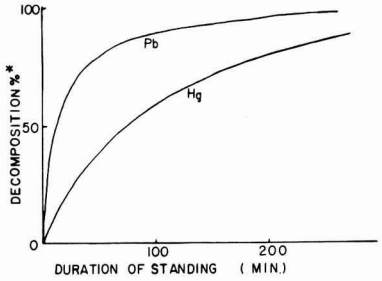

Fig. 5. Decomposition of organo-mercury and organo-lead compounds

* Decomposition % = (volume of gas evolved up to t min / total volume of gas evolved (final state)) x 100.

Table III. Decomposition of the oily substances in aqueous acidic medium

Proportion of gas produced, %	Hg cathode	Pb cathode
C_3H_8	91.5	93.5
C_3H_6	8.5	6.0
H_2	0.1	1.0

Isolation of organo-metallic compounds.—The separation and purification of the oily substances were carried out in the glass apparatus shown in Fig. 6. The crude oily substance collected on filter paper by filtration of the catholyte was dissolved in ether and the solution was quickly introduced to "reservoir A" with anhydrous potassium carbonate. The atmosphere in the system was then completely replaced by nitrogen. After standing for about 10 min in the dark, the solution was transferred into "container B" through a glass filter attached at the bottom of the glass pipe inserted in "A." Evaporation of ether in "B" was then carried out by bubbling nitrogen gas in the dark and gave a pure organo-metallic compound. The decomposition of this compound was also carried out in the same vessel "B."

The mercury compound thus obtained had properties (b.p. 118°C, 125mm Hg, $d_4^{20} = 2.125$, $n_D^{20} = 1.526$) which were identical with those of diisopropyl mercury (10). The infrared absorption spectrum of this compound pointed to the presence of only methyl and methane groups and excluded the presence of any oxygen groupings. These data confirmed the structure of the compound as diisopropyl mercury. This structure was further verified by the identification of its decomposition products. For the lead compound, the measurement of physical contents was difficult due to its instability in air. Its composition as diisopropyllead was clearly indicated from the results of the decomposition study.

Decomposition of organo-metallic compounds.—The decomposition of the mercury compound under the exposure of mercury lamp was carried out in a nitrogen atmosphere. The results are shown in Table IV.

The rate of decomposition of the lead compound seemed to be more rapid than that of the mercury compound. The results are shown in Table V. The products confirmed the structure as diisopropyl lead.

The results indicate that the organometallic compounds are the source of the propane in the electrolysis. Decomposition in the presence of 20% sulfuric acid is accelerated by light and gives practically a quantitative yield of propane and metallic ions.

The formation of propane and propylene under other conditions points to the formation of an isopropyl radical which undergoes disproportionation. This reaction apparently occurs to a slight extent in acidic medium.

The sensitivity of the organometallic compounds to light is in agreement with the work done on lead tetramethyl and mercury dimethyl by Leighton and Mortensen.

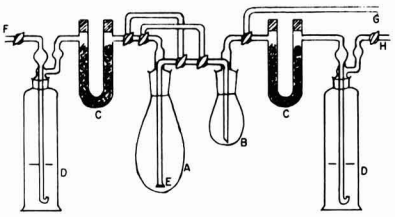

Fig. 6. Assemble glass work for purification and decomposition of organo-metallic compound: A, reservoir for crude sample; B, container of purified organo-metallic compound; C, calcium chloride for dehydration of nitrogen; D, pyrogallol alkali solution for deoxygenation of nitrogen; E, glass filter; F, gas inlet; G, to gas buret; H, gas outlet during evaporation of ether.

of hydrogen from the ether by an isopropyl radical with the formation of ethyl radicals.

Attempts to isolate an organocadmium compound in the electrolysis at a cadmium electrode, which produces a quantitative yield of propane, was not successful in agreement with the sensitivity of the compounds to acid.

In the absence of light this electrolysis gave large amounts of hydrogen and a current efficiency for propane formation of 37%. The results are shown in Table VI.

Table IV. Decomposition of organo-mercury compound in nitrogen atmosphere

	Organo-mercury compound	1.16 g	4.0 m mole*
Products	Propane	80.6 cc	3.6 m mole
	Propylene	73.3 cc	3.3 m mole
	Mercury	0.74 g	3.7 m mole

* As diisopropyl mercury.

Table V. Decomposition of organo-lead compound by light

			In N_2	In O_2	In C_6H_6	In 20% H_2SO_4	In ethyl ether
Organo-lead compound		mg	609	741	524	650	508
		m mole*	2.1	2.5	1.8	2.2	1.7
Gas produced	C_3H_8	cc	48.5	55.2	39.4	94.4	17.7
		m mole	2.2	2.5	1.8	4.2	0.8
	C_3H_6	cc	49.8	57.2	40.5	0	12.8
		m mole	2.2	2.6	1.8	0	0.6
	H_2	cc	4.5	11.2	9.0	0	0
		m mole	0.02	0.05	0.04	0	0
	C_2H_6	cc	0	0	0	0	29.8
		m mole	0	0	0	0	1.3
Residue	Total	mg	421	589	402	656	442
	Pb	mg	412	557	351	468	335
		m mole	2.0	2.7	1.7	2.3	1.6
		%**	97.7	94.6	87.3	71.3	75.6

* As diisopropyl lead.
** Pb % in residue.

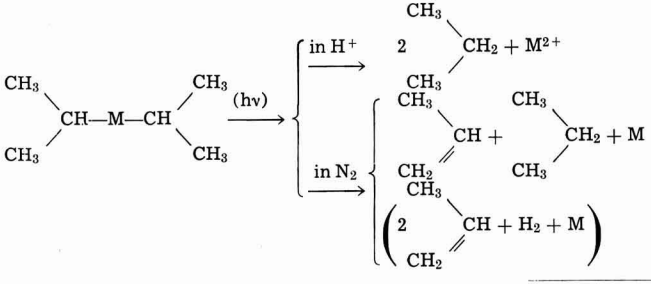

The formation of ethane in the decomposition of diisopropyl lead in ethyl ether points to the abstraction

Light had an appreciable effect also on the electrolysis at a mercury cathode. In the dark the current ef-

Table VI. Electrolysis at cadmium cathode. Effect of light

	Dark	Light
Catholyte acetone, g	82	82
20% H_2SO_4, cc	19	19
Cathode potential, v (*vs.* SCE)	−1.375	−1.375
Average current density, amp/dm²	1.9	6.1
Current consumed, amp-hr	3.3	3.4
Current efficiency, %	37	89
Products obtained		
Propane, cc	256	633
Hydrogen, cc	876	150

ficiency for the total reduction fell off to 55% or three quarters of that observed in the presence of light.

This is probably due to the slower decomposition in the dark of the intermediate organo-metallic compound.

Manuscript received Jan. 30, 1964; revised manuscript received Dec. 14, 1964. This paper was presented at the New York Meeting, Sept. 29-Oct. 3, 1963.

Any discussion of this paper will appear in a Discussion Section to be published in the December 1965 JOURNAL.

REFERENCES

1. J. Tafel and W. Schepps, *Z. Elektrochem.*, **17**, 972 (1911).
2. E. Muller, *ibid.*, **33**, 253 (1927).
3. S. Swann, Jr., *Bull.* Central Electrochem. Research Institute (India), **2**, 6 (1955).
4. K. Sugino, T. Sekine, and N. Sato, *Electrochem. Technology*, **1**, 112 (1963).
5. G. Schwarzenbach, "Die Komplexometrische Titration," Ferdinand Enke Publisher, Stuttgart (1956).
6. M. Shikata and I. Tachi, *Bull. Agr. Chem. Soc. Japan*, **4**, 91 (1928).
7. P. Zuman, *Nature*, **165**, 485 (1950).
8. J. Tafel, *Ber.*, **44**, 323 (1911).
9. C. Schall and W. Kirst, *Z. Elektrochem.*, **29**, 537 (1923).
10. M. Goret, *Bull. Sci. Pharmacol.*, **29**, 297 (1922); W. J. Jones, D. P. Evans, T. Gulwell, and D. C. Griffiths, *J. Chem. Soc.*, 45 (1935).
11. P. A. Leighton and R. A. Mortensen, *J. Am. Chem. Soc.*, **58**, 448 (1936).

Transpiration in an Open Tube GaAs/HI/H_2 System

G. Hellbardt

IBM Laboratories, Boeblingen, Germany

ABSTRACT

Etching rates and deposition rates have been measured in an open tube GaAs/HI/H_2 system for various iodine concentrations, flow rates, and temperatures between 500° and 850°C. Etching as well as deposition reactions are close to equilibrium at the surface of the solid GaAs. However, the amount of material of the vapor phase coming into contact with the solid is different in the two cases. At low flow rates the total flux through the tube takes part in the etching reaction whereas a certain fraction only takes part in the deposition reaction. It is suggested that different diffusion processes in the vapor phase cause this difference.

It has already been shown (1, 2) that etching rate measurements in open tube systems may yield results concerning the reaction mechanism.

Now the method of etching as well as deposition rate measurements has been applied to the system GaAs/HI/H_2. Whereas the thermodynamic data for the systems GaAs/H_2O/H_2 and GaAs/HCl/H_2 investigated in (2) had not been sufficiently and reliably known, in the system GaAs/HI/H_2 all the species in the gas phase and their mutual reactions are well known from thermodynamical equilibrium studies by Silvestri and Lyons (3) as well as by spectroscopic measurements by Richman (4). Furthermore, Leonhardt (5) calculated from these equilibrium data the partial pressures of all species in the vapor for a wide range of temperature. Thus we were able to compare immediately the results of our measurements with the equilibrium data. The question to be answered was how close to equilibrium the chemical reactions occur under the conditions of actual open tube vapor growth experiments.

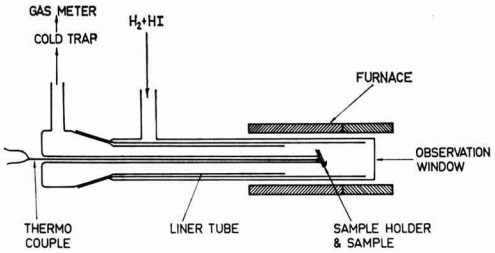

Fig. 1. Vapor etching apparatus

Experimental

Etching rate measurements.—The apparatus used in these experiments is shown in Fig. 1. Highly purified hydrogen is loaded with iodine in a U-tube filled with iodine and quartz granules and heated by a water bath to a temperature of $T_I = 50.3° \pm 0.1°C$. Additional experiments ascertained that the hydrogen/iodine mixture leaving the U-tube is saturated with iodine for all flow rates between 10 cm³/min and 500 cm³/min. The partial pressure of iodine which we found at the above mentioned temperature was $p_{I_2} = 2.01$ mm Hg. The H_2/I_2 mixture is then passed through a reaction chamber containing platinized quartz wool at 450°C approximately after which the vapor consists of $H_2 + HI$ only. This mixture is led into the double walled apparatus in which it is heated before it reacts with the GaAs sample. The reaction products leave the apparatus through a linear tube which is exchanged after each run and which prevents severe contamination of the reaction chamber.

All reaction products plus the unreacted HI are condensed in a liquid nitrogen cooled cold trap. The total volume of the pure H_2 leaving the cold trap is measured in a precision gas meter.

The face of the GaAs sample exposed to the vapor is the chemically polished (111) oriented Ga side.

Deposition rate measurements.—These experiments have been done in a simple connected tube apparatus (Fig. 2). In the first (lower) tube the seed is heated under the protection of pure H_2. In the meanwhile $H_2 + HI$ stream over the source basket containing polycrystalline GaAs as source material. As soon as

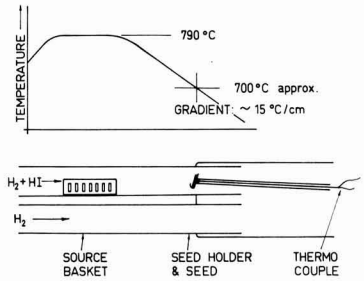

Fig. 2. Schematic sketch of the vapor deposition apparatus

the seed reaches the proper temperature it is pulled out of the lower tube and pushed into the upper one. The apparatus permits this operation to be done without opening a tube. Growth begins immediately.

The temperature profile which is the same in both tubes is such that the temperature in the source basket region is uniform within ±2°C, and the temperature gradient is constant in the vicinity of the seed. It is about 15°C/cm. Source temperature T_s and the temperature of the wafer T_w are measured by thermocouples during the run. Here, too, the exposed face of the sample is (111) oriented, Ga side.

Results

Etching rates.—Figure 3 contains all results of our etching rate experiments. The ratio of the total flux of gallium atoms in the vapor phase to the total flux of iodine atoms

$$y = \frac{n_{Ga}}{n_I} \qquad [A]$$

is plotted *vs.* the temperature of the wafer T_w. Since n_I is constant for a constant flow rate and n_{Ga} is proportional to the etching rate (cf. Eq. [1]) y itself is proportional to the weight loss per unit of time w/t in etching rate experiments. The full lines represent the theoretical values of y calculated by Leonhardt (5). The parameter is

$$\frac{P_I}{P_{tot}} = \frac{2 \times \text{partial pressure of iodine}}{\text{total pressure}} \qquad [B]$$

as measured in the iodine generator. P_{tot} used in that calculation is $P_{tot} = 1$ atm $= 735$ mm Hg, whereas we have a total (atmospheric) pressure of 720 mm Hg. We neglected this difference of 2% and calculated

$$\frac{P_I}{P_{tot}} = \frac{2 \times 2.01}{720} = 0.0056$$

This is between the values of $P_I/P_{tot} = 0.0025$ and 0.0125 available from the data of Leonhardt.

Most of the points are below the two curves. Apparently this is due to an effect of flow rate. Figure 4 shows this effect for two temperatures $T_w = 650$°C and $T_w = 800$°C; y decreases with increasing flow rate.

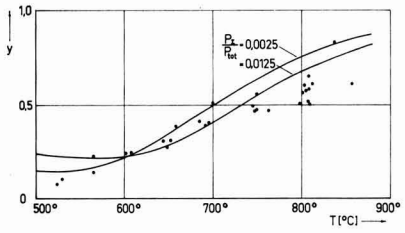

Fig. 3. Ratio of the total amount of gallium in the vapor phase to the total amount of iodine in etching experiments.

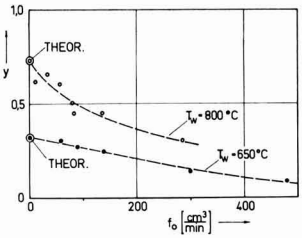

Fig. 4. Dependence of the etching rate on flow rate

The flow rate on the abscissa is in standard cm³/min. The linear velocity at $f_o = 100$ cm³/min and $T_w = 800$°C is $v = 138$ cm/min.

The theoretical values plotted at zero flow rates have been found by interpolation from the two theoretical curves in Fig. 3. Two lines can be drawn from these values through the experimental points of $T_w = 800$°C and 650°C, respectively. It appears that there is a dependence of the etching rate on the flow rate, but that for low flow rates the etching rates approach the equilibrium values.

Deposition rates.—For two different iodine concentrations corresponding to two different iodine generator temperatures T_I deposition experiments have been made. The iodine vapor pressures as determined in separate experiments were

$$T_I = 50.3, \; P_{I_2} = 2.01 \text{ mm Hg}$$

$$T_I = 60.3, \; P_{I_2} = 3.94 \text{ mm Hg}$$

The experimental deposition rates have been calculated from

$$g_{exp} = \frac{\Delta w}{M \cdot t \cdot A_w} \qquad [C]$$

where Δw, gain in weight of the wafer; M, molecular weight of GaAs; t, duration of the run; and A_w, area of the wafer.

The drawn curves (Fig. 5) represent values calculated according to

$$g_{calc.} = n_I[y_{T_s} - y_{T_w}]/A_T \qquad [D]$$

where n_I is the number of moles of iodine flowing through every cross section of the apparatus per unit of time, T_s the source temperature, T_w the wafer (seed)

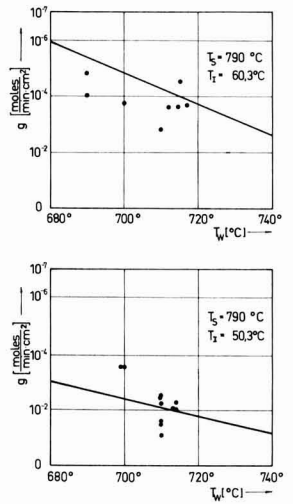

Fig. 5. Deposition rates for two different iodine concentrations

temperature, and A_T the area of the reaction tube. n_I can be calculated from the partial pressure of iodine in the iodine source and the flow rate.

For $T_I = 50.3°C$ with $P_I/P_{tot} = 0.0056$ $y_{theor.}$ has been taken from the curve of $P_I/P_{tot} = 0.0025$, while for $T_I = 60.3°C$ and $P_I/P_{tot} = 0.011$ the values have been taken from the curve of $P_I/P_{tot} = 0.0125$. In view of the scatter of the experimental points no serious error should be introduced by this approximation. The experimental points are scattered around the theoretical curves.

Discussion

Two diffusion effects have to be considered in etching rate experiments.

The first one has already been discussed in principle by Wagner and Stein (6) and others. If there is a concentration gradient along the axis of transportation, transport of the considered species will take place not only by linear flow but by diffusion also.

To calculate the magnitude of this effect in our etching rate experiments we assume the reaction

$$GaAs_s + HI_g \rightleftarrows GaI_g + \frac{1}{2}H_{2g} + \frac{1}{4}As_{4g} \qquad [1]$$

to take place.

Neglecting the partial pressure of GaI_3 is at least justified at 800°C. The mass action equation is

$$K = \frac{P_{GaI} \cdot P^{1/2}{}_{H_2} \cdot P^{1/4}{}_{As_4}}{P_{HI}} \qquad [2]$$

Furthermore, we write down an equation expressing the conservation of iodine during this reaction. HI enters the system at a partial pressure $P^1{}_{HI}$. Behind the GaAs the partial pressure of HI is constant and equal to $P^o{}_{HI}$. Consequently, no diffusion effects enhancing the transport of HI take place behind the GaAs. The amount of HI used up in the formation of GaI is given by

$$F = \frac{w \cdot q}{RT}(P^1{}_{HI} - P^o{}_{HI}) \qquad [3]$$

The flow F' of GaI from the GaAs is

$$F' = \frac{q}{RT}\left[-D\frac{dP_{GaI}}{dx} + wP_{GaI}\right] \qquad [4]$$

with D the diffusion constant of GaI in H_2, q the cross section area of the tube, x the coordinate parallel to the axis of the tube, and w the linear velocity of flow.

Under the conditions of steady state $F = \text{const}$ and $P_{GaI} = P^o{}_{GaI}$ at $x = 0$, *i.e.*, at the site of the GaAs, and $P_{GaI} = 0$ at a distance L behind the GaAs, Eq. [4] yields an expression for P_{GaI} as has been shown by Wagner and Stein (6).

$$P_{GaI} = \frac{P^o{}_{GaI}}{1 - \exp -\frac{w}{D}L}\left(1 - \exp -\frac{w}{D}(L - x)\right) \qquad [5]$$

$F = F'$ means the conservation of iodine and yields

$$P^1{}_{HI} - P^o{}_{HI} = P^o{}_{GaI}\frac{1}{1 - \exp -\frac{w}{D}L} = P^o{}_{GaI} \cdot \alpha \qquad [6]$$

With $P_{H_2} \approx \text{const} \approx 1$ atm and

$$P_{GaI} = 4P_{As4}$$

we get from [2] at $x = 0$

$$\frac{P^{o\,5/4}{}_{GaI}}{P^o{}_{HI}} = \frac{K}{0.707} = K' \qquad [7]$$

From [6] and [7] we arrive at

$$P^{o\,5/4}{}_{GaI} + K'\,\alpha\,P^o{}_{GaI} - K'\,P^1{}_{HI} = 0 \qquad [8]$$

The value of α is 1 with no diffusion going on. If α is varied by $d\alpha$ $P^o{}_{GaI}$ is varied by dP.

We then get

$$\frac{F + dF}{F} = \left(1 + \frac{dP}{P^o{}_{GaI}}\right)\left(1 + \frac{d\alpha}{\alpha}\right) \qquad [9]$$

From [8] we obtain

$$\frac{dP}{P^o{}_{GaI}} = -\frac{1}{1 + 5P^{o\,1/4}{}_{GaI}/4K'}d\alpha \qquad [10]$$

With $T = 800°C$, $D = 1$ cm²/sec,[1] $f_o = 20$ cc/min, $q = 3$ cm², $L = 10$ cm, $d\alpha$ becomes $d\alpha = 0.01$. Since it is $P^o{}_{GaI} = 0.0019$ atm and $K = 0.45$ at 800°C (5) we get

$$\frac{dP}{P^o{}_{GaI}} = -0.007$$

The change in transport rate is

$$\frac{dF}{F} = 0.003$$

At lower temperatures w/D becomes larger, since it is $w \sim T$ and $D \sim T^{3/2}$, so that diffusion effects become still less important. Consequently, the partial pressures of GaI and GaI_3 are still less changed by diffusion drain from the GaAs source.

The second diffusion effect concerns the transport of reactants from the gas stream to the surface of the GaAs. The etched or grown surfaces on the wafer very often show striations not necessarily crystal oriented which can be explained as sort of flow patterns. These could not exist if the flow in the neighborhood of the wafer were turbulent. If, however, the flow is laminar, we must assume that a diffusion process is responsible for the mass transport from the vapor to the surface of the solid GaAs. Due to this effect the etching rate should decrease as the quantity w/D increases.

A quantitative model should be able to explain Fig. 4. It should also give different magnitudes of this diffusion effect at the source and at the seed because of the different numbers and types of species diffusing to and from the surface of the GaAs. However, we have not pursued this idea to a point where we can give quantitative answers.

Since the first diffusion effect has been shown to be negligible at least at flow rates above 20 cc/min, Fig. 4 means that the concentrations approach the equilibrium values in the vicinity of the solid GaAs with decreasing flow rates. In other words, almost all of the material passing the solid GaAs in our system reacts with the GaAs to equilibrium at 20 cc/min. We therefore assume that at higher flow rates there is also equilibrium at the surface of the solid. However, not all of the material in the gas phase can get to that surface in time before it passes by. This causes a decrease in the etching rate.

A similar thing happens at the seed. Since the same reactions take place at the source and at the seed, and the temperature region is about the same, we have no reason to assume that there is no equilibrium at the surface of the solid GaAs seed. However, the diffusion of material to and from the seed can be different as explained above. Therefore, the ratio of the amount of material reacting with the GaAs to the amount of material passing by unreacted is different.

Comparison of Eq. [C] and [D] shows that in calculating the experimental g values we referred to the wafer area whereas we calculated the theoretical values referring to the cross-sectional area of the tube.

[1] This diffusion constant has been assumed to be valid at 800°C for this estimate of the diffusion effect. Assuming the $T^{3/2}$ dependence on temperature this corresponds to a value of 0.13 cm²/sec at 0°C, which is about right if one compares it with the diffusion constant of metals in H_2 (7) One has to take into account that the molecule of GaI is larger than the metal atoms, *e.g.*, Hg.

Since we used a relatively large amount of polycrystalline GaAs as source we are sure from our etching rate experiments that we are in equilibrium there. Then the coincidence of the theoretical and experimental values (Fig. 5) actually means that the ratio as quoted above is equal to the ratio $A_W:A_T$ and that very little diffusion transport takes place.

Conclusions

Etching rate as well as deposition rate measurements in the GaAs/HI/H_2 open tube system showed that chemical reactions in vapor growth experiments go on close to equilibrium at the surface of the solid GaAs in the source region as well as in the seed region. However, the amount of material from the vapor which comes into contact with the solid depends on linear flow velocities. It is much higher in the source region than at the seed.

With the results of these experiments it is possible to predict deposition rates and efficiencies of vapor growth experiments in the open tube GaAs/HI/H_2 system. However, for a better understanding of the different kinetics at the source and the seed it is highly desirable to know more about the diffusion processes taking part in open tube experiments.

Acknowledgments

The author wishes to express his appreciation of the stimulating discussion with W. Kappallo and M. Michelitsch as well as his thanks to H. Leonhardt for furnishing the tabulated results of his calculations and for permission to publish these. The help of Miss G. Fritsche and Mr. M. Schlack in the experiments is gratefully acknowledged.

Manuscript received Mar. 2, 1964; revised manuscript received Nov. 27, 1964.

Any discussion of this paper will appear in a Discussion Section to be published in the December 1965 JOURNAL.

REFERENCES

1. R. R. Fergusson and T. Gabor, *This Journal*, **111**, 585 (1964).
2. M. Michelitsch, W. Kappallo, and G. Hellbardt, *ibid.*, **111**, 1248 (1964).
3. V. J. Silvestri and V. J. Lyons, *ibid.*, **109**, 963 (1962).
4. D. Richman, *RCA Rev.*, **24**, 596 (1963).
5. H. Leonhardt, IBM Research Report, RC-997, June 1963.
6. C. Wagner and V. Stein, *Z. Phys. Chem.*, **192**, 129 (1943).
7. W. Jost, "Diffusion," p. 413, Academic Press, New York (1960).

The Thermodynamic Properties of Dilute Solutions of Oxygen in the Liquid Binary Cu-Ni Alloys

E. S. Tankins, J. F. Erthal, and M. K. Thomas, Jr.

Naval Air Engineering Center, Aeronautical Materials Laboratory, Philadelphia, Pennsylvania

ABSTRACT

Thermodynamic properties of dilute solutions of oxygen in the Cu-Ni systems have been studied by means of the hydrogen-water vapor equilibrium The following reaction

$$H_2\ (g) + [O]_{soln} = H_2O\ (g)$$

was studied for which an equilibrium ratio can be written

$$K = \frac{P_{H_2O}}{P_{H_2}[a/o\ O]} \qquad [1]$$

where P_{H_2O} and P_{H_2} are the partial pressures of water vapor and hydrogen and [a/o O] is the amount of dissolved oxygen in atomic per cent. The equilibrium reaction [1] has been investigated over a wide temperature range and also for various composition ranges. Equations are presented which show the variation of the equilibrium constant [1] as a function of composition and temperature. Equations are also presented which show the variation of the standard free energy of solution of oxygen as a function of temperature for various compositions. Evidence is presented which shows Henry's law is obeyed by oxygen within experimental error over a substantial composition range.

The copper nickel system forms a series of very important commercial alloys. Pure nickel and pure copper are resistant to oxidation. The Cu-Ni equilibrium diagram (1) shows only one solid solution and the only solid-state change is the magnetic change in the high nickel end of the diagram.

Data on the reaction between liquid metal and gases are of great practical importance to the process metallurgist as well as to the theoretical metallurgist who is trying to develop a dilute solution theory to make predictions of properties of the various multicomponent systems.

Alcock and Richardson (2, 3) have discussed the dilute solutions of molten liquids and alloys. They applied the quasi-chemical model with some success to the Cu-Ni-S system. Recently, Oriani and Alcock (4) reviewed some simple models of solution.

The object of this investigation was to determine equilibria in the following reaction from 1400° to 1600°C at the high nickel end

$$H_2\ (g) + [O]_{soln} = H_2O\ (g)$$

$$K = \frac{P_{H_2O}}{P_{H_2}[a/o\ O]} \qquad [1]$$

where P_{H_2O} and P_{H_2} are the partial pressures of water vapor and hydrogen and [a/o O] is the amount of dissolved oxygen in atomic per cent.

Experimental Procedures

Materials.—The metals used in the investigation in the equilibrium apparatus were high-purity Mond Nickel Pellets and Spectrographic Purity Copper. There was no detectable nitrogen and the initial oxygen contents were less than 0.0050 weight per cent (w/o).

Two high-purity argon-hydrogen mixtures were used with hydrogen contents of 1.02 and 0.20 in volume per cent (v/o). Further purification of the gas mixtures was effected by passing them through magnesium chips held at 630°C in a stainless steel tube furnace.

Equilibrium apparatus.—The purified hydrogen-argon mixture was led via a capillary type flow meter through a water presaturator to a condenser system submerged in a thermostatically controlled water bath. The resulting gas mixture was led through heated glass tubing to a vertical resistance heated, equilibrium furnace. Within the equilibrium furnace, the gas mixture was led through a ⅛ in. bore alumina inlet tube to the surface of the melt which was held in a pure alumina crucible, ¾ in. in diameter and 2 in. high. The pedestal which supported the crucible allowed the surface of the melt to touch the alumina inlet tube. A detailed description of the apparatus and associated electrical system has been published elsewhere (5, 6).

The temperature in the uniform temperature zone of the furnace was measured principally by a L&N Optical Pyrometer sighted through an optical flat onto the crucible pedestal. A Pt-Pt-10% Rh thermocouple was inserted from time to time into the alumina tube which supported the crucible pedestal; this served as a means of calibrating the optical pyrometer and as a double check on the temperature.

The water bath temperature was controlled by means of a mercury thermostat to better than ±0.1°C, the temperature being measured on a calibrated mercury thermometer which could be read to 0.1°C.

Analysis.—The samples were prepared for oxygen analysis by splitting the entire solidified ingot, usually vertically, with a hack-saw and then grinding at least 1/32 in. off the outside. If there were any blow holes in the sample, they were carefully ground out to ensure that any oxide which might have been formed during the quenching operation was removed and to make certain that no abrasive materials were trapped. Only the high copper alloys exhibited such blow holes. The samples were numbered, degreased, weighed, and kept in a dessicator until analyzed. Care was taken to avoid manual contact with the samples once they had been cleaned.

The oxygen analysis was by an improved vacuum fusion method which has recently been described (7). The major alloying elements were not determined since previous analysis of other alloy systems indicate that the desired composition was very close to the actual.

Procedure.—The apparatus was prepared for an experiment by replacing the alumina inlet tube, cleaning the sight window, adjusting the thermostat temperature, setting the furnace in the desired temperature range, and starting the gas flow in order to purge the system. The presaturator was adjusted until excess water precipitated in the condenser at the rate of a few cubic centimeters per hour. A pure alumina crucible was charged with a 10g heat and placed on the crucible pedestal in the bottom of the furnace tube. The pedestal was then slowly raised until the crucible was in the constant temperature zone of the furnace. When the charge had melted, the pedestal was further raised until the inlet tube was just touching the surface of the melt and a back pressure of 1-4 cm was indicated on a small water manometer placed in the gas train. The pedestal support tube was then clamped in position.

The in-flow pressure of water corresponding to the temperature of the saturator was taken from the published tables (8), and the P_{H_2O}/P_{H_2} ratio derived in the usual manner from the composition of the in-going hydrogen-argon gas mixture, with the necessary corrections for barometric pressure and the small back pressure within the apparatus. No fugacity corrections were made, as it was considered that these were too small to be significant within the experimental error.

Results and Discussion

The reactions investigated in this work may be represented by

$$H_2\,(g) + O\,[\text{in Ni-Cu}] = H_2O\,(g)$$

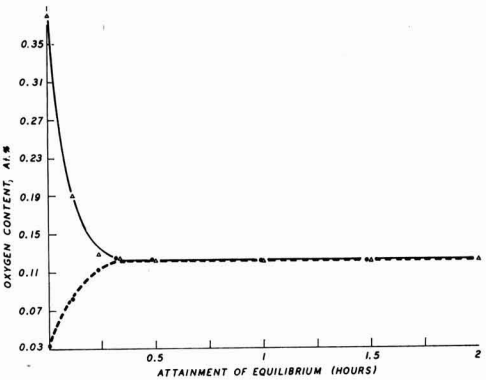

Fig. 1. Attainment of equilibrium for a 50Cu-50Ni alloy with a fixed gas composition, 1550°C: △ ——, initial oxygen 0.3800 a/o; ● - - - -, initial oxygen 0.0305 a/o.

$$K = \frac{P_{H_2O}}{P_{H_2}[\text{a/o O}]} \qquad [2]$$

where K is the equilibrium constant. The experimental results and their discussion are presented in the ensuing sections.

Attainment of equilibrium.—The attainment of equilibrium for a 50Cu-50Ni alloy with a fixed gas composition is shown in Fig. 1. The results show that in all cases except in the top line corresponding to a high oxygen content, equilibrium was reached in less than 30 min. The higher oxygen contents reached equilibrium in 30 min. The initial points on the curve probably are not as accurate because the control of temperature at the beginning is not as close as later on during each experiment. The results are also tabulated in Table I.

The melts were held at temperature with a gas flow rate of approximately 120 cc/min for at least 40 min. Earlier work on the pure metals (6) had shown equilibrium was attained in 20 min for this particular arrangement. It was assumed that copper behaved similarly to nickel, but as a further check, several duplicate runs were carried out for longer times for an alloy at the higher copper end. There was no significant change in oxygen content.

Equilibrium results for 1550°C.—In order for the derived value of K to be meaningful, either the dissolved oxygen must obey Henry's law, or a suitable extrapolation to the infinitely dilute solution must be made. It has been shown in earlier work (6) that oxygen obeys Henry's law over a substantial composi-

Table I. Experimental results obtained for a series of 50Cu-50Ni alloy at 1550°C from the attainment of equilibrium studies

Heat No.	Time	P_{H_2O}/P_{H_2}	Oxygen, a/o
	From high end Initial oxygen 0.3800 a/o		
E-1a	7 min	4.26085	0.1906
E-2a	14 min	4.26202	0.1296
E-3a	20 min	4.25417	0.1258
E-4a	30 min	4.25853	0.1220
E-5a	45 min	4.25620	0.1222
E-6a	1 hr	4.26202	0.1220
E-7a	1½ hr	4.25301	0.1216
E-8a	2 hr	4.25417	0.1220
	From low end Initial oxygen 0.0305 a/o		
E-1b	7 min	4.26085	0.084
E-2b	14 min	4.26202	0.1144
E-3b	20 min	4.25504	0.1216
E-4b	30 min	4.25853	0.1220
E-5b	45 min	4.25736	0.1220
E-6b	1 hr	4.26202	0.1224
E-7b	1½ hr	4.25301	0.1224
E-8b	2 hr	4.27311	0.1220

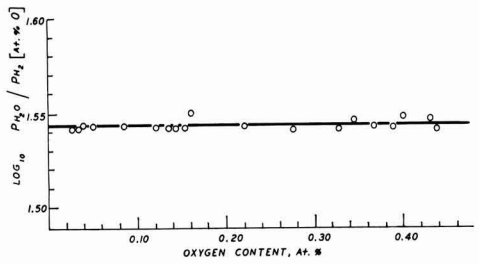

Fig. 2. Variation of the equilibrium constant $K = P_{H_2O}/P_{H_2}$ [a/o O] with oxygen content for a 50Cu-50Ni alloy at 1550°C.

tion range for pure Fe, Co, and Ni at 1550°C. Table II and Fig. 2 show the experimental results over a wide range of oxygen contents in the 50Cu-50Ni binary alloy at 1550°C. The independence of the equilibrium constant relative to the oxygen content is shown in Fig. 2. All the additional experimental runs were carried out at the lower oxygen content to insure compatability with Henry's law. A comprehensive discussion of possible discrepancies in Henry's law has been made (6).

Equilibrium results for various temperatures.—The results for various compositions of the nickel-copper alloy system are shown in Table III. The results can be represented in the usual form $\log_{10}K$ *vs.* $1/T$.

Experimental results were obtained with a computator for the least mean square calculation. Probable errors in the slopes and intercepts of the derived straight lines were calculated by the methods of Birge (9). The resulting equation for $\log_{10}K$ with probable error, are listed in Table IV.

The standard energy change for the reaction

$$H_2\,(g) + \tfrac{1}{2}\,O_2\,(g) = H_2O\,(g) \qquad [3]$$

was taken as

$$F^\circ = -59{,}905 + 13.78T \qquad [4]$$

The straight line equations for $\log_{10}K$ were converted to standard free energy equations for reaction [2] by application of the relationship

$$F^\circ = -RT \log K \qquad [5]$$

The derived equations were subtracted from Eq. [4] to yield a series of equations representing the standard free energy change, $F^\circ\%\text{-}F^\circ$ for the reaction

$$\tfrac{1}{2}\,O_2\,(\text{gas}) = [O]\ \text{soln} \qquad [6]$$

Table IV lists the derived equations; no account was taken of possible error in Eq. [4] in the listed probable errors.

The free energy of solution for the three are very close to 22 kcal at 1550°C. This means that the maximum solubility of oxygen is probably about the same in this range of alloys. The activity coefficient of oxygen due to the presence of copper in the nickel matrix is relatively constant over the 20-60% range.

Table II. Experimental results obtained for the 50Cu-50Ni alloy at 1550°C over a range of oxygen contents

Heat No.	P_{H_2O}/P_{H_2}	Oxygen, a/o	K
H-1	0.98193	0.0282	34.820
H-2	1.20632	0.0347	34.764
H-3	1.38020	0.0395	34.942
H-4	1.79659	0.0514	34.953
H-5	2.98374	0.0853	34.979
H-6	4.82476	0.1384	34.861
H-7	4.25853	0.1220	34.905
H-8	5.07400	0.1453	34.921
H-9	5.42943	0.1552	34.983
H-10	5.68682	0.1600	35.542
H-11	7.69338	0.2203	34.922
H-12	9.66969	0.2780	34.783
H-13	11.61103	0.3336	34.805
H-14	12.12911	0.3439	35.269
H-15	12.83537	0.3668	34.993
H-16	13.58081	0.3889	34.921
H-17	14.37024	0.4004	35.889
H-18	15.19531	0.4373	34.748
H-19	15.2053	0.4308	35.295

Table III. Experimental results obtained for binary alloys over a temperature range

Heat No.	Temp, °C	P_{H_2O}/P_{H_2}	Oxygen a/o	K
		80 Ni-20 Cu		
1-1	1410	6.46758	0.0570	113.466
1-2	1415	6.46758	0.0599	107.993
1-3	1420	7.07798	0.0666	106.276
1-4	1425	6.46939	0.0644	100.456
1-5	1435	6.63425	0.0714	92.917
1-6	1440	5.68843	0.0643	88.467
1-7	1450	7.07798	0.0864	81.921
1-8	1450	5.06305	0.0640	79.110
1-9	1475	5.68682	0.0851	66.825
1-10	1485	6.63044	0.1065	62.258
1-11	1490	4.26660	0.0718	59.423
1-12	1500	5.06445	0.0912	55.531
1-13	1500	4.66678	0.0830	56.226
1-14	1510	5.68361	0.1113	51.066
1-15	1525	6.61144	0.1440	45.913
1-16	1535	6.60955	0.1549	42.870
1-17	1545	4.05973	0.1020	39.801
1-18	1550	5.68361	0.1512	37.590
1-19	1550	3.31161	0.0872	37.977
1-20	1550	5.07117	0.1337	37.930
1-21	1550	4.26718	0.1119	38.117
1-22	1555	3.30873	0.0908	36.440
1-23	1575	3.30873	0.1061	31.185
1-24	1590	2.34268	0.0819	28.604
1-25	1600	2.34331	0.0875	26.781
1-26	1610	2.34208	0.0938	24.969
1-27	1620	2.34108	0.1001	23.387
		60 Ni-40 Cu		
2.1	1380	6.64285	0.0510	130.252
2.2	1390	6.47030	0.0522	123.952
2-3	1400	6.46939	0.0564	114.704
2-4	1410	6.46934	0.0620	104.345
2-5	1420	7.07798	0.0749	94.499
2-6	1435	6.63998	0.0796	83.225
2-7	1450	3.79099	0.0507	74.773
2-8	1460	3.79487	0.0549	69.123
2-9	1475	5.68682	0.0927	61.346
2-10	1485	6.62473	0.1178	56.237
2-11	1490	6.07420	0.1112	54.624
2-12	1490	5.05786	0.0927	54.561
2-13	1495	4.64765	0.0889	52.279
2-14	1500	3.80195	0.0753	50.491
2-15	1505	5.06445	0.1071	47.287
2-16	1510	5.68763	0.1226	46.392
2-17	1510	5.68763	0.1226	46.392
2-18	1515	4.05754	0.0908	44.687
2-19	1535	6.62093	0.1690	39.177
2-20	1550	5.68521	0.1632	34.836
2-21	1550	4.26718	0.1222	34.919
2-22	1550	3.83149	0.1100	34.832
2-23	1550	4.82210	0.1381	34.917
2-24	1575	3.82622	0.1309	29.230
2-25	1590	2.34108	0.0889	26.334
2-26	1600	2.34108	0.0953	24.565
2-27	1610	2.34012	0.1021	22.920
2-28	1620	2.33821	0.1090	21.451
		40 Ni-60 Cu		
3-16	1500	3.80716	0.0731	52.082
3-17	1500	6.07420	0.1165	52.134
3-18	1500	5.05849	0.0961	52.638
3-24	1550	4.82210	0.1342	35.932
3-25	1550	5.68843	0.1589	35.799
3-26	1550	6.07420	0.1692	35.899
3-27	1550	4.26718	0.1188	35.919

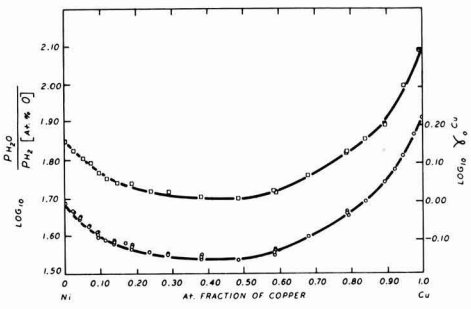

Fig. 3. Variation of the equilibrium constant $K = P_{H_2O}/P_{H_2}$ [a/a O] and the activity coefficient of oxygen with composition in the Ni-Cu alloys at 1550° (□—□—□—) and 1500°C (○—○—○—).

Table IV. Equations representing equilibrium constant and standard free energy of solution as a function of temperature

Copper w/o	$\log_{10} k$	F° $\frac{1}{2}O_2$ (g) = O soln.
20	$\frac{10{,}439\ (\pm 29)}{T} - 4.146\ (\pm 0.0165)$	$-12{,}136\ (\pm 133) - 5.192\ (\pm 0.076)T$
40	$\frac{10{,}355\ (\pm 25)}{T} - 4.138\ (\pm 0.0142)$	$-12{,}521\ (\pm 116) - 5.155\ (\pm 0.065)T$

From the consideration of the maximum uncertainties in the temperature, water ratio and oxygen analysis, one of the authors earlier suggested (6) a maximum probable error of about ±5% on the derived value of K; in general, the experimental scatter reported in this paper is consistent with this view. Analyses of many alloys in previous work for various binary alloys chosen at random showed no significant deviation in metal content (0.3%) from the stated compositions; this was ignored in considering the probable errors. The probable errors listed in Table IV suggest that the maximum probable error in the standard enthalpies of solution is of the order of 1 kcal.

Equilibrium results for binary alloys at 1550° and 1500°C.—Additional equilibrium runs are tabulated in Table V and are shown plotted in Fig. 3 for 1500° and 1550°C. There are additional runs above 60 w/o (weight per cent) Cu in order to see how the curve goes; however, the emphasis is being placed on the high nickel end of the system.

The copper-nickel system is a unique series. These alloys form a face-centered cubic lattice. The copper atom contains one more electron than the nickel atom, and to a first approximation, if a nickel atom is replaced by a copper atom in the alloy, the lattice is unaltered except that an electron is added which will raise the surface of the Fermi distribution and the lattice parameters show only slight changes.

Table V. Summary of additional data obtained for binary alloy at 1500° and 1550°C

Heat No.	Cu w/o	P_{H_2O}/P_{H_2}	Oxygen a/o	K
		Ni-Cu alloy at 1500°C		
4-1	2.50	6.07429	0.08955	67.831
4-2	5.00	6.07261	0.0940	64.602
4-3	7.50	6.06923	0.0983	61.742
4-4	10.0	6.06586	0.1034	58.664
4-5	12.0	6.06502	0.1078	56.262
4-6	13.0	6.06249	0.1091	55.568
4-7	15.0	6.12776	0.1115	54.957
4-8	25.0	6.06670	0.1169	51.896
4-9	30.0	6.12776	0.1195	51.278
4-10	50.0	6.12690	0.1222	50.138
4-11	50.0	7.06467	0.1410	50.104
4-12	70.0	6.12776	0.1064	57.592
4-13	80.0	6.07336	0.0918	66.159
4-14	80.0	3.81623	0.0578	66.025
4-15	85.0	6.06502	0.0857	70.770
4-16	90.0	6.12776	0.0780	78.561
4-17	90.0	4.64895	0.0591	78.662
4-18	95.0	6.12690	0.0688	89.054
4-19	95.0	5.06169	0.0566	89.429
4-20	100	6.07029	0.0505	120.204
		Ni-Cu alloys at 1550°C		
5-1	2.50	5.67478	0.1227	46.249
5-2	2.50	4.27815	0.09127	46.873
5-3	5.00	5.6738	0.1241	45.719
5-4	5.00	5.06536	0.1178	42.999
5-5	5.00	4.27698	0.0960	44.552
5-6	7.50	5.67798	0.1354	41.935
5-7	7.50	4.27229	0.1004	42.553
5-8	10.0	5.67959	0.1419	40.025
5-9	10.0	5.06978	0.1235	41.051
5-10	10.0	4.07144	0.0991	41.084
5-11	10.0	4.27464	0.1064	40.175
5-12	12.0	4.24863	0.1095	38.803
5-13	13.0	4.27054	0.1113	38.369
5-14	15.0	4.26704	0.1115	38.269
5-15	15.0	5.68843	0.1484	38.332
5-16	15.0	5.07119	0.1332	38.072
5-17	18.0	4.26470	0.1119	38.111
5-18	25.0	5.07259	0.1383	36.678
5-19	30.0	5.68361	0.1575	36.086
5-20	30.0	5.07259	0.1408	36.027
5-21	70.0	5.68412	0.1434	39.638
5-22	80.0	4.25612	0.0935	45.520
5-23	80.0	5.39536	0.1183	45.607
5-24	80.0	6.07958	0.1334	45.574
5-25	80.0	4.82210	0.1058	45.577
5-26	85.0	3.28285	0.0674	48.707
5-27	85.0	5.07330	0.1030	49.255
5-28	90.0	5.69005	0.1035	54.976
5-29	92.50	5.68412	0.0949	59.896
5-30	95.50	3.28728	0.0506	64.966
5-31	97.50	3.28728	0.0448	73.377
5-32	100	6.07113	0.0740	82.042

The equilibrium constant for the pure nickel is from an earlier publication (6). Two runs were made with pure copper to see how the results compare with Girardi and Siebert (10) and Sano and Sakao (11). The results are somewhat lower than those of Siebert or Sakao's; however, they are sufficient to show the trend of the curve. There is no explanation at present for the discrepancy, and an intensive investigation on pure copper is forthcoming in the near future.

Figure 3 shows the change in the activity coefficient of oxygen at the high nickel end, and then a constant range and at 0.6 copper the activity coefficient of oxygen changes. This behavior is very similar to what Alcock and Richardson (2) noted for the Cu-Ni-S system. It is interesting to note that at the corresponding composition in the solid state the alloy changes in magnetic properties.

Alcock and Richardson (2) discuss the work of Himmler (12) on the electronic effects and applied their results on the dissolved sulfur in various alloys to the model. Himmler assumed that the chemical potential of the free electrons increased as the ratio of the free electrons to atom ratio in the alloy increased. There was an excellent correlation for the chemical potential of hydrogen; however, Alcock and Richardson's work with sulfur in the several alloy systems showed that the behavior of sulfur could not be explained solely in terms of the electron to atom ratio. The electronic effect may have some effect on the dissolved oxygen and may be important, but at present there is insufficient data to make any correlation and to separate the electronic effects from other effects. The quasi-chemical model as described in great detail by Alcock and Richardson (3) was applied to the present work. The model gives the proper sign and shape to the curve for the activity coefficient of oxygen. To apply the equations that Alcock and Richardson derived (3), accurate data are needed for the activities of copper and nickel in the Cu-Ni alloy system. If one assumes Raoult's law to hold over the entire composition range for the Cu-Ni system, then the calculated values for the activity coefficient of oxygen is greater than the experimental results plotted in Fig. 3. It is interesting to note that, if one considers that the copper-nickel system exhibits positive deviation from Raoult's law, then the calculated results for the activity coefficient for oxygen will be in closer agreement with the experimental results.

Since the phase diagrams of the Cu-Ni system show an almost ideal solid solution alloy, one would suspect that Raoult's law for the liquid state would be obeyed and that the activity coefficient would be unity or close to unity. The conclusion to be drawn is that the free energy of solution would be a linear function of alloying addition for the dissolved oxygen. Figure 3 shows that this is not the case. The excess free energy of solution of dissolved oxygen is a function of the equilibrium constant. The value of $\log_{10}K$ decreases with the addition of Cu to the nickel matrix, and after reaching a minimum value remains almost constant over a wide range of composition. At the high copper end, there is a rapid increase in $\log_{10}K$ which has been observed in other binary systems. At the present time, there is no theoretical explanation for this behavior.

Activity and interaction parameter studies.—It is convenient to use a reference state which can be defined for the infinitely dilute solution of oxygen in nickel, where $a_o = 1$. The oxygen activities in the Cu-Ni alloys, therefore, are based on an activity relative to that in pure nickel.

The equilibrium for the reaction studied may be rewritten in the form

$$K_1 = \frac{P_{H_2O}}{P_{H_2}} \cdot \frac{1}{N_o{}^a \gamma_o{}^a} \qquad [7]$$

where $N_o{}^a$ is the mole fraction of oxygen in the alloy and $\gamma_o{}^a$ is the activity coefficient of oxygen in the alloy. By taking logarithms of Eq. [7] and rearranging the following expression is obtained

$$\log \gamma_o{}^a + \log K_1 = \log \frac{P_{H_2O}}{P_{H_2}} - \log N_o{}^a \qquad [8]$$

The expression on the right hand side is the experimentally determined quantity, but K_1 cannot be determined directly because of the lack of information on oxygen activity. A new equilibrium constant K_2 is defined as

$$K_2 = \frac{P_{H_2O}}{P_{H_2}} \cdot \frac{1}{N_o{}^a} \qquad [9]$$

$$\log K_2 = \log P_{H_2O}/P_{H_2} - \log N_o{}^a \qquad [10]$$

or

$$\log N_o{}^a = \log P_{H_2O}/P_{H_2} - \log K_2$$

Comparing Eq. [8] with Eq. [10], the following expression is obtained

$$\log \gamma_o{}^a = \log K_2 - \log K_1 \qquad [11]$$

Since K_2 is constant with composition, the activity coefficient is constant and, therefore, $\log K_1 = \log K_{Ni}$. Log $\gamma_o{}^a$ can be computed from the following equation

$$\log \gamma_o{}^a = \log K_2 - \log K_{Ni} \qquad [12]$$

Values for log K_2 were the experimental values determined in this study, and log K_{Ni} is obtained from earlier work (6). A plot of log K as composition, Fig. 3, will give log $\gamma_o{}^a$ which is parallel to the curve for log K with its zero at the pure Ni end of the curve.

Figure 4 shows an expanded view at the high nickel end of the diagram. Results are tabulated in Table V.

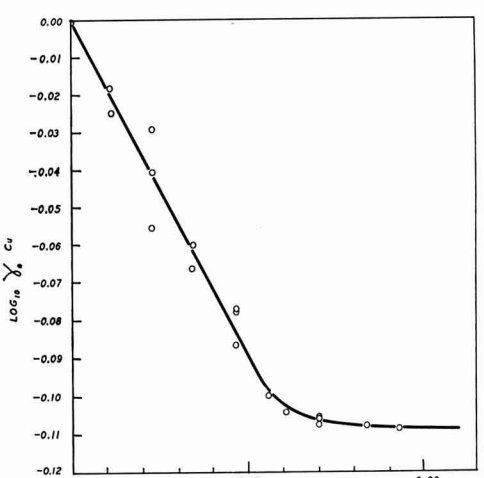

Fig. 4. Expanded view of the activity coefficient of oxygen at the nickel end of the Ni-Cu alloys at 1550°C to show the effect of Cu on the activity coefficient of oxygen in Ni.

A useful quantity can be derived from a measure of the terminal effects. The interaction parameter due to Wagner (13) can be obtained by differentiating the natural log of the activity coefficient of oxygen with respect to the mole fraction.

$$\epsilon = \left(\frac{\partial \ln \gamma_o{}^a}{\partial \text{Ni}} \right)_{\text{as Ni} \to 0} \qquad [13]$$

where ϵ is the interaction parameter, $\gamma_o{}^a$ the activity coefficient of oxygen in the alloy, and N the mole fraction of copper. From Fig. 4, one obtains a value of

$$\epsilon = -2.07$$

This value is valid up to 10% copper in nickel. The interaction parameter will allow one to calculate the excess free energy of solution.

Summary

A number of related thermodynamic equations, *e.g.*, $\Delta F°$, for the transfer of oxygen in the liquid Cu-Ni alloys have been investigated in great detail. The experimental results are represented as linear functions of $1/T$, and the related standard free energy changes are expressed as linear functions of temperature. It has been established that the dissolved oxygen in these metals follows Henry's law well within experimental errors.

The equilibrium relationships for dissolved oxygen have been investigated over a wide range of compositions for the copper-nickel alloys at two temperatures.

The interaction parameter has been determined at the high nickel end of the Ni-Cu alloy system.

Acknowledgments

Financial support for the work was from Foundational Research Project No. 9. The authors would like to thank Mr. J. Thompkins from AML for his assistance and Mr. J. Ryan for the computer work. The authors also would like to acknowledge the technical assistance of Mr. J. Hirl from AML.

The opinions expressed are the private ones of the authors and are not to be construed as official or reflecting the view of the Department of the Navy or the Naval Service at large.

Manuscript received May 11, 1964; revised manuscript received Jan. 4, 1965. This paper was presented at the Toronto Meeting, May 3-7, 1964.

Any discussion of this paper will appear in a Discussion Section to be published in the December 1965 JOURNAL.

REFERENCES

1. M. Hansan and K. Anderko, "Constitution of Biary Alloys," McGraw Hill Book Co., New York (1958).
2. C. B. Alcock and F. D. Richardson, *Acta Met.*, **6**, 385 (1958).
3. C. B. Alcock and F. D. Richardson, *ibid.*, **8**, 882 (1960).
4. R. A. Oriani and C. B. Alcock, *Trans. AIME*, **224**, 1104 (1962).
5. N. A. Gokcen, *ibid.*, **206**, 1558 (1956).
6. E. S. Tankins, N. A. Gokcen, and G. R. Belton, *ibid.*, **230**, 820 (1964).
7. N. A. Gokcen, *ibid.*, **212**, 93 (1958). N. A. Gokcen and E. S. Tankins, *J. Metals*, **14**, 584 (1962).
8. "Selected Values of Chemical Thermodynamics Properties," National Bureau of Standards, Series 111, 1956.
9. R. T. Birge, *Rev. Mod. Phys.*, **13**, 13 (1941).
10. D. J. Girardi and C. A. Siebert, *Trans. AIME*, **188**, 1168 (1950).
11. Kokich, Sano, and Sakao, *Nippon Kinzoku Gakkaishi*, **19**, 431 (1955).
12. W. Himmler, *Z. Phys. Chem.*, **195**, 244 (1950).
13. C. Wagner, "Thermodynamics of Alloys," Addison-Wesley Press, Cambridge, Mass., 1952. See also M. Ohtani and N. A. Gokcen, *Trans. AIME*, **218**, 533 (1960).

Hydrogen Adsorption on Platinum Single Crystal Electrodes

I. Isotherms and Heats of Adsorption

Fritz G. Will

Research Laboratory, General Electric Company, Schenectady, New York

ABSTRACT

The adsorption of hydrogen on the three main faces (100), (111), and (110) of platinum single crystal electrodes has been studied in 8*N* H_2SO_4 at different temperatures with the voltage sweep method. As on polycrystalline platinum electrodes, hydrogen adsorbs on each of the faces in two distinctly different binding states which present themselves as two pronounced maxima in the current-voltage sweep curves. There are indications for a third binding state giving rise to a third, less pronounced maximum. The potentials at which the maxima occur are essentially the same for polycrystalline and for each of the three single crystal electrodes. However, the relative heights of the maxima are different in each case. The adsorption isotherms and the heats of adsorption are also notably different on the three faces. Under the usual assumption of one hydrogen atom adsorbed per platinum surface atom, initial roughness factors of 1.0-1.9 result which increase to 1.9-2.4 during the experiments. The results suggest that, in fact, each of the crystal faces exposes more than one crystal plane. The left pronounced maximum is assigned to a (110) plane, the right pronounced maximum to a (100) plane, and the third small maximum to a (111) plane. Different proportions of these planes determine the different shape of the curves obtained on the different nominal faces and on polycrystalline electrodes.

The adsorption of hydrogen on polycrystalline platinum electrodes has been studied extensively in the past. Three different methods are available for these studies, (*a*) charging curves (1), (*b*) polarization with an alternating current (2), and (*c*) polarization with a triangular voltage sweep (3) also referred to as cyclic voltammetry or surface coulometry. All these methods are based on the fact that a change of the electrode potential in a certain range causes a change of the coverage of the electrode surface with hydrogen atoms. The adsorption-desorption process occurs through the charge transfer reaction

$$M\text{—}H \leftrightarrows M + H^+ + e^- \qquad [1a]$$

$$M\text{—}H + OH^- \leftrightarrows M + H_2O + e^- \qquad [1b]$$

in acid and alkaline solutions, respectively. For polarizations larger than about 50 mv, the charge transfer reaction [1] is much faster (4) than the dissociation-recombination reaction

$$H_2 + 2M \leftrightarrows 2M\text{—}H \qquad [2]$$

Hence, for a given polarization, a certain coverage of the surface with hydrogen atoms is established and maintained by fast discharge of hydrogen ions or hydroxyl ions according to the discharge reaction[1].

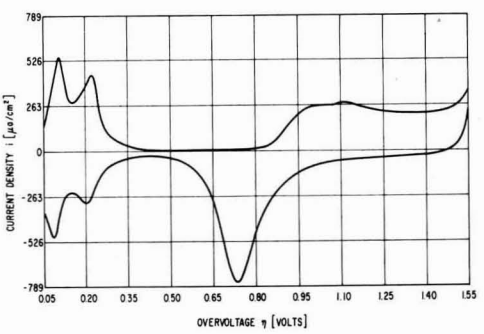

Fig. 1. Current-voltage sweep curve on polycrystalline platinum, obtained earlier (3). Sweep range 50-1550 mv, sweep rate 0.1 v/sec; surface area of electrode 0.19 cm².

The partial pressure of molecular hydrogen near the electrode surface which corresponds to that given polarization, on the other hand, is established much slower due to the slower rate of the dissociation reaction [2]. For any given polarization, the partial pressure of molecular hydrogen can be calculated from Nernst's law. At 0 volt (1 atm hydrogen pressure), the platinum surface is nearly saturated with hydrogen; at 0.4v ($\approx 10^{-14}$ atm), the surface is essentially free of hydrogen. It can thus be seen that a change of the electrode potential has the same effect on the hydrogen coverage of the surface as a change of the partial pressure of molecular hydrogen. In contrast to the latter method, however, the first method does not depend on the slow dissociation equilibrium [2].

In general, adsorption isotherms obtained on "active" polycrystalline platinum electrodes with either of the three methods exhibit three inflection points. These manifest themselves in two waves in the charging curves (5-7), and in two distinct maxima and one minimum in the differential capacity curves (8,9) and in the current-voltage sweep curves (3,10). Figure 1 shows a typical curve obtained on polycrystalline platinum with the sweep method. Apparently, hydrogen adsorbs on platinum preferentially at two distinct voltages or hydrogen pressures, *i.e.*, hydrogen exists in a strongly and a weakly bound state. Increasing voltage corresponds to decreasing hydrogen pressure, and hence the left maximum corresponds to weakly bound hydrogen and the right maximum to strongly bound hydrogen. Little conclusive information is available about the nature of the two states of adsorption.

Slygin and Frumkin (6,11) measured the amounts of anions and cations which are adsorbed on platinum as a function of the potential. They found that these amounts are influenced notably by the adsorption of hydrogen and interpret (12) their results as the adsorption of negatively polarized hydrogen at larger potentials (small coverages) followed by the adsorption of positively polarized hydrogen at smaller potentials (large coverages). Wicke and Weblus (8) found that the right maximum is influenced by the nature of the anions in the electrolyte while the left maximum does not show such a dependence. From this Eucken and Weblus (8) believe that the two maxima are not due to adsorption on two different crystallographic planes of the platinum but are due to adsorption on bare platinum (right maximum) and on oxygen atoms (left

maximum). Böld and Breiter (13) found values for the heat of adsorption of hydrogen on platinum in excess of 10 kcal/mole H_2 for coverages smaller than 0.5. This indicates that the strongly bound hydrogen is adsorbed as atoms. Kinetic considerations lead Breiter (14) to believe that the weakly bound hydrogen is also adsorbed as atoms.

Studies of hydrogen adsorption on platinum in the gas phase have also revealed the existence of strongly and weakly bonded hydrogen. Disagreement exists concerning the polarity of the two types of hydrogen and whether the weakly bound hydrogen is adsorbed as atoms or as molecules. Mignolet (15) measured the changes in the work function of a clean platinum film, which occur as a function of time, when hydrogen is being adsorbed at —190°C. Using both the condenser and the thermionic method, he found that the first 40% of the hydrogen which adsorbs increases the work function by 0.11v while the remaining 60% decreases the work function of the clean metal by 0.23v. At 20°C, under vacuum, only the initial 40% hydrogen which increases the work function remains adsorbed. These findings suggest that the initially adsorbed hydrogen is strongly bonded and negatively polarized and the subsequent 60% hydrogen weakly adsorbed and positively polarized. Mignolet also found that a volume of carbon monoxide almost equal to that of the weakly bonded hydrogen could be adsorbed in addition to the strongly bonded hydrogen. From this he believes that the weakly bonded hydrogen is adsorbed as molecules. It has been shown (16), however, that carbon monoxide displaces the weakly and strongly bonded hydrogen from the surface. Hence, the foregoing contention does not seem to be valid. Rootsaert *et al.* (17) adsorbed and desorbed hydrogen on a platinum tip in a field emission microscope by changing the temperature at a constant hydrogen pressure of 10^{-7} mm Hg. They found in agreement with Mignolet that on adsorbing hydrogen the work function first increases, passes through a maximum at a coverage of about 0.4, and then decreases with further increasing coverage. Pliskin and Eischens (18) obtained two absorption bands in infrared spectra of hydrogen adsorbed on alumina-supported platinum. When working with hydrogen and deuterium mixtures, they could not find any band corresponding to $H - D^+$ bonds. From this they deduce that the weakly bonded "positive" hydrogen is not adsorbed as molecules. Toya (19) showed that the two absorption bands correspond to a difference in heats of adsorption of only 0.8 kcal/mole H_2. This small difference makes it unlikely that the strongly and weakly bonded hydrogen discussed earlier is identical with the two types causing the two absorption bands. For the former, differences in heat of adsorption are found (10,20) which are of the order of 8 kcal/mole H_2.

The following study was undertaken to find out more about the nature of the two states of hydrogen adsorption. In particular, this study is concerned with the question whether the two states are due to adsorption on two different crystallographic planes preferentially exposed by the polycrystalline platinum. In order to test this possibility, the adsorption of hydrogen on the three main faces (100), (111), and (110) of platinum single crystals was studied. The voltage sweep method was applied because it affords a convenient and accurate way to determine the quantities of adsorbed hydrogen (3).

Experimental

The platinum single crystal was obtained by zone melting a platinum rod of 99.999% original purity in an electron beam. After orientation the crystal was cut with a diamond cutting wheel to give single crystals presenting the main faces (100), (111), and (110). These faces were then polished to optical flatness using for the final finish a 0.1μ alumina powder. The three single crystals were subsequently annealed in vacuum at 680°C for 24 hr and finally sealed into lime glass so that only the three faces of interest remained uncovered. The geometric surface areas were 0.181 cm^2 for (100), 0.328 cm^2 for (111), and 0.225 cm^2 for (110). The three crystals were symmetrically arranged in one cell compartment opposite the counter electrode. A hydrogen reference electrode was located in a second cell compartment which communicated with the main compartment via a capillary. All potentials are referred to this hydrogen electrode. The 8*N* H_2SO_4 used in the experiments was prepared with ultrapure water (21) and pre-electrolyzed for 15 hr. Although the measurements were carried out without gas-bubbling, the electrolyte was periodically flushed with prepurified argon to remove traces of hydrogen and oxygen.

Despite the cleaning procedures, reproducible results could be obtained only by applying a periodic sweep of such an amplitude that an oxide layer was formed and reduced during each sweep (compare Fig. 1) prior to the adsorption and desorption of the hydrogen layer. A sweep range of 50-1550 mv was chosen to achieve this and at the same time, hold the formation of molecular hydrogen and oxygen to a minimum. The applied sweep rate was 0.1 v/sec and, hence, the duration of one sweep was 30 sec. A modified (22) Hewlett Packard Function Generator 202A in conjunction with a potentiostat was used to apply the voltage sweeps. The resulting current-voltage (or time) curves were displayed on a Tektronix 502 x-y oscilloscope. For each face and each given temperature, photographs were taken of the first four sweeps and every 5 min thereafter for 20 min. A 35 mm "ROBOT" automatic transport and rewind camera was used for this purpose. The integration of the enlarged curves was performed graphically with an "Ott" planimeter No. 144 to a precision of 2%. Measurements on the three crystal faces were made at 0°, 10°, 25°, 40°, 60°, and 80°C. A specially designed circulating air thermostat allowed the temperature to be controlled within ±0.1°C.

While one particular face was being studied, the other two faces were kept in the solution on open circuit. When proceeding to the next face, a potential of 50 mv was always applied for 3 min before starting the periodic sweep from this potential. During the experiments which are reported here, each face was subjected to some 240 sweeps. In preceding preliminary experiments, about 160 sweeps had already been applied to each individual face.

Results

Current-voltage sweep curves.—As mentioned before, hydrogen desorbs from polycrystalline platinum electrodes preferentially at two different potentials corresponding to two distinct maxima in the current-voltage sweep curve. Figure 1 shows one such curve which was previously (3) obtained on polycrystalline platinum wires under conditions similar to those in the present study. The ratio of the currents of the "first" (less anodic) and "second" maximum I_1/I_2 is 1.2. Figure 2 shows curves which were obtained on the (100), (111), and (110) faces of platinum single crystals at 25°C. The curves correspond to sweep 260 and were photographed 10 min after starting the periodic sweep. The two striking features of the curves for (100) and (111) are: (*a*) as on a polycrystalline electrode there are still two distinct desorption maxima, and (*b*) while for the (100) face the first maximum is smaller than the second, the opposite is true for the (111) face; in fact the ratio I_1/I_2 is 0.8 for (100) and 1.5 for (111). The curve for the (111) face exhibits a small third maximum which degenerates to a shoulder in the curve for the (100) face. The curve obtained on the (110) face looks strikingly similar to the curve for (111), and the ratio I_1/I_2 is essentially the same for the two faces. However, the current densities i_1 and i_2 corresponding to the two maxima of the (110) curve are some 30% smaller than i_1 and i_2 for (111).

The effect of temperature on the curves is such that with increasing temperature the height of the maxima increases and their position is shifted toward less anodic

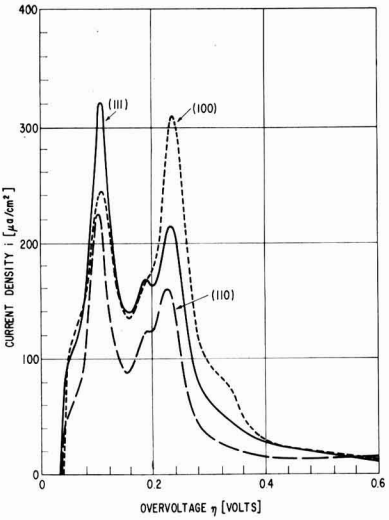

Fig. 2. Current-voltage sweep curves on platinum single crystal faces (100), (111), and (110) at 25°C. Sweep range 50-1550 mv, sweep rate 0.1 v/sec.

potentials. Both effects are larger for the first maximum.

During the 20-min duration of one experiment, the shape of the curves from the fourth sweep on remained essentially unaltered. The first curve and, to much lesser extent, the second and third curve always looked quite different from the succeeding curves.

The effect of the number of sweeps on the shape of the curves was quite pronounced, however, during the first 20 or 30 sweeps that were applied to the virgin crystal faces. Figure 3 shows this effect for the (110) face, where it is most pronounced. Curve I resulted when the 10th sweep was applied to the virgin surface. Curve II is identical to the (110) curve in Fig. 2 and was obtained after about 250 sweeps had been applied to the (110) face. While maximum 1 did not change too much, maximum 2 increased considerably with increasing number of sweeps. In fact, maximum 2 is smaller than maximum 3. After 10 sweeps, the ratio of the maxima currents I_1/I_2 is 2.9, and after 260 sweeps this ratio is 1.45. The corresponding figures for the (111) face are 2.1 (10 sweeps) and 1.5 (260 sweeps) and for the (100) face 0.79 and 0.80.

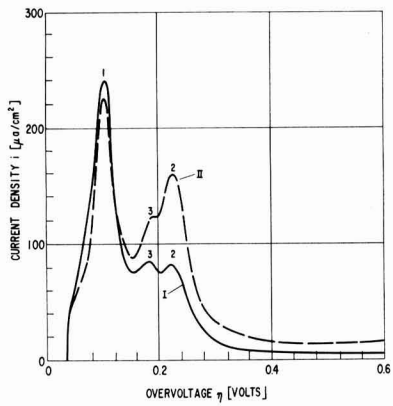

Fig. 3. Current-voltage sweep curves on the (110) face at 25°C after 10 sweeps (curve I) and after 260 sweeps (curve II).

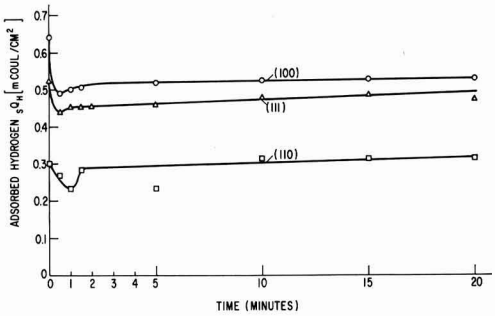

Fig. 4. Saturation amounts of hydrogen adsorbed on the three faces at 25°C.

Saturation concentration of adsorbed hydrogen.—Since a voltage is applied which changes linearly with time, the current-voltage curves in Fig. 1 and 2 also represent current-time curves. Hence, an integration of these curves yields the charge corresponding to the amount of adsorbed hydrogen plus the charge of the double layer capacity. The double layer capacity is almost constant between 50 and 400 mv (11). Its charge is only about 2% of the charge of adsorbed hydrogen and shall be neglected. The small current above potentials of about 400 mv is mostly due to the charge of the double layer (3). Below 50 mv the current decreases steeply. Therefore, the saturation concentration of hydrogen $_sQ_H$ adsorbed on the surface can be determined by integrating the curves from 50 to 400 mv. This was done for different times in the temperature range of 0° to 80°C. The result at 25°C for sweeps 240 to 280 is plotted in Fig. 4. During the first two or three sweeps of each experiment, erratic values are found for $_sQ_H$. From then on, $_sQ_H$ changes but slightly with time. This finding agrees with the finding concerning the changes in the shape of the curves with time.

For the first 10 sweeps that were applied to the virgin faces, considerably smaller amounts of hydrogen were found. The $_sQ_H$ values for 10 sweeps are 0.39 m-coul/cm² for (100), 0.23 for (111) and 0.24 for (110).[1] The corresponding values after 260 sweeps are 0.51 m-coul/cm² for (100), 0.46 for (111), and 0.30 for (110).

For the first sweep of each experiment, the total anodic charge, *i.e.*, adsorbed hydrogen plus oxygen, is always between 14% and 34% larger than the total cathodic charge. However, for the succeeding sweeps, the total anodic charge is consistently smaller than the cathodic charge, namely, by 1 to 12%.

Except for the (110) face, temperature has no systematic effect on the $_sQ_H$ values. For the (110) face, $_sQ_H$ stays roughly constant between 0° and 40°C and then decreases by about 20% from 40° to 80°C.

Adsorption isotherms.—The sweep curves obtained after 10 min for different temperatures were integrated in intervals of 50 mv between 50 and 400 mv. The degree of coverage $\theta = Q_H/{}_sQ_H$ at, *e.g.*, 300 mv, is the ratio of the charges resulting from an integration between 400 mv and, *e.g.*, 300 mv, and between 400 mv and 50 mv. The resulting adsorption isotherms for the (100) face are presented in Fig. 5. Applying Nernst's law and correcting for the vapor pressure of the sulfuric acid, the overvoltages are converted into partial pressures of molecular hydrogen. As one would expect for an exothermic process, the degree of coverage decreases with decreasing hydrogen pressure and increasing temperature. The curves display three inflection points in accordance with the three extrema

[1] Note added during revision of manuscript: According to a private communication on October 12, 1964, Dr. J. E. Oxley, Leesona Moos Laboratory, in similar experiments on Pt single crystals obtained $_sQ_H$ values of 0.30 mcoul/cm² for (100), 0.29 for (100), and 0.21 for (110). The results were obtained at a sweep rate of 18 v/sec.

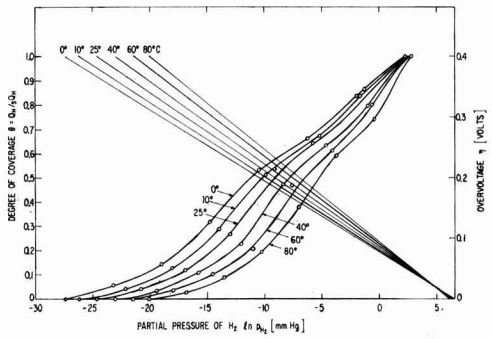

Fig. 5. Adsorption isotherms on (100) face. Straight lines relate voltage on right ordinate to partial pressure of hydrogen.

of the current-voltage sweep curves. Figure 6 shows the adsorption isotherms for the three crystal faces at 0° and 80°C. For constant hydrogen pressure, the degree of coverage decreases distinctly in the whole temperature range in the order (100)>(111)>(110). The effect is more pronounced at lower temperatures.

Heats of adsorption.—The Clausius-Clapeyron equation

$$dp/dT = \Delta H/T\Delta V \qquad [3]$$

(ΔH, ΔV enthalpy and volume change on transferring 1 mole of hydrogen from the gas phase into the adsorbed phase) may be written as

$$d \ln p_{H_2}/dT = W/RT^2 \qquad [4]$$

if one assumes ideal conditions in the gas phase and neglects the volume of the hydrogen in the adsorbed phase. The heat of adsorption $W \equiv \Delta H$ is negative for an exothermic process. If the heat of adsorption is temperature independent the integration of equation [4] gives

$$\ln p_{H_2} = -W/RT + \text{const.} \qquad [5]$$

In a plot ln p_{H_2} against $1/T$ straight lines should result whose slope is proportional to the heat of adsorption (10, 13). While this is indeed the case for the (100) and (111) faces, the heat of adsorption increases noticeably with increasing temperature for the (110) face at temperatures above 40°C.

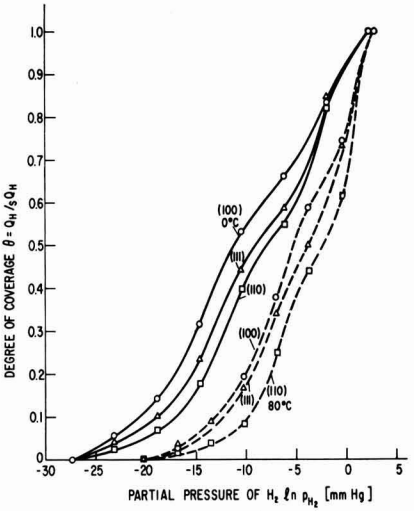

Fig. 6. Adsorption isotherms on (100), (111), and (110) at 0° and 80°C.

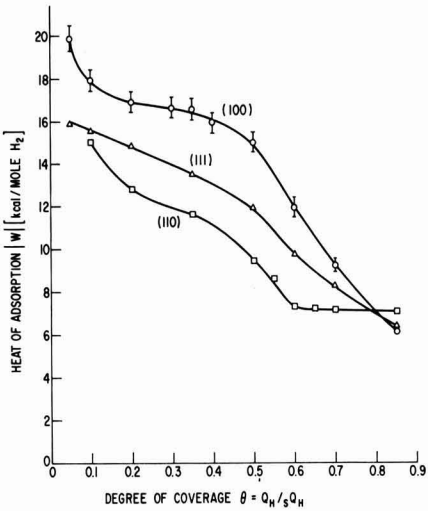

Fig. 7. Heats of adsorption of hydrogen on the three crystal faces as a function of coverage.

The heats of adsorption for the three crystal faces are plotted in Fig. 7 as a function of the degree of coverage. For the (110) face the temperature-independent values of W between 0° and 40°C are shown. For all three crystal faces, the heat of adsorption decreases substantially with increasing coverage. This agrees with results obtained on polycrystalline platinum in electrolytes (10, 13) and in the gas phase (20). Especially in the curve for the (110) face one can clearly distinguish between strongly and weakly bonded hydrogen; the latter prevails at $\theta > 0.6$ and has a heat of adsorption of about 7 kcal/mole. An increase of θ from 0.1 to 0.85 causes a decrease in the heat of adsorption of 66% for (100), 59% for (111), and 53% for (110). The other noteworthy finding is the comparatively large difference in the heats of adsorption for the different faces. Except for coverages larger than 0.8 the heats of adsorption decrease in the order (100)>(111)>(110). At coverages larger than 0.8, near saturation, this order is reversed. For coverages smaller than 0.6 the difference in W between the three faces averages between 2 and 3 kcal. For $\theta = 0.5$ the heats of adsorption are 15 kcal/mole H_2 for (100), 11.9 for (111), and 9.4 for (110).

Discussion

Roughness of the surface.—The number of platinum atoms in the surface planes of the three crystal faces are $1.5 \cdot 10^{15}$ atoms/cm^2 for (111), $1.3 \cdot 10^{15}$ for (100), and $0.92 \cdot 10^{15}$ for (110). If one makes the usual assumption that one hydrogen atom is adsorbed per platinum surface atom, the corresponding charges are 0.24 mcoul/cm^2 for (111), 0.208 for (100), and 0.147 for (110). The amounts of hydrogen that are found are considerably larger, particularly after the faces have been subjected to a large number of sweeps. This may be interpreted as a large initial roughness of the virgin faces which further increases with the number of sweeps applied. For the (100) face, for example, the roughness factor would be 1.87 after 10 sweeps and 2.45 after 260 sweeps. With such a large surface roughness, it is probable that the surface exposes more than one crystal face. The fact that the current maxima on all three faces occur to within ±5 mv at the same potentials (compare Fig. 2) could indicate that each of the faces is, in truth, a mixture of essentially two faces with a small fraction of a third face, particularly in the case of the nominal (111) and (110) face.

Effect of sweep on curve shape.—The effect of the number of sweeps on the shape of the curves (com-

pare Fig. 3) might be explained as follows. Initially (curve I), the nominal (110) face exposes a large fraction of (110) (maximum 1) and small fractions of (111) (maximum 3) and of (100) (maximum 2). After 260 sweeps have been applied (curve II), the amount of (110) has decreased slightly, the fraction of (111) stayed almost constant, but the fraction of (100) increased sharply. The periodic voltage sweep might cause the formation of etch pits with the exposure of preferred crystal faces. In this connection, it is interesting to note that the development of low-index planes by chemical etching is a standard technique in the determination of the orientation of various metal crystals (23).

The curve obtained on the (111) face (compare Fig. 2) looks always quite similar to that on the (110) face. This implies that the nominal (111) face exposes, in fact, always a large fraction of (110) (maximum 1), a considerable fraction of (100) and only a small fraction of (111). In order to rationalize this conclusion one has to assume that a thin surface layer exhibits a polishing and recrystallization texture which exposes the preferred orientations that are found. Indeed, a preferred orientation has been found on cold rolled and of polished copper and gold, with (110) planes lying parallel to the surface (24). The recrystallization texture on annealing may or may not resemble the polishing texture, depending on the severity of the surface damage and the particular annealing conditions (23). As mentioned before, the platinum crystals were annealed at 680°C for 24 hr. On platinum single crystals that had been annealed at 1100°C for 48 hr, Tucker (25) did not find evidence for faceting. However, the detection of crystal facets smaller than about 100Å in diameter is beyond the sensitivity of the slow electron diffraction apparatus.

Adsorption isotherms and heats of adsorption.—In the preceding discussion, maximum 1 has been assigned to a (110) plane, maximum 2 to a (100) plane, and maximum 3 to a (111) plane. This assignment is based on the relative heights of the current maxima for the different nominal faces in Fig. 2. It implies that the hydrogen bond is weakest on the (110) plane and strongest on the (100) plane. This agrees with the heats of adsorption for the three faces shown in Fig. 7, which increase in the order (110)<(111)<(100) for coverages smaller than 0.8. Based on considerations involving the number of nearest neighbors and their degrees of unsaturation, one would argue, however, that the bond should be weakest on the (111) plane and strongest on the (110) plane. More experiments are needed to solve this apparent contradiction.

Qualitatively, the different adsorption isotherms for the different faces can be understood with the proposed assignment of the current maxima. Since, for example, the nominal (110) face exposes a much smaller surface fraction of (100) than the nominal (100) face, it is evident that at smaller partial pressures of hydrogen, where (100) adsorbs preferentially, the surface coverage is smaller for the nominal (110) face than for the nominal (100) face. On a similar basis, the difference in heats of adsorption can be understood.

Current-voltage curves on polycrystalline wires.—The two pronounced maxima of current voltage curves obtained on polycrystalline platinum wires (compare Fig. 1) occur at essentially the same potentials as those obtained on the single crystal faces. The texture of cold-drawn wires of face-centered cubic metals, like platinum, is usually a double fiber texture with a [111] and a [100] direction parallel to the wire axis (23). With the possibility of so many different crystal planes exposed it seems surprising that only two maxima are observed. This difficulty can be reconciled by postulating that the wire surface becomes etched in the usual pretreatments of the electrodes prior to the experiments. In this etching process, the low-energy main faces are expected to develop at the expense of the large number of high-index planes.

Conclusions

The finding that the maxima have different heights for the different faces, but occur at almost the same potentials, suggests that each of the nominal faces exposes, in fact, several crystal planes in different proportions. Such an interpretation is consistent with the assumption that the large measured amounts of adsorbed hydrogen are due to a considerable surface roughness. The left pronounced maximum has been tentatively assigned to a (110) plane, the right pronounced maximum to a (100) plane and the third small maximum to a (111) plane. This implies that the bond strength of hydrogen and, hence, its heat of adsorption is smallest on (110) and largest on (100). This has been actually found. The two adsorption states of hydrogen that exist on polycrystalline platinum electrodes are also likely to be due to adsorption of hydrogen on two different crystallographic planes. The two current maxima occur within ±5 mv at the same potentials as the two pronounced maxima on the single crystals. Hence, it is concluded that cold-worked, polycrystalline platinum electrodes expose mainly crystallites with {110} and {100} planes. This conclusion is in agreement with the fact that the texture of all cold-rolled face-centered cubic metals is one in which {110} planes are parallel to the rolling plane (23). To reconcile the occurrence of only two or three current maxima on cold-drawn platinum wires with their texture of [111] and [100] parallel to the axis, one has to assume etching of the surface during the process of "activating" the electrodes. Studies with better defined crystal planes and under extreme clean conditions are needed to confirm these tentative conclusions.

Acknowledgments

The author gratefully acknowledges the loan of the platinum single crystals by C. W. Tucker which were prepared by J. W. Rutter and V. J. DeCarlo.

Manuscript received July 20, 1964. This paper was presented at the Toronto Meeting, May 3 to 7, 1964.

Any discussion of this paper will appear in a Discussion Section to be published in the December 1965 JOURNAL.

REFERENCES

1. F. P. Bowden, *Proc. Roy. Soc.*, **A125**, 446 (1929).
2. P. Dolin and B. Ershler, *Acta physicochim. URSS*, **13**, 747 (1940).
3. F. G. Will and C. A. Knorr, Internat. Polarograph. Kolloqu., Bonn 1958; *Z. Analyt. Chem.*, **173**, 87 (1960); *Z. Elektrochem.*, **63**, 1008 (1959); *ibid.*, **64**, 258 (1960).
4. J. Giner, *Z. Elektrochem.*, **63**, 386 (1959).
5. J. A. V. Butler and G. Armstrong, *Proc. Roy. Soc.*, **A137**, 604 (1932).
6. A. Slygin and A. Frumkin, *Acta physicochim. URSS*, **3**, 791 (1935).
7. M. Breiter, C. A. Knorr, and W. Völkl, *Z. Elektrochem.*, **59**, 681 (1955).
8. A. Eucken and B. Weblus, *ibid.*, **55**, 114 (1951); E. Wicke and B. Weblus, *ibid.*, **56**, 169 (1952).
9. M. Breiter, H. Kammermaier, and C. A. Knorr, *ibid.*, **60**, 37 (1956).
10. M. Breiter and B. Kennel, *ibid.*, **64**, 1180 (1960).
11. A. Slygin, A. Frumkin, and W. Medvedovsky, *Acta physicochim. URSS*, **4**, 911 (1936).
12. A. Frumkin and A. Slygin, *ibid.*, **6**, 819 (1936).
13. W. Böld and M. Breiter, *Z. Elektrochem.*, **64**, 897 (1960).
14. M. Breiter, *Electrochim. Acta*, **7**, 25 (1962).
15. J. C. P. Mignolet, *J. Chim. Phys.*, **54**, 19 (1957).
16. S. Gilman, *J. Phys. Chem.*, **67**, 78 (1963).
17. W. J. M. Rootsaert, L. L. Van Reijen, and W. M. H. Sachtler, *J. Catalysis*, **1**, 416 (1962).
18. W. A. Pliskin and R. P. Eischens, *Z. phys. Chem. N. F.*, **24**, 11 (1960).
19. T. Toya, *J. Res. Inst. Catalysis* (Hokkaido University), **10**, 236 (1962).
20. J. G. Aston, *J. Phys. Chem.*, **67**, 2042 (1963).
21. R. W. Powers, *Electrochem. Technol.*, **2**, 274 (1964).
22. F. G. Will, To be published.
23. C. S. Barrett, "Structure of Metals," McGraw-Hill Book Co., New York (1952).
24. C. S. Lees, *Trans. Faraday Soc.*, **31**, 1102 (1935).
25. C. W. Tucker, *J. Appl. Phys.*, **35**, 1897 (1964).

Technical Notes

The Preparation and Luminescence of Molybdenyl Phosphate

V. Chiola and C. D. Vanderpool

Chemical and Metallurgical Division, Sylvania Electric Products Inc., Towanda, Pennsylvania

In 1955, Schulz (1) reported the preparation and x-ray identification of molybdenyl phosphate, $MoO_2(PO_3)_2$, as one of several crystalline compounds isolated from the binary system, $MoO_3 \cdot P_2O_5$. Kierkegaard (2) investigated and proposed a crystal structure for $MoO_2(PO_3)_2$ and a number of other molybdenum phosphate compounds having low Mo:P ratios (3). In this laboratory, recent investigations of molybdenum trioxide-phosphoric acid systems led to the isolation of a crystalline product identified as molybdenyl phosphate, $MoO_2(PO_3)_2$. In the course of examining this material, it was discovered that molybdenyl phosphate, $MoO_2(PO_3)_2$, is a phosphor responding to irradiation by 3650 and 2537Å. It was found also that the same phosphor possesses electroluminescent properties. The purpose of this note is to report the preparation and properties of molybdenyl phosphate as a luminescent and electroluminescent material.

Schulz (1) prepared $MoO_2(PO_3)_2$ by heating a five-fold excess of P_2O_5 with MoO_3 to about 500°C in a steel bomb. The reaction was complete in 3-4 hr. A light-blue to light-green crystalline product was recovered after leaching the glassy reaction mixture with water to remove excess P_2O_5. Kierkegaard (2) prepared $MoO_2(PO_3)_2$ by autoclaving a mixture of 1.5 g MoO_3 and 6.6g P_2O_5 in a platinum crucible at 500°C for one week. The reaction mixture was washed and filtered to recover crystals.

Molybdenyl phosphate was prepared in this laboratory by heating one mole of MoO_3 with six moles of phosphoric acid in a silica crucible to 450°C while agitating the mixture. Crystalline $MoO_2(PO_3)_2$ began precipitating at 325°C, but a glassy mixture was formed on cooling. A bluish-white product was recovered by aqueous leaching to remove excess phosphoric acid, filtering and drying at 110°C.

An alternate procedure involved heating one mole of MoO_3 with two moles of phosphoric acid to 600°C for 1 hr to form a solid, white crystalline mass. After cooling, soluble matter was removed by leaching, and the molybdenyl phosphate product was recovered by filtration, washing with water, washing with 7% ammonium hydroxide solution, and drying at 110°C.

The typical impurity content of the molybdenyl phosphate prepared by the above procedures was determined by spectrographic qualitative analysis as follows: Al, 1-10 ppm; Ca, 1-10 ppm; Cu, 1-10 ppm; Fe, 1-10 ppm; Mg, 1-10 ppm; Mn, <10 ppm; and Si, 100-1000 ppm.

X-ray diffraction films were taken on a Philips Norelco unit having a camera diameter of 114.6 mm and using Ni-filtered CuKα radiation of 1.542Å wavelength.

Observed $1/d^2$ values agreed very well with $1/d^2$ values calculated from cell parameters furnished by Kierkegaard (2) for the compound, $MoO_2(PO_3)_2$. The observed 2θ values agree with those given by Schultz (1) for the compound having the stoichiometric composition $MoO_3 \cdot P_2O_5$.

The emission spectra were obtained with a Perkin-Elmer spectrofluorimeter (4). The spectral response of molybdenyl phosphate under 3650Å radiation is a broad-band emission which peaks at 6100Å (Fig. 1). Under 2537Å excitation a similar broad-band emission between 6100 and 6300Å is observed. Response is significantly greater at 3650 than at 2537Å radiation.

The fluorescent intensity of molybdenyl phosphate under 3650Å excitation is 79% greater than that measured on a standard calcium silicate phosphor, JEDEC No. P-25, (Sylvania No. 156). Under 2537Å radiation, the intensity is only 33% of that measured on the standard.

Electroluminescent brightness measurements were obtained using cells having dimensions of 1 x 1 x 0.006 in. and a castor oil dielectric. The electrode materials were brass and transparent conductive glass. A Photovolt Model 520 Photometer was used in conjunction with a photomultiplier detector. Figure 2 shows a semi-logarithmic plot of brightness *vs.* the reciprocal of the square root of the voltage. Although the level of brightness was low, it varied linearly with $v^{-1/2}$ from about 400 to 900v. At 400v, brightness was about 0.2% of that measured for a conventional ZnS:Cu,Cl phosphor.

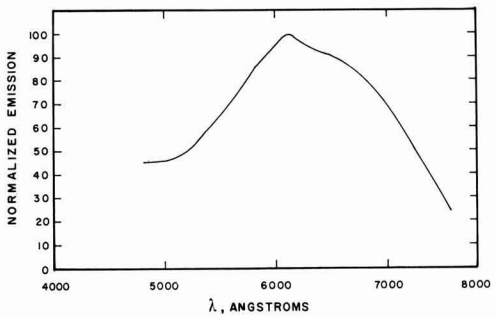

Fig. 1. Spectral response of $MoO_2(PO_3)_2$ to 3650Å excitation

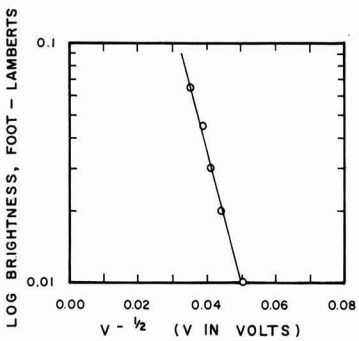

Fig. 2. Log brightness *vs.* (voltage)$^{-1/2}$

Molybdenyl phosphate electroluminesces blue-green at 60 cycles and blue at 6 kc. The results show that $MoO_2(PO_3)_2$ can be prepared from molybdenum trioxide-phosphoric acid reaction mixtures and that $MoO_2(PO_3)_2$ possesses luminescent and electroluminescent properties.

Acknowledgments

The authors wish to thank S. Faria for performing the spectral emission and electroluminescent brightness measurements and for helpful discussions concerning luminescent materials and their properties. They are also indebted to Dr. C. W. W. Hoffman and E. A. Wesley for x-ray diffraction measurements and to Dr. R. W. Mooney for advice and encouragement.

Manuscript received Aug. 18, 1964.

Any discussion of this paper will appear in a Discussion Section to be published in the December 1965 JOURNAL.

REFERENCES

1. I. Schulz, *Z. Anorg. u. allgem. Chem.*, **281,** 99 (1955).
2. P. Kierkegaard, *Arkiv Kemi*, **18,** 521 (1962).
3. P. Kierkegaard, *ibid.*, **19,** 51 (1962).
4. W. Slavin, R. W. Mooney, and D. T. Palumbo, *J. Opt. Soc. Amer.*, **51,** 93 (1961).

The Correlation between Water Contact Angle and KPR Adherence on SiO_2 Surfaces

A. A. Bergh

Bell Telephone Laboratories, Incorporated, Allentown, Pennsylvania

Kodak Photo Resist (KPR) is used in the processing of silicon planar transistors to protect selected areas of oxidized silicon surfaces from etching. KPR is an organic solvent solution of an ultraviolet-sensitive plastic. When applied to the oxide surface a thin coating is formed, and the areas where the oxide is to be protected are exposed to ultraviolet light. The nonexposed areas developed in organic solvents leaving a resist pattern that offers chemical resistance to oxide removal etchants. The oxide is usually 0.5-1.2μ thick, and the width of unprotected areas varies from a few microns to several mils. The resolution of the oxide edges depends on the adherence of the KPR to the oxide during etching. "Adherence" cannot be measured quantitatively, and it is best defined by the current of undercutting during etching as shown in Fig. 1. The sharp lines show good resolution, and the interference fringes indicate undercutting. The photoresist is not attacked by the etchant; it is only lifted at the edges. The instructions to apply KPR (1) recommend a high degree of cleanliness for both the silica surface and the photo resist solution and low relative humidity ambient to achieve good adherence. These conditions yield good results only on oxides heated to temperatures exceeding 850°C during or after oxidation. Undercutting was observed on oxides partially removed with an etchant containing fluoride ions, on oxides grown at lower temperatures, and on some deposited oxides. All the above oxides are wetted by water to a greater extent than those yielding good KPR resolution after etching.

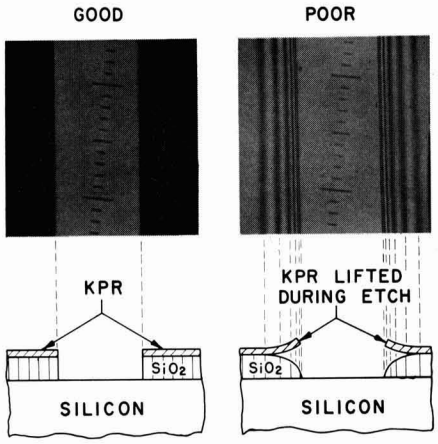

Fig. 1. Effect of KPR adherence on resolution (KPR has been removed before taking the photographs). Scale, 10 microns/division.

Experimental

One inch diameter, 5-6 mils thick, and 0.01 to 2 ohm-cm n-type silicon slices were used throughout the experiment. Oxides in the range of 0.6-1.0μ were produced under the following conditions: (*a*) 1 atm steam at 1050°C (1050°C-oxide); (*b*) 1 atm oxygen bubbled through 95°C water at 1050°C;(*c*) 120 atm steam at 650°C (650°C-oxide); (d) CO_2-oxide, deposited from a gas phase reaction at 1200°C (CO_2-oxide) (2); (*e*) reactive plasma sputtering at ~450°C (RPS-oxide) (3).

Water contact angles were measured with a reflection goniometer (4) using 4 x 10^{-3} ml size drops of high-purity water from a glass-Teflon micrometer syringe. KPR was applied over various patterns and unprotected areas of the oxide were removed with buffered HF solutions containing 15 ml of HF (49%) per 100 ml of a stock solution of 17M NH_4F. The etching rate of pure, amorphous SiO_2 is approximately 0.1 μ/min. The rate rapidly increases with increasing contamination of the oxide.

A minimum of six slices were taken from each group and contact angles were measured within 30 min after oxidation. Following this measurement slices were kept in hot concentrated HNO_3 for 10 min, rinsed in deionized water, and dried in a dust-free ambient at temperatures lower than 100°C. This treatment was used to remove any surface contamination and to evaluate the effect of water rinsing on the contact angle. (Boiling for 20 min in D.I. water produces the same change in θ.) Contact angles were measured on dry slices, KPR was applied, and the unprotected areas were etched away. The results of both readings and KPR adherence are listed in Table I. Oxides produced in atmospheric steam and wet oxygen at 1050°C showed identical values of θ and they are listed at "1050°C-oxide." Among the rinsed slices only the first group, average θ = 24°, gave good resolution.

Table I. Contact angles after oxidation and after rinsing

Type of oxide	θ After oxidation		θ After rinse		After rinse
	Average	Range	Average	Range	KPR adherence
1050°C-oxide	32	26-36	24	18-32	Good
650°C-oxide	3	0-8	3	0-8	Poor
CO_2-oxide	21	11-38	4	3-12	Poor
RPS-oxide	32	19-38	7	5-12	Poor

Table II. Change in θ after sequential treatments

Type of oxide	Treatment before heat	θ before heat	θ after heat*	θ after rinse**
1050°C-oxide	Buffered HF	4	36	24
650°C-oxide	None	<3	36	19
CO_2-oxide	HNO_3, H_2O	4	36	9
RPS-oxide	HNO_3, H_2O	13	35	9
Quartz plate	H_2O_2, H_2O	7	37	14

* 90 Min exposure to dry O_2 at 1200°C.
** 20 Min rinse in boiling DI water.

Correlation between low contact angles and poor KPR adherence was substantiated by another series of experiments. Different types of freshly oxidized slices were exposed to a buffered HF for 30 sec (etch rate~ 0.1 μ/min), rinsed in D.I. water and dried. All contact angles were lower than 6°, and poor adherence was observed on all slices with KPR.

A method to produce a low contact angle on any oxide has thus been established; different ways were tried to achieve the opposite effect. Heat-treatment in dry oxygen proved to be effective as shown in Table II. Similar results were obtained in vacuum and N_2, but O_2 is preferred because it prevents organic (usually hydrophilic) contamination. A limiting contact angle of $\theta = 40 \pm 5°$ was observed on all oxides after high-temperature baking.

Discussion

The significance of water contact angle on the structure and chemistry of SiO_2 surfaces will be discussed in detail in a forthcoming paper (5). The conclusions necessary to understand the adherence of KPR are listed below:

1. Low contact angles ($\theta < 3°$) indicate a strong adherence of water to SiO_2. Minimum contact angles are observed on completely hydroxylated surfaces.

2. The limiting value of $\theta = 40° \pm 5°$ observed on all oxides after exposure to high temperatures indicate a relatively weak bond between water and the SiO_2 surface. Heating removes water from the surface converting the silanol groups (Si — OH) into siloxane bridges (Si-O-Si). Siloxane is more hydrophobic ($\theta = \sim 40°$) than silanol ($\theta < 3°$).

3. The following can be said concerning the reaction

$$2Si{-}OH \leftrightarrows Si{-}O{-}Si + H_2O$$

(*a*) It can be completely shifted to the right at temperatures in excess of 850°C; (*b*) It can be shifted to the left only partially by boiling in water (or HNO_3). Deposited oxides hydrate easier than grown oxides (Table II, last column). (*c*) Complete hydration can be achieved (reaction shifted to the left) by breaking the siloxane bridges with HF, and hydrating the fluorinated silicon atoms, *i.e.*,

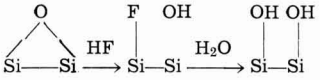

This accounts for the low contact angles after exposure to buffered HF and rinsing in water.

Table III. Effect of etch rate on the adherence of KPR

Etch rate, Å/min	Etching time, min	Hydrophobic oxide	Hydrophilic oxide
4000	2.5	Not undercut	Slight undercut
1000	10	Not undercut	Undercut
330	32	Not undercut	Heavy undercut
140	70	Undercut	All oxide removed

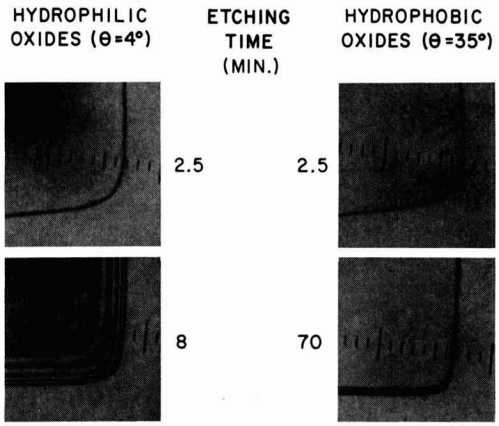

Fig. 2. Effect of etching time on undercutting. Scale, 10 microns/division.

A mechanism to explain that KPR is lifted during etching on hydrophilic surfaces can be obtained by considering the relative bond strengths at the KPR-oxide and water-oxide interfaces. Low contact angles indicate stronger, and high contact angles indicate weaker water-oxide bonds.

The contact angle of KPR, on the other hand, is nearly identical ($\theta \sim 20°$) on both hydrophilic and hydrophobic surfaces. In other words, the relative bond strengths between water-SiO_2 and KPR-SiO_2 is shifted in favor of the water on hydrophilic surfaces. Consequently, water has a greater tendency to penetrate the KPR-oxide interface on hydrophilic oxides. In view of this theory, two conditions enhance undercutting: (*a*) strong bonds at the water-oxide interface and (*b*) long exposure to aqueous solutions, *i.e.*, slow etching rates and excessive rinsing. A series of experiments were carried out, therefore, employing low and high contact angle oxides and different exposure times by changing the *p*H and thus the etch rate of the oxide removal etch. Results are shown in Table III, and some of the resolutions are illustrated in Fig. 2. Good agreement with theory can be observed. It is also evident that *p*H has an effect on the water penetration. The lifting of KPR increases with decreasing *p*H's faster than would be expected from the exposure time.

It can be concluded that the important effect of hydrophobic oxides is not in a better coupling between resist and silicon oxide, but in the decrease in the tendency of water to penetrate the resist-oxide interface.

Manuscript received Oct. 13, 1964; revised manuscript received Dec. 30, 1964. This paper was presented at the Washington Meeting, Oct. 11-15, 1964.

Any discussion of this paper will appear in a Discussion Section to be published in the December 1965 JOURNAL.

REFERENCES

1. Kodak, Photosensitive Resists for Industry, Industrial Data Book P-7, Eastman Kodak Co. (1962).
2. W. Steinmaier and J. Bloem, *This Journal*, **111**, 206 (1964).
3. J. R. Ligenza and E. I. Povilonis, Paper presented at the Washington Meeting of the Society, October 1964; W. C. Erdman and A. Androshuk, Paper presented at the Washington Meeting of the Society, October 1964.
4. T. Fort, Jr., and H. T. Patterson, *J. Colloid Sci.*, **18**, 217 (1963).
5. A. A. Bergh and M. L. White, To be published.

Strain Patterns in $GaAs_{(1-x)}P_{(x)}$ Alloy Overgrowths

R. Rosenberg

State University of New York, Stony Brook, New York

and M. Kozlowski, W. J. McAleer, and P. I. Pollak

Merck, Sharp and Dohme Research Laboratories,
Division of Merck & Company, Incorporated, Rahway, New Jersey

The objective of this note is to illustrate the occurrence of a particular type of strain pattern characteristic of $GaAs_{(1-x)}P_{(x)}$ alloy overgrowths on GaAs single crystal wafer substrates. The ultimate importance of such a strain field lies in its effect on the light emission characteristics of the heterojunction region because of disruption of crystal regularity and distortion of energy bands. Overgrowths were produced by vapor transport from GaAs and GaP charge chips to the substrate surface in an iodine ambient. The growth direction was <111>, the growth rate about 400Å/sec, and the growth surface gallium in all cases. Preparation of the wafers for observation in the <111> direction after growth consisted of removing the GaAs substrate base by lapping with a fine grit abrasive and then polishing opposite faces of the overgrowth with 0.25μ diamond paste. The strain patterns were observed by the birefringence technique and in the case of compositions transparent only to infrared lighting polaroid HR IR filters were used as polarizer and analyzer and observations made with an IR image converter tube.

Representative birefringence strain patterns are illustrated in Fig. 1 for a $GaAs_{0.8}P_{0.2}$ overgrowth. No strain was observed in pure GaAs overgrowths when viewed either parallel or transverse to the growth direction; that is, the fields were uniformly black under polarized light. The strain pattern produced in the alloy overgrowth when viewed in the <111> direction, as shown in Fig. 1a, consists of a regular block-type array of discontinuous lines which extends uniformly over the entire cross section. Figure 1b shows the strained region to extend from the original growth interface to the surface (the GaAs substrate is shown to be strain free.)

The strain was observed as a function of deposition temperature, overgrowth thickness, and overgrowth composition. Growth at 660°C (normal temperatures exceeded 800°C) did not eliminate the strain pattern, but increased the average block size suggesting a decrease in strain magnitude. Changes in overgrowth thickness did not appear to affect the strain pattern within limits of reproducibility between tests. Chem-

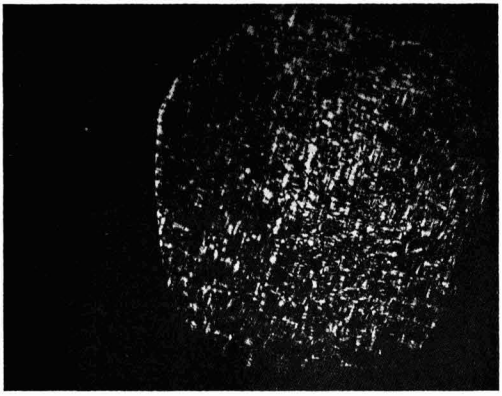

Fig. 1a. Strain pattern in $GaAs_{0.80}P_{0.2}$ alloy overgrowth produced by birefringence using polarized infrared light. Observation in <111> direction (growth direction).

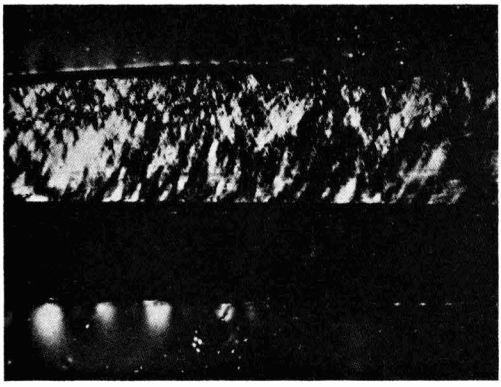

Fig. 1b. Cross-section transverse to <111> direction

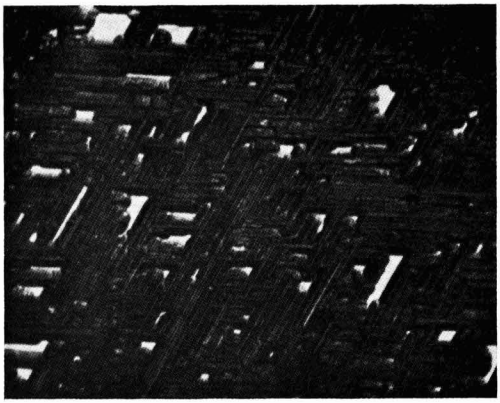

Fig. 2a. Etch-pit structure at the surface of alloy overgrowths. Slip line configuration in sample > 1 mm in thickness. Magnification approximately 100X.

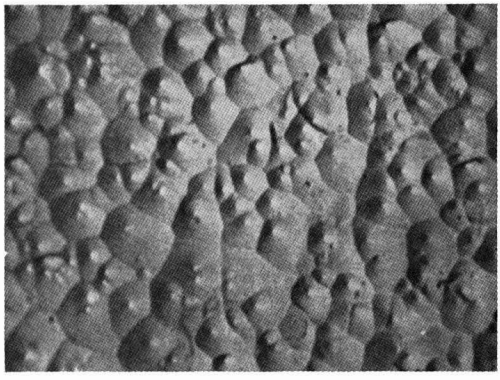

Fig. 2b. Random pits typical of thin overgrowths

ical etching of overgrowth surfaces revealed slip line configurations such as those of Fig. 2a in samples with overgrowths greater than 1mm thick, but random etch pit patterns in thinner samples, Fig. 2b. There did not seem to be a connection between the occurrence of slip and the birefringence pattern. Midrange overgrowth compositions, $0.40 < x < 0.60$, showed a tendency to fracture on cooling, with slight reduction in the observed residual strain. This was especially prevalent at low growth temperatures where release of elastic energy by deformation cannot readily take place. The strain pattern was already clearly defined in a 10% GaP alloy.

Relative rotation of the polarizer and analyzer with respect to the samples caused individual birefringence lines to be intermittently light and dark. This suggests a homogeneously distributed strain over the entire area rather than just within the observed pattern lines; the lines reflect the anisotropy produced in the crystal structure by the strain field.

Discussion

Three possible explanations can be suggested for formation of the strain pattern: lattice mismatch, thermal stresses and slip, and segregation. The lattice mismatch at the substrate overgrowth interface does not appear to be the most significant factor on several counts. First, the difference in lattice parameter between pure GaAs and pure GaP is about 4%; therefore the 10% GaP alloy has about a 0.4% mismatch (Vegard's law applies). Since the observed transition region in composition between substrate and overgrowth was found by x-ray analysis to be sufficiently broad to spread the mismatch over tens of micron distances, the resulting strain should be negligible. Second, the substrate was removed prior to observation so that the interface region was not present when observing strain patterns such as those depicted in Fig. 1a. Third, the transverse observation of Fig. 1b shows the field to extend over macroscopic distances, several orders of magnitude greater than expected on the basis of interface mismatch.

Stresses arise from thermal gradients during the cool-down period as the surface contracts more rapidly than the interior. The resulting tensile stresses, if sufficiently large, can produce slip structures such as those in Fig. 2a, or fracture in cases where slip is difficult. A recent observation by Gershenzon and Mikulyak (1) on a "pure" GaP overgrowth on GaAs showed a strain pattern similar to Fig. 1a. They attributed the pattern to the slip lines produced by the thermal stresses on cooling, relating the pattern to the familiar birefringence striations characteristic of bent crystals; also, it was argued that the strain lines were of the same orientation as slip plane traces. Several observations appear to indicate that cooling stresses were not the major cause of the strain patterns in the present work.

1. Strain patterns produced by cooling stresses usually take on a gross appearance, much like the fourfold symmetry birefringence as shown by Lederhandler (2) in silicon. The patterns in the sample of Fig. 1a and the rectangular-shaped specimen of Gerhenzon and Mikulyak were homogeneous over the entire cross section, including corners which should be most susceptible to stress concentration.

2. In the present work in which the growth direction was <111>, the strain pattern did not correspond to slip plane orientations.

3. The maximum effect of cooling should be at the outer surface of the overgrowth where the stresses are maximized. From Fig. 1b, however, it is apparent that the strain is uniform over the entire thickness of overgrowth.

4. Under exactly the same conditions of growth and cooling, pure GaAs overgrowths showed no strain patterns whereas alloy overgrowths did.

5. The GaAs substrate was found to be strain free even though the overgrowth was highly strained (see Fig. 1b). Both surfaces of the wafer were subject to approximately the same cooling rate.

The major cause of the observed strain as deduced from the findings seems to be a segregation effect. The presence of segregated impurities in silicon crystals was shown by Lederhandler (2) and Dash (3) to produce a fine striated birefringence pattern which was homogeneous with respect to the specimen cross section, much like the pattern found in the present work. As indicated by the strain-free GaAs overgrowths, the segregation effect was not produced by an impurity in the ambient or in the charge material; thus, it appears that it is the segregation of the alloy species As and P which occurs during growth (Ga segregation is probably not influential, again relying on the strain-free GaAs overgrowth). The segregation taking place must necessarily be of a local nature to give rise to the fine uniform strain pattern, and of small dimension as indicated by the homogeneous strain field suggested in a prior discussion concerning the effects of rotating the polarizer and analyzer. Segregation at sub-boundary walls is improbable on the basis that none were observed in the etch pit patterns of either the substrate or overgrowth. Also, it is difficult to conceive of segregation at individual dislocation sites causing the massive strain observed under polarization of IR or visible radiation. Two further possibilities are segregation of the species on specific habit planes, and short range ordering in the form of coherent islands, each island being consistent in composition and distribution within itself but differing from its neighbor such that a coherency strain would exist at the interfaces between islands; the sum of the local strains then appear as a long range strain. No direct evidence is available on which to base a mechanism at this time although it would seem that the driving force for segregation on habit planes should be low in this completely miscible system. Local ordering can be a result of the nucleation problem on the <111> growth surface. If it can be assumed that As, P, and Ga arrive at the surface at the same rate, then easy nucleation would give rise to a random distribution. In this case, however, the 4-atom, 2-layer triangular nucleus needed results in a nucleation problem. [Over-all growth of the nucleus occurs readily in a lateral <112> direction in the form of <110> zigzag chain units, as per Sangster (4)]. The number of stable nuclei will control the rate of growth of the surface layer. If the most stable nucleus is one which contains three atoms of P or As (the growth surface is Ga) rather than a composite, then the growth face will contain islands of GaAs and GaP nuclei. Lateral growth would then produce regions either high in As or P, with high stresses resulting in the planes of intersection between islands from lattice mismatch and differences in elastic thermal contractions on cooling. The stressed areas would be randomly oriented with respect to the growth surface and found throughout the thickness of the overgrowth, which seems to be the case. Since deposition is controlled by a chemical reaction of the growth surface, growth at low temperatures is characterized by fewer stable nuclei, slower growth, and larger and more uniform islands, resulting in a reduced strain field. Also, at the lower temperature the temperature gradients on cooling are less, decreasing contraction strains. Although experimental evidence directly confirming the above mechanisms is not available, the dependence of the strain pattern on segregation appears to be a reasonable explanation of the observations presented.

Manuscript received Oct. 19, 1964; revised manuscript received Dec. 29, 1964.

Any discussion of this paper will appear in a Discussion Section to be published in the December 1965 JOURNAL.

REFERENCES

1. M. Gershenzon and R. M. Mikulyak, *J. Appl. Phys.*, **35**, 2132 (1964).

2. S. R. Lederhandler, *ibid.*, **30**, 1631 (1959).
3. W. C. Dash, in "Growth and Perfection of Crystals," p. 383, J. Wiley & Sons, Inc., New York (1958).
4. R. C. Sangster, in "Compound Semiconductors, Vol. 1, Preparation of III-V Compounds," p. 241, Reinhold Publishing Co., New York (1962).

Thermal Expansion of GaSb at High Temperatures

J. C. Woolley

Department of Physics, University of Ottawa, Ottawa, Canada

Most of the available data on the thermal expansion of GaSb is for temperatures close to room temperature or below. Welker and Weiss (1) give a temperature coefficient α of 6.9 x 10^{-6}/°C without indicating the relevant temperature range; Sirota and Golobov (2) quote a mean expansion coefficient of 5.7 x 10^{-6}/°C over the range —100° to +20°C, whlie in a more detailed study Novikova and Abrikosov (3) have determined α as a function of temperature in the range 20-340°K and have shown a change in α from a negative value below 52°K to an almost constant value of about 6.5 x 10^{-6}/°C at 250°K and above. At temperatures above room, Bernstein and Beals (4) using an interferometric method with samples a few millimeters dimensions, give a value of α of 6.0 x 10^{-6}/°C up to 300°C. However they report that α increases rapidly above 300°C and they were unable to determine the expansion at 436°C.

It has been found (5) in electrical measurements on GaSb that the standard plot of log np/T^3 *vs.* $1/T$ shows a change in slope at approximately 450°C indicating different values of energy gap E_o above and below this temperature. It was thought therefore that a change in α at this temperature could indicate some phase change in GaSb, which would cause the change in E_o. Although x-ray powder photographs of GaSb taken at 560°C still showed a zinc blende type of line distribution (5), this did not rule out the possibility of some transition such as that from a zinc blende structure to a defect antifluorite structure, since both structures would give the same pattern of lines in a powder photograph and would differ only in the relative intensities of the lines (6).

In order to check the results of Bernstein and Beals and to extend them to higher temperatures, x-ray powder photographs have been obtained for GaSb samples in the temperature range 25°-600°C, a Unicam 19 cm high-temperature camera being used with CuKα radiation. From these photographs the change in lattice parameter of GaSb relative to its value at 25°C has been determined. Figure 1 shows the variation of δ as a function of temperature where $\delta = a_T - a_{25}/a_{25}$, a_T being the lattice parameter at temperature T and a_{25} the parameter at 25°C. It is seen that within the limits of experimental error the graph is linear, showing a constant expansion coefficient of $+(6.7 \pm 0.1)$ x 10^{-6}/°C in the temperature range 25°-600°C. There is no indication of any anomalous behavior in the range 300°-450°C and no evidence of any structure change.

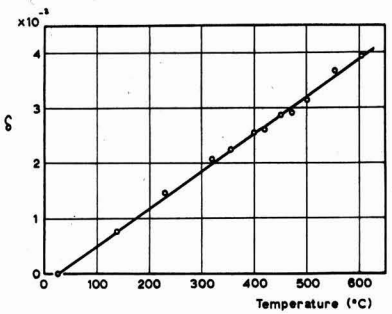

Fig. 1. Variation of δ as a function of temperature where $\delta = \frac{a_T - a_{25}}{a_{25}}$, a_T being the lattice parameter at temperature T and a_{25} the parameter at 25°C.

Acknowledgment

The author is grateful to Dr. W. B. Pearson of National Research Council, Ottawa, for the use of the high-temperature x-ray camera.

Manuscript received Oct. 28, 1964.

Any discussion of this paper will appear in a Discussion Section to be published in the December 1965 JOURNAL.

REFERENCES

1. H. Welker and H. Weiss, "Solid State Physics," Vol. 3, p. 51, F. Seitz and D. Turnbull, Editors, Academic Press, Inc., New York (1956).
2. N. N. Sirota and E. M. Golobov, *Doklady Akad. Nauk. SSSR*, **144**, 398 (1962).
3. S. I. Norikova and N. Kh. Abrikosov, *Sov. Phys. Solid State*, **5**, 1558 (1964).
4. L. Bernstein and R. J. Beals, *J. Appl. Phys.*, **32**, 122 (1961).
5. J. C. Woolley and C. M. Gillett, *J. Phys. Chem. Solids*, **17**, 34 (1960).
6. B. R. Pamplin, Thesis, Nottingham University, (1960).

The Heats of Fusion of InSb, InAs, GaAs, and InP

D. Richman and E. F. Hockings

RCA Laboratories, Princeton, New Jersey

During a study of the thermochemical properties of III-V compounds (1), information about their heats of fusion was needed. Only two compounds InSb (2, 3) and GaSb (2) have been measured by standard calorimetric methods. A rapid semiquantitative method has been used here to obtain the heats of fusion of InAs, GaAs, and InP. The application of standard techniques to these compounds is complicated by the high vapor pressures existing over the melts. This high pressure also necessitates making the measurements during the heating cycle, since quenching does not produce homogeneous, single phase materials.

The heats of fusion for the III-V compounds InSb, InAs, GaAs, and InP have been measured by a differential thermal analysis technique using apparatus of the type described by Gasson (4). Temperatures and temperature differentials were measured with Pt-Pt 13% Rh thermocouples whose outputs were displayed on an x-y recorder. Differential signals were amplified to provide a chart sensitivity of 20 μv/in. Heats of fusion were obtained from the areas of the DTA peaks after calibration with materials having known heats of fusion.

Table I. Properties of III-V compounds

Compound	Melting point, °C	Heat of fusion, kcal/mole This work	Heat of fusion, kcal/mole Other
InSb	525 ± 3	9 ± 3	12.2 ± 0.5 (2) 11.2 ± 0.4 (3)
InAs	942 ± 3	26 ± 3	
GaAs	1245 ± 5	21 ± 5	
InP	1058 ± 3	12 ± 3	15.2 (5)

The III-V compounds examined were in the form of crushed samples of single crystal, high-purity materials which had been prepared from stoichiometric melts. Heats of fusion and the melting points of these compounds are shown in Table I.

The heats of fusion for InAs and GaAs are higher than those for the other III-V compounds by an amount which exceeds the experimental error and the entropies of fusion for the arsenides are also high with respect to the other compounds. At their melting points the solids all have the zinc blende crystal structure. The liquids above the melting points can be considered as mixtures of group III atoms with monatomic and polyatomic group V species. The higher values for the entropies of fusion of the arsenides arise from differences in degree of association between arsenic and the other group V elements in these melts. Thus the observed heat of fusion of a III-V compound can be considered as composed of a heat of melting and a heat of association of the group V element.

Manuscript received March 26, 1964; revised manuscript received Jan. 8, 1965. This research was sponsored in part by the Electronics Research Directorate, Air Force Cambridge Research Center, Air Force Systems Command, under Contract AF19(604)-6152.

Any discussion of this paper will appear in a Discussion Section to be published in the December 1965 JOURNAL.

REFERENCES

1. D. Richman, *J. Phys. Chem. Solids*, **24**, 1131 (1963).
2. W. F. Schottky and M. B. Bever, *Acta Met.*, **6**, 320 (1958).
3. N. H. Nachtrieb and N. Clement, *J. Phys. Chem.*, **62**, 876 (1958).
4. D. B. Gasson, *J. Sci. Instruments*, **39**, 78 (1962).
5. M. Shafer and K. Weiser, *J. Phys. Chem.*, **61**, 1424 (1957).

Brief Communication

A Simplified Calculation of Tafel Slopes for Successive Electrochemical Reactions

G. H. Fraser[1] and R. G. Barradas

Lash Miller Chemical Laboratories, Department of Chemistry, University of Toronto, Toronto, Ontario, Canada

An electrochemical reaction may be a sequence of several elementary reactions involving one or more intermediates. To calculate the Tafel slope, if a particular step in the sequence were rate determining, the commonly employed method is to assume "quasi-equilibrium" for all preceding steps and thus to obtain the concentration of the intermediates as a function of overpotential (1, 2).

In an alternative treatment, Parsons (3) considered the passage of the representative point of a system over a series of free energy barriers. He derived the following expressions for the Tafel slopes of cathodic and anodic reactions, respectively

$$b_c = (\partial\eta/\partial \ln i)_{T,a_i} = -(\nu RT/\beta nF) - [(1-\beta)\nu/\beta nF](\partial p/\partial \ln i)_{T,a_i} - (\nu/nF)(\partial q/\partial \ln i)_{T,a_i} \quad [1]$$

$$b_a = (\partial\eta/\partial \ln i)_{T,a_i} = (\nu RT/(1-\beta)nF + (\nu/nF)(\partial p/\partial \ln i)_{T,a_i} + [\beta\nu/(1-\beta)nF](\partial q/\partial \ln i)_{T,a_i} \quad [2]$$

where a_i is the product of the activities of the reagents of the over-all reaction, n is the number of electrons involved in the over-all reaction, the stoichiometric number ν is the number of times the rate-determining step occurs when the over-all reaction occurs once, p and q are electrical work terms and η, i, β, R, T, and F have their usual significance.

In calculating Tafel slopes, most workers have preferred to use the quasi-equilibrium analysis rather than Parsons' treatment (*loc. cit.*), possibly because of uncertainty in handling the terms p and q. We shall show that these terms are really quite simple and that the method of Parsons is just as easy to use as the quasi-equilibrium treatment.

Calculations of Tafel Slopes

For the general electrochemical reaction

$$xX + gG^{+z} + ne = wW + cC^{+(gz-n)/c} \quad [3]$$

to occur, the electrochemical systems must pass over a series of free energy barriers (3, 4). Four states must be considered: namely, the initial state I, the final state F, the state P immediately before the highest free energy barrier and the state Q immediately after. The standard electrochemical free energies of these states are given by

$$\overline{G}_I^\circ = (x/\nu)\mu_x^\circ + (g/\nu)\mu_G^\circ + (gz/\nu)\phi_s F + (n/\nu)\mu_e^\circ - (n/\nu)\phi_M F \quad [4]$$

$$\overline{G}_F^\circ = (w/\nu)\mu_W^\circ + (c/\nu)\mu_c^\circ + [(gz-n)/\nu]\phi_s F \quad [5]$$

$$\overline{G}_P^\circ = \mu_P^\circ + (gz/\nu)\phi_s F - (n/\nu)\phi_M F + p \quad [6]$$

$$\overline{G}_Q^\circ = \mu_Q^\circ + [(gz-n)/\nu]\phi_s F + q \quad [7]$$

where ϕ_M is the inner potential of the electrode and ϕ_s that of the solution. p and q are the electrical parts of the standard free energies required to transfer the system from the state I to the state P and from the state F to the state Q, respectively. From these equations Parsons derived [1] and [2].

There are two sources of work in the terms p and q; namely, work done in the physical adsorption of an ion into the Helmholtz double layer, where it can be discharged, and work done in discharging an ion. The former is proportional to ψ, the potential of the Gouy-

[1] Present address: Johnson, Matthey and Mallory Ltd., Toronto, Ontario, Canada.

Helmholtz boundary of the double layer and the latter to $\Delta\phi$, where

$$\Delta\phi = \phi_M - \phi_s \quad [8]$$

Generalizing the analysis of Parsons, one derives

$$p = k^1\psi F + kF\Delta\phi; \qquad q = l^1\psi F + lF\Delta\phi \quad [9]$$

where k is the number of electrons which must be taken from the electrode to permit the rate-determining step to occur once and $(-l)$ is the number which must be removed to permit the products formed by the occurrence of one rate-determining step to be transferred to the final state F. k^1 and l^1 are defined in an analogous manner for the physical adsorption of ions. When

$$\eta = 0, \quad \Delta\phi = \Delta\phi_R$$

$$\eta = \Delta\phi - \Delta\phi_R \quad [10]$$

Therefore

$$(\partial p/\partial \ln i)_{T,ai} = kF(\partial\eta/\partial \ln i)_{T,ai} = kFb$$

and

$$(\partial q/\partial \ln i)_{T,ai} = lFb \quad [11]$$

For a process occurring on a cathode [3], the Tafel slope associated with any step proceeding in the forward direction is

$$b_c = -(RT/F)\,[k + \beta(l - k + n/\nu)\,]^{-1} \quad [12]$$

from [11] and [1]. Similarly, from [11] and [2], the Tafel slope associated with any step in a cathodic reaction proceeding in the reverse direction is

$$b_a = (RT/F)\,[(1-\beta)\,(l - k + n/\nu) - l]^{-1} \quad [13]$$

For processes occurring on anodes, the direction of the forward reaction is the opposite to that of cathodic processes, *i.e.*, anodic reactions proceed from the state formerly designated as F to the state I. We must now define l as the number of electrons which must be removed from the electrode to permit the rate-determining step to occur once, *i.e.*, to move the system from state F to state Q. Accordingly, $(-k)$ is the number of electrons which must be removed to permit the products of one occurrence of the rate-determining step to be transferred to the final state, namely to move the system from the state P to state I.

Using these new definitions of k and l, the Tafel slopes associated with any elementary reaction in an anodic process proceeding in the forward and reverse direction can be again given by [13] and [12], respectively. However, it is conventional to use the symbol β for the symmetry factor of the forward reaction (1). Therefore, for processes occurring on anodes, [13] is rewritten as

$$b_a = (RT/F)\,[\beta(l - k + n/\nu) - l]^{-1} \quad [14]$$

and by analogy, [12] as

$$b_c = -(RT/F)\,[k + (1-\beta)\,(l - k + n/\nu)\,]^{-1} \quad [15]$$

k and l are not necessarily integers. Consider the reaction scheme proposed by Conway and Bourgault (5) for the evolution of oxygen

$$M + OH^- = MOH + e \quad [16]$$

$$MOH + OH^- = MO + H_2O + e \quad [17]$$

$$MO + MOH = MHO_2 + M \quad [18]$$

$$MHO_2 + MOH = 2M + H_2O + O_2 \quad [19]$$

The [MOH] formed in [16] is converted to the final products in three ways: by [17] followed by [18] and [19], by [18] followed by [19], and by [19] alone. The first path involves an electron; the next two require no charge transfer. The average number of electrons required is 1/3, *i.e.*, $k = 1/3$. The analysis of this reaction scheme is shown in Table I as an example of the application of this method. The results agree with those of the quasi-equilibrium analysis performed by Conway and Bourgault (5).

Table I. Kinetic parameters

Rate-determining step	n	ν	l	k	b_a
[16]	4	3	0	1/3	$RT/\beta F$
[17]	4	1	−1	2	$RT/(1+\beta)F$
[18]	4	1	−3	1	$RT/3F$
[19]	4	1	−4	0	$RT/4F$

Thus the Tafel slope for an electrochemical reaction can be calculated by noting the number of electrons appearing before and after the rate-determining step.

The above treatment has, of course, the same limitations as Parsons' original treatment. It is applicable only when low-coverage Langmuir kinetic equations can be used, and when the current does not depend on ψ.

General Equivalence of the "Electron Count" Analysis to the Quasi-Equilibrium Analysis

$(n/\nu) - (k - l)$ is the number of electrons involved in the rate determining step. Let this quantity be m (m may be zero). For a rate-determining step in a cathodic reaction

$$i = A([I_1]^{x^1}[I_2]^{x^{11}}[I_3]^{x^{111}}\ldots)\exp(-m\beta\eta F/RT) \quad [20]$$

where A is a constant made up of the rate constant and the activities of the reagents, the I's represent intermediates formed by the discharge of reacting ions, and the x's represent the numbers of the corresponding intermediates appearing in the rate-determining step. The terms involving the intermediates may be symbolized by $[I]^X$. Therefore

$$i = A[I]^X \exp(-m\beta\eta F/RT) \quad [21]$$

In the quasi-equilibrium analysis, one obtains $[I]^X$ as a function of overpotential. The assumption of quasi-equilibrium implies that $\overline{G}_I = \overline{G}_P$, where these electrochemical free energies are no longer defined for the standard state. $\overline{G}_P$ can be obtained by adding a term $x(RT)\ln[I]$ to Eq. [6].

$$\overline{G}_P = \mu_P^o + x(RT)\ln[I] + (gz/\nu)\phi_s F - (n/\nu)\phi_M F + p \quad [22]$$

The activities of the reagents are considered to be constant. Therefore $\overline{G}_I$ differs from [4] only by constants. Thus

$$p = \text{constants} - x(RT)\ln[I] \quad [23]$$

From [23], [9] and [10]

$$[I]^X = (\text{constant})\exp(-\eta kF/RT) \quad [24]$$

Therefore

$$b_c = -(RT/F)\,(k + \beta m)^{-1} \quad [25]$$

which is identical to [12].

Similarly for anodic reactions

$$i = A[I]^X \exp(\beta\eta mF/RT) \quad [26]$$

$$q = \text{constants} - x(RT)\ln[I] \quad [27]$$

$$[I]^X = (\text{constant})\exp(-l\eta F/RT) \quad [28]$$

and therefore

$$b_a = (RT/F)\,(\beta m - l)^{-1} \quad [29]$$

which is identical to [14]. Thus the method of analysis developed in the previous section leads to the same Tafel slopes as in the quasi-equilibrium analysis.

Summary

The kinetic analysis of electrochemical reactions consisting of several steps, which was derived by Parsons, has not been widely used. By an extension of his treatment we have derived expressions by which

it is possible to calculate Tafel slopes merely by counting the number of electrons which are involved in various parts of the reaction, *i.e.*, those that appear before and those that appear after the rate-determining step, as well as the total number of electrons involved in the reaction. The stoichiometric number of each step must also be known. The general equations for the Tafel slopes of cathodic and anodic reactions, which we have derived, make Parsons' treatment just as convenient as the better known quasi-equilibrium analysis. It is shown that both treatments predict the same Tafel slopes.

Acknowledgments

The authors are indebted to the National Research Council of Canada and to the University of Toronto for financial assistance. One of them (G.H.F.) wishes to record his gratitude to the Province of Ontario Government for the award of a Postgraduate Fellowship.

Manuscript received Aug. 11, 1964; revised manuscript received Nov. 20, 1964.

Any discussion of this paper will appear in a Discussion Section to be published in the December 1965 JOURNAL.

REFERENCES

1. J. O'M. Bockris, *J. Chem. Phys.*, **24**, 817 (1956).
2. B. E. Conway, *Trans. Royal Soc. Canada*, **54**, (III), 19 (1960).
3. R. Parsons, *Trans. Faraday Soc.*, **47**, 1332 (1951).
4. J. O'M. Bockris, "Modern Aspects of Electrochemistry," pp. 180 *et seq.*, No. 1, Butterworth's, London (1954).
5. B. E. Conway and P. L. Bourgault, *Can. J. Chem.*, **37**, 292 (1959).

Manuscripts and Abstracts for Fall 1965 Meeting

Papers are being solicited for the Fall Meeting of the Society, to be held at the Statler-Hilton Hotel in Buffalo, N. Y., October 10, 11, 12, 13, and 14, 1965. Technical sessions probably will be scheduled on: Batteries (including Symposia on Charging Characteristics of Batteries and Characteristics of Electrodes during Charging), Corrosion, Electrodeposition (including Symposium on Thin Film Technology), Electronics-Semiconductors, Electrothermics and Metallurgy (including a Symposium on Zirconium and Its Alloys).

To be considered for this meeting, **triplicate copies of the usual 75-word abstract, as well as of an extended abstract of 500-1000 words** (see notice on page 112C of this issue), must be received at The Electrochemical Society, 30 East 42 St., New York, N. Y., 10017, *not later than May 17, 1965.* (Papers solely sponsored by the Corrosion Division **do not** require an extended abstract.) *Please indicate on 75-word abstract for which Division's symposium the paper is to be scheduled, and underline the name of the author who will present the paper.* No paper will be placed on the program unless one of the authors, or a qualified person designated by the authors, has agreed to present it in person. Clearance for presentation of a paper at the meeting should be obtained before the abstract is submitted. An author who wishes his paper considered for publication in the JOURNAL OF ELECTROCHEMICAL TECHNOLOGY should send triplicate copies of the manuscript to the Managing Editor of the appropriate publication 30 East 42 St., New York, N. Y., 10017. Concerning papers to be published in the JOURNAL, see notice on per page charge on page 105C of this issue.

Presentation of a paper at a technical meeting of the Society does not guarantee publication in the JOURNAL or ELECTROCHEMICAL TECHNOLOGY. However, all papers so presented become the property of The Electrochemical Society, and may not be published elsewhere, either in whole or in part, unless permission for release is requested of and granted by the Editor. Papers already published elsewhere, or submitted for publication elsewhere, are not acceptable for oral presentation except on invitation by a Divisional program Chairman.

FUTURE MEETINGS OF
The Electrochemical Society

★ ★ ★

San Francisco, Calif., May 9, 10, 11, 12, and 13, 1965

Headquarters at the Sheraton Palace

Sessions will be scheduled on Electric Insulation, Electronics (including Luminescence and Semiconductors and a Symposium on Optical Masers), Electro-Organic (including a Symposium on Industrial Organic Chemistry and a Symposium on Elucidation of Electro-Organic Electrode Processes jointly with the Theoretical Electrochemistry Division), Electrothermics and Metallurgy (including joint Symposium on Molten Salts jointly with the Theoretical Electrochemistry Division and, also, a Symposium on Strengthening Mechanisms in Nonmetallics), Industrial Electrolytic (including a Symposium on Electrolytic Diaphragms and Battery Separators jointly with the Battery Division and, also, a Symposium on the Production of Chlorine without Caustics)

★ ★ ★

Buffalo, N. Y., October 10, 11, 12, 13, and 14, 1965

Headquarters at the Statler-Hilton Hotel

Sessions probably will be scheduled on Batteries (including symposia on Charging Characteristics of Batteries and Characteristics of Electrodes during Charging), Corrosion, Electrodeposition (including Symposium on Thin Film Technology), Electronics—Semiconductors, Electrothermics & Metallurgy (including a Symposium on Zirconium and its Alloys)

★ ★ ★

Cleveland, Ohio, May 1, 2, 3, 4, and 5, 1966

Headquarters at the Sheraton-Cleveland Hotel

★ ★ ★

Philadelphia, Pa., October 9, 10, 11, 12, and 13, 1966

Headquarters at the Sheraton Hotel

★ ★ ★

Dallas, Texas, May 7, 8, 9, 10, and 11, 1967

Headquarters at the Hilton Hotel

★ ★ ★

Papers are now being solicited for the meeting to be held in Buffalo, N. Y., October 10, 11, 12, 13, and 14, 1965. **Triplicate copies of the usual 75-word abstract, as well as of an extended abstract of 500-1000 words** (see notice on p. 112C of this issue), are due at The Electrochemical Society, 30 East 42 St., New York, N. Y. 10017, *not later than May 17, 1965 in order to be included in the program.* (Papers sponsored solely by the Corrosion Division **do not** require an extended abstract.) *Please indicate on 75-word abstract for which Division's symposium the paper is to be scheduled, and underline the name of the author who will present the paper.* No paper will be placed on the program unless one of the authors, or a qualified person designated by the authors, has agreed to present it in person. Clearance for presentation of a paper at the meeting should be obtained before the abstract is submitted. An author who wishes his paper considered for publication in the JOURNAL or ELECTROCHEMICAL TECHNOLOGY should send triplicate copies of the manuscript to the Managing Editor of the appropriate publication, 30 East 42 St., New York, N. Y., 10017. Concerning papers to be published in the JOURNAL, see notice on per page charge on page 105C of the issue.

Presentation of a paper at a technical meeting of the Society does not guarantee publication in the JOURNAL or in ELECTROCHEMICAL TECHNOLOGY. However, all papers so presented become the property of The Electrochemical Society, and may not be published elsewhere, either in whole or in part, unless permission for release is requested of and granted by the Editor. Papers already published elsewhere, or submitted for publication elsewhere, are not acceptable for oral presentation except on invitation by a Divisional program Chairman.

Current Affairs

San Francisco Meeting of the Society May 9-14, 1965

The Spring Meeting of The Electrochemical Society will be held from May 9 through 14 in San Francisco, Calif., at the Sheraton Palace Hotel. The complete program for the meeting appeared in the March 1965 issue of the JOURNAL, pp. 47C-91C.

San Francisco owes much of its individuality to three natural endowments: its site, topography, and climate.

The city occupies a 46 square mile fingertip between the Pacific Ocean and one of the world's greatest natural harbors. Being thus confined has caused San Francisco, like Manhattan, to grow up rather than out and kept its distinctive urbanity intact.

Since temperatures seldom rise above 75° or drop below 45°, cool weather clothes are comfortable summer and winter. In May, you will find clear, sunny days and a spring-like crispness to the air; the average maximum temperature of this season is 63.4°, the average minimum 50.8°. Rain is a rarity in May.

There are more than a dozen art museums and galleries in the city. As the acknowledged cultural capital of Northern California, it is also devoted to the performing arts. In addition to a glittering opera season, San Francisco has its own symphony orchestra and ballet, legitimate playhouses presenting the best of Broadway and London; an annual International Film Festival; innumerable movie theaters, many specializing in foreign and art films, and a flock of professional caliber repertoire theater groups.

San Francisco's compactness is an advantage to sightseers; much of it can be seen conveniently on foot.

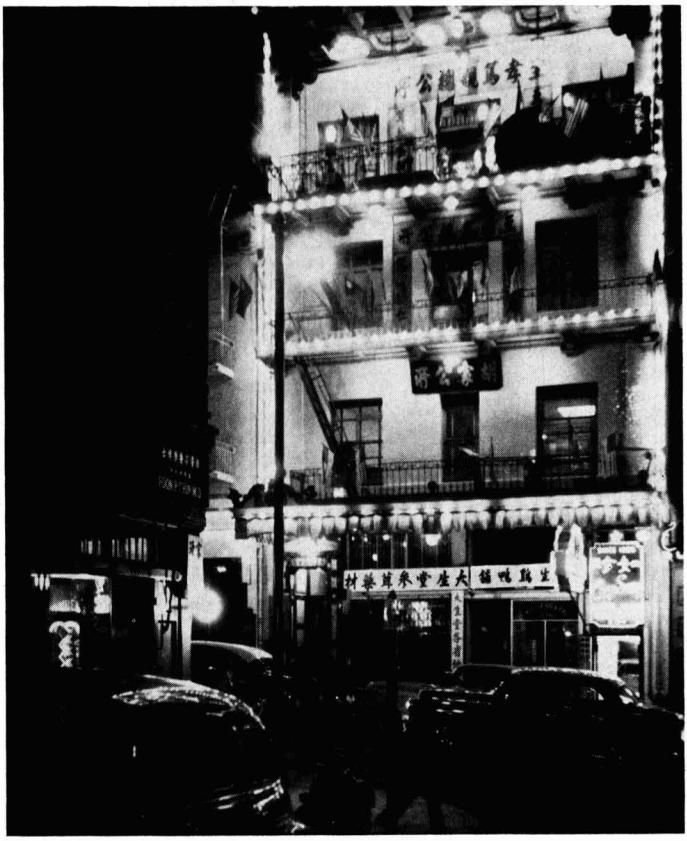

San Francisco's Chinatown

There's Nob Hill for example; the hill's two highest hotels have rooftop skyrooms where the cocktails come with an intoxicating view. And, of course, there are the cable cars which will take you there. Both the Golden Gate and Bay Bridges should be crossed and the attractions on the opposite shores explored—not the least of which are Marin County's Mediterranean-like boating communities with their many open deck restaurants . . . And last, but not least, San Francisco's Chinatown is a place not to be missed. Chinatown's main stream, Grant Avenue, is lined with up-curved roofs, dragon-entwined lampposts, shops crammed with Oriental merchandise, and restaurants serving exotic dishes.

One of the interesting features of the technical part of the meeting will be an Educational Lecture Series sponsored by the Electrothermics and Metallurgy Division. For additional information see the March issue for complete details.

Telephone Message Center

The Pacific Telephone and Telegraph Co., will make available to Members and Guests attending the ECS Meeting in San Francisco, a Telephone Message Center.

A staff of trained personnel will take messages for participants of the meeting during convention hours.

A special telephone number, area code 415-421-0900, is assigned to the Message Center. The Message Center will take incoming calls only. No outgoing calls may be made from the Message Center.

Messages will be posted in the Message Center area.

Division News

Electronics Division

The nominating committee has prepared a slate of candidates for the new officers of the Electronics Division. All candidates have express the willingness to serve. The election will be held at the Spring 1965 San Francisco Meeting of the Society.

The following is a list of candidates:

ECS San Francisco Local Committee

Ray A. Zimmerly

J. F. Aicher

Francis J. Bowen

Herbert Bandes

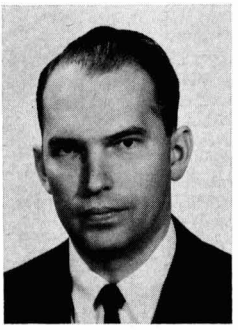

Bruce E. Deal

Donald V. Doub

Mrs. C. Tobias

Members of the Convention Committee under General Chairman Ray A. Zimmerly are: J. F. Aicher (Finance); Francis J. Bowen (Registration); Herbert Bandes (Entertainment); Bruce E. Deal (Arrangements); Donald V. Doub (Secretary); and Mrs. C. Tobias (Ladies' Committee).

Chairman—F. Hubbard Horn, General Electric Co., Research Labs., P.O. Box 1088, Schenectady, N.Y.

Vice-Chairman (General Electronics)—David E. Kinney, General Electric Co., 1099 Ivanhoe Rd., Cleveland, Ohio.

Vice-Chairman (Luminescence)—Paul Goldberg, General Telephone & Electronics Labs., Bayside, N.Y.

Vice-Chairman (Semiconductors)—Morton E. Jones, Semiconductor Exploration Lab., Texas Instruments Inc., P.O. Box MS 130, Dallas, Texas.

Secretary-Treasurer—Henry F. Ivey, 401-3B4, Westinghouse Research Labs., Pittsburgh, 35, Pa.

Additional nominations may be made by a petition signed by five members of the Division and that such petition must be in the hands of the Chairman of the Nominating Committee Robert J. Ginther, 5507 Myrtle Ave., Washington 22, D.C., at least ten days prior to the date of election May 12, 1965.

Austin E. Hardy,
Chairman

Theoretical Electrochemistry Division

The list of nominees for officers of the Theoretical Electrochemistry Division is:

Chairman—S. Schuldiner, 3101 P St., S. E., Washington, D. C.

Vice-Chairman—D. A. Vermilyea, General Electric Research Labs., P. O. Box 1088, Schenectady, N. Y.

Secretary-Treasurer—C. G. Enke, Frick Chemical Lab., Princeton University, Princeton, N. J.

Members of the Executive Com-

Page Charge Adopted for the JOURNAL

Increased costs of publication have made it necessary for The Electrochemical Society to institute a per page charge for publication in the JOURNAL.

At the Meeting of the Board of Directors held in New York on September 29, 1963 a charge of $35.00 per printed page was established by the Board of Directors, on recommendation of the Publication and Finance Committees, for papers published in the JOURNAL. This action becomes effective for papers received after February 1, 1964.

A 10% reduction in the page charge will apply to papers authored by one or more members of The Electrochemical Society and/or by one or more employees of Patron or Sustaining Members of the Society.

Papers are accepted for publication on the basis of merit by established practices of review. Acceptance of future papers for publication will not be dependent on payment of this invoice. Where funds are not available for payment of this charge it will be waived by The Electrochemical Society.

mittee—R. E. Meredith, Chemical Engrg. Dept., Oregon State College, Corvallis, Ore., and Manfred Breiter, General Electric Co., Res. Labs., P. O. Box 1088, Schenectady, N. Y.

At the Annual Business Meeting of the Theoretical Division to be held in San Francisco action will be taken on proposed amendments to the present Bylaws of the Division. This notice of change in Bylaws is in compliance with the requirements of the existing Bylaws of the Division.

D. A. Vermilyea,
Secretary-Treasurer

Section News

Boston Section

The forty-sixth meeting of the Boston Section was held on Thursday, January 21, 1965 at the Ledgemont Laboratory of the Kennecott Copper Corp., Lexington, Mass. Mr. Owen Meeghan, Corporation Counsel, Sylvania Electric Products, Inc., Danvers, Mass., presented an interesting talk on the "U.S. Patent System." He emphasized the legal technicalities and principles of the patent system, pointing out that a patent is the property of the inventor and that assignment of it to a company is equivalent to a sale. He discussed the reasoning which motivates the patent attorney to encompass a broad technical area in the claims of a patent. Under the U.S. system, the "patent pending" label offers no protection, since patent rights take effect at the date of issue. The speaker also discussed aspects of trade secrets as they affect technical people and noted that only 40 to 45 percent of patents which are litigated are held to be valid.

M. D. Banus,
Secretary

Indianapolis Section

The Indianapolis Section held its second meeting of the season on Wednesday, January 27, 1965. Dr. Harold J. Read, Vice-President of the Society, spoke on "Recent Developments in Electroplating." Before his talk, Dr. Read gave a brief review of recent activities at the Society Headquarters.

Dr. Read's talk covered a wide range of subjects. Examples of electron microscope studies of electroplated nickel, tin and brass and electroless nickel were given. The structure of plated tin coatings was compared with their ability to fuse properly. Electroplated brass which gave a uniform coating initially and then appeared to have migrated was described with the help of electron micrographs taken after very short plating times. Some anomalous relationships between hardness and ductility in electrodeposited and electroless nickel were presented. Evidence of semiconductor properties in electroplated manganese-aluminum alloys were demonstrated. The meeting ended with a lively discussion.

Lowell F. Howard,
Secretary

Pittsburgh Section

To fill a vacancy created when the Pittsburgh Section Vice-Chairman, Dr. G. K. Notman, returned to England, the Executive Committee met and appointed J. R. Conner as Vice-Chairman and M. G. Vucich as Secretary-Treasurer for the remainder of the year 1964-1965, in accordance with Section 5, Article III of the Section Bylaws.

On Monday, January 25, 1965, a joint meeting of The Electrochemical Society and the American Chemical Society, Pittsburgh Sections, was held at Carnegie Institute of Technology, Pittsburgh Pa. The speaker was Dr. Morris Cohen, National Research Council, Ottawa, Canada. Dr. Cohen's most interesting talk on "Anodic Oxide Films on Iron" was well attended. The talk was preceded by a dinner at Stouffer's Restaurant.

J. R. Conner,
Secretary-Treasurer

Southern California-Nevada Section

The Southern California-Nevada Section met on January 26, 1965, at the Roger Young Auditorium in Los Angeles to hear Dr. Ernest Yeager discuss "Fundamental Aspects of Fuel Cells." Dr. Yeager discussed fundamental problems associated with various types of cells, with particular emphasis on hydrogen-oxygen type cells. Present status of alkali metal, alcohol, and various hydrocarbon cells were considered.

Notice to Members

April 1 is Cut-Off Date

All ECS members are required to remit dues by April 1 if names are to be retained on 1965 mailing lists. This cut-off date is in accordance with the Constitution of the Society, Article III, Section 9: "Any member delinquent in dues after April 1 of each year shall no longer receive the Society's publications . . . ." and no exceptions can be made. Members who have not sent in 1965 payments were mailed a second notice on February 5 and are urged to make payment promptly in order to avoid delay in receipt of JOURNALS.

The Section is planning to hold a two day conference on the effects of defects in the creptalline state on the optical and conductivity properties of materials at the UCLA Lake Arrowhead Lodge during September 19-21, 1965. Mr. Ted La Chappelle was appointed conference Chairman and should be contacted for details. A Symposium on Advances in Battery Technology is being planned for late 1965. Dr. C. Berger is Chairman of this one day meeting.

Two interdivisional meetings were held on January 22 and February 11, 1965 at UCLA. Dr. J. S. Newman spoke on "Polarized, Diffused Double-Layers" at the first meeting and Professor T. Kuwana spoke on "Electro-Illuminescent Processes" at the second meeting.

Dr. D. N. Benion was appointed Chairman of the Theoretical Electrochemistry Division of the Section.

C. M. Botchek,
Secretary-Treasurer

Obituaries

Samuel C. Lind

Dr. Samuel Colville Lind, internationally known pioneer in radium chemistry, drowned on February 13 while trout fishing in the Clinch River near Oak Ridge, Tenn.

Dr. Lind invented the interchangeable electroscope for radium measurements and originated the ionization theory of the chemical effects of radium rays.

He served in recent years as a senior consultant to the Atomic Energy Commission's Oak Ridge National Laboratory.

Dr. Lind was elected president of The Electrochemical Society (American Electrochemical Society) in 1927.

I. Melville Stein

I. Melville Stein, former president and chairman of the Board of Directors of Leeds & Northrup Co., Philadelphia, Pa., died on Sunday, January 24 in Germantown Hospital, Philadelphia. He was 70.

Mr. Stein, who was born in Long Branch, N. J., attended Edison Technical School and Columbia University.

He joined Leeds & Northrup in 1919 after serving during the war years as a personal assistant to Thomas A. Edison, the chairman of the Naval Advisory Board. Mr. Stein served successively as a sales engineer, manager of technical sales, director of research, and vice-president before becoming executive vice-president in 1951.

In July 1953 he became president of the firm, holding this post until September 1963 when he was elected chairman of the Board. He resigned as chairman and as a director of the

company in May 1964 after reaching, as he put it, "my goal for complete retirement at the age of 70."

Among the honors held by Mr. Stein were an Emeritus Membership in The Electrochemical Society, an honorary Doctor of Science degree from Rensselaer Polytechnic Institute, a presidental certificate of merit and distinguished life memberships in the American Society for Metals and the Instrument Society of America. In 1961, he was the recipient of the "Engineer of the Year" award from the Philadelphia chapter of the National Society of Professional Engineers. He also held the Award for Outstanding Contributions to the Advancement of Art and Science of Management conferred by the Philadelphia Chapter of the Society for Advancement Management. A former director of the Scientific Apparatus Makers Association, Mr. Stein received the organization's 1964 annual award in recognition of his leadership in the growth of the scientific instrument industry.

Mr. Stein was a Fellow of the Institute of Electrical and Electronic Engineers, the American Society of Mechanical Engineers, and the American Association for the Advancement of Science. Prior to relinquishing his duties in May of 1964, Mr. Stein was chairman and a member of the Board of Directors of Leeds & Northrup's international subsidiary companies in Canada, England, and Italy. He held 14 patents in the field of measuring and control instruments and authored numerous technical papers.

Mr. Stein is survived by his wife, the former Grace Lawton of Philadelphia, a daughter and a grandson.

News Item

Corrosion Week

A symposium on corrosion designated "Corrosion Week" will be held in Brussels, Belgium, June 7-11, 1965 under the auspices of the Belgium Center for Corrosion Studies (CEBELCOR), the European Federation of Corrosion, and the International Committee for Electrochemical Thermodynamics and Kinetics. The first half of the week will be devoted to a discussion of corrosion in the building and public works industry. The second half will be concerned with fundamental research in the electrochemistry of corrosion reactions and practical applications to corrosion studies. Papers are invited covering corrosion control of heating systems, cold and hot water distribution systems, roofing, curtain walls, reinforced and pre-stressed concrete, and metal structures in general. Similarly, papers are invited dealing with electrochemical methods for the study of corrosion reactions of metals and alloys in general, as well as of metallic, inorganic, and organic coatings.

Papers will be presented in either English, French, Dutch, or German. Further information can be obtained from Dr. Marcel Pourbaix, Manager of CEBELCOR, 24, Rue des Chevaliers, Brussels, Belgium.

Submitted by H. H. Uhlig

Calendar of Events

Other Organizations

Frontiers in Chemistry lectures will be held at the Western Reserve University, Cleveland, Ohio, April 2, 9, and 23, 1965.

The First International Conference on Crystal Growth to be held in Boston, Mass., June 20-24, 1966.

The 16th Meeting of C.I.T.C.E. will be held in Budapest, Hungary, Sept. 5-10, 1965.

The 20th Annual International ISA Conference & Exhibit on Instrumentation, Systems, and Automatic Control will be held in Los Angeles, Calif., Oct. 4-7, 1965.

The International Conference on Energetics sponsored by the American Society of Mechanical Engineers will be held at the University of Rochester, Rochester, N. Y., Aug. 18-20, 1965.

New Books

"Proceedings of the 18th Annual Power Sources Conference." Published by PSC Publications, P. O. Box 891, Red Bank, N.J., 1964. 186 pages; $10.00.

These are the collected papers presented at the May 1964 Conference at Fort Monmouth, N. J. Twelve papers were presented in the sessions on Fuel Cell Batteries; eight were presented on Primary and none on Secondary Batteries; seven papers were presented on Electrical to Electrical Energy Conversion; nine papers were presented on Thermal Energy Conversion; and four on Solar Energy Conversion. Most papers list references.

"Chemical Transport Reactions," by Harold Schäfer. Published by Academic Press, New York, 1964. 161 pages; $6.80.

This is the updated and partially revised English translation of the 1962 German edition. The author is concerned with chemical transport, the formation of volatile unstable intermediates which after vaporization break down to reform the original substance. The effect is that of distillation or sublimation of materials with low vapor pressures. ECS members will be interested in the section on preparation of single crystals.

"Handbook of Electron Beam Welding," by R. Bakish and S. S. White. Published by John Wiley & Sons, Inc., New York, 1964. 269 pages; $11.50.

Chemical or Electrical Engineer

Experienced in storage battery manufacturing Southwest U. S. area. Mail details of education, experience, and personal background to *Box A 304*, c/o The Electrochemical Society, Inc., 30 East 42 St., New York, N. Y., 10017.

Book Reviews

"Standard Aqueous Electrode Potentials and Temperature Coefficients at 25°C," by A. J. de Bethune and N. A. S. Loud. Published by Clifford A. Hampel, 8501 Harding Ave., Skokie, Ill. 19 pages; $1.95 + 8 cents postage (also available at college bookstores).

The tabular storage of exact thermodynamic data for the chemical substances is of great importance in predicting the possibility and extent of reactions. The use of electrode or half-cell potentials and their temperature coefficients makes it possible to condense such information into extremely compact form. The present booklet of only 19 pages (large ones, 21.6 x 28 cm) contains useful material out of all proportion to its size.

The 9-page table of potentials lists 467 half cell reactions for 90 elements and their most common compounds, with temperature coefficients in most cases and the second derivative where possible. The potentials are from direct measurements or calculated from other data. All partial reactions are written as oxidations. The potentials are given the experimentally observed sign (D. C. polarity) of the appropriate electrode *vs.* the standard hydrogen electrode (an eminently sound system since, fortunately, standard cells

and potentiometers are labeled uniformly throughout the world). This is sometimes called the I.U.P.A.C.-Gibbs-Stockholm system; the "European" system.

"Isothermal" temperature coefficients are listed and assume the value zero for the standard hydrogen electrode at all temperatures. "Thermal" temperature coefficients are also given and assume the coefficients +0.871 mv/°C for the hydrogen electrode (the exact value is open to some question since it ignores thermal liquid junction potential in saturated KCl, influence of Soret effect and the negligible thermoelectric potential in the metallic leads.)

The table of potentials appeared in "Encyclopedia of Electrochemistry" (Reinhold Publishing Corp., 1964). In the booklet it is accompanied by a table of thermodynamic data for water, its elements and ions; and a table of third law entropies and heat capacities for 91 elements. Dr. de Bethune has written an introduction and exposition of the use of the data (7 pages) which is lucid, definitive and immensely useful in showing what calculations can be made and how to make them. Examples illustrate calculation of the free energy and enthalpy of formation; entropy and heat capacity of ions and compounds; water constant, solubility products and other equilibria and their temperature coefficients; entropy transport in thermal cells, *etc.*

This booklet can be highly recommended for students and teachers of physical chemistry at all levels; it can serve as an excellent basis for the study of this phase of thermodynamics and for the formulation and solving of both easy and difficult problems. Further, since the authors have taken particular care to obtain the most reliable data available and have presented the values to the appropriate degree of precision, research workers can employ them without hesitation. There are no typographical errors of any consequence and evidently every effort has been made to eliminate any kind of error.

C. V. King
American Gas & Chemicals, Inc.

"The Encyclopedia of Electrochemistry," Edited by Clifford A. Hampel. Published by Reinhold Publishing Corp., New York, 1964. 1206 pages; $35.00.

This book is an encyclopedic presentation of over 360 articles that pertain to the science and technology of electrochemistry and closely related subjects. The editor has succeeded admirably in the formidable task of securing authoritative contributions from 271 collaborators who are identified and listed with their assigned topics. His contributors are well known, respected and qualified. An interesting and appropriate feature of the book is the inclusion of biographical sketches of 48 scientists who, during the past 200 years, have made basic and notable contributions to electrochemistry. Another important feature is presentation of the most complete and up-to-date table of electrode potentials and temperature coefficients that has been compiled. There is a table of the oxidation potentials of the elements. There is a concise exposition of the conventions governing the algebraic sign of the electrode potential.

The articles are specific, informative, and short. This is well illustrated in the treatment of the broad subject of corrosion and corrosion control. There are more than 30 articles on discrete aspects of corrosion no one of which exceeds 4000 words; yet taken together they require more than 80 pages for presentation. The book provides a ready source of information on all aspects of electrochemistry as well as on topics which physical scientists in general and electrochemists in particular will find useful when they need brief authoritative information outside their areas of specialization. All articles provide references for anyone who may wish to pursue the subjects further.

Space does not permit mention of more than a small fraction of the topics covered in the book. One finds, as expected, all of the basic aspects of electrochemistry both scientific and technological. The variety of related subjects is indicated by the following topics: lasers, plasmas, electron beam welding and melting, bioelectrogenesis, fuel cells, xerography, electrolytic restoration of ancient metals, Electron Paramagnetic Resonance, Flade potential, electrophysiology, electrochromatography, electrocardiology, electrostatic coating processes, dielectrophoresis, electroencephalography, electrostriction, ferroelectricity, thermoelectric thermometry, thermoelectric power generation, solar energy converters, magneto-hydrodynamics, *etc.* The reader will be delighted to find how readily he may become knowledgeable on the varied and timely topics of which the foregoing are representative.

Teachers and students, as well as practicing scientists and engineers, will find that the book meets its objective "to be helpful to those seeking an introduction to new areas of science, those looking at some unfamiliar facets of their own general field of physical science, or those wishing to refresh their knowledge of a specific subject."

This is a 1200-page book, well printed and sturdily bound. As an encyclopedia in an important area of science and technology it will be a useful addition to the professional man's library whether he be in academic, governmental or industrial work.

R. M. Burns

(Note: A brief review of "The Encyclopedia of Electrochemistry" appeared in the January 1965 JOURNAL. *We are happy to publish this additional information.—Ed.)*

"Recent Progress in Surface Science, Vol. I," Edited by J. F. Danielli, K. C. A. Pankhurst, and A. C. Riddiford. Published by Academic Press New York, 1964. 414 pages; $16.00.

This first volume of what is intended to be a serial publication presents 11 articles on various phases of surface science. Of these, ECS members will be most interested in the articles by D. A. Haydon on the Electrical Double Layer, Sigmund Schuldiner on Electrode Processes, C. V. King on Corrosion of Metals, and perhaps in the article by E. Tannenbaum Handelman on the Chemistry of the Semiconductor Surface. The articles appearing are as follows:

M. Joly—Surface Viscosity

J. A. Kitchener—Foams and Free Liquid Films

W. Black—Surface-Active Substances

W. D. Stein—Facilitated Diffusion

E. J. Ambrose—Cell Contacts

E. H. Mercer—External Surface of the Cell and Intercellular Adhesion

P. Mueller, D. O. Rudin, H. T. Tien, and W. C. Wescott—Formation and Properties of Bimolecular Lipid Membranes

Haydon's article on the Double Layer omits discussion of the metal/solution interface, and the semiconductor/aqueous solution interface. The Gouy-Chapman equations are

TECHNICAL SERVICE ENGINEER

For Metal Plating of Plastics

To provide field service to electro-platers, molders and end users; conduct seminars and make presentations to conferences and customers; participate in product development for plating field.
B.S. degree in engineering or chemistry 3-5 years experience with two years in metal plating.
Rapid development of Cycolac brand ABS plastic in metal plating has created this exceptional opening. MARBON—the growth division of Borg Warner Corporation—has an excellent achievement record.
Send resume and salary history to N. H. Petersen, Manager of Professional Employment, *MARBON CHEMICAL*, Division of Borg-Warner Corporation, P. O. Box 897, Parkersburg, West Virginia.

Equal Opportunity Employer

derived and various improvements and corrections are discussed. Experimental data are given for comparison with theory. The Stern equation is discussed together with Grahame's modifications. The double layers at air/water, hydrocarbon/water, and silver halide/solution interfaces are then discussed in the light of recent experimental results and theoretical developments.

Schuldiner's article on Electrode Processes is essentially a noncritical review covering the development of measurement techniques and of kinetic theories during the period 1955-1961 and a review of work on the electrolytic hydrogen reaction. The discussion is descriptive and almost completely nonmathematical. Metal deposition and corrosion, anodic processes, such as oxygen and halogen evolution, and work in fused salts and in other nonaqueous media are not covered. In the section on Measurements, most of the discussion concerns the interrupter technique, potentiostatic techniques, and alternating current and galvanostatic methods. From the number of new developments in hydrogen overvoltage theory as well as the repeated revivals of older theories, in one form or another, it is apparent that the late D. C. Grahame was over optimistic in 1952 when he concluded that the problem of hydrogen overvoltage was solved.

King's article on Corrosion is restricted to a survey of metallic corrosion in aqueous media, omitting such topics as stress corrosion, high temperature oxidation, *etc.* The approach is didactic and the material presented is explained, discussed, interpreted, and occasionally criticized. Much specific information is presented. The special topics discussed are the interpretation of polarization curves, cathodic polarization, anodic passivation and polarization, the use and effect of nonoxidizing inhibitors, and transport-controlled dissolution.

Handleman's very brief article on the Chemistry of Semiconductor Surfaces develops some of the necessary concepts and terminology. The subheadings mentioned are Atomically Clean Germanium and Silicon Surfaces, Catalysis, Compound Semiconductors, and Organic Semiconductors.

H. W. Salzberg

"Ellipsometry in the Measurement of Surfaces and Thin Films." Edited by E. Passaglia, R. R. Stronberg, and J. Kruger. Published by the National Bureau of Standards, Washington, 1964. 359 pages; $2.25.

This book consists of the collected papers of a symposium of the same title held in Washington in September 1963. The papers and their discussion were presented by an international group and give an up-to-date version of the "state-of-the-art." Although there has been an attempt to separate theory and techniques from the experimental applications, there is considerable overlap in the introductions to all the papers. About one-third of the papers deal directly with the oxidation and corrosion of metals. Others treat adsorption from both gases and solutions. The book should be of interest to all members of the Society who deal with the formation of thin films on solid surfaces.

M. Cohen
National Research Council

Announcements from Publishers

"Research and Development on Advanced Graphite Materials, Vol. XXXIV, Oxidation-Resistant Coatings for Graphite," Report AD 606 892N,* $4.00.

"X-Ray Diffraction Microscopy of Imperfections in Semiconductor Crystals," Report AD 608 335N;* $5.00.

"Research on Applications of Krypton-85 and Other Radioactive Isotopes," Report NYO-2906-1N,* $1.75.

"Effects of Purity and Structure in Arc-Melted Tungsten," Report N64-33085N,* $1.25.

"Tungsten-Oxygen Vapor Species," Report AD 608 103N,* $2.00.

"Hot-Salt Stress-Corrosion Cracking of Titanium Alloys," Report N64-32829N,* $1.25.

* Order from Office of Technical Services, U. S. Department of Commerce, Springfield, Va., 22151.

Advertiser's Index

Now With Guaranteed Upper Limit To The Residual Current

ULTRA-PURE EUTECTIC SALTS

For basic and applied electrochemical research, Anderson Physics Laboratories now offers ultra-pure eutectics and salt mixtures. Available are dehydrated and purified LiCl, and eutectic mixtures of LiCl-NaCl, LiCl-KCl, LiCl-CsCl and LiCl-LiF. All salts are shipped in sealed Pyrex or fused silica ampoules, and have a guaranteed upper limit to the residual current.

Also available are high-purity alkali halides and custom-purification of other salts to your specifications. For complete information, write or call

ANDERSON PHYSICS LABORATORIES, INC.

Box 177, Station A Champaign, Illinois 61824

Phone (217) 356-1347

Buffalo, N. Y. Meeting Symposia

Battery Symposium Plans

The Battery Division of the Society is planning symposia on "Charging Characteristics of Batteries" and on "Characteristics of Electrodes During Charging" for the 1965 Fall Meeting in Buffalo, N. Y., October 10-14, 1965. General sessions are also planned.

Triplicate copies of the usual 75-word abstract, as well as of an extended abstract of 500-1000 words (see notice p. 112C of this issue) should be sent to The Electrochemical Society, 30 East 42 St., New York, N. Y., 10017, or to Mr. T. J. Hennigan, Goddard Space Flight Center, Code 636-2, Greenbelt, Md., 20771, *not later than May 17, 1965.*

Corrosion Symposia Plans

General Sessions

Inasmuch as the symposia this year are rather specific in nature it is both anticipated and hoped that more papers than usual will be submitted for the general sessions. Authors who have material for a paper which does not fit in with one of the symposia are urged to submit it for the general session.

Any inquiries or suggestions regarding these sessions should be addressed to the Divisional Chairman, Ernest L. Koehler, Continental Can Co., 7622 S. Racine Ave., Chicago, Ill., 60620.

For all papers at any of the Division's sessions, three copies of an abstract of 75-words or less must be received at The Electrochemical Society, 30 East 42 St., New York, N.Y., 10017, by May 17, 1965.

The Corrosion Division does not require extended abstracts.

Symposium on Corrosion Inhibition of Organic Compounds

Announcement is made by Chairman Ernest L. Koehler of the Corrosion Division that symposia plans for the 1965 Fall Meeting of the Society include "Corrosion Inhibition of Organic Compounds." Symposium Chairman is Dr. Z. A. Foroulis, Esso Research & Engineering Co., P.O. Box 101, Florham Park, N.J.

Papers are now solicited for presentation at this symposium. Contributions concerning the mechanism of corrosion inhibition by organic compounds and, in particular, the effects of their chemical and structural characteristics on adsorption and the kinetics of corrosion reactions are particularly suitable. Papers concerning both mercury and solid metals are invited.

To be considered for this meeting, triplicate copies of the usual 75-word abstract should be sent to The Electrochemical Society, 30 East 42 St., New York, N. Y., 10017, not later than May 17, 1965.

Inquiries and suggestions should be sent to the Symposium Chairman. Anyone considering submitting a paper for this symposium, should notify him as soon as possible.

Symposium on Microbiological Corrosion

The Corrosion Division is planning a symposium on "Microbiological Corrosion" for the 1965 Fall Meeting of the Society. There has been a considerable amount of effort in this field during the last few years in a number of laboratories. It is hoped that, with the work accomplished, it will be possible to appraise some of the theories and propositions that have been advanced to explain the relationship between microbial growth and corrosion. Papers reporting advances in the field are now being solicited.

To be considered for this meeting, triplicate copies of the usual 75-word abstract should be sent to The Electrochemical Society, 30 East 42 St., New York, N.Y., 10017, not later than May 17, 1965.

Inquiries on the technical content of the symposium or expressions of willingness to participate should be directed to Dr. R. T. Foley, Chemistry Dept., The American University, Washington, D.C., 20016.

Symposium on Corrosion in Nonaqueous Media

The Corrosion Division is planning a Symposium on "Corrosion in Nonaqueous Media" for the 1965 Fall Meeting of The Society.

"Corrosion in Nonaqueous Media" is to be considered as inclusive of research in organic and inorganic solvents, molten salts, and gas systems. Papers which may relate properties of the corrosion products to corrosion performance or to the corrosion mechanism are especially, but not exclusively, desired.

Suitable papers are solicited for the Symposium. Three copies of the usual 75-word abstract must be received at The Electrochemical Society, 30 East 42 St., New York, N.Y., 10017, not later than May 17, 1965.

Inquiries and suggestions should be sent to the Symposium Chairman, Sheldon Evans, Rocketdyne D/991-356, 6633 Canoga Ave., Canoga Park, Calif., 91304. Anyone considering submitting a paper for the symposium should so notify the Chairman.

Electrodeposition Symposium Plans

The Electrodeposition Division of the Society is planning a symposium on "Thin Film Technology" for the 1965 Fall Meeting to be held in Buffalo, N. Y., October 10-14, 1965. Papers are solicited in both basic and applied areas. Communications and inquiries should be addressed to Dr. I. W. Wolf, Ampex Corp., 401 Broadway-Ms 3-21, Redwood City, Calif.

Triplicate copies of the usual 75-word abstract as well as of an extended abstract of 500-1000 words (see notice p. 112C of this issue) should be sent to The Electrochemical Society, 30 East 42 St., New York, N. Y., 10017, *not later than May 17, 1965.*

Electrothermics and Metallurgy Symposium Plans

General Session

A general symposium on subjects that come within the scope of activity of the Electrothermics and Metallurgy Division is being organized by the Division as part of its 1965 Fall Meeting of the Society to be held in Buffalo, N.Y., October 10-14, 1965

To assist potential contributions to decide whether their papers fall within the field of interest of the Division, the following paragraph from the Division's tentative statement of scope has been reproduced as follows:

In general, the purpose of the Division is to aid and encourage the advancement of electrochemical science and industry concerned with specialty materials and processes.

As specific examples of fields in which the Division has maintained interest and activity, there may be cited: Materials such as refractory metals and compounds, intermetallics, graphite, fused salts, and rare earths metals; Equipment for the utilization of electrical energy and materials synthesis; Processes using arcs, vacua, plasma, and electron and ion beams; and Phenomena such as melting, vaporization, reaction, sintering, diffusion or oxidation occurring at high-temperatures, high pressures or involving high temperature materials.

Papers of both the fundamental and applied nature are welcomed.

Triplicate copies of the usual 75-word abstract as well as an extended abstract of 500-1000 words must be received at The Electrochemical Society, 30 East 42 St., New York, N.Y. 10017, *not later than May 17, 1965.* Inquiries may be sent to W. E. Kuhn, Chairman, Electrothermics and Metallurgy Division, c/o Spindletop Research, Iron Works Pike, Lexington, Ky.

Symposium on Zirconium and Its Alloys

A Symposium on Zirconium and Its Alloys is being organized by the Electrothermics and Metallurgy Division as part of the 1965 Fall Meeting of The Electrochemical Society to be held in Buffalo, N. Y., October 10-14, 1965.

Sessions will be held on: Mechanisms of Corrosion and Oxidation Processes; Mechanisms of Hydrogen Pickup; Deformation and Fracture; Transformation and Diffusion; and Irradiation Effects.

Papers should consider the fundamental nature of the processes involved.

Symposium Co-Chairmen are: E. C. W. Perryman, Chemistry and Metallurgy Div., Atomic Energy of Canada Ltd., Chalk River, Ont., Canada and J. P. Pemsler, Ledgemont Lab., Kennecott Copper Corp., 128 Spring St., Lexington, Mass., 02173.

Triplicate copies of the usual 75-word abstract, as well as an extended abstract of 500-1000 words must be received at Society Headquarters, 30 East 42 St., New York, N. Y., 10017, *not later than May 17, 1965.*

Publication of papers from this Symposium is planned.

Authors are therefore requested to submit three copies of each manuscript to Dr. W. W. Smeltzer, Dept. of Metallurgical Engineering, McMaster University, Hamilton, Ont., Canada, as soon as is possible, prior to presentation of the paper at the National Meeting of the Society.

RESEARCH & DEVELOPMENT OPPORTUNITIES

GROUP LEADER—R & D LABORATORY

Leading battery company offers career opportunities in research and development on silver-zinc batteries at the Research and Development Laboratory in Minneapolis, Minnesota.

M.S. or Ph.D. Physical or Physical Organic Chemist-Group leader to direct the efforts of a group of chemists and support personnel in exploratory research and applied research in separators for silver-zinc batteries. 2-5 years experience. Background in electrochemistry and/or polymer chemistry helpful.

PRODUCT DEVELOPMENT SECTION HEAD
ALKALINE BATTERY DIVISION

B.S. in chemistry or Chemical Engineering. Will be responsible for directing the design and development of remotely activated silver-zinc primary batteries.

For further information, write in confidence to G. W. Vinton, E-1300 First National Bank Building, St. Paul, Minnesota 55101

GOULD NATIONAL®

An equal opportunity employer

GOULD-NATIONAL BATTERIES, INC.

FIRST NATIONAL BANK BLDG. • ST. PAUL, MINNESOTA • 55101

ATTENTION, MEMBERS AND SUBSCRIBERS

Whenever you write to The Electrochemical Society about your membership or subscription, please include your Magazine address label to ensure prompt service.

ATTACH LABEL HERE

Change of Address

To change your address, please give us five weeks' advance notice. Place magazine address label here. Print your NEW address below. If you have any question about your subscription or membership, place your magazine label here and clip this form to your letter.

Mail to the Circulation Department, The Electrochemical Society, Inc., 30 East 42 St., New York, N. Y., 10017.

name

address

city state zip code

WHY GUESS?

MEASURE PLATING THICKNESS

to a millionth of an inch

Your profits depend on meeting tight specifications, maintaining quality control and reducing rejects. Can you afford to guess at plating thickness when it is so easy to *measure and be sure*?

UNITRON'S PL-MEC PLATER'S MICROSCOPE **substitutes facts for uncertainty. The plated deposit is observed through a Filar Micrometer Eyepiece and measurements are read directly from a micrometer drum. This compact microscope is easy to use, portable around the shop and has a built-in light source. It also doubles as a metallurgical microscope for examining grain structure etc. at magnifications of 25X-1500X. Permanent photographic records may be made using an accessory 35mm. camera attachment and provide valuable legal protection for subcontractors.**

UNITRON'S PLATER'S MICROSCOPE **will save its initial cost many times over. Prove this for yourself — as so many firms in the plating industry have done—by requesting a FREE 10 DAY TRIAL in your own plant. There is no cost and no obligation.**

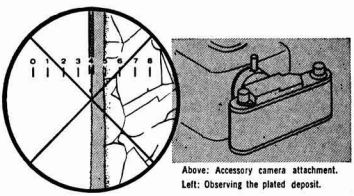

Above: Accessory camera attachment.
Left: Observing the plated deposit.

$468 Model PL-MEC complete with all optics and standard accessories	As above with built-in camera attachment, but without 35mm. camera back: **$540**

THE TREND IS TO UNITRON

UNITRON

INSTRUMENT COMPANY • MICROSCOPE SALES DIV.
66 NEEDHAM ST., NEWTON HIGHLANDS 61, MASS.

Please rush UNITRON's Microscope Catalog 86-I

Name_____

Company_____

Address_____

City_____ State_____

Extended Abstract Book Publication Program for the Society's 1965 Fall Meeting in Buffalo, N. Y.

The Board of Directors has provided that the National Office shall assist Divisions with the mechanics of publishing Extended Abstracts for sessions involving 15 or more papers at our National Meetings.

The Divisions will handle the technical editing of the abstracts following which the Society Office will arrange for the printing and distribution of the books, thus relieving Division representatives of this responsibility. Each Division program will be the subject of a separate Extended Abstract Book. Papers sponsored solely by the Corrosion Division **do not** require an extended abstract.

This means that each author who submits a paper for presentation at our meeting should do three things:

1—Submit *three* copies of the usual 75-word abstract of the paper for publication in the printed program of the meeting;

2—Simultaneously submit *three* copies of an extended abstract of the paper of 500-1000 words; and

3—Send the 75-word abstract and the 500-1000-word extended abstract to Society Headquarters, 30 East 42 St., New York, N. Y., 10017, *not later than May 17, 1965.*

The Extended Abstract Books will be published by photo-offset reproduction *from typewritten copy submitted by the author.* Special care should therefore be given to the following typing instructions so as to establish uniformity in printing:

1—Abstracts are to be 500-1000 words in length.

2—Use white bond paper, size 8½ x 11 inches.

3—Abstracts should be typed SINGLE space.

4—Use 1¼ inch margins at the top and bottom and at the sides of each page.

5—All copy, including figures, symbols, and corrections, should be in black ink.

6—Figures should be pasted in within the typing dimensions indicated. Captions should be typed not wider than figure dimensions and pasted in proper place in the abstract. Figure captions should appear at bottom of figure. Table titles should appear at top of tables.

7—Wherever possible, avoid use of halftones.

8—Title of paper should be in capital letters. Author(s) name and affiliation should be typed immediately below. It is not necessary in the heading or body to designate paper as "Extended Abstract," or quote the Divisional Symposium involved.

9—Mail to Society Headquarters *unfolded.*

Members and JOURNAL subscribers will receive notice of Extended Abstracts Books to be scheduled for publication. The notices will be accompanied by order blanks for the copies desired. Orders should be submitted with remittance. The advance orders will be necessary for estimating numbers of books to be printed and will be mailed to purchasers prior to the Buffalo meeting. Some extra copies will be available at the meeting but the advance-paid order is the only way to be assured of getting copies.

The Electrochemical Society

Patron Members

Aluminum Co. of Canada, Ltd.,
Montreal, Que., Canada
The Dow Chemical Co.,
Chemical Dept., Midland, Mich.
Metals Dept., Midland, Mich.
International Nickel Co., Inc.,
New York, N. Y.
General Electric Co.
Capacitor Dept., Hudson Falls, N. Y.
Chemical Laboratory, Knolls Atomic Power Laboratory, Schenectady, N. Y.
Chemical and Materials Engineering Laboratory, Advanced Technology Laboratories, Schenectady, N. Y.
Chemistry Research Dept., Schenectady, N. Y.
Direct Energy Conversion Operation, West Lynn, Mass.
Lamp Division, Cleveland, Ohio
Materials & Processes Laboratory, Large Steam Turbine-Generator Dept., Schenectady, N. Y.
Metallurgy and Ceramics Research Dept., Schenectady, N. Y.
Olin Mathieson Chemical Corp.,
Chemicals Div., Research Dept., New Haven, Conn.
Union Carbide Corp.
Divisions:
Carbon Products Div., New York, N. Y.
Consumer Products Div., New York, N. Y.
Westinghouse Electric Corp.
Electronic Tube Div., Elmira, N.Y.
Lamp Div., Bloomfield, N.J.
Molecular Electronics Div., Elkridge, Md.
Research Laboratories, Pittsburgh, Pa.
Semiconductor Div., Youngwood, Pa.

Sustaining Members

Air Reduction Co., Inc., New York, N. Y.
Allen-Bradley Co., Milwaukee, Wis.
Allied Chemical Corp.
General Chemicals Div., Morristown, N. J.
Alloy Steel Products Co., Inc., Linden, N. J.
Aluminum Co. of America,
New Kensington, Pa.
American Metal Climax, Inc.,
New York, N. Y.
American Potash & Chemical Corp.,
Los Angeles, Calif.
American Smelting and Refining Co.,
South Plainfield, N. J.
American Zinc Co. of Illinois,
East St. Louis, Ill.
American Zinc, Lead & Smelting Co.,
St. Louis, Mo.
M. Ames Chemical Works, Inc.,
Glen Falls, N. Y.
Ampex Corp., Redwood City, Calif.
Armco Steel Corp., Middletown, Ohio
Basic Inc., Bettsville, Ohio
Bell Telephone Laboratories, Inc.,
New York, N. Y. (2 memberships)
Bethlehem Steel Co., Bethlehem, Pa.
(2 memberships)
Boeing Co., Seattle, Wash.
Burgess Battery Co., Freeport, Ill.
(2 memberships)
Burndy Corp., Norwalk, Conn.
Canadian Industries Ltd., Montreal,
Que., Canada
Carborundum Co., Niagara Falls, N. Y.
Chrysler Corp., Detroit, Mich.
Consolidated Mining & Smelting Co. of Canada, Ltd., Trail, B. C., Canada
(2 memberships)
Continental Can Co., Inc., Chicago, Ill.
Corning Glass Works, Corning, N. Y.
Diamond Alkali Co., Painesville, Ohio
Wilbur B. Driver Co., Newark, N. J.
(2 memberships)
E. I. du Pont de Nemours & Co., Inc.,
Wilmington, Del.
Eagle-Pitcher Co., Chemical and Metals Div.,
Joplin, Mo.
Eastman Kodak Co., Rochester, N. Y.
Eltra Corp.,
Prestolite Div., Toledo, Ohio
C&D Batteries, Conshohocken, Pa.
Electric Storage Battery Co.,
Philadelphia, Pa. (2 memberships)
Engelhard Industries, Inc., Newark, N. J.
(2 memberships)
The Eppley Laboratory, Inc., Newport, R. I.
Exmet Corp., Bridgeport, Conn.
Fairchild Semiconductor Corp., Palo Alto, Calif.
FMC Corp.
Inorganic Chemical Div., Buffalo, N. Y.
Chlor-Alkali Div., South Charleston, W. Va.
Foote Mineral Co., Exton, Pa.
Ford Motor Co., Dearborn, Mich.
General Motors Corp.
Allison Div., Indianapolis, Ind.
Delco-Remy Div., Anderson, Ind.
Research Laboratories, Warren, Mich.
General Telephone & Electronics
Laboratories Inc., Bayside, N. Y.
(2 memberships)
Globe-Union, Inc., Milwaukee, Wis.
B. F. Goodrich Chemical Co.,
Cleveland, Ohio
Gould-National Batteries, Inc.,
Minneapolis, Minn.
Great Lakes Carbon Corp., New York, N. Y.
Hanson-Van Winkle-Munning Co.
Matawan, N. J. (2 memberships)

(Sustaining Members con'd)

Harshaw Chemical Co., Cleveland, Ohio
(2 memberships)
Hercules Powder Co., Wilmington, Del.
Hill Cross Co., Inc., West New York, N. J.
Hoffman Electronics Corp., Semiconductor Div., El Monte, Calif.
Honeywell Inc., Minneapolis, Minn.
Hooker Chemical Corp., Niagara Falls, N. Y. (3 memberships)
HP Associates, Palo Alto, Calif.
Hughes Research Laboratories, Div. of Hughes Aircraft Co., Malibu, Calif.
International Business Machines Corp., New York, N. Y.
International Minerals & Chemical Corp., Skokie, Ill.
International Resistance Co., Philadelphia, Pa.
ITT Federal Laboratories, Div. of International Telephone & Telegraph Corp., Nutley, N. J.
Jones & Laughlin Steel Corp., Pittsburgh, Pa.
K. W. Battery Co., Skokie, Ill.
Kaiser Aluminum & Chemical Corp.
Div. of Chemical Research, Permanente, Calif.
Div. of Metallurgical Research, Spokane, Wash.
Kawecki Chemical Co., Boyertown, Pa.
Kennecott Copper Corp., New York, N. Y.
Leesona Moos Laboratories, Div. of Leesona Corp., Jamaica, N. Y.
Arthur D. Little, Inc., Cambridge, Mass.
Lockheed Aircraft Corp., Missiles & Space Div., Sunnyvale, Calif.
Mallinckrodt Chemical Works, St. Louis, Mo.
P. R. Mallory & Co., Indianapolis, Ind.
Melpar, Inc., Falls Church, Va.
Metal Pumping Services Cleveland, Ohio
Miles Chemical Co., Div. of Miles Laboratories, Inc., Elkhart, Ind.
Monsanto Chemical Co., St. Louis, Mo.
M&T Chemicals Inc., Detroit, Mich.
National Cash Register Co., Dayton, Ohio
National Lead Co., New York, N. Y.
National Steel Corp., Weirton, W. Va.
North American Aviation, Inc., El Segundo, Calif.
Northern Electric Co., Montreal, Que., Canada
Norton Co., Worcester, Mass
Owens-Illinois Glass Co., Toledo, Ohio
Pennsalt Chemicals Corp., Philadelphia, Pa.
Phelps Dodge Refining Corp., Maspeth, N. Y.
Philco Corp., Research Div., Blue Bell, Pa.
Philips Laboratories, Inc., Briarcliff Manor, N. Y.
Pittsburgh Plate Glass Co., Chemical Div., Pittsburgh, Pa.
Potash Co. of America, Carlsbad, N. Mex.
Radio Corp. of America
Electronic Components and Devices, Lancaster, Pa.
Tube Div., Harrison, N. J.
RCA Victor Record Div., Indianapolis, Ind.
Raytheon Co., Waltham, Mass.
Republic Foil Inc., Danbury, Conn.
Reynolds Metals Co., Richmond, Va.
Shawinigan Chemicals Ltd., Montreal, Que., Canada
Socony Mobil Oil Co., Inc., Dallas, Texas
Speer Carbon Co.
International Graphite & Electrode Div., St. Marys, Pa.
Sprague Electric Co., North Adams, Mass.
Stackpole Carbon Co., St. Marys, Pa.
Stauffer Chemical Co., New York, N. Y.
Texas Instruments, Inc., Dallas, Texas
Metals and Controls Corp., Attleboro, Mass.
3M Company, St. Paul, Minn.
Titanium Metals Corp. of America, Henderson, Nev.
Tyco Laboratories, Inc., Waltham, Mass.
Udylite Corp., Detroit, Mich.
(4 memberships)
United States Borax & Chemical Corp., Los Angeles, Calif.
United States Steel Corp., Pittsburgh, Pa.
Univac, Div. of Sperry Rand Corp., New York, N. Y.
Universal-Cyclops Steel Corp., Bridgeville, Pa.
Upjohn Co., Kalamazoo, Mich.
Western Electric Co., Inc., Chicago, Ill.
Wyandotte Chemicals Corp., Wyandotte, Mich.
Yardney Electric Corp., New York, N. Y.

97 941